

# LAUNCH CANADA 2024 CHALLENGE



Final Design Report for Borealis  
Competing Team 31 - Waterloo Rocketry

## TABLE OF CONTENTS

|  |           |
|--|-----------|
| <b>1 INTRODUCTION</b>                                  | <b>11</b> |
| 1.1 Team History . . . . .                             | 11        |
| 1.2 Team Organization . . . . .                        | 12        |
| 1.3 Outreach Activities . . . . .                      | 12        |
| <b>2 INITIAL REQUIREMENTS AND DESIGN GOALS</b>         | <b>14</b> |
| <b>3 MISSION CONCEPT OF OPERATIONS OVERVIEW</b>        | <b>18</b> |
| <b>4 CYCLE BASED DESIGN APPROACH</b>                   | <b>22</b> |
| 4.1 Linear vs Cyclical Design . . . . .                | 22        |
| 4.2 Advantages of Cyclical Design . . . . .            | 23        |
| 4.3 Borealis Execution . . . . .                       | 24        |
| 4.4 Impact On Borealis Project . . . . .               | 24        |
| <b>5 SYSTEM ARCHITECTURE OVERVIEW</b>                  | <b>26</b> |
| <b>6 FLIGHT DYNAMICS</b>                               | <b>29</b> |
| 6.1 Flight Dynamics History . . . . .                  | 29        |
| 6.2 LOTS Retrospective . . . . .                       | 29        |
| 6.3 Borealis Design Goals . . . . .                    | 31        |
| 6.4 Setting Eridium Engine Design Targets . . . . .    | 32        |
| 6.5 Fin Aerodynamic Design . . . . .                   | 33        |
| 6.6 Nosecone Aerodynamic Design . . . . .              | 35        |
| 6.7 Design Data Tracking and Mass Budgeting . . . . .  | 35        |
| 6.8 Choice of Simulation Software . . . . .            | 37        |
| 6.9 RSE File Generation . . . . .                      | 38        |
| 6.10 Airbrakes Location . . . . .                      | 39        |
| 6.11 Airbrakes Ansys Simulation . . . . .              | 40        |
| 6.12 Ansys and OpenRocket Integration . . . . .        | 40        |
| 6.13 Monte Carlo Simulations with OpenRocket . . . . . | 41        |
| 6.14 Loads Analysis . . . . .                          | 41        |
| 6.15 Painting . . . . .                                | 44        |
| 6.16 Current Simulation Results . . . . .              | 47        |
| 6.17 Weather Launch Commit Criteria . . . . .          | 50        |
| <b>7 AEROSTRUCTURE</b>                                 | <b>51</b> |
| 7.1 Overview . . . . .                                 | 51        |
| 7.2 Nosecone . . . . .                                 | 52        |
| 7.3 Composite Bodytubes . . . . .                      | 55        |
| 7.3.1 Layup Schedule Calculations . . . . .            | 55        |
| 7.3.2 Manufacturing Process . . . . .                  | 56        |
| 7.4 Upper Bodytube and Parachute Bay . . . . .         | 57        |
| 7.4.1 Payload bay . . . . .                            | 58        |

|          |                                 |            |
|----------|---------------------------------|------------|
| 7.4.2    | Payload Bay Manufacturing       | 59         |
| 7.5      | Oxidiser Tank Aft Skirt         | 60         |
| 7.5.1    | Longerons                       | 60         |
| 7.5.2    | Fairings                        | 64         |
| 7.5.3    | Fill Disconnect Hatch           | 64         |
| 7.6      | Fin Can                         | 65         |
| 7.6.1    | Fin Testing                     | 70         |
| 7.6.2    | Fin Manufacturing               | 72         |
| 7.6.3    | Boattail                        | 75         |
| 7.7      | Couplers                        | 78         |
| 7.7.1    | Geometry                        | 78         |
| 7.7.2    | Structure                       | 79         |
| 7.7.3    | Manufacturing and Bonding       | 81         |
| <b>8</b> | <b>PROPELLION</b>               | <b>82</b>  |
| 8.1      | Overview                        | 82         |
| 8.2      | Injectors                       | 82         |
| 8.2.1    | Injector Characterization       | 83         |
| 8.2.2    | Injector Bulkhead               | 86         |
| 8.3      | Combustion Chamber              | 88         |
| 8.3.1    | Combustion Chamber Casing       | 89         |
| 8.3.2    | Ablative Liners                 | 90         |
| 8.3.3    | Custom Ablative Development     | 90         |
| 8.3.4    | Nozzle Retention                | 91         |
| 8.3.5    | Igniter                         | 91         |
| 8.4      | Feedsystem                      | 92         |
| 8.4.1    | Propellant Tanks                | 92         |
| 8.4.2    | Piston                          | 92         |
| 8.4.3    | Fill Bulkhead                   | 92         |
| 8.4.4    | Vent Bulkhead                   | 93         |
| 8.5      | Injector Valves                 | 95         |
| 8.6      | Fill/Dump Valve                 | 99         |
| 8.7      | Vent Valve                      | 101        |
| 8.8      | Engine Testing                  | 102        |
| 8.8.1    | Thrust Curve                    | 102        |
| 8.8.2    | Pressure Data                   | 103        |
| 8.8.3    | Changes for Flight              | 104        |
| <b>9</b> | <b>AVIONICS AND TELEMETRY</b>   | <b>106</b> |
| 9.1      | RocketCAN                       | 107        |
| 9.1.1    | Bus Topology and Harness Design | 108        |
| 9.1.2    | Common RocketCAN Hardware       | 110        |
| 9.1.3    | Common RocketCAN Software       | 111        |
| 9.1.4    | Message Format and Arbitration  | 112        |
| 9.1.5    | Telemetry Architecture          | 112        |

|   |            |
|---|------------|
| 9.1.6 Power Architecture . . . . .                  | 114        |
| 9.2 Charging Board . . . . .                        | 115        |
| 9.3 Propulsion Board . . . . .                      | 116        |
| 9.3.1 Actuators . . . . .                           | 116        |
| 9.3.2 Sensors . . . . .                             | 117        |
| 9.4 GPS Board . . . . .                             | 118        |
| 9.5 Live Telemetry Transmitter . . . . .            | 120        |
| 9.6 Camera/Logger Board . . . . .                   | 120        |
| 9.6.1 Scope . . . . .                               | 120        |
| 9.6.2 Electrical Design . . . . .                   | 121        |
| 9.7 BigRedBee GPS . . . . .                         | 122        |
| <b>10 RECOVERY SYSTEM</b> . . . . .                 | <b>124</b> |
| 10.1 Overview . . . . .                             | 124        |
| 10.2 Reefing Design . . . . .                       | 125        |
| 10.3 Physical Design . . . . .                      | 125        |
| 10.4 Past Failures and New Changes . . . . .        | 130        |
| 10.5 Parachute Folding and Deployment Bag . . . . . | 132        |
| 10.6 Remote Arming . . . . .                        | 132        |
| 10.6.1 Failing Safely . . . . .                     | 134        |
| 10.6.2 Remote Arming ConOps . . . . .               | 134        |
| 10.6.3 Power Management . . . . .                   | 135        |
| 10.6.4 Altimeter Control . . . . .                  | 136        |
| 10.6.5 Telemetry . . . . .                          | 137        |
| 10.6.6 Remote Arming Testing . . . . .              | 138        |
| 10.6.7 Revisions . . . . .                          | 138        |
| 10.7 Bulkhead and Cameras . . . . .                 | 139        |
| 10.8 Potential Sources of Failure . . . . .         | 140        |
| 10.9 Risk Assessment . . . . .                      | 141        |
| 10.10 Testing . . . . .                             | 141        |
| <b>11 GROUND SUPPORT EQUIPMENT</b> . . . . .        | <b>143</b> |
| 11.1 Remote Launch Control System . . . . .         | 143        |
| 11.1.1 Clientside . . . . .                         | 144        |
| 11.1.2 Towerside . . . . .                          | 145        |
| 11.1.3 System Safety . . . . .                      | 148        |
| 11.2 Data Acquisition System . . . . .              | 149        |
| 11.3 Omnibus . . . . .                              | 154        |
| 11.4 Ground Side Power Distribution . . . . .       | 155        |
| 11.4.1 GSPD Boards . . . . .                        | 155        |
| 11.4.2 GSPD Case . . . . .                          | 157        |
| 11.5 Tank Heating . . . . .                         | 159        |
| 11.6 Electrical Umbilical . . . . .                 | 161        |
| 11.7 Launch Tower . . . . .                         | 162        |
| 11.8 Antenna Towers . . . . .                       | 164        |

|  |            |
|--|------------|
| 11.9 Fill Plumbing . . . . .                                     | 164        |
| <b>12 AIRBRAKES</b>  | <b>166</b> |
| 12.1 Mechanical . . . . .  | 166        |
| 12.1.1 Constraints and Criteria . . . . .                        | 166        |
| 12.1.2 Conceptual Design . . . . .                               | 166        |
| 12.1.3 Implementation . . . . .                                  | 167        |
| 12.1.4 Integration . . . . .                                     | 171        |
| 12.1.5 Testing . . . . .   | 171        |
| 12.1.6 Conclusion . . . . .                                      | 174        |
| 12.2 Controller . . . . .  | 174        |
| 12.3 Processor Board . . . . .                                   | 174        |
| 12.3.1 Scope . . . . .   | 174        |
| 12.3.2 Electrical Design . . . . .                               | 175        |
| 12.3.3 Firmware . . . . .  | 175        |
| 12.4 Simulations . . . . .                                       | 176        |
| 12.5 PyAnsys Automation . . . . .                                | 180        |
| <b>13 PAYLOADS</b>   | <b>182</b> |
| 13.1 Vibration . . . . .   | 182        |
| 13.1.1 Vibration Board . . . . .                                 | 182        |
| 13.1.2 Vibration Plates . . . . .                                | 182        |
| 13.2 Peristaltic Pump . . . . .                                  | 183        |
| 13.2.1 Arms . . . . .  | 184        |
| 13.2.2 Tubing and Bagging . . . . .                              | 185        |
| 13.2.3 Fluid . . . . .   | 185        |
| 13.3 Tubing Track . . . . .                                      | 186        |
| 13.3.1 Pump Assembly . . . . .                                   | 186        |
| 13.4 CubeSat . . . . .   | 187        |
| 13.5 Fabrication . . . . .                                       | 188        |
| 13.6 Testing & Risks . . . . .                                   | 188        |
| <b>14 COMPLETED AND PLANNED SYSTEM TESTING</b>                   | <b>192</b> |
| 14.1 Static Fire . . . . .                                       | 192        |
| 14.2 Rocket Assembly . . . . .                                   | 192        |
| 14.3 Wet Dress Rehearsal . . . . .                               | 192        |
| 14.4 Competition Simulator . . . . .                             | 194        |
| <b>15 PROGRAMMATIC/TECHNICAL RISKS AND MITIGATION STRATEGIES</b> | <b>195</b> |
| <b>APPENDICES</b>  | <b>201</b> |
| <b>A Aerostructure Component Calculations</b>                    | <b>201</b> |
| A.1 Bodytube Safety Factor Calculation Example . . . . .         | 201        |
| A.2 Longeron Calculations . . . . .                              | 203        |
| A.3 Payload Bay Calculations . . . . .                           | 204        |

|  |            |
|--|------------|
| A.3.1 Bolt Failure . . . . .           | 204        |
| A.3.2 Bolt Thread Engagement . . . . . | 205        |
| <b>B Remote Arming Schematics</b>      | <b>206</b> |
| <b>C Charging Board Schematics</b>     | <b>209</b> |
| <b>D Borealis P&amp;ID</b>             | <b>214</b> |
| <b>E Launch Operations Procedure</b>   | <b>215</b> |

## LIST OF FIGURES

|   |    |
|---|----|
| Figure 1 2024 Nominal CONOPS . . . . .                                    | 18 |
| Figure 2 2024 CONOPS Flowchart . . . . .                                  | 21 |
| Figure 3 Linear Design Approach . . . . .                                 | 22 |
| Figure 4 Cyclical Design Approach . . . . .                               | 23 |
| Figure 5 Functional Architecture Map . . . . .                            | 27 |
| Figure 6 Assemblies and Subassemblies . . . . .                           | 28 |
| Figure 7 Predicted Apogee with Cycle for LOTS . . . . .                   | 29 |
| Figure 8 Total Mass Evolution During LOTS Design Cycle . . . . .          | 30 |
| Figure 9 Dry Mass CG Evolution During LOTS Design Cycle . . . . .         | 31 |
| Figure 10 Fin Parameters . . . . .  | 33 |
| Figure 11 Rocket Sections . . . . .                                       | 36 |
| Figure 12 Cycle 4.1 Mass/CG Tracking Sheet . . . . .                      | 36 |
| Figure 13 Engine Flight Configuration Center of Gravity vs Time . . . . . | 39 |
| Figure 14 Airbrakes and Fin Flow Interference . . . . .                   | 40 |
| Figure 15 BENDIT7 Inputs . . . . .  | 42 |
| Figure 16 Takeoff Axial Loads Graphed . . . . .                           | 44 |
| Figure 17 MaxQ Bending Loads Graphed . . . . .                            | 44 |
| Figure 18 Borealis Dry Mass Breakdown by Section and Subsystem . . . . .  | 48 |
| Figure 19 Borealis Dry Mass Breakdown by Section . . . . .                | 48 |
| Figure 20 Aerostructures Layout . . . . .                                 | 52 |
| Figure 21 Nosecone Mould Halves . . . . .                                 | 53 |
| Figure 22 Scarf Joint . . . . .   | 53 |
| Figure 23 Nosecone Curing Under Vacuum . . . . .                          | 53 |
| Figure 24 Nosecone Compression Testing . . . . .                          | 54 |
| Figure 25 Stress-Strain Curve For Bodytube Test . . . . .                 | 56 |
| Figure 26 Infusion Setup . . . . .  | 57 |
| Figure 27 Fin Can and Combustion Chamber Bodytube Demoulding . . . . .    | 57 |
| Figure 28 Payload Bay Assembly . . . . .                                  | 58 |
| Figure 29 Payload Base Plate . . . . .                                    | 59 |
| Figure 30 Front Profile of Longeron . . . . .                             | 61 |
| Figure 31 Side Profile of Longeron . . . . .                              | 61 |
| Figure 32 Curved Tab . . . . .  | 62 |

|           |  |     |
|-----------|--|-----|
| Figure 33 | Metal Bracket  | 62  |
| Figure 34 | Buckling Simulation on a Longeron                                      | 63  |
| Figure 35 | Screw Layout of Curved Tabs  | 63  |
| Figure 36 | Fill Disconnect Hatch  | 64  |
| Figure 37 | Carbon Fibre Fins  | 65  |
| Figure 38 | Bonding Jigs Fixed on Fin Can  | 66  |
| Figure 39 | Fillet Being Formed Using Popsicle Stick                               | 67  |
| Figure 40 | Sanded Fillets   | 68  |
| Figure 41 | Fabric Being Wetted Out With Resin                                     | 69  |
| Figure 42 | Fabric Being Laid on the Fin Can                                       | 69  |
| Figure 43 | Vacuum Bagging   | 69  |
| Figure 44 | Final Vacuum Bagged Assembly   | 70  |
| Figure 45 | Fin Plate Testing Samples - SRAD (right) and COTS (left)               | 71  |
| Figure 46 | Load (N) Response of SRAD Plate Against Time (s)                       | 72  |
| Figure 47 | Load (N) Response of COTS Plate Against Time (s)                       | 72  |
| Figure 48 | Layer Thickness Test Piece   | 73  |
| Figure 49 | Plate Layer Assembly   | 74  |
| Figure 50 | Plate During Infusion  | 74  |
| Figure 51 | Fin With Small Hole on Bonding Edge                                    | 75  |
| Figure 52 | Boattail CAD   | 76  |
| Figure 53 | Boattail Assembly  | 76  |
| Figure 54 | Boattail As-Manufactured   | 77  |
| Figure 55 | Side Profile of Bonded Boattail  | 78  |
| Figure 56 | Injector Cross-Section   | 83  |
| Figure 57 | Cold Flow Test Load Cell Set-up  | 84  |
| Figure 58 | COTS Nozzle Spray Angle  | 85  |
| Figure 59 | Injector Joints  | 86  |
| Figure 60 | Top View of Asymmetric Manifold of the Injector Bulkhead               | 87  |
| Figure 61 | Cross Section of Injector Bulkhead                                     | 87  |
| Figure 62 | FEA Study on the Injector Bulkhead                                     | 88  |
| Figure 63 | Combustion Chamber Cross-Section                                       | 89  |
| Figure 64 | Ablative Characterization Testing Setup and Test                       | 91  |
| Figure 65 | Tank Assembly with Bulkheads   | 92  |
| Figure 66 | Fill Bulkhead Cross Section  | 93  |
| Figure 67 | FEA of Vent Bulkhead   | 94  |
| Figure 68 | Centering Features of Vent Bulkhead                                    | 94  |
| Figure 69 | Vent Bulkhead Port Placement and Integration                           | 95  |
| Figure 70 | Cross section of the Fuel Injector Valve - Closed                      | 96  |
| Figure 71 | Cross section of the Fuel Injector Valve - Open                        | 96  |
| Figure 72 | Fill Bulkhead with Integrated Valves                                   | 97  |
| Figure 73 | Changes in seat geometry between 2023 and 2024 oxidizer injector valve | 98  |
| Figure 74 | Flight Oxidizer Injector Valve   | 98  |
| Figure 75 | Flight Fuel Injector Valve   | 99  |
| Figure 76 | Cross section of the Fill/Dump Valve                                   | 100 |
| Figure 77 | Finished Fill/Dump Valve   | 101 |

|            |  |     |
|------------|--|-----|
| Figure 78  | 2023 Vent Valve . . . . .  | 102 |
| Figure 79  | Flight Qualification Static Fire Thrust Curve . . . . .                  | 103 |
| Figure 80  | Flight Qualification Static Fire Pressure Data . . . . .                 | 104 |
| Figure 81  | Flight vs Static Fire 2 Thrust Curves . . . . .                          | 105 |
| Figure 82  | RocketCan Block Diagram . . . . .  | 106 |
| Figure 83  | Male and Female Gecko Cable Assemblies . . . . .                         | 109 |
| Figure 84  | Female and Male Harwin Connector Assembly . . . . .                      | 109 |
| Figure 85  | Tefzel Jacket . . . . .  | 109 |
| Figure 86  | Schematic of Standard PIC18F26K83 Connections . . . . .                  | 110 |
| Figure 87  | Schematic of CAN Transceiver and Programming Header . . . . .            | 111 |
| Figure 88  | CAN Connector and Current Sensing Schematic . . . . .                    | 111 |
| Figure 89  | Example CAN Message . . . . .  | 112 |
| Figure 90  | PCB Trace Antenna on Rocket Side . . . . .                               | 113 |
| Figure 91  | Propulsion Board Actuator Circuit . . . . .                              | 116 |
| Figure 92  | Propulsion Board Barometric Pressure and Temperature Sensor . . . . .    | 117 |
| Figure 93  | Propulsion Board Connection Points for External Analog Sensors . . . . . | 118 |
| Figure 94  | GPS Connections Schematic . . . . .                                      | 119 |
| Figure 95  | GPS Power Supply Schematic . . . . .                                     | 120 |
| Figure 96  | The BigRedBee Mount in the Nosecone . . . . .                            | 123 |
| Figure 97  | Deployment Architecture . . . . .  | 124 |
| Figure 98  | Truck Testing a Previous Year's Parachute . . . . .                      | 126 |
| Figure 99  | Deployment Test . . . . .  | 127 |
| Figure 100 | Recovery Electronics Sled . . . . .                                      | 128 |
| Figure 101 | Routed and Folded Reefing Wire and Shock Cord Bundles . . . . .          | 129 |
| Figure 102 | Integrated Recovery Bulkhead with Slipring Shroud . . . . .              | 130 |
| Figure 103 | Packed Parachute and Rigging . . . . .                                   | 131 |
| Figure 104 | Lipo Mount . . . . .   | 131 |
| Figure 105 | Remote Arming Block Diagram . . . . .                                    | 133 |
| Figure 106 | Complete Remote Arming System . . . . .                                  | 133 |
| Figure 107 | Remote Arming Power Circuit for One of Two Batteries . . . . .           | 135 |
| Figure 108 | Recovery Batteries Current Sensing Circuit . . . . .                     | 136 |
| Figure 109 | One of Two Altimeter Arming Circuits . . . . .                           | 136 |
| Figure 110 | Stratologger Telemetry Level Shifting Circuit . . . . .                  | 137 |
| Figure 111 | CNC Recovery Bulkhead . . . . .  | 139 |
| Figure 112 | FEA of the Recovery Bulkhead . . . . .                                   | 140 |
| Figure 113 | Site Layout . . . . .  | 143 |
| Figure 114 | RLCS Clientside . . . . .  | 144 |
| Figure 115 | RLCS towerside . . . . .   | 145 |
| Figure 116 | RLCS Towerside Power Board . . . . .                                     | 146 |
| Figure 117 | RLCS Relay Board . . . . .   | 147 |
| Figure 118 | RLCS Tank Heating Relay Board . . . . .                                  | 148 |
| Figure 119 | Star Shaped Voltage Headers . . . . .                                    | 150 |
| Figure 120 | DAQ Connectors . . . . .   | 151 |
| Figure 121 | DAQ Interior . . . . .   | 152 |
| Figure 122 | DAQ Power Buck Schematic . . . . .                                       | 153 |

|            |  |     |
|------------|--|-----|
| Figure 123 | DAQ Power LDO Schematic  | 153 |
| Figure 124 | Omnibus Dashboard Screenshot   | 154 |
| Figure 125 | Connections Between Boards for GSPD                                    | 155 |
| Figure 126 | Schematic for Input Board  | 156 |
| Figure 127 | Schematic for Converter Board  | 157 |
| Figure 128 | Schematic for Connector Board  | 157 |
| Figure 129 | Inside the Fully Assembled GSPD Case                                   | 158 |
| Figure 130 | CAD for the Fan Cover  | 159 |
| Figure 131 | Tank Heater Flex PCB   | 160 |
| Figure 132 | Electrical Disconnect  | 161 |
| Figure 133 | Assembled Launch Tower   | 162 |
| Figure 134 | Raised Launch Tower  | 163 |
| Figure 135 | Assembled Nitrous Oxide Panel  | 165 |
| Figure 136 | Airbrakes Mechanism Top View   | 167 |
| Figure 137 | Airbrakes Mechanism Bottom View  | 167 |
| Figure 138 | Airbrakes Assembly Section View  | 168 |
| Figure 139 | Airbrakes Parametric Curve   | 168 |
| Figure 140 | Moment About Linear Rails  | 169 |
| Figure 141 | Bearing Stack  | 170 |
| Figure 142 | Airbrakes Mechanism Cross Section                                      | 170 |
| Figure 143 | Airbrakes Integration  | 172 |
| Figure 144 | Airbrakes Testing  | 172 |
| Figure 145 | Assembled Airbrakes  | 173 |
| Figure 146 | Assembled Airbrakes - Isometric  | 173 |
| Figure 147 | Processor Board Firmware Architecture                                  | 176 |
| Figure 148 | Rocket Model Used for CFD Simulation                                   | 177 |
| Figure 149 | Enclosure Created from Rocketry Geometry, with Bodies of Influence     | 177 |
| Figure 150 | Closeup View of the Mesh   | 178 |
| Figure 151 | Pressure Contour of the Rocket at Mach 0.8 and 0% Airbrake Extension   | 179 |
| Figure 152 | Drag Plot at 0-100% Extension  | 180 |
| Figure 153 | Drag Plot of 0-100% Extension Overlaid                                 | 181 |
| Figure 154 | Vibration Exploded   | 183 |
| Figure 155 | Peristaltic Arms   | 184 |
| Figure 156 | Bagging  | 185 |
| Figure 157 | Tubing Track   | 186 |
| Figure 158 | Pump Assembly  | 187 |
| Figure 159 | Pump Assembly  | 188 |
| Figure 160 | Exploded View  | 189 |
| Figure 161 | Machined CubeSat   | 190 |
| Figure 162 | Gasket Example   | 190 |
| Figure 163 | Assembled Rocket   | 193 |
| Figure 164 | Nitrogen and Water Being Sent Through the Injector Valves During WDR 1 | 194 |
| Figure 165 | Remote Arming Schematic - Microcontroller                              | 206 |
| Figure 166 | Remote Arming Schematic - Power  | 207 |
| Figure 167 | Remote Arming Schematic - Altimeters                                   | 208 |

|            |   |     |
|------------|---|-----|
| Figure 168 | Charging board - Microcontroller and System | 209 |
| Figure 169 | Charging Board - Battery Charger            | 210 |
| Figure 170 | Charging Board - Power                      | 211 |
| Figure 171 | Charging Board - Current Sense              | 212 |
| Figure 172 | Charging Board - Motor Control              | 213 |
| Figure 173 | Borealis P&ID                               | 214 |

## LIST OF TABLES

|          |   |     |
|----------|---|-----|
| Table 1  | Primary Functional Requirements for Borealis  | 14  |
| Table 2  | Borealis Design Cycles  | 25  |
| Table 3  | Final Fin Parameters  | 34  |
| Table 4  | Cycle 4 Takeoff Loads   | 43  |
| Table 5  | Cycle 4 MaxQ Loads  | 43  |
| Table 6  | Borealis Cycle 4 OpenRocket Simulations of Various Surface Finishes                     | 47  |
| Table 7  | Cycle 4 Simulation Inputs   | 47  |
| Table 8  | Cycle 4 Expected Case Simulation Results OpenRocket Based                               | 49  |
| Table 9  | Cycle 4 Expected Case Simulation Results CFD Based with 50% Airbrakes Control Authority | 49  |
| Table 10 | Composite Components Overview   | 51  |
| Table 11 | Resin System and Method Used to Make Composite Parts                                    | 52  |
| Table 12 | Payload Bay Safety Factor Calculations  | 59  |
| Table 13 | Coupler Geometries and Failure Modes  | 81  |
| Table 14 | Key Engine Parameters   | 82  |
| Table 15 | Summary of RocketCAN systems and locations  | 107 |
| Table 16 | CAN Bus Power Consumption   | 114 |
| Table 17 | CAN Bus Power Schedule  | 115 |
| Table 18 | Recovery Programmatic and Technical Risks, Hazards and Mitigation Strategies            | 141 |
| Table 19 | Recovery Tests  | 142 |
| Table 20 | Payload technical risks, hazards, and mitigation strategies                             | 191 |
| Table 21 | Likelihood and severity categories  | 195 |
| Table 22 | Team-wide programmatic risks  | 195 |
| Table 23 | Bodytube Parameters   | 201 |
| Table 24 | Bodytube Loads  | 202 |
| Table 25 | Longeron Calculation Parameters for Column Buckling                                     | 203 |
| Table 26 | Longeron Calculation Parameters for Tensile Failure                                     | 203 |
| Table 27 | Longeron Calculation Parameters for Compressive Failure                                 | 204 |
| Table 28 | Payload Bay Bolt Loads  | 204 |
| Table 29 | Payload Bay Bolt Parameters   | 204 |
| Table 30 | Payload Bay Bolt Failure Calculations   | 205 |
| Table 31 | Minimum Thread Engagement   | 205 |

## 1 INTRODUCTION

Waterloo Rocketry is a student team representing the University of Waterloo, from Waterloo, Ontario, Canada. The team is entering their bipropellant liquid rocket "Borealis" in the advanced category with a primary mission goal of a nominal ascent, followed by a successful recovery. The secondary mission goal is to perform our payload experiment, which intends to validate the process of blood transfusion in high-G environments. For the first time in the team's history, Borealis will also contain airbrakes to actively control the rocket's final apogee.

The primary objective of the team is to provide students with opportunities to engage in hands-on learning through practical engineering challenges. Team growth and continuity is contingent on the teams ability to maintain this atmosphere of learning and collaboration while remaining competitive and improving year-to-year. Many past and present members have dedicated significant time and effort to the team, and continued success is a recognition of this commitment. Additionally, the team owes much to the institutions and resources that the University of Waterloo makes available to student teams. The team's advisors, both from within the University and from industry, share knowledge and provide insight as the team continues to develop more complex and sophisticated systems.

This document details the design, analysis, implementation, and testing of all rocket and ground support systems, including the aerostructure, engine, avionics, recovery system, simulations, active controls, and onboard payload. There is also some discussion of risks and testing. Note that the unit system in this report is a mix of metric and US customary units. All technical descriptions have preserved the original design units, with occasional conversions where relevant.

### 1.1 Team History

Waterloo Rocketry was founded in 2009 and has competed at the Intercollegiate Rocket Engineering Competition since 2011. The team has entered IREC with an SRAD hybrid rocket each year except for 2012, where the team competed with a liquid bipropellant rocket. Starting in 2023, the team has attended Launch Canada. Below is a summary of the team's recent competition results:

- 2017: successful launch of the Vidar III hybrid rocket; winner of the 10,000ft SRAD hybrid/liquid category; awarded the Jim Furfaro award for technical excellence.
- 2018: successful launch of the Unexploded Ordnance hybrid rocket; winner of the 10,000ft SRAD hybrid/liquid category.
- 2019: successful launch of Shark of the Sky hybrid rocket; 2nd place in the 30,000ft SRAD hybrid/liquid category.
- 2021: 2nd place in the 30,000ft SRAD hybrid/liquid category; awarded the Gil Moore award for innovative design.
- 2022: 3rd place in the 30,000ft SRAD hybrid/liquid category; runner-up for the Jim Furfaro award for technical excellence.
- 2023: successful launch of the Leviathan of the Sky (LotS) hybrid rocket; 2nd place in the 30,000ft SRAD hybrid/liquid category; finalist for the Dr. Gil Moore Award for Innovation.

- 2023: successful launch of the 10K KOTS Solid solid rocket; Tied 3rd place in the basic category of Launch Canada

More information about the team can be found at the team's website: [waterloorocketry.com](http://waterloorocketry.com).

## 1.2 Team Organization

Waterloo Rocketry currently consists of around 100 members from a wide range of faculties, including Engineering, Math, Arts, and Science. The team's active members are largely undergraduate students, though the team has some graduate students and consults with alumni.

The teams faculty advisor is Dr. Andrew Milne, an engineering professor at the University of Waterloo who specializes in thermofluids. Dr. Milne often provides insight as the team works to develop more complex systems, as well as assisting with some high-level administrative tasks and decisions. The team has two co-leads: Jack Christensen and Tessa Pugh, who act as project and team managers, as well as technical supports. The Team Leads are responsible for overall project management and team direction, including overseeing all technical, administrative, and operational activities necessary to achieve team objectives. The Chief Safety Officers, Matthew Gordon, Rida Sayed, and Rhea Scollie consult with team members on practices and procedures to ensure that they are being done in the safest way possible. The Chief Safety Officers are also responsible for oversight of all safety documentation. Although this role is given to three people, safety practices are considered the responsibility and priority of every team member.

Organizationally, the team is structured into both technical and administrative systems. These are led by System Leads, who coordinate timelines and communication for each project undertaken. Each technical project is overseen by a Project Lead, who is responsible for managing all aspects of the project including, but not limited to, design, manufacturing, testing and integration. Team members are encouraged to work on any project, or projects, that interest them, and there is often collaboration and significant overlap between project teams and systems.

## 1.3 Outreach Activities

Waterloo Rocketry makes an effort to involve itself in university and community outreach each year. This serves the dual purpose of recruiting new members, as well as promoting awareness of student rocketry and Canadian rocketry as a whole. The team participates in the following outreach activities.

- Open House: The University of Waterloo holds two annual open houses for potential students. The team is always present at these events to showcase the rocket and the benefit of student teams.
- Giving Tuesday: This year, we will be participating in the university's Giving Tuesday, a university-wide fundraising event where donations to various organizations within UWATERLOO are matched by the university. The team has been involved with fundraising on the Student Design Centre's behalf.

- Model Rocket: Since 2014, the team has held an annual model rocket event in the fall. Participants are able to design, assemble, and launch their very own model rockets for a weekend, introducing potential new recruits to the rocket design process.
- Aviation Fun Day: The team has participated in the Region of Waterloos Aviation Fun Day since 2018, as a means to interact with the community and help fundraise for local food banks.
- High School Outreach: Members of the team conduct outreach activities at local high schools in the Kitchener-Waterloo region and surrounding areas to promote student rocketry and STEM.

In addition, Waterloo Rocketry intends to host an outreach activity at Launch Canada 2024. The team will present a video game which allows players to control both the airbrakes of a real-time simulated rocket and a physical model of Borealis' airbrakes. The endeavour of this activity is to encourage interest in model rocketry and demonstrate firsthand the engineering and mathematical challenges involved in it. This activity is particularly suitable for young children.

## 2 INITIAL REQUIREMENTS AND DESIGN GOALS

The primary mission goal of Borealis is to have a nominal flight with a successful recovery in a reflyable state. The flight also has two secondary goals. The first is to carry a 3U cubesat payload containing a peristaltic pump experiment to validate the ability to perform blood transfusions in high-G environments. The second is to validate the new active controls system, with the success criteria being that they bring the vehicle closer to the contract apogee than Borealis would have been otherwise. This rocket embodies the spirit of SRAD, with a design goal of having as many components as possible be student designed and fabricated.

After an incredibly successful hybrid launch at IREC 2023, the team has decided to retire its hybrid engine and move on to a nitrous oxide/ethanol liquid bipropellant engine. The team has now successfully tested a liquid engine three times, including once in Borealis' flight configuration. This certifies the engine as ready for flight.

The airframe of the rocket will be fabricated out of a mix of SRAD carbon fiber and fibreglass body tubes using improved processes and designs derived from destructive testing of existing body tubes. The rocket also contains some COTS fibreglass bodytubes where SRAD fibreglass was infeasible.

Reliability improvements also extend to the recovery system with the transfer of SRAD pyro-cutters from the shroud lines to the parachute canopy to reduce tangling risk and avionics improvements to prevent electrical shorts.

The list of primary functional requirements for the rocket can be seen below:

Table 1: Primary Functional Requirements for Borealis

| 1 Vehicle Requirements           |  |
|----------------------------------|--|
| 1.1                              | Borealis shall ascend nominally.<br><br>Final verification of this requirement will be performed at the Launch Canada Challenge with the rockets first launch attempt. Preliminary verification has been accomplished through flight simulation using data from static fire testing. Borealis does not have an apogee requirement.   |
| 1.2                              | Borealis shall descend safely from apogee and land without significant damage.<br><br>Meeting this requirement is the primary responsibility of the recovery system. Recovery system derived requirements are detailed under requirement section 3 Recovery System Requirements. Final verification of this requirement will be performed at the Launch Canada Challenge with the rockets first launch attempt. Derived requirements will be verified through a series of ground tests and drop tests. |
| 1.3                              | Borealis shall maintain stability throughout ascent. Generally targeted as between 1.5 and 7.0 static stability margin calibers throughout ascent.<br><br>Verification will be accomplished through flight simulation using data from static fire testing.   |
| 1.4                              | Borealis shall have an off-the-rail velocity greater than 30 m/s<br><br>Verification has been accomplished through flight simulation showing off rail velocity of 43m/s.   |
| 2 Propulsion System Requirements |  |
| 2.1                              | The total impulse of the engine shall not exceed the impulse limit defined in the Launch Canada Rules & Regulations  |

|  |  |
|--|--|
| <p>As the Eridium engine is intended for use at the Launch Canada Challenge it must not exceed the total impulse limits stated by rules and regulations of this competition. As fired in June, the engine had 24 000 Ns of impulse, and for flight is planned to have 28 150 Ns, well below the limit. This requirement is met.</p>  |  |
| 2.2  | The engine shall employ a method by which the amount of oxidizer loaded into the oxidizer tank can be reliably estimated.      |
| <p>The fill sensing system uses a load cell on the launch tower to measure the difference in rocket weight when loading propellant. A thermistor at the vent port will additionally indicate when the oxidizer tank level has reached the dip-tube. A propellant loading test using a proxy fluid for nitrous oxide (liquid CO<sub>2</sub>) will be performed to verify that this system is correctly able to measure the level of oxidizer.</p> |  |
| 2.3  | The aluminum shell of the combustion chamber shall not exceed a temperature of 250 °C.   |
| <p>This ensures the combustion chamber is not annealed by the engine burn. Temperatures are kept low using an ablative G-3 fibreglass liner. While no temperature over time data was collected, the maximum temperatures of the combustion chamber remained below 200 °C on single use temperature stickers. This requirement is met.</p>  |  |
| 3  | Recovery System Requirements   |
| 3.1  | The recovery system shall deploy the main parachute in a reefed state when Borealis reaches apogee.                            |
| <p>The deployment of the parachute was tested during a crane droptest. This requirement is met.</p>  |  |
| 3.2  | The recovery system shall trigger the disreefing event when Borealis has descended to an altitude of 1500 ft AGL.              |
| <p>This requirement has been tested using simulations built in to the altimeters. The requirement is met.</p>  |  |
| 3.3  | The recovery system shall be capable of being armed remotely.  |
| <p>Ground testing of the remote arming system will take place prior to the launch campaign to verify that the system can be remotely armed and disarmed. Testing of all safe states and contingencies will also be done.</p>   |  |
| 3.4  | A communication failure with the remote arming system shall not prevent the recovery system from being disarmed.               |
| <p>The recovery system can always be disarmed from outside of Borealis using its internal magnetic switches. Ground testing will be performed on this system to verify the disarming method.</p>   |  |
| 4  | Avionics Systems Requirements  |
| 4.1  | Borealis shall transmit telemetry regarding altitude, velocity, and attitude throughout the flight from ignition to touchdown. |
| <p>This functionality will be performed by the RocketCAN Live Telemetry Transmitter Board. Telemetry functionality and range testing will be performed on the ground.</p>  |  |
| 4.2  | Borealis shall log all system commands and sensor data gathered during flight for post-flight analysis and troubleshooting.    |

|   |   |
|---|---|
| <p>This is the function of the RocketCAN Logger Board. All RocketCAN boards communicate over a shared CAN bus, and Logger Board records and saves every CAN message to an SD card. This SD card can be recovered after the flight. Electrical system integration tests will be performed to ensure Logger Board is capable of logging every message when all boards are active and message throughput is high.</p>  |   |
| 4.3   | It shall be possible to replace any avionics board with an identical copy without compromising or negatively affecting the avionics system.   |
| <p>All boards must be trivially replaceable. This ensures that if a component on one board fails in the field during final assembly, it can be replaced with an identical board without issue. RocketCAN is designed with modularity and ease of replacement in mind, and several copies of each board will be assembled and packed to ensure sufficient spares are on hand. All replacement boards will have identical hardware, so no configuration changes will be necessary.</p>  |   |
| 4.4   | All flight electronics shall comply with the Launch Canada Safety Critical Wiring Guidelines.   |
| <p>Although the Safety Critical Wiring Guidelines are only explicitly binding on wiring associated with recovery systems and air-start motors, it is desirable to ensure all flight wiring is in compliance. This ensures all flight systems are robust and reliable. It also makes pre-flight inspection easier, as all wiring must be held to the same standard. Design considerations (selection of components) will be verified for compliance during the electrical design review process. Assembly considerations will be verified for compliance during pre-flight inspection.</p> |   |
| 5   | Airframe Requirements   |
| 5.1   | Borealis' fins shall have an aeroelastic flutter threshold velocity higher than the maximum rocket airspeed.  |
| <p>Simulation and numerical-based methods have taken place to validate that the fins as-built have an aeroelastic flutter threshold higher than the maximum rocket airspeed. This requirement is met.</p>   |   |
| 5.2   | The airframe shall withstand all bending, compression, and impact loads encountered throughout flight.  |
| <p>Preliminary design validation will use analytical methods of determining loads experienced by the structure. These analytical methods have been flight-tested on all rockets since 2019.</p>   |   |
| 5.3   | Airframe manufacturing processes shall endeavour to reduce surface roughness in the interest of drag reduction wherever possible.   |
| <p>This will be accomplished through surface finishing techniques such as sanding, polishing, and use of glossy coatings.</p>   |   |
| 6   | Payload Requirements  |
| 6.1   | The payload shall conform to the CubeSat standard with a form factor of 3U.   |
| <p>Compliance will be ensured throughout all design reviews leading up to manufacturing. Final verification will be accomplished via measurement of dimensions and mass. This requirement is met.</p>   |   |
| 6.2   | The payload shall be unnecessary for nominal rocket performance - that is, if the payload is replaced with a dead weight of equivalent mass and form factor, all non-payload mission objectives shall still be met. |

|   |   |
|---|---|
| <p>The payload performs no flight functions. Although it is capable of interfacing with the Rocket-CAN communications bus to provide an additional stream of sensor data, this data is redundant and not necessary for flight or for post-flight analysis of vehicle trajectory. This requirement is met.</p> |   |
| <p><b>6.3</b> Simulations shall be done to verify the CubeSat as flight worthy before launch.</p>   |   |
| <p>Ansys FEA has been used to evaluate the CubeSats performance, including static structural, modal, and vibrational analysis.</p>  |   |
| 7   | Ground Support Equipment Requirements   |
| 7.1   | The fill and ignition process shall be operable remotely from a range of at least 2,000 ft.<br><br>Verification of the remote fill and ignition systems will take place during static fire testing and Wet Dress Rehearsals. Launch control system range testing will be separately held to verify the operating range of radio communication.                                      |
| 7.2   | An electrical or software failure in the launch control system shall not cause the rocket to enter an unsafe state when personnel are nearby.<br><br>All actuators will have power disabled and controls locked out via key switch when any personnel are at the launch pad.  |
| 7.3   | There shall be a method of remotely disconnecting the fill system plumbing from the rocket prior to launch.<br><br>This system is expected to be similar to the system used last year, which was validated at IREC 2023.  |
| 8   | Airbrakes Requirements  |
| 8.1   | Airbrakes shall not compromise nominal flight of the rest of the rocket.<br><br>Verification shall be performed by ensuring symmetric actuation of airbrakes at all times and simulations to determine their effect on overall static stability   |
| 8.2   | Airbrakes shall bring Borealis closer to the target apogee than it would have been without airbrakes.<br><br>Verification can be performed with simulations to determine expected apogee, and true apogee as read by the onboard altimeters   |
| 9   | Operational and Safety Requirements   |
| 9.1   | Rocket final assembly (all assembly steps that can happen only immediately prior to launch) shall take no longer than 3 hours to complete.<br><br>This requirement is important to ensure that launch day operations are efficient and can be completed in a timely manner. Verification will take place through assembly rehearsals prior to the launch campaign.                  |
| 9.2   | A safe perimeter shall be established around test and launch sites prior to fill system pressurization. Only designated test personnel with proper PPE shall be permitted to enter this perimeter while the fill system is in a pressurized state.<br><br>Procedural checks are in place to ensure that the test site or launch pad are clear prior to the start of pressurization. |

### 3 MISSION CONCEPT OF OPERATIONS OVERVIEW

The mission concept of operations (CONOPS) for Borealis is made up of 9 phases, beginning with pre-launch operations and ending with vehicle recovery. The main phases are illustrated in Figure 1, with a more detailed breakdown of events in Figure 2. The primary mission objective is a nominal flight. Therefore while a target apogee has been defined, the magnitude of this value is of no consequence to the team. It is required instead to gauge airbrakes performance. As such, the target apogee for this flight is 6660m (21 850ft).

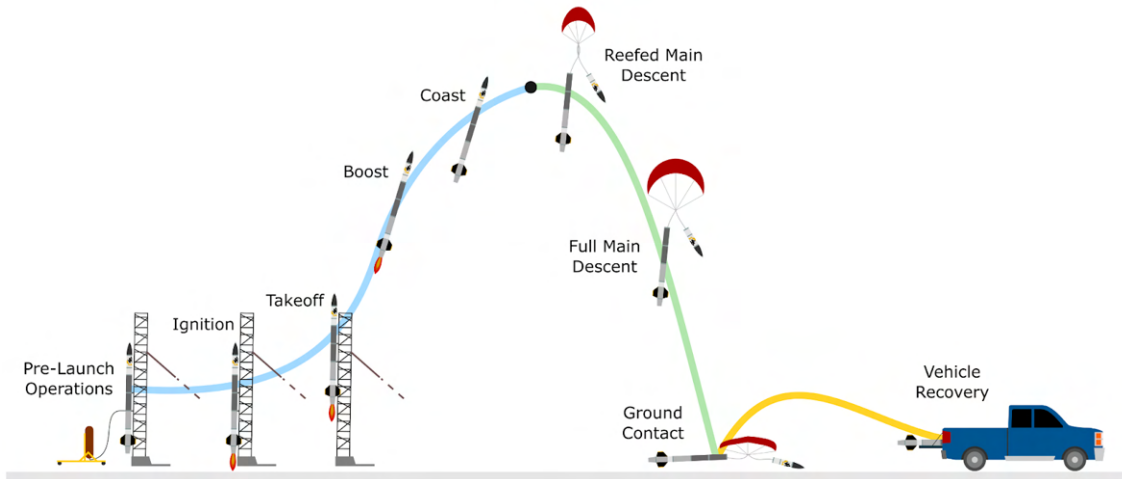


Figure 1: 2024 Nominal CONOPS

#### A. Pre-Launch Operations

Pre-launch operations begin when Borealis and the launch tower have been fully assembled. The rocket departs for the launch site and is loaded onto the launch rail upon arrival. The tower is then raised. All team members return to either mission control or base camp apart from the primary and secondary operators who don the necessary personal protective equipment, as outlined in the fill procedure. The operators perform the required system verifications and arm the recovery system, then retreat to the minimum safe distance before the remote fill procedure commences. Throughout fill, the remote launch control system (RLCS) and the data acquisition system (DAQ) provide feedback on the rocket mass and pressures from the fill lines and oxidizer tank. The fill system is disconnected when fill is complete, which is indicated by the rocket reaching a predetermined mass and oxidizer tank pressure. Pre-launch operations end when clearance to begin ignition is received.

#### B. Ignition

The ignition phase begins when the ignition command is sent to the primary ignition puck via RLCS. If necessary, the flight dynamics officer will monitor windspeed and provide simulation data on stability prior to the decision to sending the ignition command. When the puck ignites successfully, determined by a change in the igniter current or the observation of black smoke, the injector valves are opened, and the propellant ignites. The payload, recovery and avionics systems continue to acquire data. The ignition phase ends when the rocket begins to accelerate.

## C. Take-off

The take-off phase begins as the rocket accelerates up the launch rail. When the first launch rail button departs the rail, the velocity of the rocket shall be sufficient to keep the rocket stable and on the correct flight path. The recovery system, avionics, and payload experiment will continue to acquire data. The take-off phase ends when the aft launch lug of the rocket clears the launch rail.

## D. Boost

The boost phase begins when the rocket departs the launch rail. The engine will continue to burn, accelerating the rocket through the period of maximum dynamic pressure. The recovery, avionics, and payload systems will continue to acquire data. This phase ends at engine burnout.

## E. Coast

The coast phase begins following engine burnout, at which point the engine stops producing thrust and the rocket begins to decelerate. At the time of burnout, the active controls begin to take effect, braking the rocket to more closely reach the target apogee. The coast phase ends when the rocket reaches apogee.

## F. Reefed Descent

When the rocket reaches apogee, the altimeters will detect a decrease in altitude and trigger deployment of the main parachute, which opens initially in a reefed state. This will slow descent to a constant velocity of approximately 120ft/s. The avionics and payload systems will continue to acquire data, and the propulsion system will remain inactive. Airbrakes will be commanded to retract. Reefed main descent ends when the rocket descends to a predetermined altitude and the parachute is disreefed.

## G. Full Main Descent

When the altimeters detect that a pre-set altitude of 457m (1,500 ft) AGL has been reached, they trigger a disreefing event, expanding the main parachute to its full size. This will slow descent to a constant 30 ft/s. The recovery system will track the rocket's position as it descends. The avionics and payload systems will continue acquiring data, and the propulsion system will remain inactive. This phase ends when the rocket touches down on the ground.

## H. Ground Contact

This phase begins when the rocket makes contact with the ground, and the vehicle and parachute come to rest. This action renders all systems inactive, with the exception of the payload and avionics, which will continue to acquire data.

At the launch site, the fill system is safed using RLCS, and the primary and secondary operators approach from the minimum safe distance in order to complete the venting procedure. The phase ends when the fill system has been vented, indicated by all sensors in the lines and tanks reading atmospheric pressure.

## I. Rocket Retrieval

The rocket retrieval phase begins when a retrieval route is planned, and a retrieval team is formed. When the retrieval team has received safety kits and permission to depart, they proceed to the received location. When they arrive at this location, a primary damage inspection is done. If any energetics failed to discharge during the flight, they are safely disarmed by trained personnel. Borealis is then returned to mission control for a full post-flight evaluation.

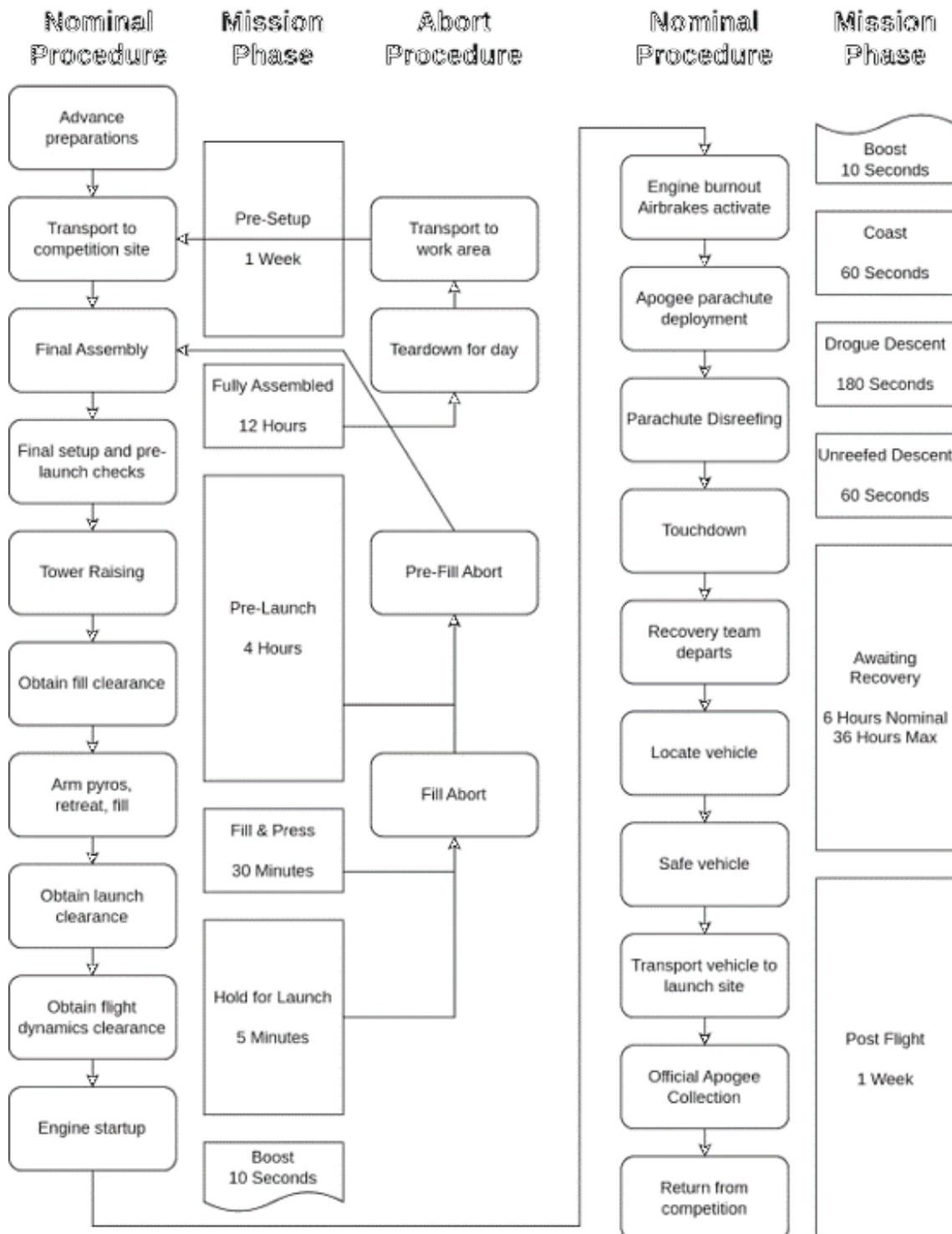


Figure 2: 2024 CONOPS Flowchart

## 4 CYCLE BASED DESIGN APPROACH

### 4.1 Linear vs Cyclical Design

As discussed in a retrospective report on last year's 2023 hybrid rocket, the team has developed a cycle-based design approach [1]. This replaces the linear approach the team had previously used and which is used by many student design teams. This typical linear design approach is shown in Figure 3.

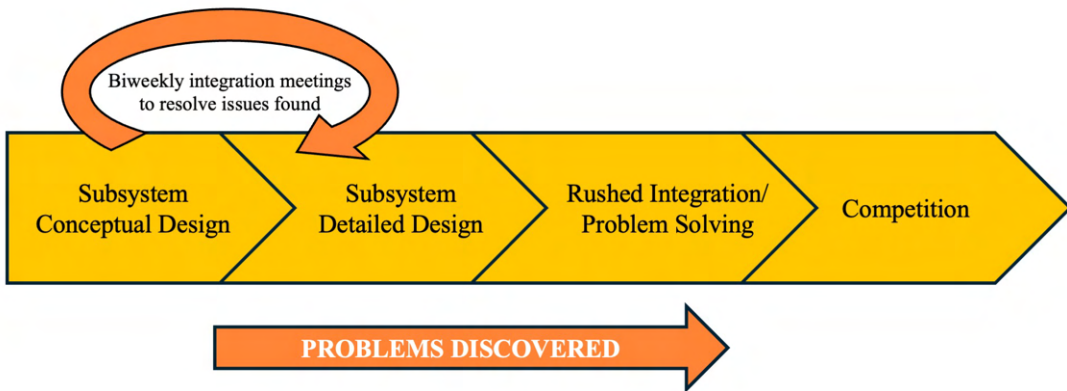


Figure 3: Linear Design Approach

In this linear approach,

"individually, each subsystem would create a conceptual design of what they were considering. Next each subsystem would create a detailed design and work out interfaces with other subsystems through bi-weekly integration meetings. These meetings were intended mainly to fight major issues being discovered throughout the design process. As issues were found and competition grew closer, the team entered into rushed integration and problem solving. Bringing many components designed in relative isolation together resulted in major issues being found very close to competition. An infamous team example happened when assembling the payload into the rocket a few weeks prior to competition. It was found that the payload did not fit through the opening in the rocket. While this issue was resolved, it raises serious concerns about this approach and how robust it is for integration purposes" [1].

To replace the linear design approach, a cyclical approach was created shown in Figure 4.

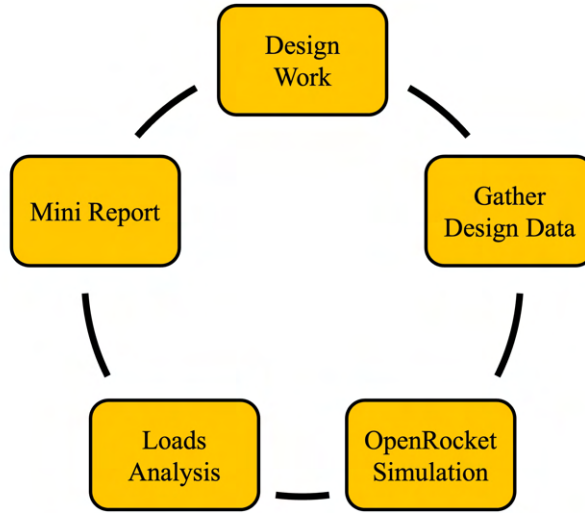


Figure 4: Cyclical Design Approach

The nominal use of this system is that:

"design work is completed as before, individually by each designer. Then periodically, this design data (mainly mass and position data) is collected into a large spreadsheet. Based on this data, OpenRocket simulations are completed. This provides the key flight characteristics of the current rocket as it exists in each designers mind. Based on the outputs of the OpenRocket simulation, loads analysis is completed. This enables each designer to know what the limiting load scenario is for their parts. After each of these steps is complete, the relevant data is collected and presented in a 10- to 20-page mini report. This cycle was repeated throughout the design process at key project milestones to ensure the information remained recent enough to be representative. This also has a side benefit of driving design progress and keeping each subsystem aligned in terms of design progress" [1].

## 4.2 Advantages of Cyclical Design

Some of the key advantages of the cyclical design approach, in no particular order, are:

- Early architecture decisions such as engine performance targets, rocket diameter, or section locations can be decided earlier with data driven confidence that the decided path is the most efficient.
- The deadlines for submitting design data act as checkpoints in the development of the rocket, improving timeline adherence.
- Architecture and timeline problems/inefficiencies can be spotted and proactively corrected before components are fully designed to improve performance based on simulation data.
- Provides design history documentation recorded in a trustworthy and accessible location.

- Enables the entire team to be on the same page about design priorities and overall system design. Everyone pulling in the same direction.
- Through the team regularly completing cycles, the data collection and simulation processes are optimized and familiar. This means that if schedules slip, the team is capable of incredibly quick data collection and simulation with high quality control. The team follows the philosophy that nothing being done at competition should be done for the first time, and mass collection and simulation is no different.
- Reduction of team stress levels due to deep understanding of the current and desired states of the rocket.

There are also many other benefits of this design approach that are less tangible.

### 4.3 Borealis Execution

In practice, the ideal items in each cycle are not always completed in order or for every cycle. For example, for most of the cycles in Borealis' development, there was a competition report being written at the end of the cycle. In this case, a mini-report was not needed. For cycles without a competition report, a google sheet summarizing the results and a slack message was deemed sufficient to communicate the learning's without the engineering resources required for a formal report.

As discussed in the retrospective report, a key consideration of the project was how many cycles to complete and when to do them [1]. The rationale was that a cycle should be completed when:

- New data is available that significantly changes the flight profile (i.e. completing a static fire test).
- A major architecture design needs to be made and data is required to make that decision (i.e. fin sizing or thrust requirement definition).
- A major competition deliverable is required and updated numbers are desired (i.e. competition final design report).

The cycles completed for Borealis are shown below in Table 2.

More details on gathering design details and OpenRocket simulations are discussed in Section 6.7. A detailed explanation of loads analysis is provided in Section 6.14.

### 4.4 Impact On Borealis Project

The cyclical design approach benefited the team greatly for the Borealis project. Some of the key successes of this project for Borealis were:

- Defining the scope of the project as a whole intentionally barely within the team's capabilities. This stretched the team to learn and grow but reduced the risk of a failed project. Defining scope well can be difficult when introducing new systems as it is tempting to let scope continually expand.

Table 2: Borealis Design Cycles

| Cycle   | Date             | Purpose  |
|---------|------------------|--|
| Cycle 0 | July 2023        | Early architecture decisions, set project goals and engine requirements, define scope.   |
| Cycle 1 | November 2023    | Subsystem conceptual designs, further define scope and objectives, early optimization.   |
| Cycle 2 | March 2024       | Finalize fin design using somewhat detailed subsystem designs, RSE based on first engine static fire.                          |
| Cycle 3 | May 2024         | Integration of detailed subsystem designs.   |
| Cycle 4 | July 2024        | Integration of almost all components "as-fabricated", new RSE based on static fire data.                                       |
| Cycle 5 | July/August 2024 | Assembly-based mass measurements to include smaller components / paint mass that may have been missed in previous cycles.      |
| Cycle 6 | August 2024      | Final simulations at competition to verify whether launch commit criteria or adjust to any problems discovered at competition. |

- Initial engine target performance parameters were set in September 2023 before full conceptual subsystem designs were made. Instead, this was based upon data driven system requirements and a very early conceptual rocket design as discussed in Section 6.4. This allowed high risk engine development to start detailed design work, testing, and iteration early to reduce risk and improve quality. The system level goals which engine targets were based on were all met without significantly changing the engine targets, showing the success of this approach.
- Technical risk of airbrakes was successfully brought down quickly through showing CP impact would be acceptable before detailed CFD models and mass data were available as discussed in Section 6.10.
- Timeline slip was kept in check successfully due to the regular rocket system progress updates from each cycle.

There are additionally many other impacts of this design approach on the design of Borealis which there is not space to discuss. The introduction of this design approach is a significant part of why the team was able to consistently produce innovative and capable rockets for two years in a row and it is expected to serve the team well in the future. Additionally, it more closely approximates a true industry development approach helping students to learn in a realistic engineering environment. The team recommends this type of design approach to all student teams, even those not focused on rocketry. An easily digestible presentation on this approach and its use in LOTS was done at the TMU Rocketry Conference which is an easy way to share the method [2].

## 5 SYSTEM ARCHITECTURE OVERVIEW

Borealis' system architecture is composed of a few broad systems that work together to fulfill the goals and requirements of the mission. The major rocket systems consists of a liquid engine to propel the rocket, an electronics system to communicate with and provide active control to the rocket in the form of airbrakes, a payload to collect sensor data through flight, a recovery system to return the rocket to earth safely, and an airframe to structurally and aerodynamically support the other 4 systems. These broad systems are broken into 9 distinct subsystems which are broken into 41 different subassemblies. The subsystems are categorized by location and function within the rocket. Breaking these further into their subsystems, they are useful to identify interfaces within the rocket. These can be one or more of mechanical, fluid, electrical, and informational interfaces. The system architecture map below illustrates the relationship between all of the systems in the rocket. This is a key part of ensuring that the vehicle will integrate together to fulfill the mission goal. At this stage in the design, the system architecture is finalized, the components are fabricated, and the various interfaces between the systems are being tested, characterized, and pushed to failure to better understand them.

Borealis has also been decomposed into a physical architecture, which is a representation of the mechanical assembly of the system. This architecture is being used as the structure for the CAD assembly of the vehicle, for mass data management, and is being used to plan assembly order and procedures. The physical architecture breaks the vehicle into the 6 major physical sections, the nosecone, the recovery system, the payload bay, the airbrakes, the feed system (including the propellant tanks and Ox Tank Aft Skirt section), and the combustion chamber and fin body. A detailed breakdown of the physical architecture can be seen in Figure 6.

It is critical that the rocket system integrates properly with its ground support equipment at the launch site. The team's GSE and launch pad performed exceptionally well at IREC in 2023, and a similar layout is intended for Launch Canada 2024. The GSE system consists broadly of the launch tower, the rocket fill disconnect arm, the electrical umbilical, the plumbing GSE panel, the Remote Launch Control System, the Data Acquisition System, Ground Side Power Distribution, the antenna towers, and the nitrous oxide tank inverters.

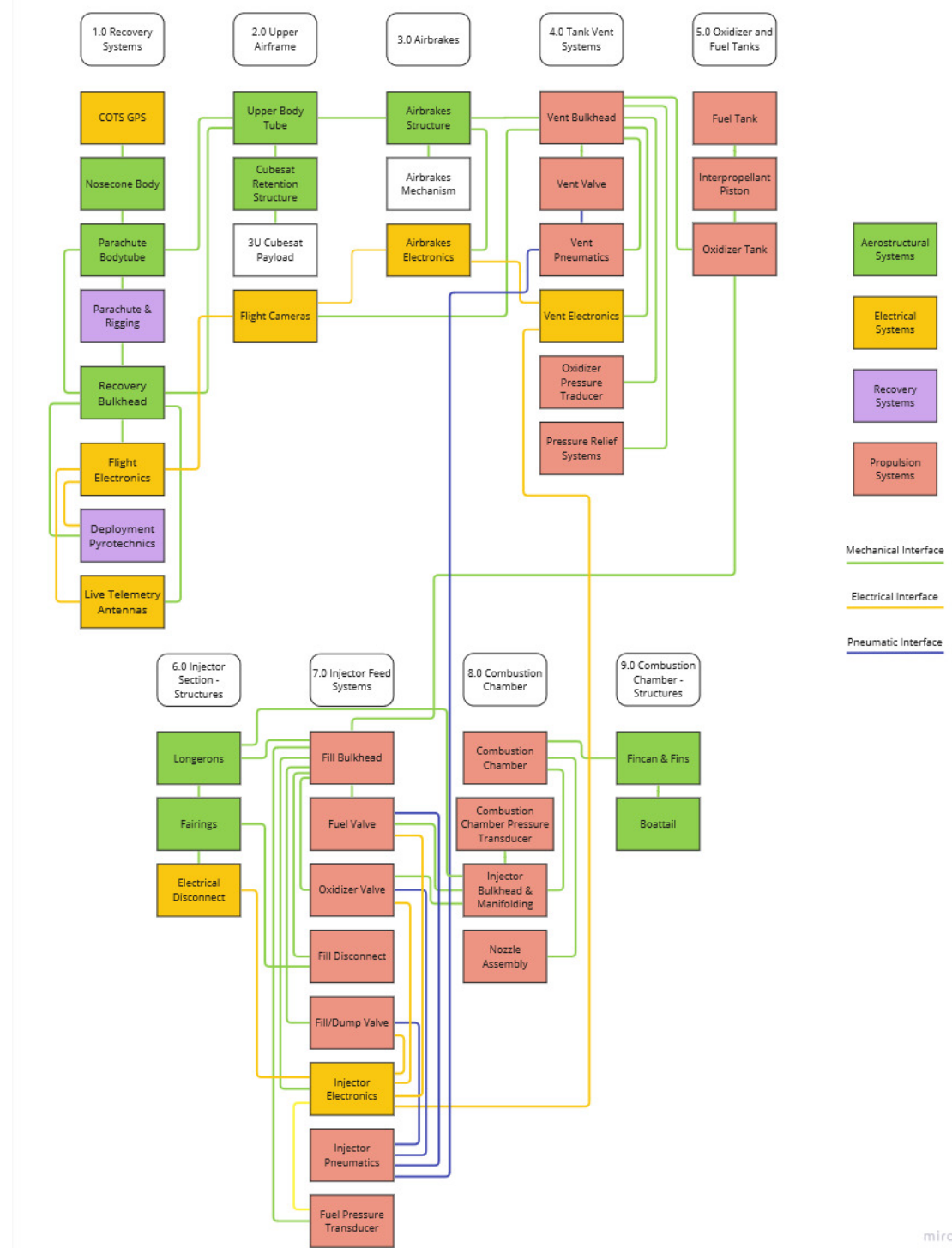


Figure 5: Functional Architecture Map

1. Nosecone
  - 1.1. Nosecone Bodytube
  - 1.2. Nosecone Tip
  - 1.3. Big Red Bee GPS
2. Recovery Section
  - 2.1. Recovery Bodytube
  - 2.2. Recovery Harness
  - 2.3. Recovery Rigging
  - 2.4. Recovery Bulkhead
  - 2.5. Recovery Electronics Sled
3. Payload Bay
  - 3.1. Upper Bodytube
  - 3.2. Payload
  - 3.3. Payload Bay Harness
4. Airbrakes
  - 4.1. Airbrakes Bodytube
  - 4.2. Airbrakes Harness
  - 4.3. Airbrake panels
    - 4.3.1. Mechanical Actuators
    - 4.3.2. Electronics
    - 4.3.3. Panels
5. Feedsystem
  - 5.1. Feedsystem Harness (Raceway)
  - 5.2. Vent Section
    - 5.2.1. Vent Bulkhead
    - 5.2.2. Vent Valve
    - 5.2.3. Vent section Pneumatics
    - 5.2.4. Vent section Electronics
    - 5.2.5. Pressure Relief Systems
    - 5.2.6. Flight Cameras
  - 5.3. Tanks
    - 5.3.1. Inner Tank
    - 5.3.2. Outer Tank
    - 5.3.3. Fuel Piston
  - 5.4. Injector Section (Engine components)
    - 5.4.1. Fill Bulkhead
    - 5.4.2. Fuel Valve
    - 5.4.3. Ox valve
    - 5.4.4. Fill/Dump Valve
    - 5.4.5. Injector Electronics
    - 5.4.6. Injector Pneumatics
    - 5.4.7. Injector Bulkhead
    - 5.4.8. Fill Disconnect
    - 5.4.9. Electrical Disconnect
    - 5.4.10. Longerons
    - 5.4.11. Fairings
6. Engine Bay
  - 6.1. Combustion Chamber
  - 6.2. Fincan & Fins
  - 6.3. Boattail

Figure 6: A breakdown of Assemblies and Subassemblies of the Physical Architecture

## 6 FLIGHT DYNAMICS

### 6.1 Flight Dynamics History

LOTS (the team's SAC rocket in 2023) was the first Waterloo Rocketry project where the flight dynamics of the vehicle were managed throughout the entire design and development process. A cycle-based system was implemented focusing on the continuous iteration of a few models. This approach enabled intentional tuning of every subsystem to achieve the established performance goals. Last year, the objective was to improve the apogee of an already existing hybrid rocket. This approach led to astounding results. The apogee of LOTS was improved by 23% over the design cycle by improving engine efficiency, system integration, dry mass, and much more [1]. This is clear looking at the predicted apogee throughout the overall design cycle as shown in Figure 7.

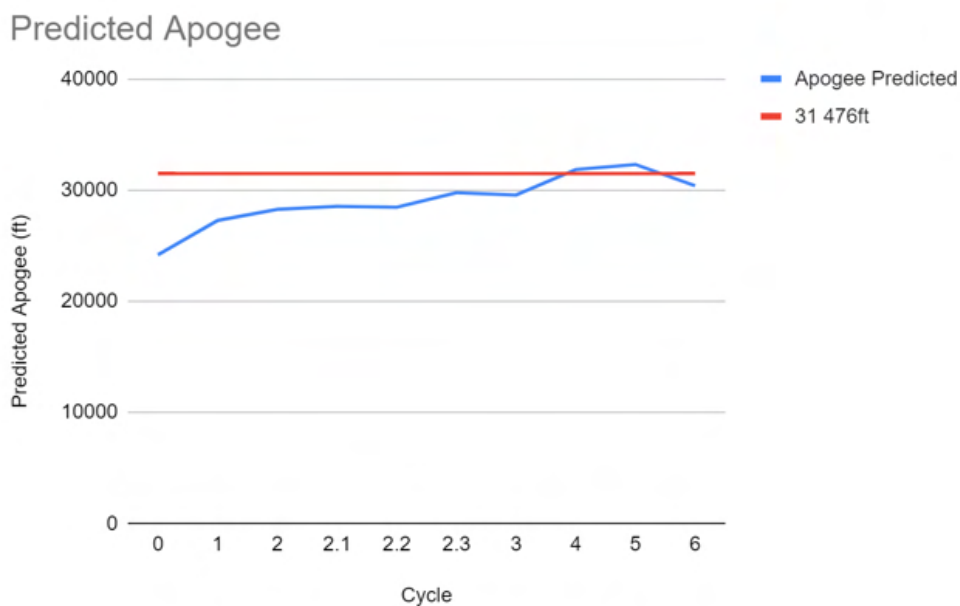


Figure 7: Predicted Apogee with Cycle for LOTS

In fact, the apogee increase was significantly more than 23%, but the amount of oxidizer loaded was reduced in order to target 30,000ft. This was also successful as evidenced by LOTS being the closest rocket to it's predicted apogee ever at Spaceport America Cup in the 30k ft Hybrid category (3.7% error).

### 6.2 LOTS Retrospective

After the team's success with LOTS, some time was spent documenting lessons learned and how they can be applied for future projects. The main relevant lessons learned were:

- Meticulous mass, length, and center of gravity tracking of all components throughout the design process allowed us to obtain accurate rocket simulations. This also enabled easier retrospective analysis.

- Conversely as the adage goes, "garbage in, garbage out". Simulations created using bogus data simply result in more bogus data.
- OpenRocket can be used to effectively simulate high powered rockets with SRAD engines if good engineering practices are followed.
- Early design input based on simulated data (not intuition) can be critical in creating an efficient architecture.
- Clear design goals are important to distinguish system requirements from "features" that may be interesting but would not contribute to the stated design goals.
- Surface finish is critical to increasing apogee and predicting it adequately.
- Most if not all student team rockets are not truly optimized for maximum apogee as this can be impossibly difficult and not in scope.
- When estimates are made with good engineering judgement, even early mass estimates can be surprisingly accurate at the vehicle level. The team found that both mass and center of gravity only decreased by 6% between the first design cycle and the last, as shown in Figures 8 and 9 below.

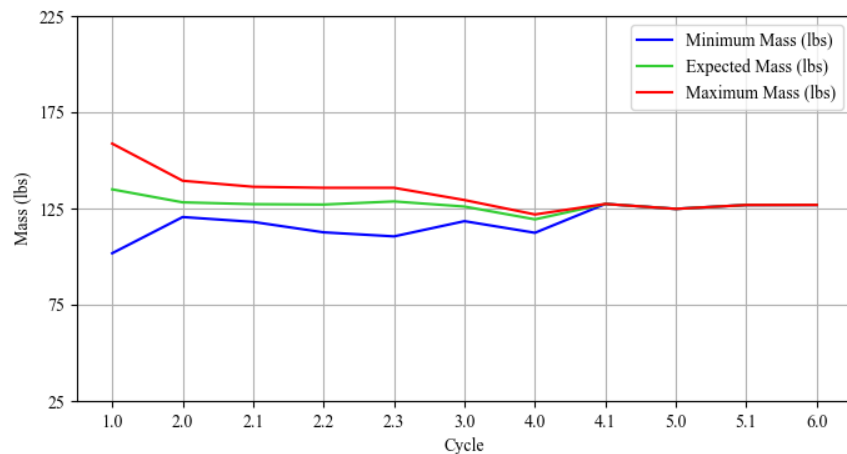


Figure 8: Total Mass Evolution During LOTS Design Cycle

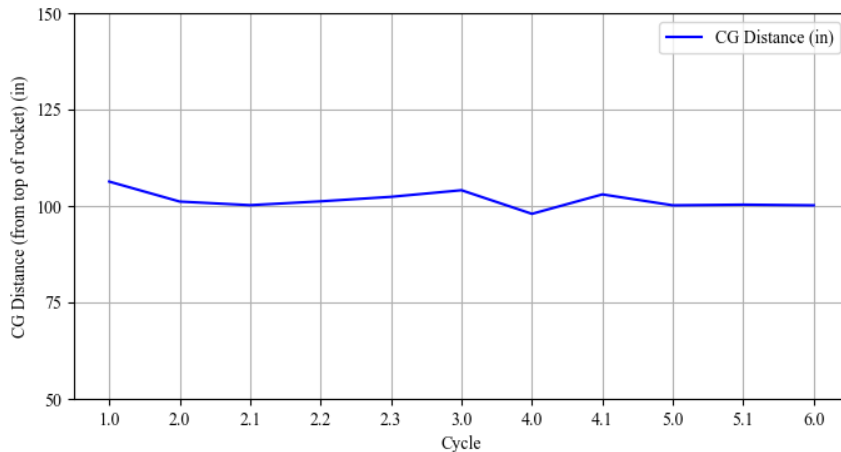


Figure 9: Dry Mass CG Evolution During LOTS Design Cycle

### 6.3 Borealis Design Goals

As mentioned, one of the major lessons learned from LOTS is that defining key project goals is critical to good system design. The architecture of Borealis is driven by the requirements and project goals as set out in Section 2, along with the team history discussed in Section 1.1 and 6.1. The primary flight goal is to fly a nominal ascent and recovery with a significant amount of new innovative design elements listed below:

- A completely new liquid engine as opposed to the previous hybrid engine.
- An airbrakes system designed to precisely control apogee.
- A novel reefing recovery system which has been greatly improved from previous attempts at similar systems.

This amount of unproven systems introduces technical and programmatic risks that are inherently different from last year's project. Since the focus was on iterating a previously flown architecture LOTS required an intense focus on apogee improvement and targeting a specific and fairly high apogee throughout the program. The team learned how much focus this requires and how difficult it can be. Instead of attempting to retain this intense focus on a target apogee while introducing new systems, the decision was made to prioritize chance of success for the new systems more than a high apogee. This means the rocket architecture is not optimized for apogee but is instead focused on validating the new designs integrated this year and increasing the likelihood of success. This is evident throughout Borealis' system design. A few examples are:

- Engine design parameters were determined based on practicality and demonstration of a successful liquid engine as discussed in section 6.4.
- General physical architecture for the sections of the rocket has remained the same as LOTS. Many decisions enabled this, a few examples are:

- Fins sized for high stability in high wind conditions which provides stability margin in some airbrake failure modes.
- Concentric tanks (piston based) which were chosen to reduce complexity in pressurization, routing of plumbing/electrical around a lower tank, and ease of physical integration.
- Airbrakes in the upper section to reduce physical integration challenges with the combustion chamber and injector sections. This is unconventional as the airbrakes are ahead of the center of gravity.
- Many reused/iterated design elements from LOTS (bulkheads, couplers, valves, nosecone, fin can, payload structure, boattail, main tank design, etc.) to increase design focus on new innovative elements.
- Very similar but slightly lower off rail velocity, length, and general flight characteristics to LOTS. This was chosen to create flight loads which are slightly lower than what LOTS faced to reduce risk of structural problems.
- Design for predictable apogee, not increased apogee. As mentioned before, the team decided to focus on achieving the apogee target accurately, while remaining indifferent to the specific value of the target itself. Some of the design choices relevant to this are:
  - Fin leading edge being rounded as opposed to an aerofoil shape which could improve efficiency but would be harder to model in OpenRocket and CFD.
  - Paint designed to mimic the surface finish of LOTS such that the measured surface roughness values and flight heritage can be used.
  - Precise and detailed mass tracking despite mass optimization not being a major goal.
  - Effort taken to reduce protrusions from the rocket surface such as bolt heads. These can be hard to properly model in CFD and OpenRocket.
  - Rocket propellant loading strategy designed to load a specific determinate amount of propellants.

## 6.4 Setting Eridium Engine Design Targets

Initial engine performance targets focused largely on the off-rail velocity of the rocket. A general guideline for minimum off-rail velocity is 100 ft/s and a 20% safety margin gives 120 ft/s as the chosen target for off-rail velocity. While it is possible to set engine performance targets related to stability and apogee, doing so during cycle 0 and 1 is difficult due to the variation in design possibilities. Therefore, these two parameters were used only for reference to ensure no extreme flight possibilities occur. Based on the 120 ft/s requirement, a minimum thrust to weight ratio of 15 was established. A tentative mass estimate for the rocket was compiled from 2023 mass data and was used to set an initial minimum engine thrust of 1500 lbf. To determine burn time, a few factors were considered. Firstly, the team did not want to fly incredibly high, both because of the challenging Timmins recovery environment and the scope of new changes being made throughout the rocket. Originally the target apogee was going to be 10 000 feet, however coupled with the minimum thrust, this gave an extremely short burn time. A requirement was thus established that

the engine burn for a minimum of 5 seconds. This was chosen so that there was ample burning time to get a good idea of engine transient behavior as the tank pressure drops, as well as enough thermal stress on the ablatives to evaluate their performance. Later in the design cycle these targets were adjusted to have a slightly higher target thrust. This was done to reflect mass increases in the rocket and also the allow the fins to remain small. The decision to use 3 fins was made early on. However, if became difficult to keep the rocket stable with only 3 fins without making them very large. At a higher off-rail velocity, the fins can remain small and preserve the required stability.

## 6.5 Fin Aerodynamic Design

Fin design must be preceded by creating a good model of the rocket in OpenRocket. Any major inaccuracies in the model may render any simulation results useless and lock the team into a poor design. Cycle based data collection ensures that key rocket information is kept up to date. Fin design was finalized in March 2024. The design was finalized around this time to enable long lead time, high risk, SRAD fin can manufacturing processes to start. This is quite early in the design process and highlights how knowing that early mass estimates are fairly representative of the final rocket is important. For those more inexperienced in fin design, it is important to understand the different variables involved and how they can affect the rocket's flight. Key fin parameters are shown in Figure 10.

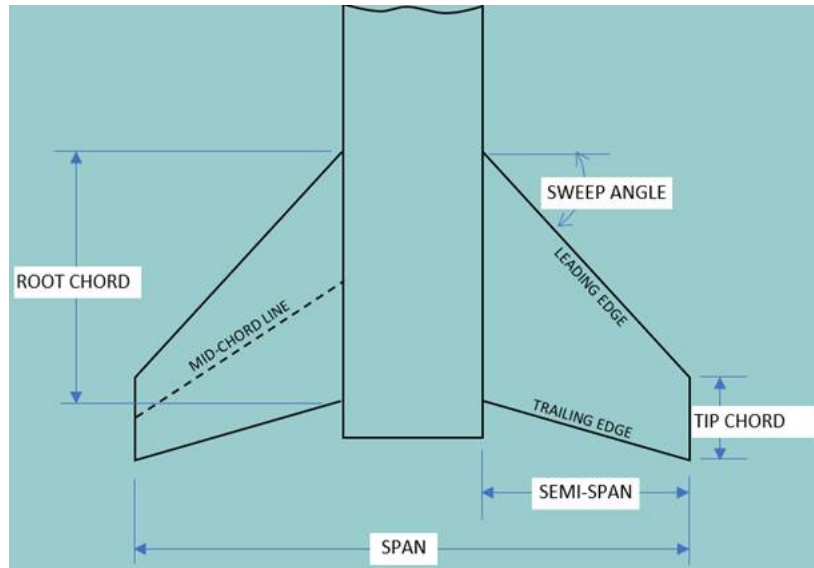


Figure 10: Fin Parameters

The fin parameters that were found to most affect flight results include the semi-span, sweep length, fin thickness, and fin positioning. Some common fin designs such as rectangular, clipped delta, swept, and trapezoidal are generally easier to manufacture and are often used as a starting point. However, knowledge of the specific shapes is not strictly required as experimenting with fin parameters during the fin design process tests many different shapes.

The team set two main criteria that the fins should ideally fulfill: maintain a minimum launch stability of 2 cal in 15 mile per hour winds and have a minimum fin flutter velocity FOS of 1.5. The first design choice was how many fins to have. Early simulations showed that four fins instead

of three would increase apogee (which for student teams is almost always the case). However, a three-fin design was chosen to minimize the risk of aerodynamic interference between the fins and the airbrakes system. To compensate for this, stability can be gained easily by increasing fin semi-span, but this inversely affects the fin flutter FOS. This can be offset by increasing the thickness of the fin, but fin thickness is restricted by how many layers of twill can be bonded and weight will necessarily increase. Therefore, it was important to determine early on the limits on the number of layers, and balance the fin semi-span and thickness. Smaller changes to the stability could be further obtained by shifting the CP forwards or backwards using the sweep angle, while keeping in mind that the aft end of the tip cord should not extrude past the boattail to avoid damage on landing. Weighing all of these effects, fin parameters are iterated many times (50+) in OpenRocket until an optimal fin shape is determined. The resulting values can be seen in Table 3.

Table 3: Final Fin Parameters

|                   |         |
|-------------------|---------|
| Number of fins    | 3       |
| Fin cant          | 0°      |
| Root chord        | 9"      |
| Height            | 7"      |
| Sweep length      | 4.5"    |
| Sweep angle       | 32.7°   |
| Thickness         | 0.235"  |
| Fin cross section | Rounded |

Fin positioning and boattail parameters must also be taken into account. The fins require a 0.5" clearance on both sides in the root chord direction for the composite manufacturing process. The total engine bay length not including the bulkhead flange is 14". Having a longer boattail and a more aggressive taper is beneficial for apogee due to a decrease in base drag. However, a significantly increased taper angle was found to decrease stability, and a longer boattail pushes the fins upwards, also hurting stability. When stability is decreased through these methods it forces the fins to be larger which results in lowering the apogee and decreasing the fin flutter FOS. Balancing the need for stability and reducing overall rocket drag and mass is a key consideration during the fin design process. This was achieved through iterating many designs with various section lengths and making intentional trade-offs. Ultimately the boattail length was set to 3.125" and the aft diameter was set to 5.5" with the fins positioned as far back as possible (0.5" from the start of the boattail). Note that not having a boattail and instead just extending the bodytube would decrease apogee by about 500 ft when comparing it to the 5.5" aft diameter boattail.

Fin cross section options include rounded, rectangular, and various airfoils. Rectangular cross sections have increased drag compared to other cross sections and airfoil cross sections are harder to manufacture due to complicated geometry. Rounded cross sections help with reducing drag and can be achieved by sanding down the edges. This also has the benefit of rounded edges being easy to model in both OpenRocket and CFD enabling them to be more directly compared against each other.

## 6.6 Nosecone Aerodynamic Design

In 2019 when the team first investigated SRAD composite components, a nosecone with a von Karman shape and 4:1 fineness ratio was chosen. This shape is optimized for the transonic and supersonic flight conditions that the team's rockets typically experience. This year, a very quick study was done to ensure that other nosecone shapes would not lead to a dramatic performance improvement. It was shown to still be a near-ideal shape. Therefore, to reduce the scope and risk for the airframe subsystem, the previous nosecone moulds were used as is, and the von Karman 4:1 was preserved.

## 6.7 Design Data Tracking and Mass Budgeting

Mass and CG of each part and length of each section are tracked throughout the design and development of the rocket in 6 distinct cycles as discussed in Section 4, each with their own separate spreadsheet. There are many advantages to this approach to mass tracking:

- Up-to-date and accurate mass and CG estimates allows for better simulation results, and increases the confidence in rocket design.
- Simple and easily accessible databases for all team members of both previous and current rockets.
- Enables cross-cycle tracking in order to catch any significant design changes that may affect overall mass and CG.
- Google Sheets functionality allows reverting to any previous version of the spreadsheet which can be used to control quality (especially in reviewing previous years data and building confidence it has not been changed)

The rocket is divided into distinct sections as shown in Figure 11. These sections are chosen typically at couplers or other locations that easily detach and can be individually transported. Each item on the BOM of the rocket is grouped by section and listed in order of axial position. For each component, team members are asked to record the following information:

- Minimum and maximum mass, primarily important in early design cycles where the design is not finalized
- Expected mass
- Expected CG location relative to the front of the section
- The initials of the team member who recorded the value, ensuring traceability
- The date the value was recorded
- The source of the value, whether it be an educated guess based on previous years, a CAD measurement, or a direct measurement

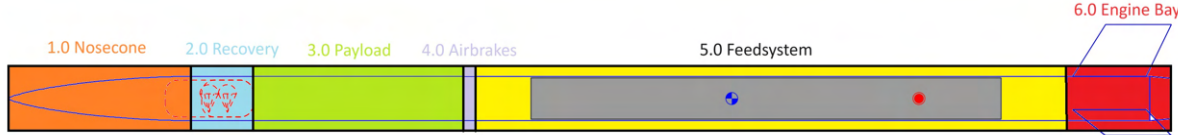


Figure 11: Rocket Sections

Figure 12 below shows part of the completed cycle 4.1 spreadsheet to show what the sheet looks like (lengths are tracked in another tab of the same spreadsheet).

| DO NOT EDIT THIS SHEET! IT IS NOW ARCHIVED AS OF 2024-10-07 AND SHOULD NOT BE CHANGED.<br>IF YOU THINK IT MUST BE CHANGED PLEASE REACH OUT TO JOEL BEFORE CHANGING. |  |             |              |            |  |                 |          |  |                 |        |  |                 |
|---|--|-------------|--------------|------------|--|-----------------|----------|--|-----------------|--------|--|-----------------|
|   |  |             |              |            |  |                 |          |  |                 |        |  |                 |
|   |  |             |              |            |  |                 |          |  |                 |        |  |                 |
|   |  |             |              |            |  |                 |          |  |                 |        |  |                 |
| Nose cone   | Second layer                             | Third layer | Fourth layer | Mass (lbs) | Source   | Initials & date | Expected | Source   | Initials & date | Max    | Source   | Initials & date |
| Nosecone Harness  |  |             |              | 0.01       | LOTS   | SA 2023-10-30   | 0.01     | Guess based on LOTS                                | JG 2023-07-10   | 0.02   | Guess  | SA 2023-10-31   |
| Nosecone Tip  | Tip + Tip Spacer                         |             |              | 0.23       | Measured for flight                                | KD 2024-06-25   | 0.232    | Measured for flight                                | KD 2024-06-25   | 0.232  | Measured for flight                                | KD 2024-06-25   |
| BigRedBe  | Tip Eyebolt                              |             |              | 0.166      | Measured for flight                                | KD 2024-06-25   | 0.166    | Measured for flight                                | KD 2024-06-25   | 0.166  | Measured for flight                                | KD 2024-06-25   |
| Nosecone Structure  | With mag switch + lipo                   |             |              | 0.29       | Measured <a href="https://wakil">https://wakil</a> | JG 2024-07-07   | 0.29     | Measured <a href="https://wakil">https://wakil</a> | JG 2024-07-07   | 0.29   | Measured <a href="https://wakil">https://wakil</a> | JG 2024-07-07   |
| Nosecone  |  |             |              | 1.374      | Measured   | TP 2023-07-06   | 1.374    | Measured   | TP 2024-07-06   | 1.374  | Measured   | TP 2023-07-06   |
|   | Shear Pin Coupler                        |             |              |            |  |                 |          |  |                 |        |  |                 |
| Overall:  |  |             |              | 2.07       |  |                 | 2.07     |  |                 | 2.08   |  | 12.71           |
| Recovery  | Recovery Rigging                         |             |              | 5.69       | Weighed by Stefan                                  | JG 2024-07-08   | 5.69     | Weighed by Stefan                                  | JG 2024-07-08   | 5.69   | Weighed by Stefan                                  | JG 2024-07-08   |
|   | Parachute and Rigging                    |             |              |            |  |                 |          |  |                 |        |  |                 |
|   | Pyrocutter assy                          |             |              |            |  |                 |          |  |                 |        |  |                 |
|   | Recovery Bulkhead                        |             |              |            |  |                 |          |  |                 |        |  |                 |
|   | Recovery Electrical Sled                 |             |              | 1.78354    | Estimated uncertainty                              | AL 2024-07-01   | 1.79897  | Measured   | AL 2024-07-01   | 1.8144 | Estimated uncertainty                              | AL 2024-07-01   |
|   | Bulkhead + eyebolt + slings              |             |              | 1.4        | Measured from last y                               | SA 2024-01-28   | 1.7      | SW + LOTS  | SA 2024-05-27   | 2      | Guess  | SA 2023-10-23   |
|   | Parachute Bay Body                       |             |              | 1.296      | Measured   | TP 2024-07-06   | 1.296    | Measured   | TP 2024-07-06   | 1.296  | Measured   | TP 2024-07-06   |
|   | Shear pin doubler                        |             |              |            |  |                 |          |  |                 |        |  |                 |
|   | Recovery coupler                         |             |              |            |  |                 |          |  |                 |        |  |                 |
|   | Bodytube                                 |             |              |            |  |                 |          |  |                 |        |  |                 |
| Overall:  |  |             |              | 10.17      |  |                 | 10.48    |  |                 | 10.80  |  | 4.91            |
| Payload Bay   | Payload Bay Harness                      |             |              |            |  |                 |          |  |                 |        |  |                 |
|   | Cubesat Payload                          |             |              |            |  |                 |          |  |                 |        |  |                 |
|   | Upper Bodytube                           |             |              |            |  |                 |          |  |                 |        |  |                 |
|   | Recovery Coupler                         |             |              |            |  |                 |          |  |                 |        |  |                 |
|   | Airbrakes forward doubler                |             |              |            |  |                 |          |  |                 |        |  |                 |
|   | Bodytube                                 |             |              |            |  |                 |          |  |                 |        |  |                 |
|   | Payload Plates (3 Combined)              |             |              |            |  |                 |          |  |                 |        |  |                 |
|   | Payload top ring                         |             |              |            |  |                 |          |  |                 |        |  |                 |
|   | Payload centering ring                   |             |              |            |  |                 |          |  |                 |        |  |                 |
| Overall:  |  |             |              | 13.73      |  |                 | 13.69    |  |                 | 13.73  |  | 19.73           |
| Airbrakes   | Entire system (includes 1 payload plate) |             |              |            |  |                 |          |  |                 |        |  |                 |
| Overall:  |  |             |              | 3.36       | Measured <a href="https://wakil">https://wakil</a> | JG 2024-07-07   | 3.36     | Measured <a href="https://wakil">https://wakil</a> | JG 2024-07-07   | 3.36   | Measured <a href="https://wakil">https://wakil</a> | JG 2024-07-07   |
| Feedsystem  | Feedsystem Harness                       |             |              |            |  |                 |          |  |                 |        |  |                 |
|   | Vent Bulkhead                            |             |              |            |  |                 |          |  |                 |        |  |                 |
|   | Dip Tube                                 |             |              |            |  |                 |          |  |                 |        |  |                 |
|   | Ox tank + Fuel Tank                      |             |              |            |  |                 |          |  |                 |        |  |                 |
|   | Tank heating                             |             |              |            |  |                 |          |  |                 |        |  |                 |

Figure 12: Cycle 4.1 Mass/CG Tracking Sheet

Additionally one of the team leads updates the length of each section according to the flight CAD or measured values for each cycle.

The first four design cycles are between one and two months each. The first week is spent collecting design data. The second week is spent ensuring the data collected is of adequate quality. This is done by every row in the spreadsheet being reviewed and signed off by both a team lead and the flight dynamics lead. They ensure that the source is the best possible current source, no parts are forgotten, and look for typos, excel formula errors, or other mistakes. At this point, the RSE file is also reviewed by the propulsion lead and the flight dynamics lead. This verification step is important as it is surprising how many errors are caught each time. To an external observer, this amount of reviewing may seem excessive but it is necessary to ensure accurate simulations and apogee estimates. As mentioned previously, "garbage in, garbage out". Any data which is not adequate is updated and signed off before continuing. The third week is typically spent in OpenRocket simulations and loads analysis. Lastly the fourth week is spent documenting everything that was

done and communicating the results to the wider team. Often the schedule overruns slightly due to difficulty in achieving the quality standards set by the team.

Cycle 0 was completed in July 2023 and focused on enabling early architecture decisions and setting project goals. Cycle 1 was completed in November 2023 and focused on integrating the conceptual designs from each subsystem and continued architectural decision making. Cycle 2 was completed in March 2024 and focused on enabling fin design. This requires a much higher level of confidence in the data and thus takes significantly longer than the other cycles. Cycle 3 was completed in May 2023 and focused on integration of detailed designs for each subsystem. Cycle 4 was completed in July and focuses on integrating as many "as-fabricated" components in time for this report. Cycle 5 is focused on ensuring that every part included is based on as-fabricated weighed values. Cycle 6 is used for the simulations that are completed at competition (masses are not collected here unless absolutely required).

When parts are weighed in order to ensure quality of data, team members are asked to take a picture of the scale showing what is being weighed and the value. This is also helpful in troubleshooting issues when they arise. These pictures are sent in slack and a link to the message is included in the spreadsheet for traceability when possible.

In later cycles, entire assemblies are weighed in order to ensure that the mass of small components (nuts, bolts, batteries, zip ties, etc.) that may have been missed when tracked individually are captured. This also ensures a more accurate CG can be captured.

Once all the required data has been collected, each section on the mass spreadsheet is modeled as a point mass with a length on OpenRocket. This substantially decreases the work required to enter data into OpenRocket and the potential for error. This eliminates the need to add numerous "mass components" to the rocket in the simulation to correctly model the rocket's weight. Instead, the entire section has its own total mass and CG, both of which are overridden in OpenRocket. Once all of the data is translated into OpenRocket, the total rocket mass and CG are verified to match between the spreadsheet and the OpenRocket file.

## 6.8 Choice of Simulation Software

The team has mainly used OpenRocket in the past and continued to do so this year. OpenRocket is extremely well documented, user friendly, and trustworthy. While other simulation software such as RASAero are sometimes touted as more accurate, this advantage is minimal in Borealis's flight speeds. Additionally, OpenRocket has been proven to work effectively for the team in previous projects and is much more accommodating of additional development work to simulate unusual design elements and unusual mass distributions. OpenRocket's advantages shine in the early project stage, where the rapid iteration of concepts can be quickly completed, as discussed in Section 6.10. This kind of analysis is much more difficult in all other simulation software the team has used. The standard version of OpenRocket will be used for the majority of tasks but the team has implemented a few changes for specific purposes. Monte Carlo functionality was added in previous years and is discussed in Section 6.13. Additionally, this year, functionality for airbrakes modeling using the team's CFD analysis was created, as discussed in Section 6.12.

## 6.9 RSE File Generation

Modelling the engine well is critical to be confident in the accuracy of our apogee. This increases the chances of the airbrakes system working well. It can also be challenging due to the complex fluids involved. Initial RSE files before static fire data was available were made using adjusted nitrous blowdown data from the 2023 hybrid static fires. Mass flowrate and thrust were predicted by coupling linearly scaled pressure-mass flow nitrous curves with single phase incompressible fuel flowrate modeling. This provided a good estimate of what kind of performance could be achieved. The curves were also double checked using data from other groups who had static fired similar styles of nitrous blowdown liquid engines.

While thrust and mass over time are measured data points during the flight qualification static fire, in order to accurately model the shift in the Cg of the propellant tanks, a time-step-based excel calculator was written. This calculator also serves as a prediction model that allows for the extension of the burn time of the engine. To accurately model the extended burn time, the mostly linear engine curve can simply be extended by a time corresponding to the increased fuel propellant mass. To model the Cg shift of the tanks over time, both the fuel, the oxidiser, and the propellant piston are modelled within the tanks. While the incompressible fuel and piston moving down a cylinder are relatively straightforward to model, the nitrous oxide presents a more complicated process.

Assuming thermodynamic equilibrium between the vapor and liquid, and using the current nitrous tank volume (which changes every timestep due to the fuel moving in the tank), the vapor fraction can be calculated from the tank pressure. Using this, the mass of liquid nitrous can be calculated and modeled as a hollow cylinder around the bottom of the fuel tank. The nitrous vapor is split into a few volumes, notably the hollow cylinder up to the top of the fuel tank, the volume above the fuel tank and the volume above the propellant piston. Individual centers of gravity are calculated for each discrete section, and a weighted average of the entire tank can be calculated using the masses of each volume. Interestingly, the initial and final center of gravity are almost identical. This makes sense because as the fuel runs out and the entire tank is full of vapor, it returns to a homogeneous density where the center of gravity will be very close to the middle of the tank. A graph of the Cg shift within the tank over time is shown in Figure 13. The combustion chamber is not included in the RSE file because the change in mass of the ablatives over the burn is negligible.

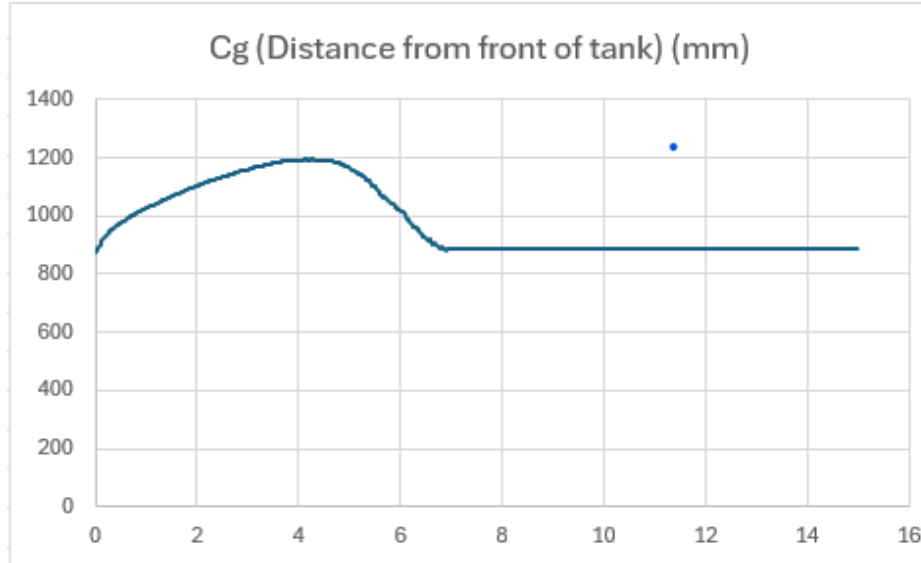


Figure 13: Engine Flight Configuration Center of Gravity vs Time

## 6.10 Airbrakes Location

From the beginning of the Borealis design process, a critical question was whether the airbrakes system needed to be nested into the engine. This was explored and ultimately found to be extremely difficult. This is fairly evident by looking at the injector section of Borealis. A potential solution to avoid this is to place the airbrakes assembly above the oxidizer tank, well above the CG of the rocket. At a glance, this seems risky due to potential interactions with the fins. More importantly, it variably reduces stability in a way that is hard to model without CFD when the airbrakes are deployed. A literature review was conducted of other student design teams but no other teams could be found with airbrakes ahead of the rocket CG. The majority also had the airbrakes behind the CP thus requiring almost no stability analysis.

To resolve this, in September 2023 (well before reliable rocket CFD was available) this possibility was explored using a simple OpenRocket model. Circular "bodytube pods" with no length were used to roughly approximate drag produced by a flat disk which was used to roughly set the size of the airbrakes for this study. After this nosecone pods at the same location were used to approximate the CP effect using published CFD results on flat plates at similar speed ranges to estimate where the CP should be. Note that OpenRocket does not allow changing the shape of the rocket shape mid-flight so airbrakes being "deployed" during engine burn had to be accounted for along with some other complications. Despite all of these simplifications, this approach showed that confidence in stability was still easy to achieve despite locating the airbrakes ahead of the vehicle CG. This was later validated by more detailed CFD simulations which agreed with the above approach by  $\pm 10\%$ .

It was also decided to have 3 fins and 3 airbrakes spaced as far apart as possible to minimize wake interactions between the fins and the airbrakes. This is because 3 fins is the least amount required to provide stability thus providing the greatest possible axial distance between fins and airbrakes with this approach. The disturbed flow from the airbrakes was shown to not impact the fins as shown in figure 14.

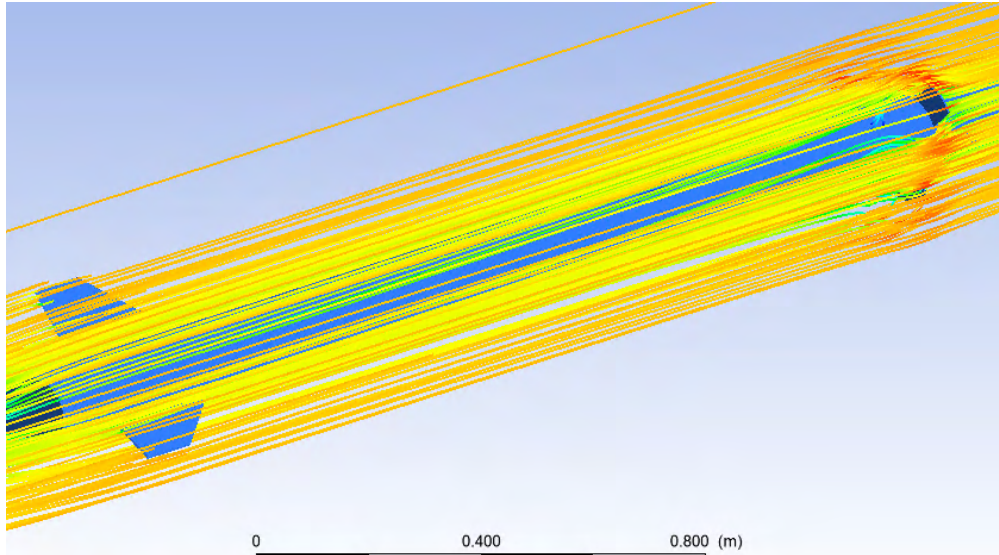


Figure 14: Airbrakes and Fin Flow Interference

A simple hand calculation was done to ensure that even with extremely high axial rotation at low vertical speeds, the flow will still not interfere with the fins.

### 6.11 Airbrakes Ansys Simulation

Since OpenRocket was incapable of computing an accurate center of pressure for calculating static stability margin, it was necessary to perform this calculation in Ansys instead for those cases where the airbrakes were extended. In order to verify the CoP results being provided by Ansys, it was decided to compare them against OpenRocket for the 0% extension case where they could be expected to agree. This process began with a comparison of LOTS Cycle 6 data versus the LOTS model in Ansys. The criteria for this test were:

- Drag force within 5% deviation from OpenRocket
- Centre of Pressure location within 2 inches of OpenRocket location, favouring a rearward positioning to account for base drag not considered in OpenRocket.

Upon this successful verification of the LOTS model, the focus shifted to developing a more intricate model that reflects the geometry of the 2024 liquid rocket before tabulating the drag of the rocket at various altitudes, velocities and airbrake extension rates.

### 6.12 Ansys and OpenRocket Integration

To determine airbrake sizing and validate controller software, a custom OpenRocket extension was designed to model the effect of airbrakes by overriding simulation drag force. The drag force is sourced from CFD data which relates dynamic pressure and airbrake extension to rocket drag force. This data is interpolated to provide values given any reasonable flight condition and airbrake extension. Then, the extension and other factors, such as the angle of attack, are considered

negligible. This approach combines the complex airbrakes CFD simulations with OpenRocket to provide reliable, applicable results for modelling the effect of airbrakes on flight.

### 6.13 Monte Carlo Simulations with OpenRocket

A custom extension of the OpenRocket simulation software runs thousands of flight simulations with randomized launch and flight conditions. This Monte Carlo technique provides calculations of both the average apogee and other flight statistics and isolated cases of potential instability. The flight conditions are randomized based on a normal distribution of historical weather conditions at the launch site. This is useful for development to catch edge cases and consider statistical likelihood. It was also shown to be an incredibly useful tool for launch operations last year at Spaceport America Cup where 99th percentile winds were observed. Monte Carlo simulation ability allows the team to quickly generate data driven launch commit criteria which was critical to launching LOTS last year.

### 6.14 Loads Analysis

The publicly available spreadsheet BENDIT7 was used to estimate bending, axial, and sheer moments experienced by the rocket at the maximum acceleration (takeoff) and at maximum dynamic pressure (max Q). Having an estimate of these moments is essential for designing an airframe and couplers that are strong enough to withstand the loads of launch. The flight condition inputs come from OpenRocket simulation data that use RSE files based on static fire data, as well as mass and length measurements taken of flight hardware. Thus, stress analysis of components on the rocket during the boost phase considers both bending and axial forces due to acceleration.

The fin profile on Borealis caused some difficulties with the loads analysis, as the fin shape was not valid in the supersonic Barrowman equations spreadsheet that the team has historically used for three BENDIT7 input values. This prompted a sensitivity study in order to determine the magnitude of difference depending on the fin configuration. Three different profiles were used in this study: 4 fins with the same shape as Leviathan of the Sky (LotS), 3 LotS fins, and 3 modified LotS fins using a shape similar to the Borealis fin shape. Analyzing the results, the 3 modified LotS fins profile had the largest bending moment at max Q with a body bending moment of 1414.77 lb-in, and the 4 LotS fins showed the least body bending moment of 1389.41 lb-in. Using these vastly different profiles and seeing a difference of at most 25 lb-in indicated that the fin profile seemed to be relatively unimportant for rocket loads and the large FOS used would negate the slightly increased loading.

Considering these results, the 4 LotS fins profile was used to guide design choices such as couplers and longerons. It is also worth noting that these loads are not used to size the fins and the only joint that was designed based solely on the bending loads has a FOS of 4. The plots shown in Table 4, Table 5, Figure 16, and Figure 17 show the results of the analysis, while Figure 15 shows the spreadsheet inputs.

|  | Loadcases   |         |             | Unit                |
|--|-------------|---------|-------------|---------------------|
| Bendit inputs, unformatted                                   | Takeoff     | Burnout | MaxQ        |                     |
| Altitude, ft AGL   | 0.083       |         | 4528.057    | ft                  |
| Launch Altitude, ft  | 968         |         | 968         | ft                  |
| Launcher Length, ft  | 326         |         | 326         | in                  |
| Mach Number  | 0.012       |         | 1.281       |                     |
| Flight Speed, fps  | 7.415       |         | 1409.766    | fps                 |
| q, Dynamic pressure, lb/ft <sup>2</sup>                      | 0.064744846 |         | 2,060.44    | lb/ft <sup>2</sup>  |
| Sref, Aerodynamic reference area,                            | 28.3        |         | 28.3        | in <sup>2</sup>     |
| Reference Length, Max Body Diameter, in                      | 6           |         | 6           | in                  |
| Pr (no failure)  | 0.99        |         | 0.99        |                     |
| Axial Acceleration, a, ft/sec <sup>2</sup>                   | 371.602     |         | 31.401      | ft/sec <sup>2</sup> |
| Thrust, lb   | 1577.641    |         | 437.44      | lb                  |
| 1σ C.G. Lateral Offset                                       | 0.1         |         | 0.1         | in                  |
| 1σ Thrust misalignment angle, rad.                           | 0.07        |         | 0.07        | deg                 |
| Body Station of Nozzle Throat, in                            | 145.37      |         | 145.37      | in                  |
| Element where the thrust is applied                          | 13          |         | 13          |                     |
| Analysis Condition Right after ignition?                     | TRUE        |         | FALSE       |                     |
| I <sub>xx</sub> , Roll Moment of Inertia, sl-ft <sup>2</sup> | 0.140800613 |         | 0.140800613 | sl ft <sup>2</sup>  |
| E, Nose Shell Modulus of Elasticity, psf                     | 250416356.5 |         | 250416356.5 |                     |
| Element to use as base for nose aeroelastic effect           | 2           |         | 2           |                     |
| Nose Static Aeroelastic Effect?                              | FALSE       |         | FALSE       |                     |
| N, number of fin panels                                      | 4           |         | 4           |                     |
| 1σ gust amplitude, fps                                       | 29.3334     |         | 45.56722076 |                     |
| Gust Longitudinal Autocorrelation Length, ft                 | 1000        |         | 1000        |                     |

Figure 15: BENDIT7 Inputs

Table 4: Cycle 4 Takeoff Loads

| Section        | Body Station (in) | Shear Force (lb) | Bending Moment (lb-in) | Axial Force (lb) |
|----------------|-------------------|------------------|------------------------|------------------|
| Nosecone       | 0.0               | 0.0              | 0.0                    | 0.0              |
| Recovery       | 25.1              | 0.1              | 1.4                    | -73.9            |
| Recelec        | 33.6              | 0.1              | 2.3                    | -372.3           |
| Payload Bay    | 42.8              | 0.1              | 3.3                    | -431.7           |
| Airbrakes      | 63.1              | 0.1              | 5.3                    | -862.4           |
| Top of Tank    | 72.1              | 0.1              | 6.1                    | -959.2           |
| Middle of Tank | 96.1              | 0                | 7.1                    | -1670.1          |
| Bottom of Tank | 120.1             | -0.1             | 6.0                    | -2110.7          |
| OTAS           | 136.4             | -0.2             | 3.3                    | -2382.4          |
| CC             | 145.4             | -0.2             | 1.2                    | -2390.1          |
| Boattail       | 156.5             | 0                | 0                      | 381.6            |

Table 5: Cycle 4 MaxQ Loads

| Section        | Body Station (in) | Shear Force (lb) | Bending Moment (lb-in) | Axial Force (lb) |
|----------------|-------------------|------------------|------------------------|------------------|
| Nosecone       | 0.0               | 0.0              | 0.0                    | 0.0              |
| Recovery       | 25.1              | 26.3             | 372.0                  | -9.7             |
| Recelec        | 33.6              | 25.1             | 590.1                  | -50.5            |
| Payload Bay    | 42.8              | 24.5             | 819.6                  | -59.0            |
| Airbrakes      | 63.1              | 17.0             | 1250.0                 | -124.2           |
| Top of Tank    | 72.1              | 10.2             | 1367.4                 | -164.4           |
| Middle of Tank | 96.1              | -0.8             | 1489.3                 | -212.4           |
| Bottom of Tank | 120.1             | -16.1            | 1294.7                 | -260.4           |
| OTAS           | 136.4             | -52.6            | 744.0                  | -353.2           |
| CC             | 145.4             | -54.4            | 262.5                  | -357.3           |
| Boattail       | 156.5             | 6.0              | -9.4                   | 80.2             |

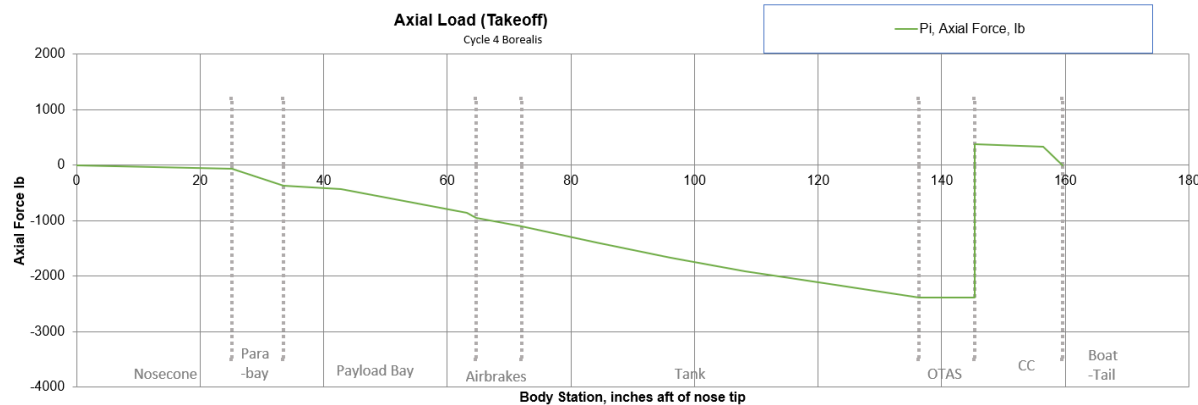


Figure 16: Takeoff Axial Loads Graphed

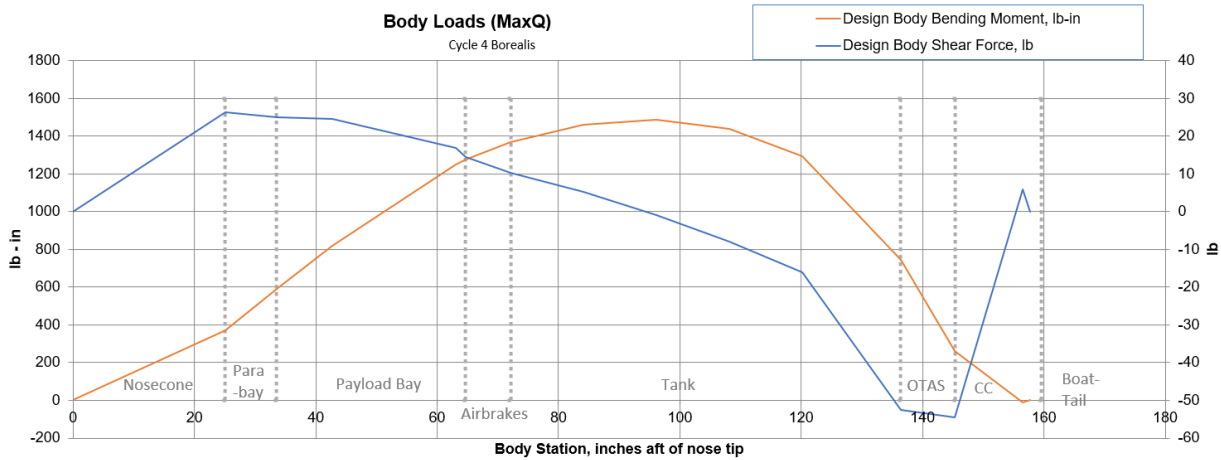


Figure 17: MaxQ Bending Loads Graphed

## 6.15 Painting

The effect of surface finish on the apogee of our rocket was first considered in 2023 when optimizing the rocket for a 30,000ft apogee was a primary requirement. At the time, going from a regular paint finish (0.787 mil) to a smooth paint finish (2.36 mil) could result in an apogee difference of 2,200 ft. While this is intuitive in retrospect, this is an astronomical difference. For comparison, a similar apogee increase would require a vehicle dry mass reduction of 13% (11lbs).

A significant amount of work to figure out what the most time-effective method to increase apogee was done during the LOTS project. The majority of this analysis still applies. While the team considered looking at developing great CFD models to enable things such as "delay[ing] the onset of turbulence in the airflow across the rocket, [...] the team does not have much experience with the computational fluid dynamics analysis required to predict it or its effects. [...] Therefore, it was decided that [this] would not be a feasible approach to reduce the skin friction drag"[\[3\]](#). It

was instead determined that the most straightforward way to increase apogee would be to "simply make the surface of the rocket as smooth as possible" [3].

When it came time to considering how to achieve this effect, a lot of testing was conducted on what would achieve the smoothest and most consistent surface finish. However, the team also considered the amount of effort and money that each method required. The report written on this topic[3] summarizes the result of these efforts:

The first option considered was to simply sand the exterior surfaces of the rocket to a very fine finish. All the large exterior surfaces of the rocket are either painted composite materials [...] suitable for fine sanding, making this a feasible option that could be accomplished without much cost or complexity. However, this option would be relatively labour-intensive due to the large amount of sanding expected to be required to achieve a sufficiently fine finish, so time would need to be set aside in the fabrication schedule in the rocket for this purpose.

The next option considered was the use of a commercial epoxy resin system to coat the exterior surfaces of the rocket. Several products specifically designed to produce smooth, durable coatings exist and are used by amateur rocketeers for this purpose. This approach might be a relatively low-effort way to produce a smooth surface, but [...] an epoxy coating would be more expensive than the exterior paint already used by the team. [...] If the team were to rely on a specialty coating, it could become challenging to source an alternative if the selected product became unavailable [...]. Additionally, it was expected that an epoxy coating would be thicker than an equivalent coating of paint, thus adding additional mass to the rocket when compared to the paint option.

The final option considered was the use of a vinyl wrap. This was expected to have a very smooth surface finish, and like the epoxy coating, would probably require less manual labour by team members to achieve a good result. [...] However, like the epoxy coating, it also represented a sourcing challenge to the team, in that it would be more expensive to implement than paint and could pose issues with availability and/or lead time. Furthermore, [...] there is no obvious method of repairing the vinyl wrap surface if it were to become damaged. [Finally], application onto surfaces that do not have regular curvature, such as the fins or nose cone, would be difficult or even completely unfeasible.

Due to the sourcing challenges presented by epoxy resin and vinyl wraps, as well as the flexibility of paint, it was decided that the team would simply paint and sand the rocket. However, the process that was decided upon turned out to be extremely labour intensive, which necessitated a new approach for Borealis. The previous procedure involved using diluted paint to paint one layer, then sanding it smooth with 800grit sand paper, and repeating that for anywhere from three to five coats per color. Due to the large surface area of the airframe, this was a very time consuming process. In total around a 150 working hours were spent on painting with a few team members solely dedicated to this for a few weeks. Sanding was by far the most time-consuming operation of this process. This is obviously not desirable.

With this in mind, the team focused on minimizing the amount of sanding involved in painting for the current rocket. For last years design cycle, to obtain surface roughness values, samples of paint on the body tubes were sent to the MSAM laboratory. Due to the tight timelines of this years design cycle, we were unable to obtain any concrete surface roughness values, but it was determined that so long as the paint was even and sanded to 2000 grit, the numbers acquired last year should be realistic for simulations. The finish achieved can also be visually compared with the paint from last year. After multiple rounds of testing methods, it was concluded that spray paint was an acceptable way to paint the rocket. With spray paint, each layer could be applied evenly and thick enough that there was no need to sand in between each layer, nor was there a need for more than 2 coats of each color. This significantly reduced the amount of drying time and halved the number of days it took to finish painting each part. With these results in mind, the painting team drew up a procedure for the entire process, detailed as follows:

1. Sand all the body tubes to 800 grit to ensure a smooth surface for paint application.
2. Apply a base coat of white paint of around 5 layers. Wait for 30 to 40 minutes between each layer of base coat.
3. Apply the first layer of base coat as a tack. No need to cover the entire surface of the body tube. Just enough so that the next layer has a surface to stick to.
4. Apply next 4 layers until a thick finish is achieved.
5. Wait 24 hours for the base coat to cure.
6. Sand last layer of base coat with increments from 800 grit to 2000 grit to obtain smooth base for further application of colour layers.
7. Apply colours coat and use stencils as per the paint scheme. Each colour should have 5 to 6 layers but if they seem inadequate and there is fear of sanding chipping away the paint to reveal base coat, then add 1 to 2 more layers as a precaution.
8. Wait for 24 hours for the colour coat to cure.
9. Remove any stencils. You should feel a subtle bump when you run your finger along the seam where the stencil was placed. This is expected.
10. Sand from 800 grit to 2000 grit to obtain a smooth and lustrous surface finish. Pay extra attention at the seams where the stencils were placed, intend to make them uniform.

This is expected to significantly reduce labour time on painting while achieving similar results. This is important to increase the confidence in the surface finish data being used in simulation. Similar to LOTS, in OpenRocket and CFD simulations, a slight knockdown factor is used to account for joint misalignment, protruding bolts (for OpenRocket) and other manufacturing defects which make the overall rocket surface finish not equivalent to the measured surface finish values. As LOTS was very close to it's target apogee, there is some confidence this approach will result in a reasonable simulation accuracy. Again this is important to ensure the airbrakes system has the highest chance of being properly demonstrated.

Table 6: Borealis Cycle 4 OpenRocket Simulations of Various Surface Finishes

| Surface Roughness ( $\mu\text{m}$ ) | Apogee (ft) |
|-------------------------------------|-------------|
| 150 (unfinished)                    | 19 475      |
| 60 (regular paint)                  | 20 485      |
| 20 (smooth paint)                   | 21 598      |
| 5 (optimum paint) Bay               | 22 441      |
| 2 (aircraft sheet-metal)            | 22 441      |

As a comparison tool, simulations were completed of Borealis with different surfaces finishes and the results are summarized below in Table 6.

Despite the high labour requirements it is surprising how achieving a good surface finish is one of the lowest energy to apogee increase activities that can be done.

## 6.16 Current Simulation Results

The total Borealis dry mass estimate from Cycle 1 to Cycle 4 has decreased by 10%. This is a much larger percent change than LOTS which is primarily due to the architecture change of introducing a new liquid engine and airbrakes. Introducing new innovative components increases the uncertainty of early estimates, especially compared to LOTS which had the advantage of being the 4th iteration of the team's hybrid engine. This error in early mass estimates validates the team's decision to not focus on apogee.

Current (cycle 4) expected mass, length, and CG of each section are included below in Table 7. A mass breakdown by subsystem can be seen in Figure 18 and a mass breakdown by section is also included in Figure 19.

Table 7: Cycle 4 Simulation Inputs

| Section               | Mass (lb)     | Length (in)   | CG (in from top of section)      |
|-----------------------|---------------|---------------|----------------------------------|
| Nosecone              | 2.07          | 25.1          | 12.71                            |
| Recovery              | 10.48         | 8.45          | 4.91                             |
| Payload Bay           | 13.89         | 29.56         | 19.73                            |
| Airbrakes             | 3.36          | 1.60          | 0.29                             |
| Feedsystem            | 39.68         | 80.66         | 42.56                            |
| Engine Bay            | 17.83         | 14.25         | 7.95                             |
| <b>Dry Mass Total</b> | <b>87.32</b>  | <b>159.62</b> | <b>94.87</b>                     |
| Oxidizer              | 28.66         |               | In RSE file                      |
| Fuel                  | 9.37          |               | In RSE File                      |
| <b>Wet Mass Total</b> | <b>125.35</b> | <b>159.62</b> | <b>98.48</b> (prior to ignition) |

Note that at the end of Cycle 4.1 data collection, there remains a  $\pm 0.8\text{lb}$  total uncertainty in the rocket dry mass. This is due to some items being fabricated in the late stage. There is also a few small items currently not being tracked such as paint or suspected of being missed (a few small screws are typically missed in Cycle 4). These additional items are expected to weigh around 0.1-1lbs. Higher accuracy will be achieved in Cycle 5 where each section will be weighed as an

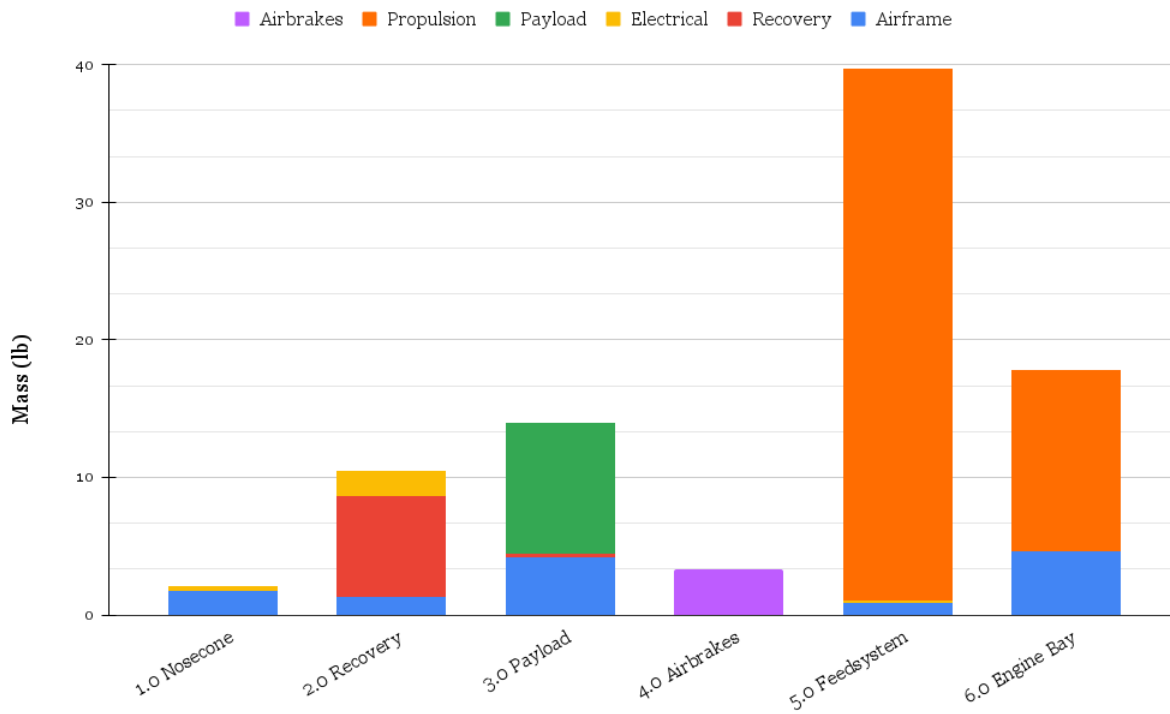


Figure 18: Borealis Dry Mass Breakdown by Section and Subsystem

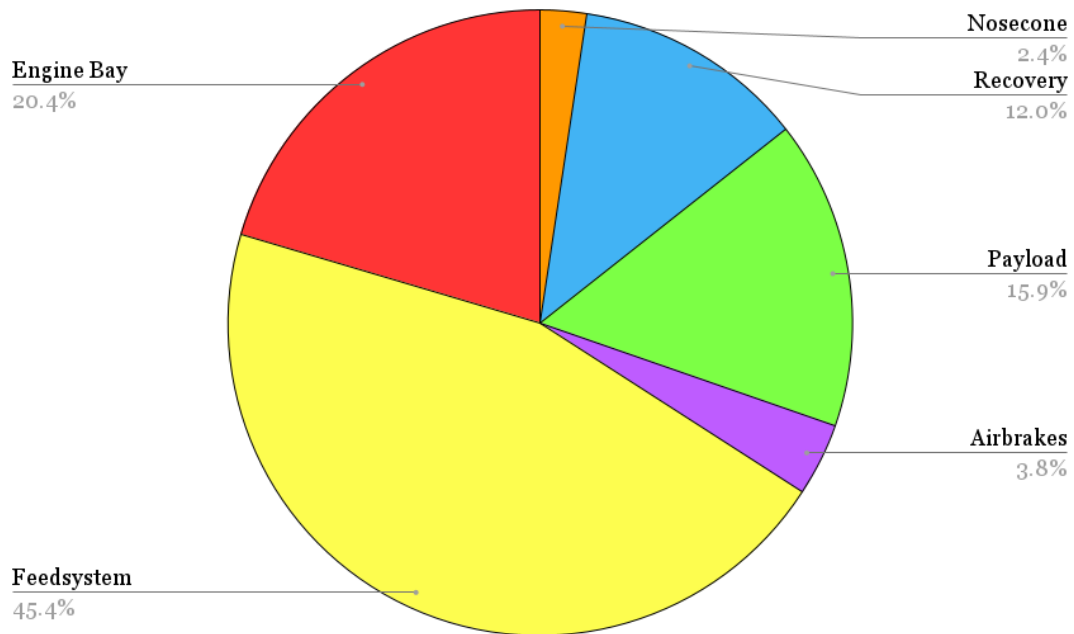


Figure 19: Borealis Dry Mass Breakdown by Section

assembly with all its components fabricated. It is expected that the rocket dry mass as launched will be around  $\pm 0.25\text{lbs}$  of the recorded mass simply due to remaining process uncertainty.

Initial OpenRocket simulations are done in each cycle without considering the airbrakes. This avoids the complexity of CFD and simultaneously allows us to compare the OpenRocket aerodynamic model with the team's own. Once this is done the CFD integrated with OpenRocket model is created and compared. The values are not expected to match exactly but be within a reasonable error. Since the airbrakes system affects the flight characteristics after engine burn out, the values for this flight segment are not expected to line up.

The initial key flight characteristics as simulated in cycle 4 without considering airbrakes are shown in Table 8. Off-rail stability and stability at apogee are both listed, as one of them is always the lowest stability in Borealis's flight (without airbrakes).

Table 8: Cycle 4 Expected Case Simulation Results OpenRocket Based

|                          |        |
|--------------------------|--------|
| Apogee (ft)              | 21,617 |
| Off-Rail Velocity (ft/s) | 142    |
| Maximum Velocity (ft/s)  | 1410   |
| Off-Rail Stability (cal) | 2.99   |
| Maximum Stability (cal)  | 5.62   |
| Apogee Stability (cal)   | 4.34   |

The same characteristics with the CFD integrated into OpenRocket model are shown below in Table 9

Table 9: Cycle 4 Expected Case Simulation Results CFD Based with 50% Airbrakes Control Authority

|                          |        |
|--------------------------|--------|
| Apogee (ft)              | 21,850 |
| Off-Rail Velocity (ft/s) | 142    |
| Maximum Velocity (ft/s)  | 1393.6 |

Note that the CFD based calculation without airbrakes gives around a 1 000ft higher apogee than the openrocket values. The team has decided to trust the CFD value as last year LOTS flew 3.7% higher than predicted and OpenRocket is known to under predict apogee for supersonic rockets. However, the apogee above is not 1 000ft greater than the OpenRocket value. This is because it is considering using 50% of the airbrakes control authority. This is the nominal or ideal case such that if the rocket under performs the airbrakes can retract more, and if the rocket over performs then the airbrakes can extend more.

It can also be noted that stability is missing from the CFD based results above. The final calculation for this was delayed to ensure that all possible inputs could be used. When these inputs were used and the simulation run, it resulted in a value much higher than expected (previously OpenRocket and the teams CFD were only 2in different in CP). It is believed that a simulation or data entry error was made and so this data is not included in this report. The team is confident this can be understood fully prior to launch and if the correct value is anywhere in the range of all values currently simulated this will not adversely affect the flight as the vehicle is already very stable due to late stage mass increases near the top of the rocket.

These OpenRocket results are calculated using a wind speed of 6.8 mph, ground level pressure of 1015 mbar and temperature of 62°F. These are based on launch site weather data during the launch window from the last 5 years. However, pressure and temperature were noted to have minimal effect.

## 6.17 Weather Launch Commit Criteria

The highest wind speed which the team can safely launch Borealis in is currently 21.5 mph. This is based on the Cycle 4.1 off-rail stability being greater than 1.5 cal calculated using OpenRocket. According to the analysis of previous weather data in Timmins, Ontario, this wind speed has never happened during the launch window in the last 5 years.

That being said, the team designed LOTS to be launch-capable in 95th percentile high winds, yet the recorded winds at the SAC competition were 99th percentile. Again, this year's main flight goal is to fly a nominal ascent and recovery with a significant amount of new innovative design elements. Due to this requirement, it is highly important to have as wide of a launch commit criteria as possible to increase the chance of launch regardless of launch day issues. Designing to this level of wind speed decreases the apogee achieved of the vehicle, but the gains in the likelihood of a successful launch far outweigh the losses in apogee.

## 7 AEROSTRUCTURE

### 7.1 Overview

Aerostructures on Borealis can be subdivided into composite components and metallic components. The former includes the majority of the outer airframe; details can be found in Table 10 and Table 11. The latter includes the oxidizer tank, couplers between bodytubes, and the longerons. The Borealis aerostructure breakdown can be found in Figure 20.

Table 10: Composite Components Overview

| Component                           | Stacking Sequence | Fabric Used  |
|-------------------------------------|-------------------|--|
| Nosecone                            | $[45]_4$          | Composites Canada Plain Weave Fibreglass   |
| Parachute Bay                       | N/A               | MadCow Rocketry COTS G12 Fibreglass  |
| Upper Bodytube                      | N/A               | MadCow Rocketry COTS G12 Fibreglass  |
| Vent Shroud                         | $[45]_2$          | A&P 6" OD Fibreglass Biaxial Sleeving  |
| Oxidizer Tank Aft Skirt Fairings    | $[45, 0, 45, 0]$  | 4HS Fibreglass Cloth, Textreme 80 Spread Tow Carbon Fibre, A&P 6" OD Braided Carbon Fibre Biaxial Sleeving                             |
| Fin Can/Combustion Chamber Bodytube | $[45_3, 0]$       | Composites Canada 4HS Fibreglass Cloth, A&P 6" OD Braided Carbon Fibre Biaxial Sleeving, Textreme 80 Spread Tow Carbon Fibre           |
| Fins                                | $[45_6, 0]$       | 2x2 Twill Double Bias A&P Carbon Fibre, Textreme 80 Spread Tow Carbon Fibre laid up on COTS 1/8" Thick [0,90] Carbon Fibre Plate Stock |

Table 11: Resin System and Method Used to Make Composite Parts

| Component                           | Epoxy System                                | Manufacturing Method             |
|-------------------------------------|---|----------------------------------|
| Nosecone                            | Aeropoxy PR 2032 resin and PH 3663 hardener | Vacuum Bag Hand Layup            |
| Parachute Bay                       | N/A   | COTS                             |
| Upper Bodytube                      | N/A   | COTS                             |
| Vent Shroud                         | Airstone 780E resin and 786H hardener       | Resin Infusion                   |
| Oxidizer Tank Aft Skirt Fairings    | Airstone 780E resin and 786H hardener       | Resin Infusion                   |
| Fin Can/Combustion Chamber Bodytube | Airstone 780E resin and 786H hardener       | Resin Infusion                   |
| Fins                                | Airstone 780E resin and 786H hardener       | Vacuum Assisted Tip-to-Tip Layup |

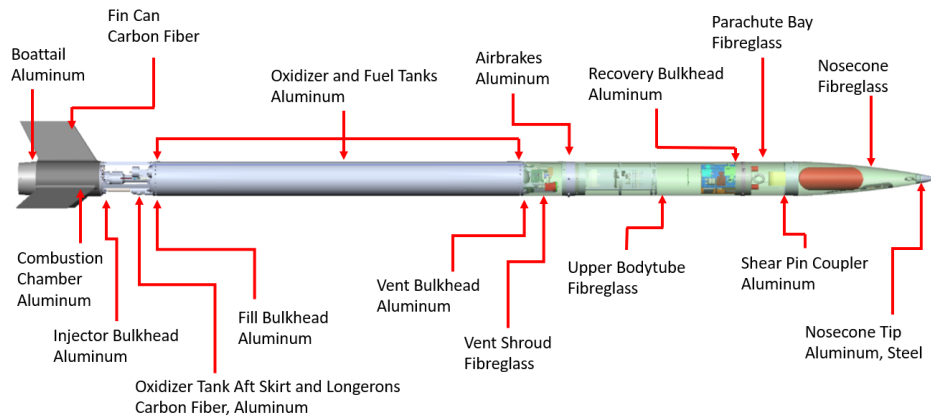


Figure 20: Aerostructures Layout

The oxidizer tank, boattail, couplers, and various internal structural components are machined out of aluminum. The entire structure is monocoque, with the oxidizer tank aft skirt supported by longerons meant to resist compression. The outer diameter of the airframe is 152.4 mm (6 inches).

## 7.2 Nosecone

The fibreglass nosecone is a Von Karman shape with a 4:1 fineness ratio as discussed in Section 6.6. It was manufactured in a vacuum bag layup process using a female mold as shown in Figure 21. Each of the 2 halves used 4 fibreglass plies arranged in a scarf joint, shown in Figure 22. The

entire mold was left in vacuum as shown in Figure 23 to evenly distribute the epoxy, remove excess epoxy, and help the nosecone maintain its shape while curing.

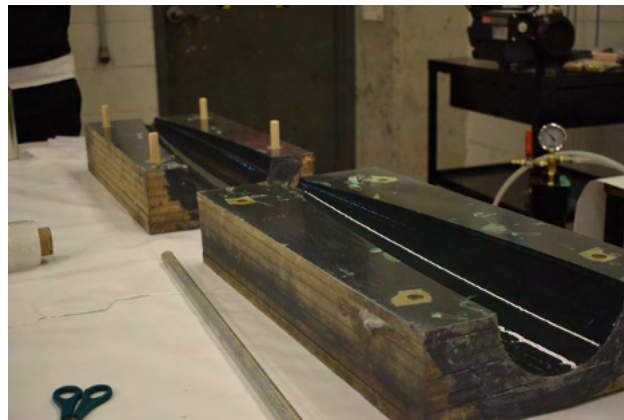


Figure 21: Nosecone Mould Halves

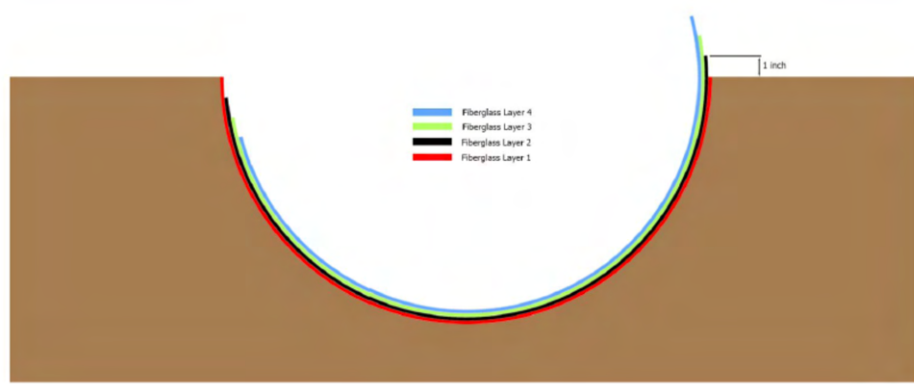


Figure 22: Scarf Joint



Figure 23: Nosecone Curing Under Vacuum

The shape of the nosecone remains unchanged since Shark of the Sky, the team's 2019 rocket, which had a successful launch at SAC. Shark of the Sky (2019), Kraken of the Sky (2020-2022), Leviathan of the Sky (2023) and this year's Borealis all fly in the transsonic and supersonic regimes, which allow for the continued use of the 4:1 fineness Von Karman nosecone shape. The nosecone tip will be machined stainless steel and aluminum bonded together with epoxy. The stainless steel provides wear resistance as well as thermal protection from aerodynamic heating, and the aluminum provides a more lightweight medium in which threads for an eyebolt can be tapped. A line from the parachute connects to this eyebolt which keeps the nosecone attached to the rocket after parachute deployment. The parachute itself is also partially located inside the nosecone along with a 3D printed BigRedBee GPS enclosure. A shear pin coupler is epoxied to the aft of the nosecone to allow it to come off during parachute deployment. The nosecone is made from plain weave fibreglass in a stacking sequence of  $[\pm 45]_4$ , which is the number of plies used to create the scarf joint as shown in Figure 22. Due to the 4 plies, the nosecone is thicker than the SRAD bodytubes. Some manufacturing flaws appeared in the nosecone after manufacturing, caused by excessive use of Super 77 during the layup (see Figure 24). This caused some concerns about the structural ability of the nosecone, and whether it was fit to fly. Compression testing was done by adding 50 lb plates on series to the top of the nosecone until 350 lb was reached as shown in Figure 24. No signs of cracking or buckling were present at this weight, which is greater than the loads the nosecone is expected to experience during flight (just under 300lb). This validates the nosecone's fitness for flight, as per DTEG R8.6.2.

Rounds of Bondo body filler followed by sanding will be used to create the final surface finish of the nosecone.



Figure 24: Nosecone Compression Testing

## 7.3 Composite Bodytubes

Borealis features a combination of COTS and SRAD composite bodytubes that make up the airframe. The SRAD composite bodytubes were designed to be superior to COTS bodytubes in a number of specific ways. First, the SRAD bodytubes can be made to variable length, increasing material uniformity and reducing manufacturing complications. As well, in-house bodytube fabrication removes the need to deal with external vendors who may have long or inconsistent lead times, which allowed for greater flexibility and better project planning. Next, the stacking sequence of the bodytubes can be tailored to the load case experienced by each specific tube, which creates around a 50% weight saving while still maintaining the required strength. Finally, it provides an opportunity for team members to get hands on experience at composites manufacturing, which further develops the team's composite knowledge and manufacturing capabilities. For these reasons, the goal was for the Borealis bodytubes to be SRAD. The vent shroud and fin can bodytube are SRAD. The upper bodytube and parachute bay are COTS due to various defects in the manufacturing process of the respective SRAD bodytubes which made the components unfit for flight. Due to timeline constraints, it was decided to use COTS bodytubes instead of attempting to manufacture another tube.

### 7.3.1 Layup Schedule Calculations

Calculations were performed to determine the required number of plies and type of fabric needed to create the bodytubes based on the predicted loads. It was known that the upper sections of the rocket needed to be made of fibreglass. This was due to a requirement for RF transparency in order to ensure proper function of the avionics components located in those sections, including both GPS modules and the Live Telemetry Transmitter. The lower sections of the rocket, including the oxidizer tank aft skirt fairings and the fin can, were made of carbon fibre due to it having a higher strength-to-weight ratio than fibreglass and having no requirement for RF transparency. The oxidizer tank aft skirt fairings in particular did not have a strength requirement, because load in the oxidizer tank aft skirt is entirely supported by the longerons. The SRAD bodytubes that did have a strength requirement were the vent shroud and fin can. The fin can has a minimum safety factor of 3.0, and the vent shroud has a minimum safety factor of 4.4. The calculations for these are detailed in Appendix A.1.

As of now, one fibreglass bodytube with ply orientations  $[\pm 45]_4$  has been compression tested and failed in buckling at 37kN of force. The stress-strain chart derived from that test can be found in Figure 25. The data was a conservative case since the buckling occurred near the top of the body tube, where there would normally be a metal coupler or bulkhead. In the absence of a larger data set, high FOS and non-destructive testing have also been employed to ensure all components are unlikely to undergo structural failure. The 37kN was used as a contingency to calculate safety factors.

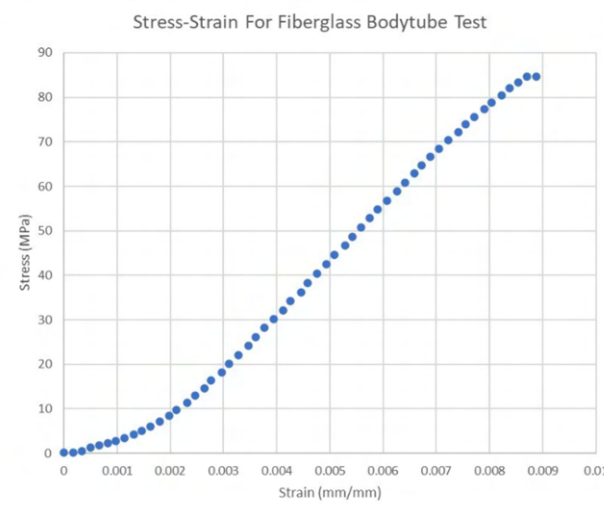


Figure 25: Stress-Strain Curve For Bodytube Test

The safety factor was dependent on the thickness of the bodytube, which itself was dependent on the specific fibre and number of plies used. Using the thickness of the composite at 50% fibre volume given by the manufacturer, the layup schedule was iteratively refined by adding/removing material until the desired safety factor was reached. The upper bodytube and parachute bay were intended to be SRAD bodytubes, however as mentioned earlier, the part had defects when it was manufactured and therefore was deemed not fit for flight. Due to time constraints, COTS G12 fibreglass tubes shall be flown instead.

### 7.3.2 Manufacturing Process

The composite bodytubes were manufactured using a Vacuum Assisted Resin Transfer Molding (VARTM) process, also known as resin infusion. First, a surface preparation process was done through cleaning, waxing, and applying Polyvinyl Alcohol (PVA) to ensure that no contaminants were cured onto the part, and that the bodytubes were released from the mold without damage. Next, plies of fibreglass and/or carbon fibre were laid out in a female mold using Super 77 spray adhesive. Then, the part was placed under vacuum through poly-tubing attached on one end, with resin allowed to enter from the other via vinyl-tubing. As a result, the resin was pulled through the fibreglass by the vacuum, which ensures an optimal surface finish and low void content. The infusion setup is displayed in Figure 26, along with an image of the combustion chamber-fin can bodytube manufactured using the VARTM process displayed in Figure 27.



Figure 26: Infusion Setup



Figure 27: Fin Can and Combustion Chamber Bodytube Demoulding

All composite components including bodytubes were post-cured in the team's SRAD PID controlled curing oven to raise the components' glass transition temperatures above the maximum temperatures they are expected to see before or during flight.

#### 7.4 Upper Bodytube and Parachute Bay

An infusion was completed to create the upper bodytube and the parachute bay. However, due to some manufacturing defects, it was deemed not suitable for flight. Instead, a COTS upper bodytube was purchased, cut, sanded, and squared to the desired length for both tubes. The COTS bodytubes are much heavier and thicker than the SRAD bodytubes, which affected the results of

previous simulations. This change also affected some parts which are to be bonded into the upper bodytube and parachute, changing their outer diameters or fit constraints.

### 7.4.1 Payload bay

The purpose of the payload bay is to prevent the unwanted movement of the payload during flight. As shown in Figure 28, the payload bay consists of two centering plates, one top clamping plate, and one payload base plate. The centering plates prevent rotation of the payload. They are each made from 1/4" thick aluminum 6061 and are permanently bonded in place using West Systems 105/206 epoxy resin. The clamping plate prevents movement of the payload throughout flight, and is fastened to the bodytube via 4x #6-32 screws and Loctite Threadlocker Blue 242. The design is similar to the 2023 version, with the centering plates epoxied to the body tube, and with a removable top clamping plate to allow for the payload to be removed or installed as needed during the competition.

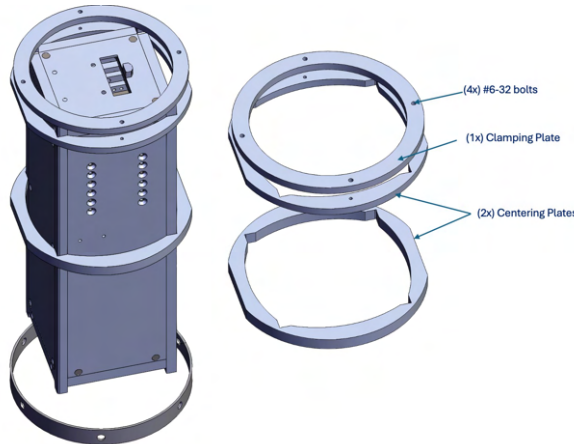


Figure 28: Payload Bay Assembly (baseplate not shown)

The payload base plate was designed with two primary considerations. The first was to support the load from the payload. The second was to serve as the top plate that the airbrakes mechanism could clamp on to for support. Secondary considerations were given to mass optimization. The final design resulted in a surrounding ring with three structural supports across the center. It is made of 1/8" Aluminum 5052 sheet and was validated to support the weight of the payload and the pre-load of the clamping bolts using Solidworks FEA. It is shown in Figure 29

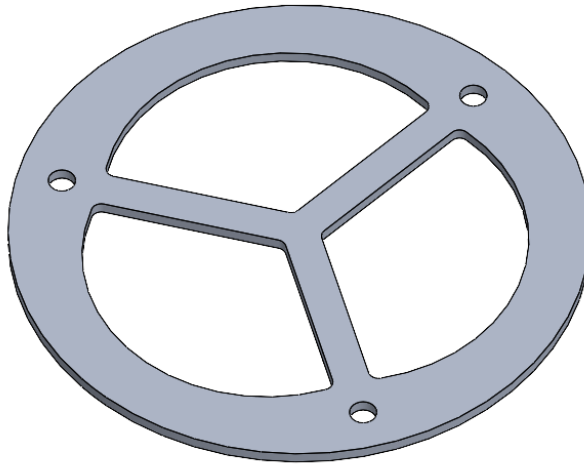


Figure 29: Payload Base Plate

To verify the safety of the design, safety factors were calculated for the top clamping plate and bolts. FEA and hand calculations were performed with a 1000N load acting on the bottom of the clamping plate based on the mass of the payload (4 kg) and acceleration during descent (25g's) based on load analysis. Table 12 summarizes the safety factors calculated for the bolt failure, internal thread shear, and bolt tear out (see Appendix A.3 for detailed calculations).

| Components     | Safety Factor |
|----------------|---------------|
| Clamping Plate | 40            |
| Bolt           | 6.6           |

Table 12: Payload Bay Safety Factor Calculations

#### 7.4.2 Payload Bay Manufacturing

Aluminum plate stock was used to manufacture the clamping and both centering plates using a waterjet cutter. The #6-32 holes in the top centering plate were then tapped. Afterwards, the centering plates were bonded to the body tube. The bonding surfaces were prepared by sanding the surfaces with a file and washing the surfaces with Simple Green Household Degreaser, water, and acetone. Next, West Systems 105 Epoxy Resin and 206 Hardener were mixed. The mixture was split into two portions: one mixed with cabosil for thickening, and the other without thickener. The unthickened mixture was first used to wet out the bonding surfaces. The thickened epoxy was then used on the bonding surfaces; the centering plates were then inserted into the body tube to cure for 24 hours.

Significant difficulties were experienced bonding the plates into the composite body tubes. On the first attempt, the centering ring bond failed, requiring another attempt. On the second attempt, both bonds failed when inserting the payload afterwards. This is likely due to poor surface

preparation. Both plates were successfully bonded on the third attempt, and have been load tested to confirm their suitability for flight.

## 7.5 Oxidiser Tank Aft Skirt

The oxidizer tank aft skirt uses 3 structural aluminum longerons to transmit thrust loads from the combustion chamber during takeoff and boost, and tensile loads at deployment. The longerons also allow for the pneumatics, fill plumbing, and injector valve in the oxidizer tank aft skirt to be accessible for maintenance while the rocket is on the launch tower. The entire section is covered by three SRAD carbon fibre fairings, which each cover a third of the section and serve no structural purpose. They are easy to remove and provide the outer aerodynamic surface of the section.

In the fairings, there are fluid connections for propellant loading, as well as an electrical umbilical used to charge batteries on the rocket while the rocket is on the pad. This umbilical is attached to the rocket using magnets and disconnects passively as the rocket ascends.

### 7.5.1 Longerons

The longerons are composed of 8.125" long 6061-T6 aluminum columns and are designed to transfer the loads from the engine to the rest of the rocket, shown in Figure 30. Attached to the aluminum columns are 0.1875" thick 6061-T6 curved tabs as displayed in Figure 31 that allow the columns to be easily bolted into the fill and injector bulkheads, respectively. The final parts of the longeron assembly are the 11-gauge aluminum sheet metal brackets in Figure 32 used to mount the fairings in Figure 33, which are thirds of a thin-walled carbon fibre body tube.



Figure 30: Front Profile of Longeron



Figure 31: Side Profile of Longeron



Figure 32: Curved Tab



Figure 33: Metal Bracket

Longerons and fairings are used in place of a traditional body tube as they provide better access to the inside of the rocket, improving section ease of assembly. The longeron columns were designed following a similar methodology to 2023 and 2022 design cycles (LotS and KotS).

Firstly, a set of possible solutions were conceptualized, each with a unique cross-sectional shape but with equal properties such as cross-sectional area. The set of solutions were then compared using a list of predetermined constraints and criteria like mass budget, FoS considerations, space optimization, manufacturing constraints, and analysis constraints, which allowed for the selection of an optimal cross-sectional shape. From this comparison, it was found that C cross-sections and I cross-sections were optimal, with C cross-sections being slightly better for buckling

resistance but also weighing more. In the 2023 design cycle (LotS), the I cross-section was selected over the C cross-section for its ease of assembly, even though it had less resistance to buckling. This year, the C cross-section column was chosen as it results in a smaller footprint altogether, which greatly improves the injector section.

Once an optimal cross-section shape had been selected for the current design cycle, iterative changes were made to the cross-sectional geometry to obtain a minimum FoS of 2.0 on buckling. Buckling was determined to be the limiting failure mode through extensive hand calculations (see Appendix A.2), also accounting for potential eccentricities due to out-of-spec machining and unexpected load cases. Finally, thorough linear and non-linear buckling simulations were conducted on the finalized longeron geometry using Ansys Mechanical to validate the hand calculations as shown in Figure 34. The mounting of the columns to the bulkhead and the mounting of the fairings to the longerons is nearly identical to previous implementations (2022 and 2023). However, due to the significant decrease in footprint, the screw layout for mounting the curved tabs to the columns had to be changed, and the screw size also had to be decreased, given in Figure 35. In the 2022 and 2023 design cycles, #10-32 screws were used side by side to fasten the columns to the curved tabs. This year, #4-40 screws aligned vertically as the columns are deeper than they are wide.

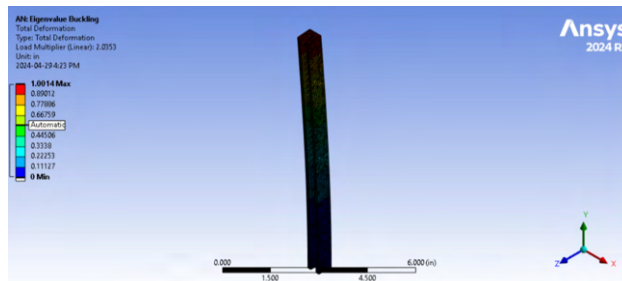


Figure 34: Buckling Simulation on a Longeron



Figure 35: Screw Layout of Curved Tabs - 2024 (Bottom) and 2023 (Top)

## 7.5.2 Fairings

The fairings are designed to make the injector section easy to access. Each panel can be removed by unscrewing 4x #6-32 bolts, which hold each one in place. They are manufactured using the same resin infusion process used to manufacture the rocket's structural bodytubes. After being trimmed and sanded to size, they provide smooth and flush transitions from the oxidizer tank above to the injector bulkhead and combustion chamber bodytube below. The fairings are also the mounting position for the fill disconnect hatch and electrical disconnect systems. These are bonded into the fairings using West Systems 105 epoxy resin and 206 hardener, securing them in place.

## 7.5.3 Fill Disconnect Hatch

The fill disconnect hatch provides an opening in the body tube covering the fill section for the pneumatic and oxidizer fill system to interface with the rocket. The hatch is mounted to a cutout in the body tube, must accommodate the fill disconnect mechanism, and must automatically close under its own means when the fill system is disconnected from the rocket following filling. The hatch consists of a 3D printed PETG frame and hatch with torsion spring sprung pins and magnets for a secure closure.

The design architecture was selected to ensure closure of the hatch by aerodynamic loading in case the hatch bounces open during flight or fails to close under its own means. The hatch is set to be flush with the body tube to minimize parasitic drag. The size of the hatch was determined based on the profile of the fill disconnect system. Small torsion springs were chosen for compactness, with the understanding that they would be relied upon for keeping the hatch shut during flight alongside the magnets.

Two 180 degree bent torsion springs were implemented to ensure hatch closure after the fill disconnect mechanism is removed. Neodymium magnets were attached to the inside face of the hatch and the frame for secure latching. This was desired and necessary due to the low torque of the small torsion springs, and high expected acceleration of the rocket. The magnets were attached with adhesive, and the frame is attached to the inside surface of the body tube with epoxy. The CAD for this assembly is shown in Figure 36. This design was flown and tested in 2023 and performed as expected.

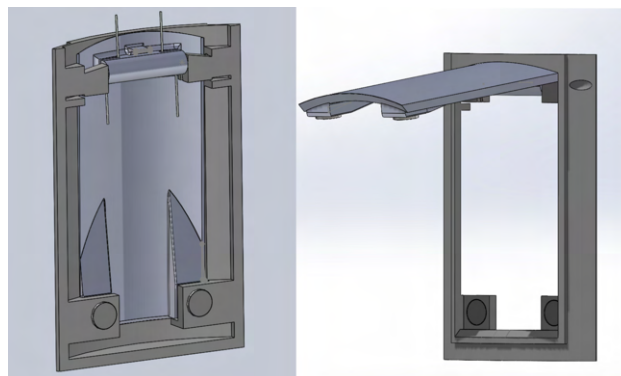


Figure 36: Rear view of fill disconnect hatch assembly including springs, magnets, hatch door and frame (left) and front view of open hatch (right).

## 7.6 Fin Can

The fin can is the bodytube that surrounds the combustion chamber and holds the fins. The bodytube is an SRAD carbon fibre tube made using two layers of 194gsm 2x2 carbon fibre twill, one layer of 4HS fibreglass and 1 layer of Textreme 80gsm as discussed in subsection 7.3.

The fins were cut using both a CNC router and a waterjet (Figure 37). The plate stock was then bonded using Aeropoxy ES6228 to the fin can. A two part laser cut jig was used to ensure alignment, which was properly positioned and fixed using spacers. The bonding setup can be seen below (Figure 38). All three fins were bonded at once and left to cure for two days.

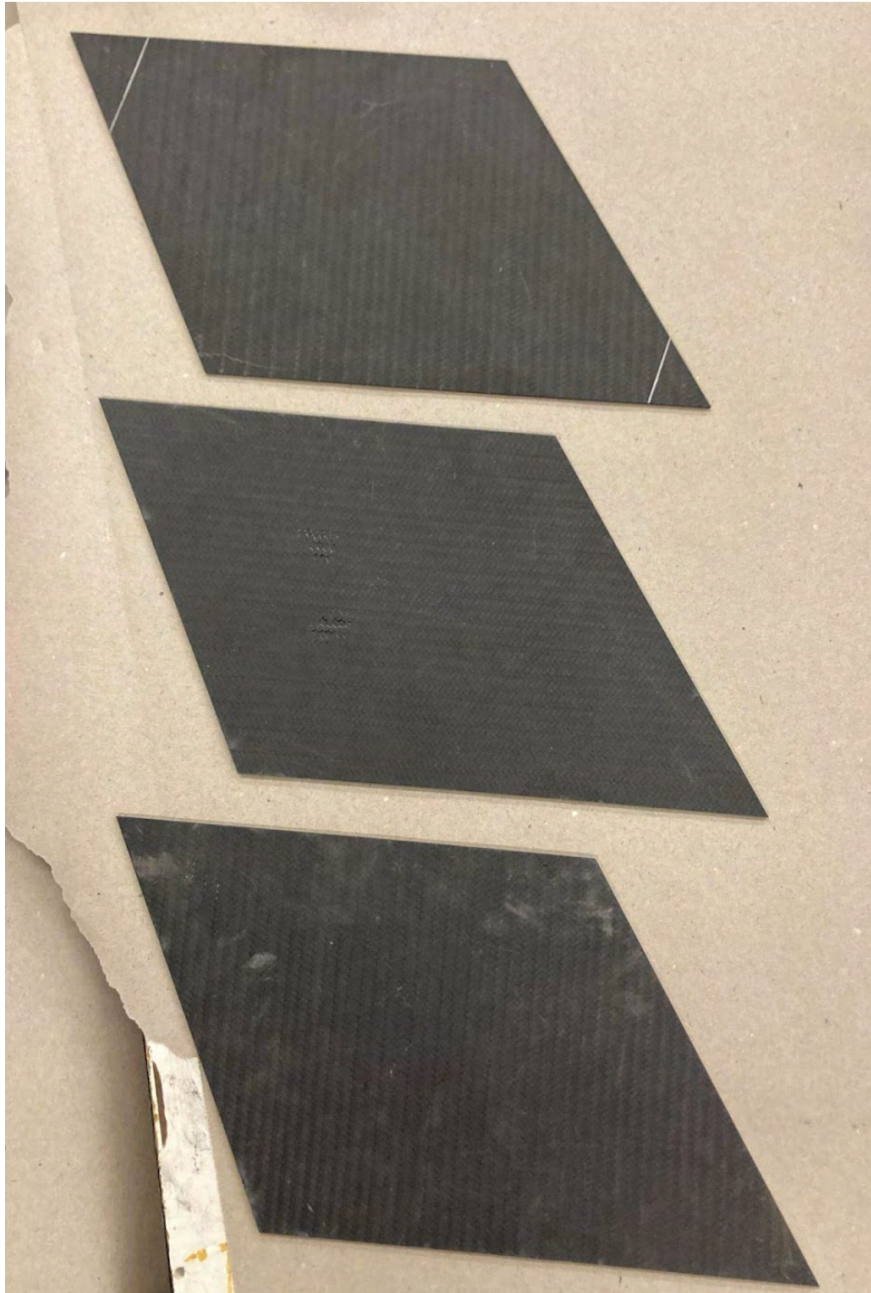


Figure 37: Carbon Fibre Fins

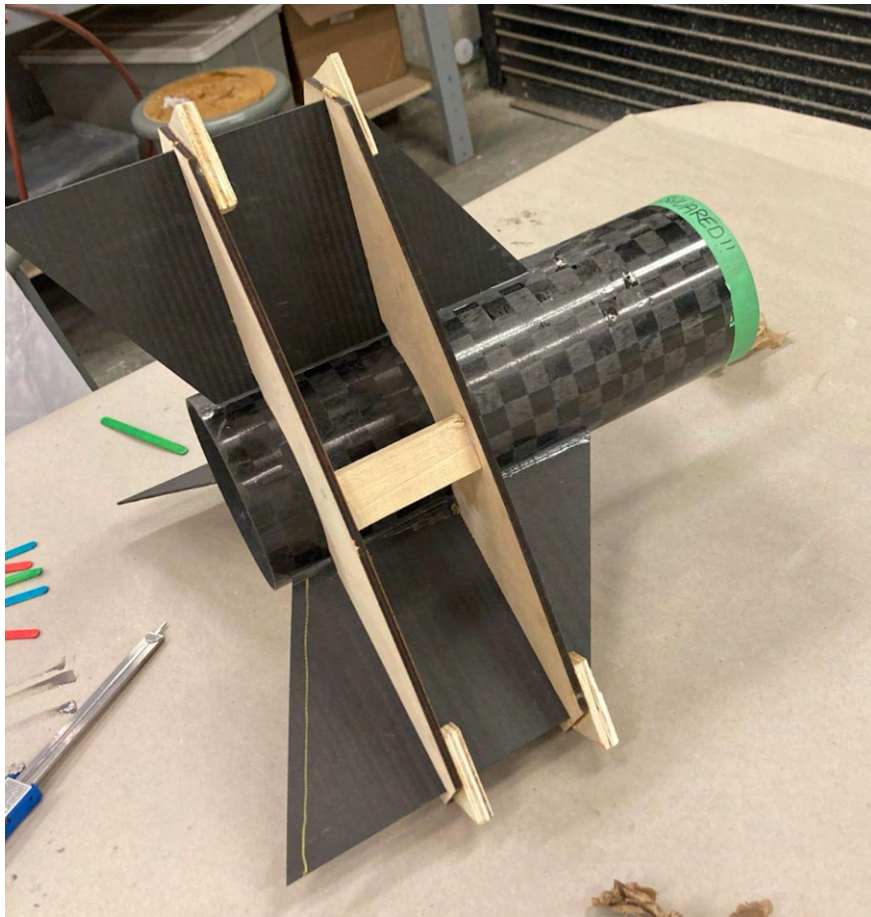


Figure 38: Bonding Jigs Fixed on Fin Can

Fillets were then formed using Aeropoxy PR2032 and PH3663 at each fin root to create a smoother transition between the fins and the tube (Figure 39). A 1" wooden dowel was used to create a constant cross section. The fillets were sanded by hand and using the same wooden dowel to form the final shape (Figure 40).



Figure 39: Fillet Being Formed Using Popsicle Stick



Figure 40: Sanded Fillets

The tip to tip layup is the largest manufacturing step of the fin can, which involves placing layers of fabric from the edge of one fin, across the tube, and to the edge of the next. To achieve the desired fin thickness (0.235"), the layup consisted of seven layers of 194gsm 2x2 twill and one layer of Textreme 80gsm. The number of layers in the tip to tip is typically only 2-3 as the inner plate is stiffer than those added in the layup. However, fin thickness had not yet been determined at the time of plate manufacturing, which is why more layers had to be added to make up the difference from a thinner plate. The twill forms the structure of the layup and the textreme creates a smoother surface finish. Each layer of fabric was wet out between plastic sheeting and placed onto the fin can (Figure 41). All the twill layers were placed on each third before rotating, followed by the entire layer of textreme at the end (Figure 42). The layup was then vacuum bagged to pull out any excess epoxy to obtain a better fibre volume fraction and a lighter part (Figure 43 and Figure 44).



Figure 41: Fabric Being Wetted Out With Resin



Figure 42: Fabric Being Laid on the Fin Can



Figure 43: Vacuum Bagging



Figure 44: Final Vacuum Bagged Assembly

The layup was left to cure for two days before demoulding. The part had excess fabric removed from the edges using a dremel, and was then sanded by hand to create the desired profile. Rounds of Bondo body filler followed by sanding will be used to create the final surface finish of the fin can.

The forward coupler and boattail were bonded into the fin can using West Systems 105. Fillets will be formed using Aeropoxy PR2032 and PH3663 to have a smoother transition between the fin can and the metal components.

### 7.6.1 Fin Testing

To validate the strength of the SRAD carbon fibre plate, a uniaxial tensile test was conducted following ASTM D3518 - Standard Test Method for In-Plane Shear Response of Polymer Matrix Composite Materials by Tensile Test of a  $\pm 45^\circ$  Laminate [4]. The samples were cut from the plate stock using the CNC router to 25mm x 200mm (Figure 45). Five were cut from the SRAD stock and five were cut from a COTS plate of the same thickness for comparison.



Figure 45: Fin Plate Testing Samples - SRAD (right) and COTS (left)

The tests were conducted at the Fatigue and Stress Analysis Lab at the University of Waterloo. The displacement was set to 2 mm/min and the tests were run until failure. Figure 46 and Figure 47 show the load response of the SRAD and COTS samples respectively, where the SRAD plate outperformed the COTS plate by a factor of 2.695 (maximum of 14.4354 kN vs. 5.35539 kN). Lateral and longitudinal strain were recorded with extensometers during the test. Following the shear modulus formula provided by ASTM D3518 [4], a shear modulus of 666984.3929 psi was calculated for the SRAD plate. This value was subsequently used in fin sizing, as the shear properties of the plate determine fin flutter reactions.

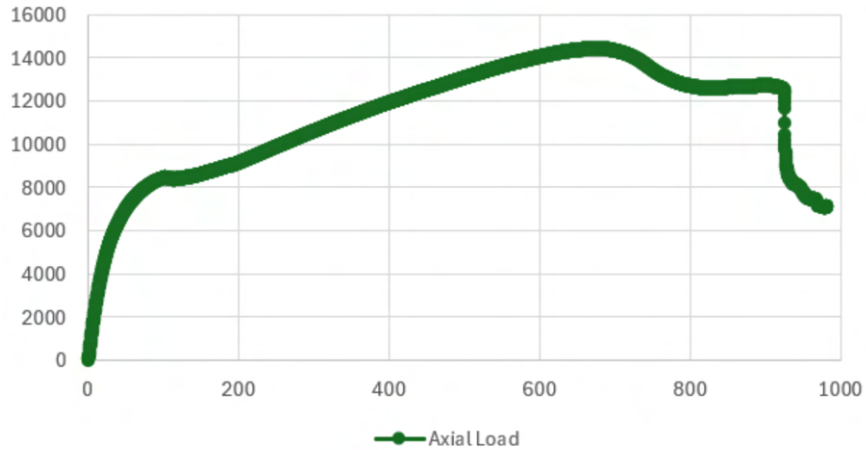


Figure 46: Load (N) Response of SRAD Plate Against Time (s)

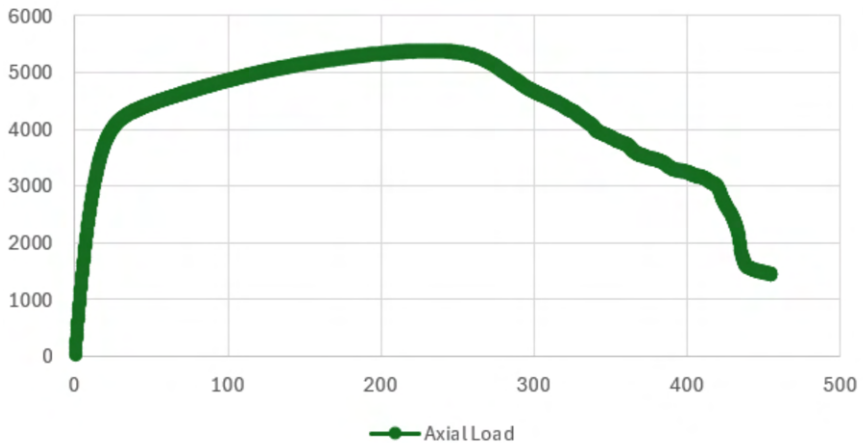


Figure 47: Load (N) Response of COTS Plate Against Time (s)

### 7.6.2 Fin Manufacturing

The fins were made from SRAD 1/8in carbon fibre plate stock. The plate was manufactured through Vacuum Assisted Resin Transfer Molding (VARTM), also known as resin infusion. The number of carbon fibre layers was determined through a small sample piece with a gradual increase in layers, targeting 0.125 (Figure 48). A 4'x8' glass table was used as the moulding surface and was prepped with eight layers of mold release wax. 13 layers of 194gsm 2x2 carbon fibre twill were sandwiched between peel ply using Super 77 spray adhesive on the molding surface (Figure 49). A top layer of infusion mesh was placed under the vacuum bag, which was then sealed with gum tape. The plate was then infused with Airstone 780E + 786H (Figure 50).

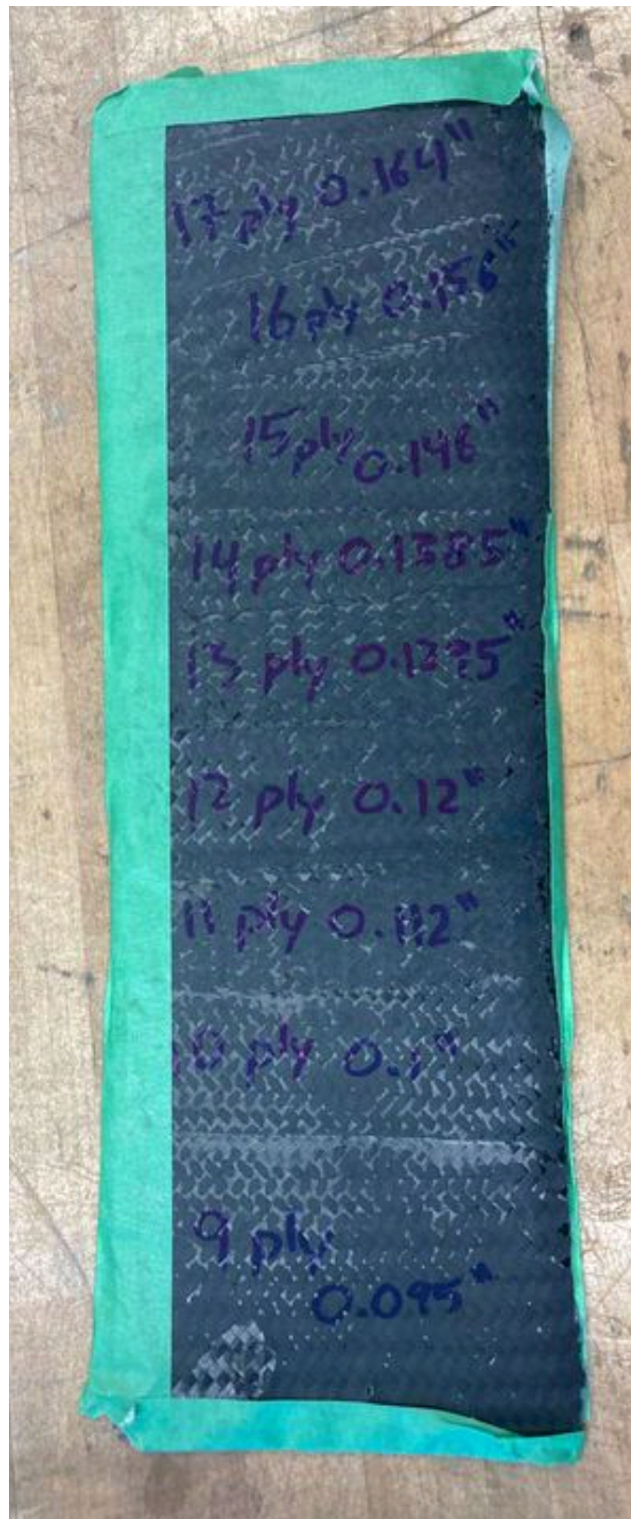


Figure 48: Layer Thickness Test Piece

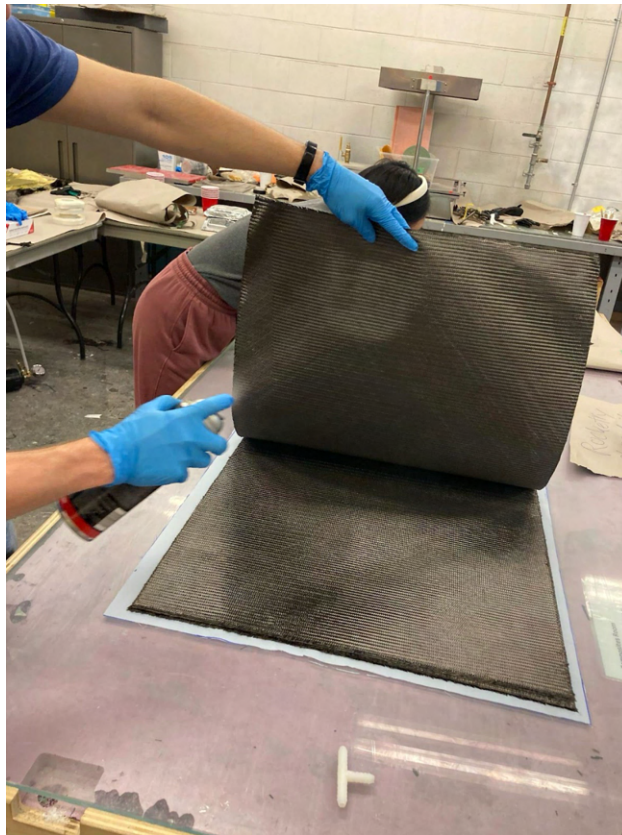


Figure 49: Plate Layer Assembly



Figure 50: Plate During Infusion

Due to a limited amount of plate stock available for cutting fins, one fin has a small hole on

the bonding edge (Figure 51). This is obviously a concern as the strength of the bond and the fin itself will be altered. However, it was decided that the strength would not be considerably compromised due to a combination of factors. First, the process of adding epoxy fillets filled the hole and continued the epoxy matrix across the gap. Additionally, the plate stock only represents part of the fin. The fin consists of 13 layers while the tip to tip comprised seven on each side, more than doubling the thickness. It is for these reasons that the team proceeded with manufacturing with no significant adjustments to account for this defect.

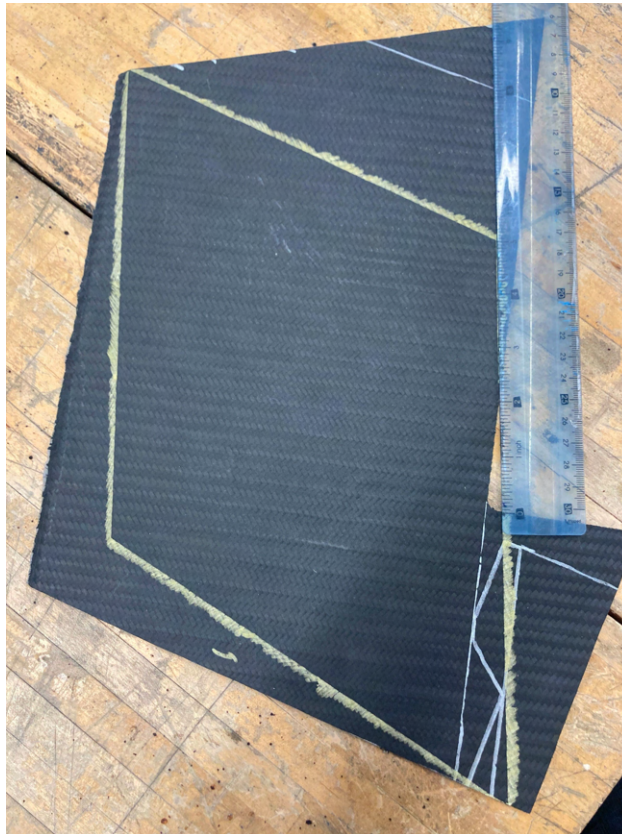


Figure 51: Fin With Small Hole on Bonding Edge

No tests have been conducted to validate the strength of the as-built fin can since properly characterizing the ultimate load that each fin is able to withstand would require destructive testing. Additionally, no tests have been conducted to validate the aeroelastic response of the damaged fin since properly characterizing this would require a large supersonic wind tunnel or extremely complicated test design/correlation.

### 7.6.3 Boattail

The conical boattail completes the aft end of the engine and surrounds the rocket's nozzle. The purpose of the boattail is to reduce the base drag of Borealis by producing a more streamlined vehicle shape. The aerodynamic design is discussed in section 6.5. The geometry of the boattail

and the position of the boattail on the rocket are shown in Figure 52 and Figure 53. Retaining pins are used instead of machine screws to seal the aft end of the combustion chamber, so that only 4 counterbored screw heads are protruding, giving a smoother profile to reduce drag.



Figure 52: Boattail CAD

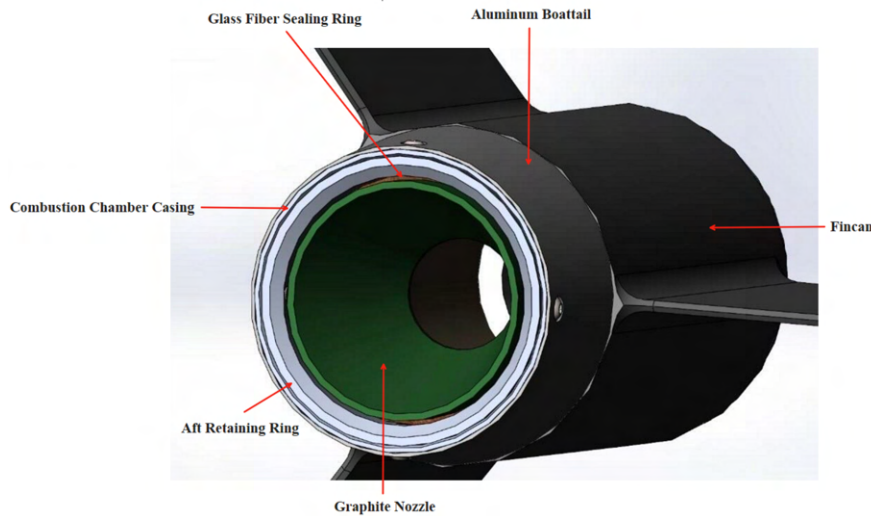


Figure 53: Boattail Assembly

On the team's previous rockets, Leviathan of the Sky (2023) and Kraken of the Sky (2022), a

boattail made from carbon fibre was proposed but ultimately rejected due to integration concerns, the potential of damage from landing, and negligible weight savings. From a integration perspective a composite boattail would have unfavourable bonding surfaces, bolt locations, and pre-set thicknesses based on the number of plies. A carbon fibre boattail is much more likely to crack on landing due to its fairly low toughness. In comparison, an aluminum boattail is extremely unlikely to fail on landing. The LotS boattail impacted the ground at around 120km/h due to partially failed recovery and did not suffer any damage. Lastly, when the team compared conceptual design masses for a carbon fibre vs aluminum boattail designed for the same loads, the mass was almost identical. This is partially due to features required for integration and due to the aluminum boattail being machined very thin by a sponsor. In summary, a carbon fibre boattail would increase risk of cracking, manufacturing and integration complexity and not reduce weight in any measurable way. Images of the final product are shown in Figure 54 and Figure 55.

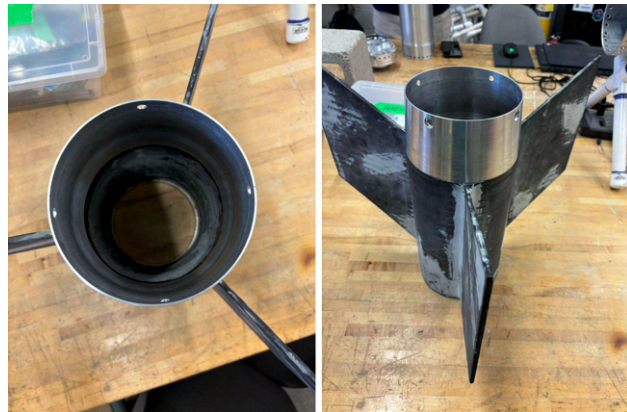


Figure 54: Boattail as-Manufactured and Bonded Into the Fin Can

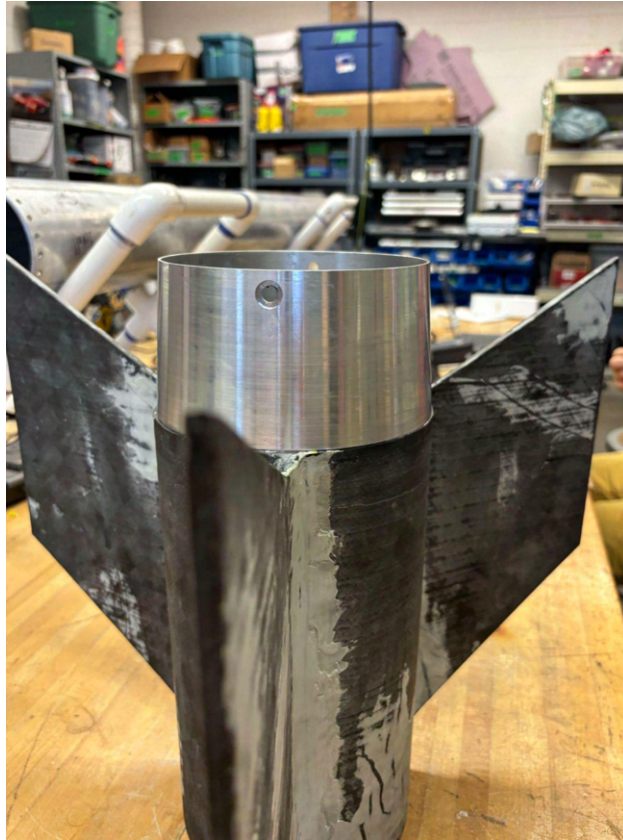


Figure 55: Side Profile of Bonded Boattail

## 7.7 Couplers

Every connection between composite bodytubes is made by a metal coupler bonded into each side of the bodytube. The couplers are made of Aluminum 6061 and fastened by 6x 1/4"-28 radial socket head cap screws. Having a standard joining interface between couplers simplifies the design and provides a certain amount of backwards compatibility, allowing the use of past rocket hardware for testing. Radial patterns are chosen for their simplicity to machine with the tools available in the student machine shop. Other joint types, like radax joints, have been considered but ultimately rejected due to their machining complexity.

Joint design is driven primarily by two constraints, geometry and structural need. It is also to a lesser extent driven by ease of machining, ease of assembly, and similarity to joints used historically on the team.

### 7.7.1 Geometry

The primary joint type used on the rocket is a composite/metal joint. This involves an outer composite ring and an inner threaded aluminum ring. Typically, there is also an aluminum stiffening ring bonded into the composite outer tube. This stiffening ring serves two purposes. The first is to guarantee circularity. The second is to guarantee structural integrity. There is also one joint on the rocket which joins the upper recovery section to the rest of the vehicle. It involves an outer metal

ring bonded to the aft end of the joint, a center aluminum ring bonded to the forward end of the joint, and an inner recovery bulkhead used to hold all recovery electronics and seal pressure inside the recovery bay.

Geometry of the joints is designed first, typically by iterating on sketches. The key parameters to address are:

- What is the diameter of the tube sections, and is there sufficient clearance to mate them?
- Will the designed joint be simple to machine with the available tools?
- Will everything entering through this side of the bodytube be able to fit past the designed joint?
- Does the team have experience or reference material for making this joint?
- If the team decides this joint is unsuitable down the line, how can it be adapted?
- Where can this joint be weight optimized or strength optimized?

After developing a joint profile, design can then begin on the structural analysis.

### 7.7.2 Structure

All joints on the vehicle are made of 6061-T6 aluminum tubes. Failure modes of these joints are always failure around the bolt circles, and therefore bearing failure and tearout failure at takeoff, max-Q, and recovery deployment are the limiting cases. FOS 2.0 is kept for all cases. For information on how the team develops those load profiles, see section 6.14. For metal/metal joints, the analysis is relatively straightforward, as the bearing and shear strengths of aluminum are well understood. However, for bolts bearing directly on composite, the bearing and shear strength of the composite is less well understood or consistent. Therefore, as well as being effective for guaranteeing circularity, the inner aluminum stiffening ring must also be independently capable of handling the full load of the vehicle in all three load cases.

Inputs to the structural analysis of the joints are the geometry of the joint, as well as the load inputs described in section 6.14. For takeoff and max-Q, the axial and bending load and the given geometry are converted to a bearing and shear stress, taking the bearing area to be the thickness of the joint multiplied by the minor diameter of the bolt and the shear area to be twice the thickness of the joint multiplied by the distance from the bolt to the edge of the coupler. Dividing the bearing yield strength and shear strength of the material by the bearing and shear stresses experienced by the joint gives the factor of safety, which is kept above 2.0. In the recovery deployment loading case, an axial load in tension with a magnitude of 25Gs of deceleration acting on the entire dry mass below aft of that joint is assumed. The specific geometry of the joint is then designed by tuning the inner and outer diameters of the parts until they are above FOS 2.0 for all load cases. Shear loads are neglected, and the bending is modelled as an additional axial load in tension/compression

A sample calculation shall be done on the airbrakes forward stiffening ring at max-Q, which has the following geometry and loads:

- Axial load (P): -491lbf

- Bending moment (M): 1188lbf-in
- Coupler Inner Diameter (CID): 5.69in
- Coupler Outer Diameter (COD): 5.82in
- Coupler Edge Distance (CED): 0.325in
- Bolt Diameter (BD): 0.25in
- Number of bolts: 6
- Bearing yield strength, 6061-T6: 56000psi [5]
- Shear yield strength, 6061-T6: 30000psi [5]

note that the load cases found here are different than those in section 6.14. This is because all designs were done on an earlier load profile with a weaker engine. However, a review of all coupler designs with the most up to date load profile has been completed and all couplers are still above FOS 2 in every load case

$$\text{Additional axial load from bending (worst case)} = \frac{M}{4 \times 1.5\text{in} \times \sqrt{3}} = \frac{1188\text{lbf-in}}{4 \times 1.5\text{in} \times \sqrt{3}} = 114\text{lbf}$$

$$\text{Maximum axial force per bolt}(F) = \frac{P}{6} \pm \text{Additional axial load from bending} = \frac{-491\text{lbf}}{6} \pm 114\text{lbf} = 32\text{lbf}, -195\text{lbf}$$

- For bearing, take largest magnitude. For tearout, take positive.

$$\text{Coupler Thickness (CT)} = \frac{(\text{COD} - \text{CID})}{2} = \frac{(5.82\text{in} - 5.69\text{in})}{2} = 0.065\text{in}$$

$$\text{Bearing area } (A_{\text{Bearing}}) = \text{BD} \times \text{CT} = 0.25\text{in} \times 0.065\text{in} = 0.01625\text{in}^2$$

$$\text{Bearing Stress } (\sigma_{\text{Bearing}}) = \frac{F}{A_{\text{Bearing}}} = \frac{195\text{lbf}}{0.01625\text{in}^2} = 12000\text{psi}$$

$$\text{Bearing FOS} = \frac{\text{Bearing yield strength}}{\sigma_{\text{Bearing}}} = \frac{56000\text{psi}}{12000\text{psi}} = 4.7$$

$$\text{Tear out area } (A_{\text{Tear}}) = 2 \times \text{CT} \times (\text{CED} - \frac{\text{BD}}{2}) = 2 \times 0.065\text{in} \times (0.325\text{in} - \frac{0.25\text{in}}{2}) = 0.026\text{in}^2$$

$$\text{Tear out stress } (\sigma_{\text{Tear}}) = \frac{F}{A_{\text{Tear}}} = \frac{32\text{lbf}}{0.026\text{in}^2} = 1231\text{psi}$$

$$\text{Tear out FOS} = \frac{\text{Shear yield strength}}{\sigma_{\text{Tear}}} = \frac{30000\text{psi}}{1231\text{psi}} = 24.4$$

A complete list of all load bearing coupler geometries and failure modes can be found in Table 13. Note that the failure point of all joints on Borealis is either bearing failure or tearout failure on parachute deployment.

| Coupler                | COD (in) | CID (in) | CED (in) | Position (in) | Min. FOS |
|------------------------|----------|----------|----------|---------------|----------|
| Recovery Fore Coupler  | 5.66     | 5.518    | 0.5      | 32.3          | 2.6      |
| Recovery Aft Coupler   | 5.8      | 5.66     | 0.5      | 32.3          | 2.6      |
| Airbrakes Fore Doubler | 5.82     | 5.69     | 0.325    | 59.1          | 2.5      |
| Airbrakes Fore Coupler | 5.69     | 5.45     | 1.5      | 59.1          | 5.5      |
| Airbrakes Aft Coupler  | 5.73     | 5.6      | 0.325    | 61.32         | 2.9      |
| Airbrakes Aft Doubler  | 5.86     | 5.73     | 0.325    | 61.32         | 2.9      |
| Vent Bulkhead Doubler  | 5.87     | 5.68     | 0.37     | 80.7          | 4.9      |
| Vent Bulkhead Tabs     | 5.68     | 5.48     | 0.23     | 80.7          | 2.3      |

Table 13: Coupler Geometries and Failure Modes

### 7.7.3 Manufacturing and Bonding

All couplers were machined in the Engineering Student Machine Shop on a manual lathe. All mating surfaces were machined to fit wherever possible. Interfaces between metal and composite components were permanently bonded in place using West Systems 105/206 epoxy resin and left to cure for 24h. Radial holes were then drilled on the rotary table. This machining and bonding process has been used since 2019 and has never seen an in-flight failure since it was implemented (3 total flights).

## 8 PROPULSION

### 8.1 Overview

Borealis is powered by Waterloo Rocketry's first flight ready liquid rocket engine, named Eridium. The engine runs on Nitrous Oxide ( $\text{N}_2\text{O}$ ) and Ethanol, drawing on heritage from the team's successful hybrids program to reduce the scope of changes that needed to be made. The goal for the engine this year was not to be extremely optimized, but rather to be reliable and achieve baseline thrust goals set by flight dynamics to ensure rocket stability, without sweeping changes operationally that would be out of scope for a single year of changes.

A P&ID diagram for the engine is shown in Appendix D, and key engine parameters are summarized in Table 14.

Table 14: Key Engine Parameters

| Parameter                  | Value                              |
|----------------------------|------------------------------------|
| Oxidizer                   | 13 kg $\text{N}_2\text{O}$         |
| Fuel                       | 4.25 kg Ethanol                    |
| Impulse                    | 28 150 Ns                          |
| Burn Averaged $I_{sp}$     | 184 s                              |
| Thrust (peak)              | 8.1 kN                             |
| Thrust (sustained)         | 4.5 kN                             |
| Burn duration              | 5.6 s                              |
| O/F ratio                  | 3.4 (initial), 2.65 (Burn Average) |
| Oxidizer tank pressure     | 800 psi                            |
| Chamber pressure           | 480 psi (peak), 300 psi (average)  |
| Chamber length             | 14.25"                             |
| Chamber OD                 | 5.2"                               |
| Chamber wall               | 0.1"                               |
| Nozzle geometry            | 15° Conical                        |
| Throat diameter            | 1.975"                             |
| Expansion ratio            | 4.1                                |
| Characteristic Length (L*) | 31"                                |

### 8.2 Injectors

The injector design chosen for the engine is a 6 element coaxial swirl injector. This injector was selected due to its combination of enabling rapid small scale testing while maintaining reasonable propellant mixing properties. The injector is fuel centered, using modified COTS brass spray nozzles to reduce complexity and machining time. The outer swirl elements are brass sleeves with tangential holes drilled in 5 locations equally spaced around the outer diameter, and the assembly was to be brazed together to create a seal between propellants. An injector element cross section is shown in Figure 56.

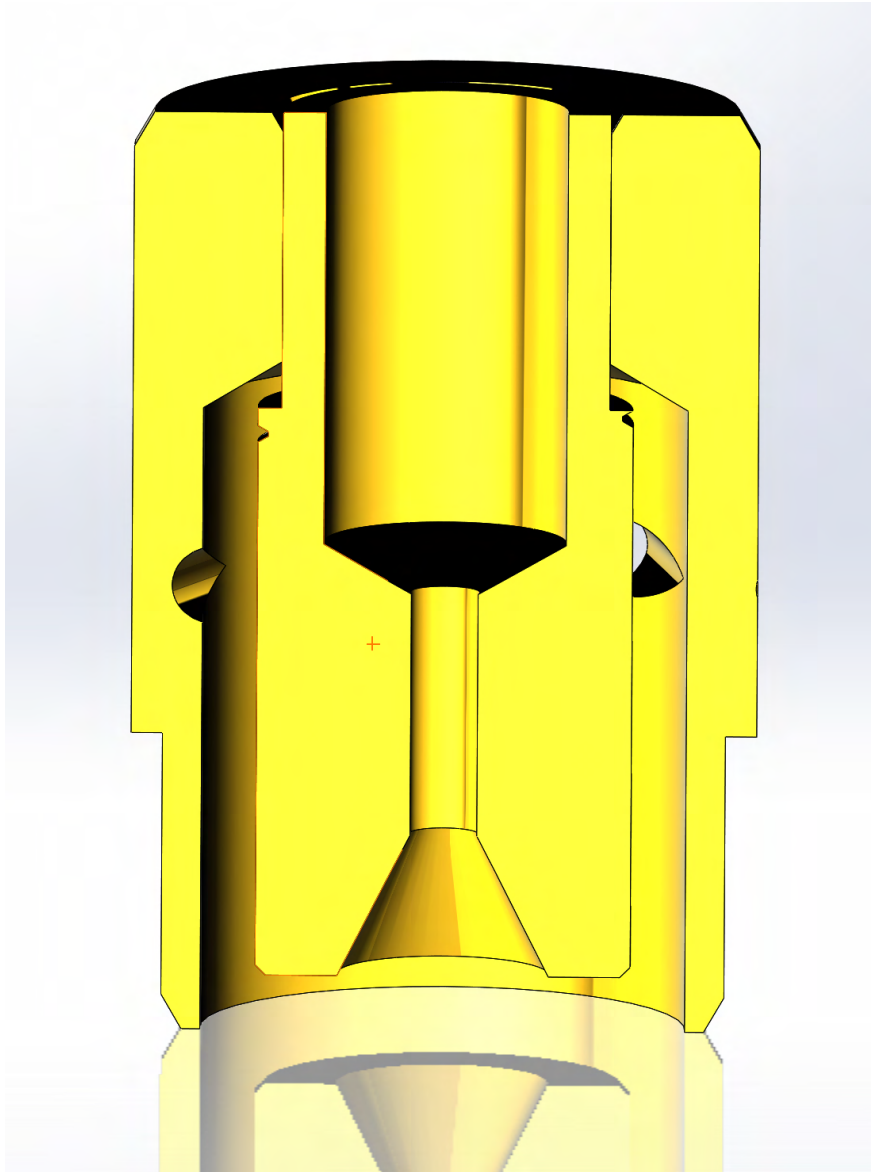


Figure 56: Injector Cross-Section

### 8.2.1 Injector Characterization

Cold flow testing was conducted using CO<sub>2</sub> as a simulated propellant for N<sub>2</sub>O, and water as a substitute for ethanol. To allow rapid testing, the elements were tested as single elements in a custom test jig to reduce required machining time. The measurement method of flowrate was by tank mass hanging from a load cell. However, due to vibrations in the tank, this data was difficult to characterize.



Figure 57: Cold Flow Test Load Cell Set-up

Additionally, since the nitrous injection holes are quite small, there were concerns that at lower pressure drops the flow would not become critical, and thus the models used would not accurately predict the flowrate. This was especially concerning as Waxman [6] notes that at low L/D ratios the flow choking was not accurately predicted by his models. To avoid this, it was conservatively assumed that the flow would not choke in the nitrous holes, and the engine was designed to have adequate injector pressure drop margin to handle higher flow rates. In practice, the flow appears to be choked during static fires, meaning the O/F ratio of the engine ended up being fairly fuel rich. This is an acceptable result for the goals of this year's engine, since it reduces the likelihood of melting the chamber or the injectors and still produces adequate thrust and efficiency.

After initial testing, the swirl angle on the oxidiser side has been visually characterized to be approximately  $10^\circ$ , which is a significantly narrower cone than initially predicted. The suspected cause of this narrower cone is the turbulence caused by vaporization of the nitrous oxide as it

flashes through the injector orifices negating the tangential momentum of the fluid. This is not a significant concern for propellant mixing, as the spray angle of the COTS spray nozzles (which also underperformed on spray angle) has been visually characterized to be approximately  $40^\circ$ , as shown in Figure 58. The fuel and oxidizer flow paths should impinge given the injector elements are fuel centered. As well, we expect to see shear effects which should also help mixing.



Figure 58: COTS Nozzle Spray Angle

For the initial static fire, it was attempted to use low temperature silver solder to join the fuel injectors and oxidiser sleeves together. This proved to be more difficult than initial small scale testing would have suggested, and there were significant leaks that could not be fully eliminated. For the following static fire, the interpropellant seals were changed to large press fits above the threshold for plastic deformation in the materials. These joints successfully passed hydrostatic testing at 1200 psi pressure difference and were used successfully in the second static fire. The front plate of the injectors is brazed to the outer sleeve, to allow for clearance on the holes, thereby avoiding press fits where multiple components needed to line up to tight tolerances simultaneously. Figure 59 shows the permanent interpropellant seal configuration of the injectors.

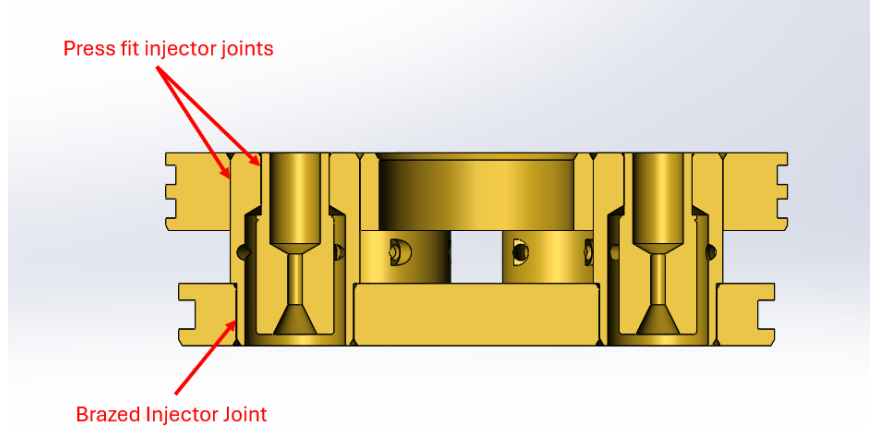


Figure 59: Injector Joints

### 8.2.2 Injector Bulkhead

The injector bulkhead is designed to be simple to assemble and avoid complex fluid paths. The oxidiser is fed directly from the outlet flange of the valve down the center of the fuel manifold and into the lower oxidiser volume. The fuel is introduced asymmetrically, with a large volume to keep the velocity of the propellant low in the manifold to minimize flow distribution issues. The fuel dome is raised above the injector bulkhead for weight savings and to allow the oxidiser valve to mount directly to a flange on the dome. The removable seals in the injector are all Buna-N O-rings, with 2 O-rings at the interpropellant seals. Additionally, the fuel manifold is asymmetric to accommodate the inlet while allowing space for longerons and other hardware on the bulkhead, meaning an asymmetric face seal O-ring was used for the primary fuel dome seal.

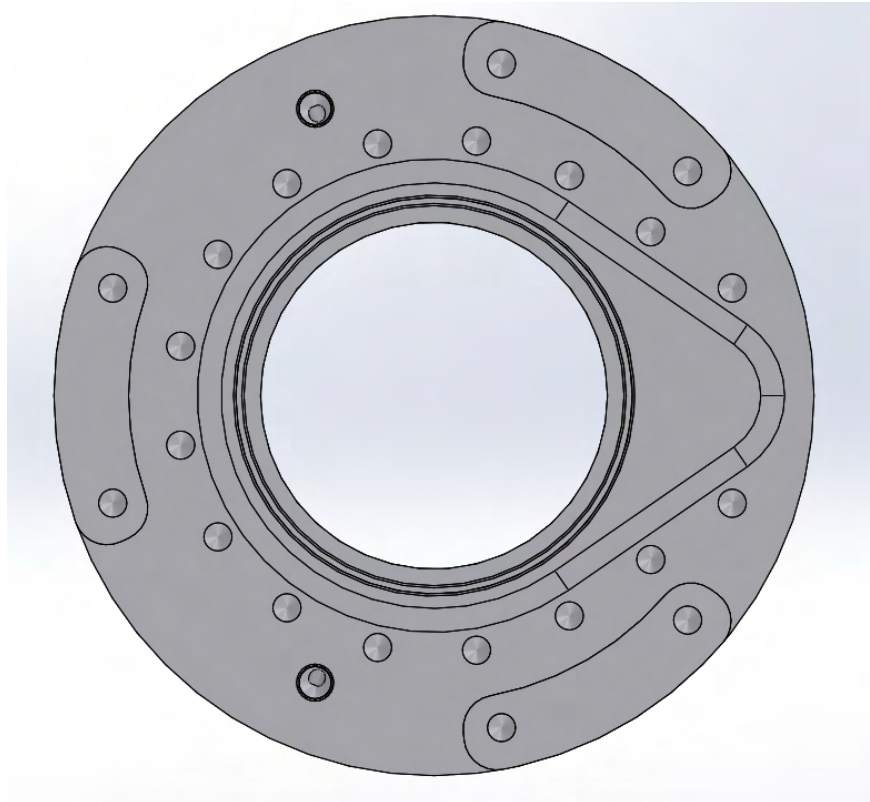


Figure 60: Top View of Asymmetric Manifold of the Injector Bulkhead

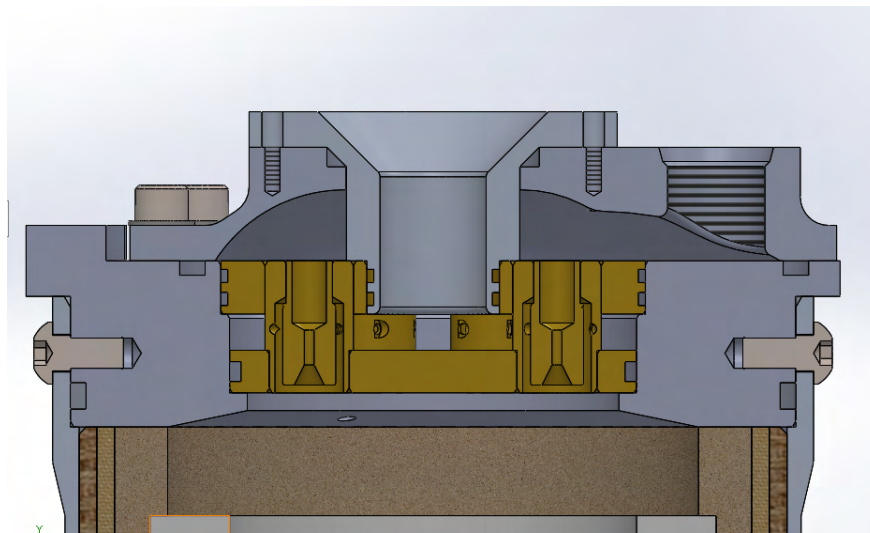


Figure 61: Cross Section of Injector Bulkhead

The injector bulkhead also accommodates 2 pressure transducer ports, allowing for chamber pressure data to be acquired during the burn. A single pressure transducer will be flown, due to space limitations and a limited number of electrical sensing ports on the propulsion board. The second unused port will be plugged for flight.

The fuel dome was analyzed using the Ansys Mechanical FEA package. In particular, both the stress in the dome and stress created by preloaded bolts were analyzed. This was done because there was concern that the material removed around the bolted joints combined with the asymmetrical pressure loading could lead to bending in the bolts at those joints, or separation of the flange from the O-ring groove under pressure. The analysis shows that the flange maintains FOS 2 even at an extremely conservative preload uncertainty. The bulkhead was initially designed for 75 in-lbs of preload across the 16 flange bolts, but due to threads in the injector bulkhead not being as deep as intended, the applied torque was reduced to 50 in-lbs to avoid tearing out the aluminum female threads in the bulkhead. The full FEA analysis documentation is cited here [7] as a representative example of how FEA studies are conducted on the team.

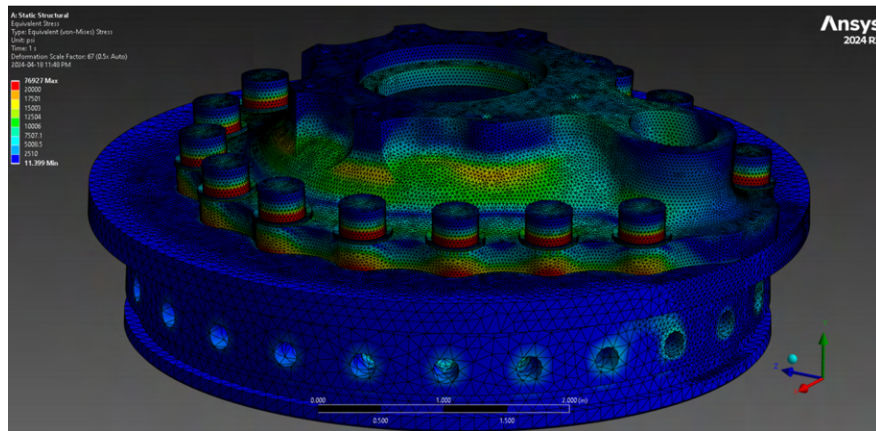


Figure 62: FEA Study on the Injector Bulkhead

### 8.3 Combustion Chamber

The combustion chamber comprises a structural pressure vessel containing various ablatives to protect the aluminum pressure vessel and the nozzle, as well as retaining the injector bulkhead at the head of the chamber. O-rings are used for the main seals at the forward and aft ends of the chamber. To prevent hot combustion gases from reaching the casing and/or O-rings, most interfaces between internal components of the combustion chamber are sealed with high-temperature RTV gasket maker (Permatex 26BR). A high-temperature synthetic grease (Super Lube 41160) is applied liberally to the exterior surface of the stack of internal components to fill the gap between the liner and the casing, which facilitates disassembly of the combustion chamber assembly after the burn, as well as helping to transmit radial pressure forces into the casing. A sectional view of the combustion chamber is shown in figure 63.

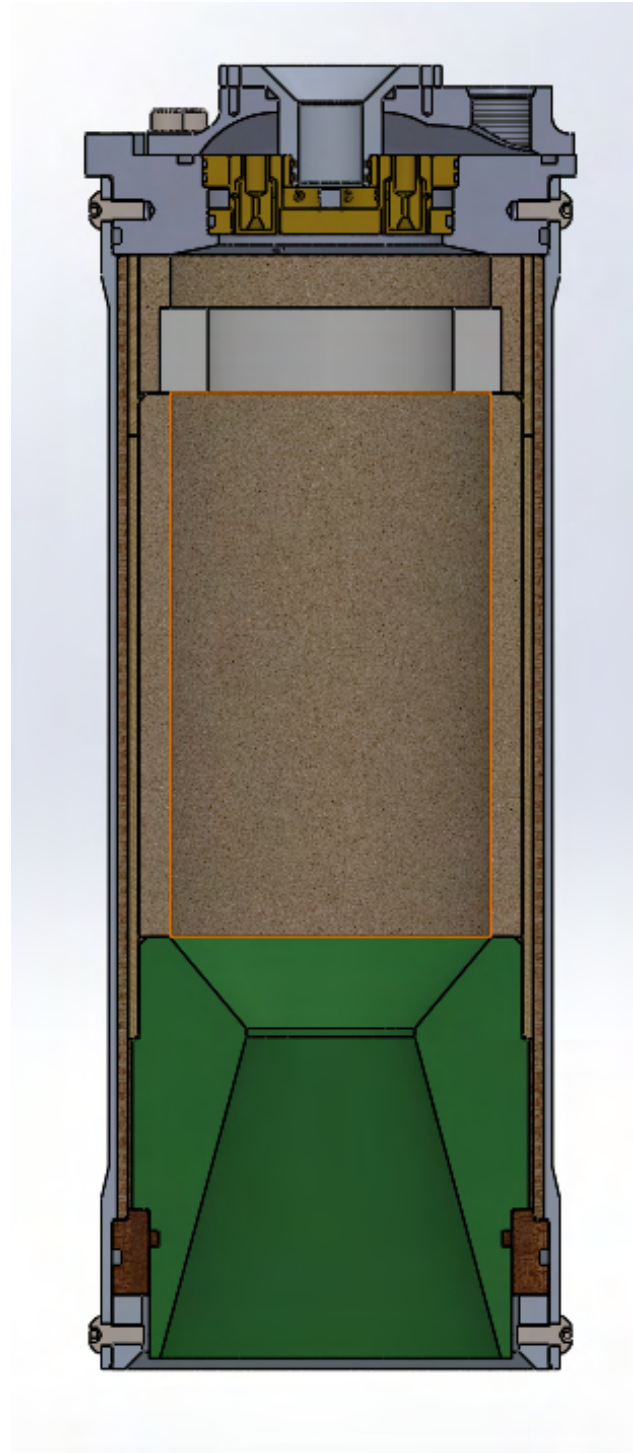


Figure 63: Combustion Chamber Cross-Section

### 8.3.1 Combustion Chamber Casing

The combustion chamber casing is made of 6061-T6 aluminum and consists of a main section in the middle containing ablative components, and two enlarged end sections which are bored out

to accommodate the O-ring seals for the injector bulkhead and sealing ring. The casing is 14" in length. The outer diameter is 5.2" in the main section and 5.375" at the forward and aft ends. The wall thickness is 0.1" in the main section and 0.125" in the end sections. These dimensions were chosen to minimize mass while still maintaining adequate strength against the pressure load produced by the burn. The casing was hydrostatically tested to 1000 psi before engine testing.

### **8.3.2 Ablative Liners**

The ablative liner for the combustion chamber reuses phenolic tubing from the 2023 Kismet hybrid rocket engine. A 1/8" thick G3 phenolic composite tube runs the entire length of the combustion chamber, serving as a final barrier to prevent heat from reaching the walls. It also acts as the shield to keep the graphite from the nozzle from contacting the aluminum, since heat soak through graphite can be extremely hot after the burn. Inside of the G3 tube, another 1/8" thick G11 glass epoxy composite tube is used. The tube mates around the converging section of the graphite nozzle, and is split in two sections near the top of the chamber to allow for the igniter to be cast inside. The G11 tube serves as the casting tube for the 3/8" thick custom cast ablative that makes up the main contact area with the combustion gasses.

### **8.3.3 Custom Ablative Development**

Inspired by Half Cat Rocketry's CHAMBERSAFE, various combinations of epoxy, glass fibres, ceramic powders, phenolic micro balloons, and boric acid were tested to determine the formula. The testing setup involved an oxy-acetylene torch which was retained in a mount at a fixed distance and angle from the samples. A thermocouple was placed underneath the sample, with ample thermal paste, and the samples were heated for a fixed amount of time. While not an accurate test of combustion chamber conditions, this setup allowed for comparison of different samples in a repeatable way. The testing setup is shown in Figure 64 below. The test setup's accuracy was verified since identical samples generally fell within 5% of each other's temperature curves. The final formula selected uses 63.3% epoxy, 31.7% boric acid and 5% phenolic micro-balloons by mass. It should be noted that because phenolic micro-balloons have a very low density they make up a significant portion of the mixture by volume.



Figure 64: Ablative Characterization Testing Setup and Test

In both static fire tests, this custom ablative was more than adequate to provide thermal protection to the combustion chamber, generally regressing approximately 1/8" over the duration of the burn during both static fires. Although no thermocouple data was acquired during either static fire due to instrumentation issues, single use temperature indicating stickers were used during the flight qualification static fire as a backup and did not show any temperature values above 200 °C, well below the temperature required to anneal the T6 temper on the aluminum casing for the duration that it would be hot.

### 8.3.4 Nozzle Retention

The retention of the nozzle is accomplished using a ring made from G3 plate stock. The ring is water jet cut and then the O-ring groove and final dimensions are turned on a lathe. The sealing ring and the graphite nozzle are both baked for 6 hours at 300 °F (150 °C) to avoid water absorption that could lead to steam formation and cracking. The G3 ring sits on a secondary aluminum retaining ring, which contains holes for twenty 1/4" pins and four 1/4"-28 screws. The pin holes are blind, and are retained from the outside of the combustion chamber by the boat tail. The four 1/4"-28 screws join the boat tail (and fin can) to the rest of the rocket.

### 8.3.5 Igniter

The igniter borrows heavily from previous hybrid engine igniters. The igniter sits in the combustion chamber, and uses a modified version of Richard Nakka's RNX propellant, with the burn rate modifiers removed to keep the burn rate slower. The igniter is bonded directly to the custom ablative, and sits on a 1/8" thick lip to avoid getting blown out of the chamber when the valves open. Ignition is achieved through 2 redundant nichrome wires that are cast directly into the surface of the RNX. Speaker wire is run from the nichrome out the nozzle to the ground support equipment. The only significant change that has been made from 2023's ignition system is that the nichrome was moved from being 2 distinct coils to being wrapped around the inner diameter of the igniter. This style of ignition puck has successfully ignited the last 3 liquid engine static fires that have been conducted.

## 8.4 Feedsystem

### 8.4.1 Propellant Tanks

Nitrous oxide is an excellent propellant for small liquid rocket engines due to its high vapor pressure at room temperature. This allows for the rocket to avoid using a secondary high pressure gas to pressurize the propellant tanks, significantly reducing both complexity and mass. Concentric tanks were selected for Borealis, allowing the vapor pressure of the nitrous to also pressurize the concentric ethanol tank. A piston is used to avoid mixing oxidiser and fuel inside the propellant tanks.

Both propellant tanks are made of 6061-T6 aluminum, due to its light weight and reasonable cost. The oxidiser tank has an outer diameter of 6", with a thickness of 3/16", and is 64" long. The fuel tank has an outer diameter of 3", with an average thickness of 0.08". The fuel tank is held concentric with a sealed attachment point to the fill bulkhead at the aft end, and centering tabs that extend downward from the vent bulkhead at the front. The tank bulkheads are retained to the tank using a circle of 24 1/4"-28 bolts, and the bolted closures are designed to a factor of safety of 2 at a maximum operating pressure of 1000 psi. The flight tanks have passed hydrostatic testing at 1500 psi. Both ends of the tank are sealed with two Buna-N O-rings.

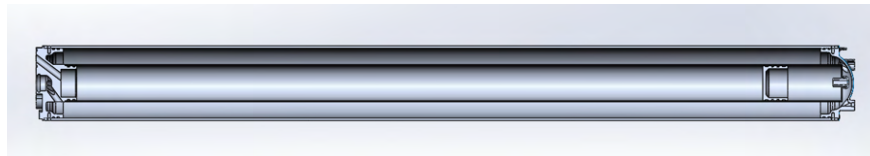


Figure 65: Tank Assembly with Bulkheads

### 8.4.2 Piston

To ensure that the piston will adequately seal the length of the fuel tank, drawn aluminum tubing is used for the internal tank. Both ends of the tube were measured and a maximum difference of 3.5 thou across the ID was found. This is more than acceptable to keep good compression and avoid extrusion on the piston O-rings at 1000 psi. The piston has two O-rings that make up the interpropellant seal. Unlike many O-ring seals on the rocket that have relaxed tolerances to allow for easier assembly and more forgiving fabrication, the piston strictly follows the Parker O-ring handbook's dynamic seal design guidelines [8] to ensure reliability. Additionally, 2 PTFE wear rings are added to the piston on the outside of the O-rings to ensure that the aluminum piston body does not scratch the inside surface of the fuel tank. The wear rings also help to reduce the chance that the piston will bind in the tank. The length added by the wear rings also helps to avoid the "sticky drawer effect" [9]. Finally, the piston is generously lubricated with oxidiser safe Krytox synthetic grease to ensure that it slides well in the tank. The piston has been successfully tested in the second static fire as well as multiple cold flows during preparation and wet dress rehearsals.

### 8.4.3 Fill Bulkhead

The fill bulkhead is the lower bulkhead of the rocket, and serves as both the interface for filling the tanks as well as the interface to the propellant feed lines. To save space, both the fuel injector

valve and the fill/dump valve are mounted directly to the bulkhead, avoiding extra flanges. The bulkhead also includes a small access port to the fuel tank that allows for filling fuel as well as a pressure transducer to ensure that the piston is correctly transmitting pressure before firing the engine. The most notable feature of the bulkhead is the angled holes that invert the positions of the fuel and oxidiser. In the tank, the fuel is central but in the injectors the oxidiser needs to be in the center, so angled holes drilled on a 5 axis CNC are used to move the propellants to the opposite position, while avoiding complicated bent tube geometry elsewhere in the feedlines. The bulkhead is made of 6061-T6 aluminum and is designed to a minimum factor of safety of 2 at 1000 psi. The bulkhead's strength was verified using hand calculations, SolidWorks FEA, and hydrostatic testing to 1500 psi.

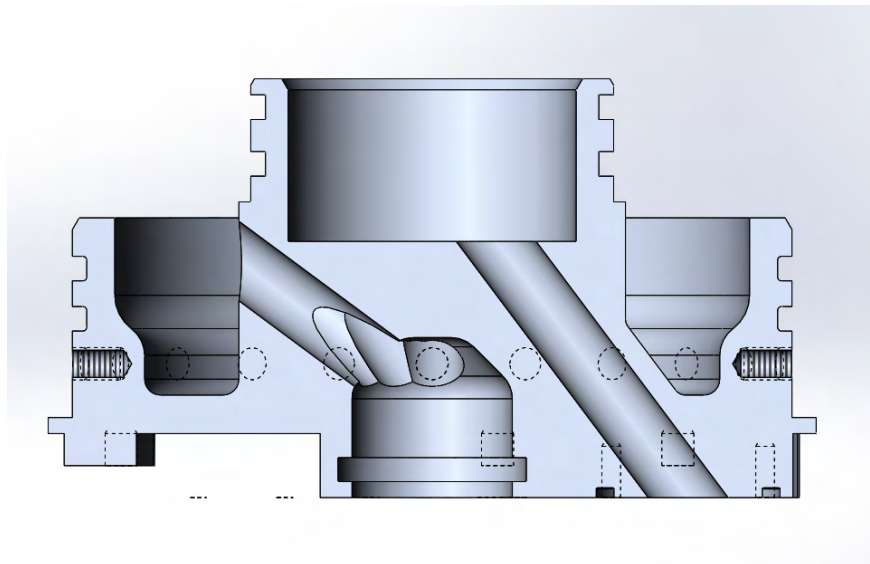


Figure 66: Fill Bulkhead Cross Section

#### 8.4.4 Vent Bulkhead

The vent bulkhead caps the top end of the concentric tanks and connects to the vent section plumbing. The previous multiport bulkhead also featured three ports for the pressure transducer, vent valve, and pressure relief valve. This year, 6061-T6 aluminum is used instead of 7075 aluminum so the wall thicknesses are changed accordingly and FEA confirms a minimum FOS of 2, as shown in Figure 67.

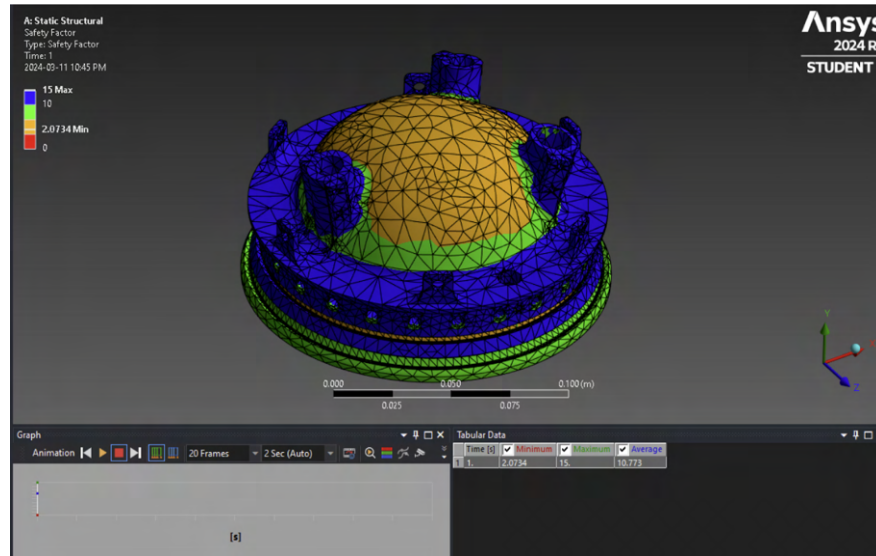


Figure 67: FEA of Vent Bulkhead

Additionally, the ports are spaced to allow for printed circuit boards to be mounted in between and to make space for the centering features for the inner tank. (Figure 68).



Figure 68: Centering Features of Vent Bulkhead

Port placement is changed from last year's design to accommodate the centering tabs and board mounts for printed circuit boards, as shown in Figure 69.

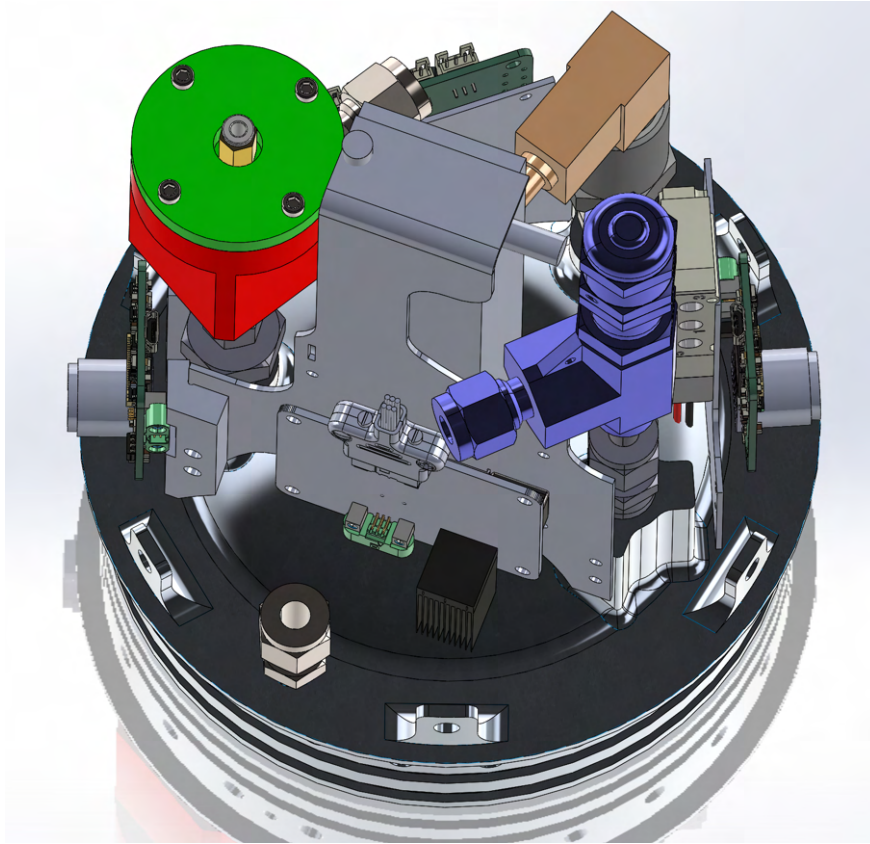


Figure 69: Vent Bulkhead Port Placement and Integration

## 8.5 Injector Valves

Both the fuel and oxidizer valves are coaxial sleeve style valves based on the oxidizer injector valve used successfully in 2023. A representative cross-section of the fuel injector valve is shown in Figure 70 and Figure 71

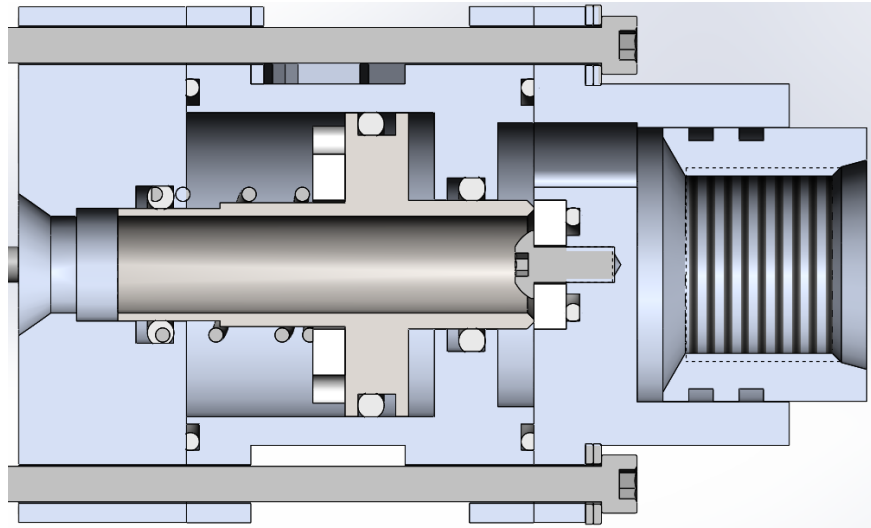


Figure 70: Cross section of the Fuel Injector Valve - Closed

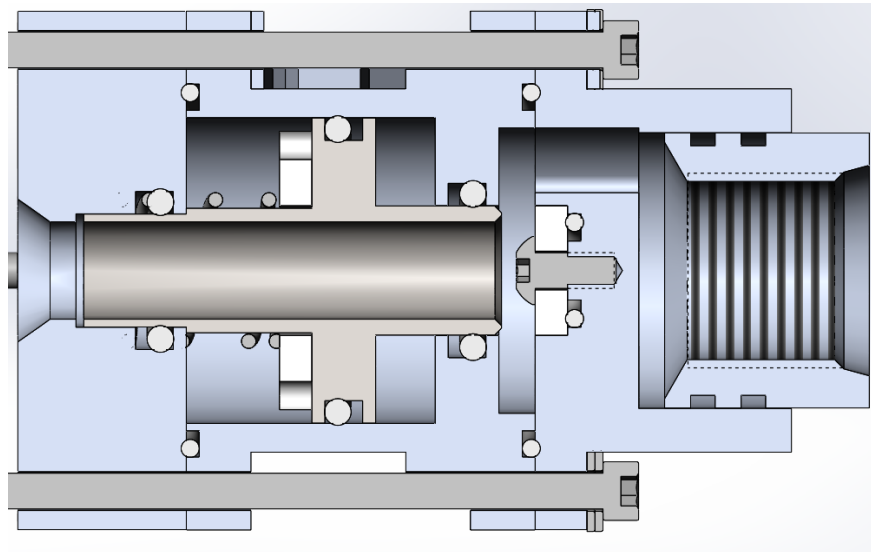


Figure 71: Cross section of the Fuel Injector Valve - Open

Both valves feature a sleeve that is moved by pneumatic pressure to open or close the flow path, and have biasing springs to return the valve to the closed position if pneumatic pressure is lost. The sleeves of both valves are also sized such that the downstream projected area is larger than the upstream projected area. This design choice was made so that in the event the injector valves lose pneumatic pressure while open, the unbalanced force due to fluid pressure will be larger than the spring force and will keep the valves open until the tank pressure drops below about 300 psi. This behaviour is desirable in order to ensure the burn is not cut short in the event pneumatic pressure is lost immediately upon liftoff, and so the engine will burn long enough for the rocket to reach an altitude where the recovery system can safely deploy. The valves are designed to actuate with FOS 1.5 at 100 psi pneumatic pressure, and have been verified to actuate at as low as 50 psi

during a cold-flow test prior to the June static fire.

The fuel injector valve is mounted directly to the underside of the fill bulkhead, and the oxidizer injector bulkhead is mounted to the injector bulkhead. This allows the valves to be fully assembled and mounted before injector section assembly. Additionally, both valves/propellant feedlines have length compensators (static O-ring piston seals that allow the length of the oxidizer and fuel feedlines to fluctuate about .15" in either direction). This was done to ensure the structural longerons are the only item constraining the length of the injector section, unlike in 2023 where both the oxidizer feedline and longerons constrained the height. The layout of the Fuel injector and Fill-Dump valves mounted on the fill bulkhead is shown in Figure 72.



Figure 72: Fill Bulkhead with Integrated Valves

The fuel injector valve is designed to maintain a pressure drop of less than 50 psi across the fuel feedline, using the simple incompressible assumption for ethanol. The oxidizer valve is sized so that the equivalent flow area is at least 3x the total area of the injector elements so that the nitrous oxide does not flash to vapour in the valve.

The most significant change from the 2023 Oxidizer sleeve valve design to this year's design is the valve seat geometry. The previous valve seat used a chamfered PTFE seat, which the sleeve created an edge seal on. Manufacturing this seat involved turning the part on a lathe and was a relatively time-consuming process. For Borealis, the seal was changed to be a face seal, with the PTFE seat now flat and recessed into the downstream connector. This means that the seat can be waterjet, allowing spare seats to be made very easily, and that the seat is supported against extrusion.

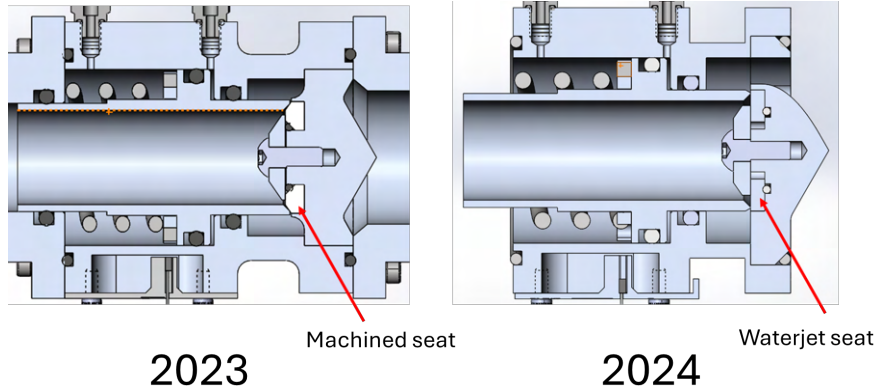


Figure 73: Changes in seat geometry between 2023 and 2024 oxidizer injector valve

To size the face seal, the actuator force and the contact area were sized such that the sealing pressure (sealing force divided by contact area) is greater than 1.5x the fluid pressure the contact surface must seal against. Initially, the sleeves were made out of 6061-T6 aluminum, however the sealing surface of these sleeves was damaged easily. Given the face sealing mechanism is less tolerant of surface imperfections than the edge seal due to larger contact area and thus reduced seat stress, the sleeve material was changed to stainless steel to be harder and more resistant to damage from handling. The finished valves are shown in Figures 74 and 75.



Figure 74: Flight Oxidizer Injector Valve



Figure 75: Flight Fuel Injector Valve

Both valves were validated in the June 2024 static fire of the Eridium liquid engine. For more details on the specifics and design process of the original sleeve valves, see the design report on the 2023 oxidizer injector valve [10].

## 8.6 Fill/Dump Valve

The Fill/Dump valve is a pneumatically-actuated poppet valve that allows oxidizer to be filled into and retained in the oxidizer tank, and can be re-opened to drain the tank out the inlet line in the event of an abort. A cross-section of the valve is shown in Figure 76.

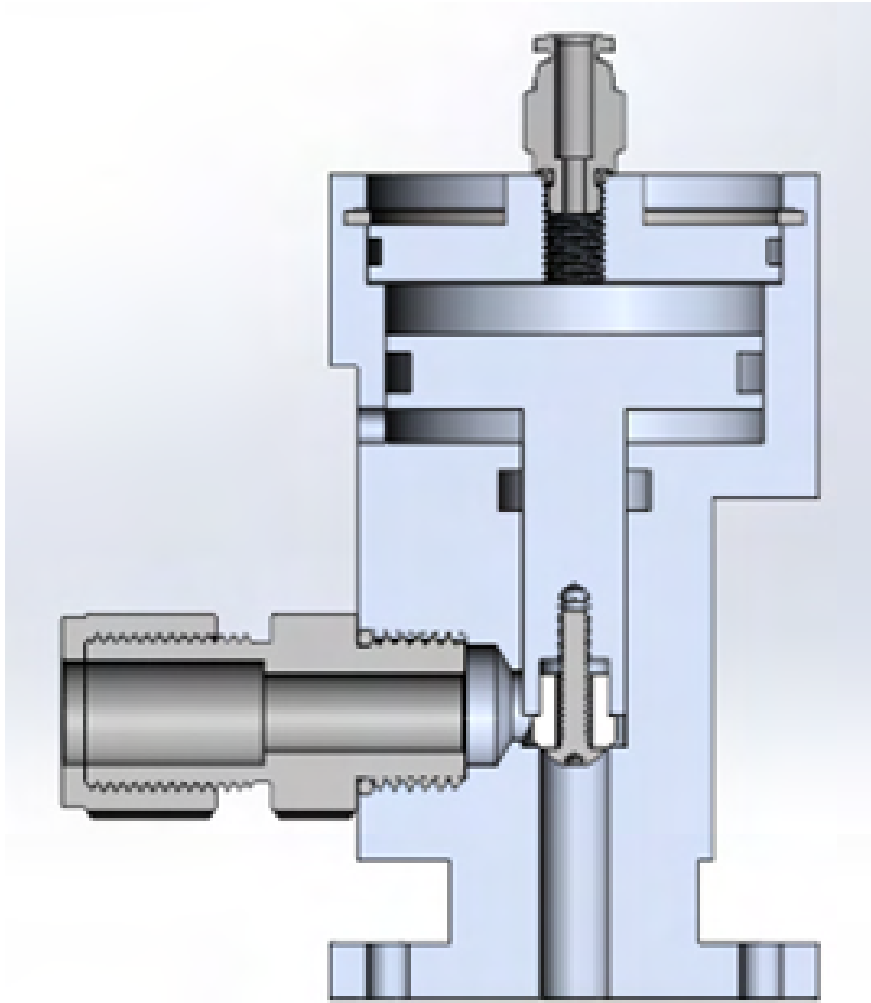


Figure 76: Cross section of the Fill/Dump Valve

This valve replaces the check valve which was present on Waterloo Rocketry's previous rockets, and means aborting and safing the rocket is now much faster - previously, the only way to drain the oxidizer tank without flowing through the combustion chamber was to wait for the nitrous oxide to boil off through the 2mm orifice in the vent valve, a process which has historically taken up to 1 hour. The inlet of the valve is on the left hand side, coming directly from the fill port that connects to the ground-side fill system, and the outlet of the valve is at the bottom as oriented in this figure. Pneumatic pressure enters from the top port, and pushes the valve stem down to close the valve. The outlet connection of the valve is a flanged connection that mounts directly to the fill bulkhead on the bottom of the tank, allowing it to be installed before the injector section is assembled and held securely in place during flight. The PTFE sealing tip of the stem is also designed to be replaceable so that damage to the seat does not require the entire stem to be remade. Currently, 2 spare seats have been machined, and at least one more will likely be made before competition. The valve was machined entirely by members of the team. the finished valve is shown in Figure 77.



Figure 77: Finished Fill/Dump Valve

The valve is pneumatically actuated given the presence of pneumatic systems already on the rocket, and the knowledge the team has developed in pneumatic SRAD valve design in recent years. The actuator is designed such that the pneumatic pressure provides 1.5x the force required to close the valve, which was the driving requirement for this design. This also means that the sealing force when the valve is closed is much higher than the sealing force of a passive check valve, which should eliminate the issue experienced in flight in 2023 where the check valve failed due to a combination of back pressure at the end of the burn and vibration. Additionally, the flow area of the valve is significantly larger than that of the Swagelok check valve used in 2023, which should make this valve more resistant to any FOD that manages to make it through the groundside filters, as much larger objects can pass through the valve compared to the check valve where even small pieces of debris would get caught at the stem and prevent sealing. The pressure force acting on the part of the seat exposed to fluid when the valve is closed valve stem is at least 1.5x the conservative O-ring running friction as calculated using the Parker O-ring handbook, so no biasing spring was needed to make this valve fail to the open state. This pressure force was calculated using the minimum pressure that has been observed immediately after tank fill at winter static fires, and is therefore the minimum nitrous vapour pressure that can be reasonably expected. The normally-open behaviour has been validated in hydrostatic tests, even under hose pressure (20 psi).

More details on the valve design can be found in the design report for the fill/dump valve, cited here: [11].

## 8.7 Vent Valve

The SRAD vent valve that will be used on Borealis is the same valve as was used on Leviathan of the Sky in 2023, and experienced no significant issues during the flight or ground test campaign leading up to it. The vent valve is a poppet-style pneumatically actuated valve, with a biasing spring that ensures it fails open. The SRAD vent valve has a 2mm orifice which allows nitrous

vapour to escape but restricts the flow enough for liquid to be filled into the oxidizer tank. A diptube is connected to the inlet of the vent valve and sized such that at least 15% ullage gas by volume will be maintained in the oxidizer tank. [12]

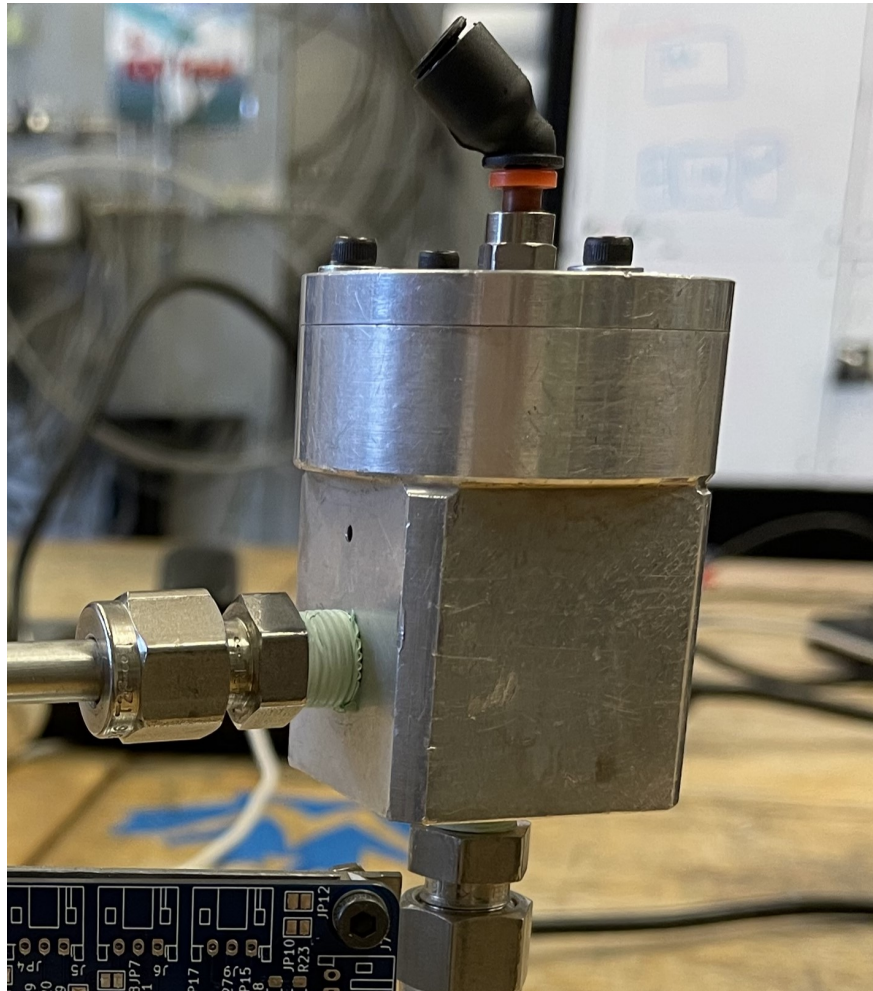


Figure 78: 2023 Vent Valve

## 8.8 Engine Testing

The Eridium rocket engine successfully completed 2 static fires this design cycle. The first static fire focused on the injectors and the engine ablatives, while the second static fire was a minor iteration on the combustion chamber and a test of the flight injector valves and flight tank configuration. The second static fire was the flight-like static fire, and will be the centerpoint of this discussion. Video of both tests can be found on the Waterloo Rocketry YouTube Channel: <https://www.youtube.com/@WaterlooRocketry>

### 8.8.1 Thrust Curve

The thrust curve for the burn is shown below in Figure 81. The three bursts at the end of the burn should be noted, which are consistent with loud popping seen in the video. It is suspected that

this was caused by the excess nitrous oxide that was loaded for this burn, allowing decomposition in the hot chamber after the burn. The large thrust spike at the start of the burn was expected, since a similar thrust profile occurred both on the 2023 hybrid and the first liquid static fire earlier in the year. While a small spike at the beginning of the burn is common in nitrous blowdown engines, it does not appear to be nearly as dramatic on most other amateur nitrous bi propellant rocket thrust curves that are available, suggesting that this is unique to the team's ignition system. Since this spike is consistent and predictable across all recent Waterloo Rocketry engines, it has been determined to not be of concern, and has mild benefits for off-rail stability.

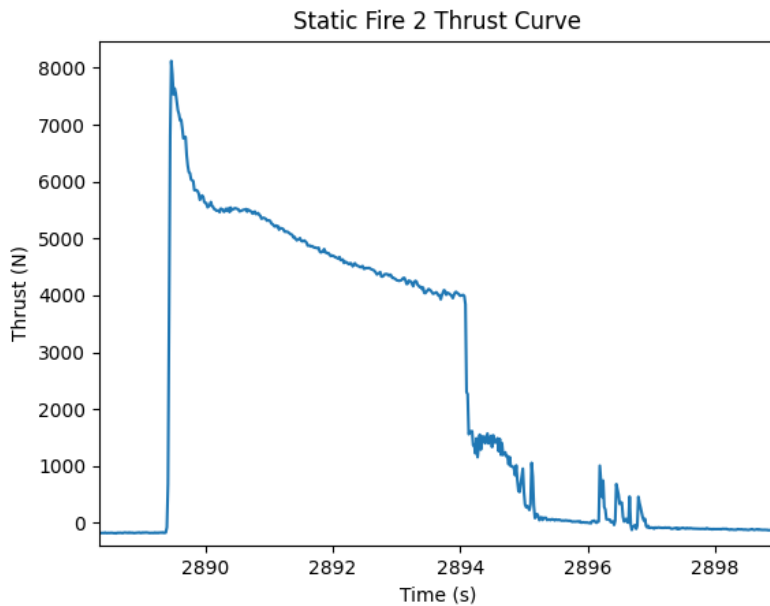


Figure 79: Flight Qualification Static Fire Thrust Curve

### 8.8.2 Pressure Data

Combustion chamber pressure, as well as both tank pressures are shown in Figure 80 below. This plot highlights a few interesting behaviors. Firstly, the transition from liquid nitrous oxide boiling to gaseous nitrous oxide blowdown is fairly obvious, and confirms that there was significant  $\text{N}_2\text{O}$  residuals. Additionally, it can be seen that there is a large injector pressure drop margin across the entire burn, which gives confidence that there is sufficient margin for slight performance differences. Finally, the fuel tank pressure data clearly shows the moment where the fuel tank piston bottoms out in the tank, as the pressure immediately drops. Interestingly, but not unexpectedly, from this point onwards the fuel tank pressure mirrors the combustion pressure. This means that the fuel is being compressed backwards in the injector, avoiding significant combustion gas ingestion into the fuel manifold. This is confirmed by the lack of soot inside this manifold, and the presence of fuel residuals when the feedline hose was disassembled. While this does leave an opportunity for fuel to drip out after the burn in flight, this has not caused a significant issue for other similar rocket engines.

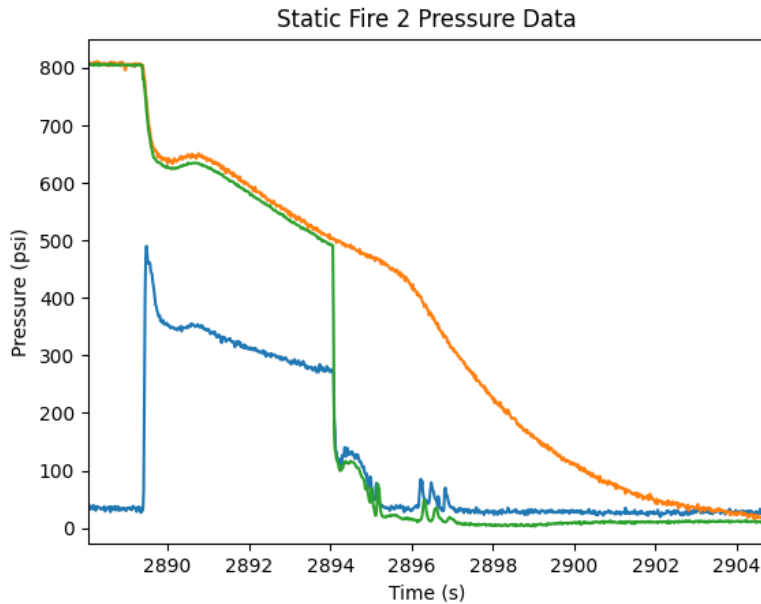


Figure 80: Flight Qualification Static Fire Pressure Data

### 8.8.3 Changes for Flight

There are a few minor differences between this static fire and the planned flight configuration. Firstly, the feedline lengths will be shorter. This should slightly reduce the pressure drop across the feedsystem, slightly improving performance. Additionally, the flight engine will not have a nitrogen purge after the burn. Other amateur liquid flights have demonstrated that the lack of a purge in flight is not a significant concern, with the prevailing theory being that the low pressure zone behind the rocket is more than sufficient to put out any residual burning. Finally, the propellant masses for flight are being altered to slightly increase the fuel load, while reducing the nitrous load. The effect of this can be seen in Figure 81. This should reduce the leftover liquid nitrous to just under half a second of excess, improving performance but not significantly changing the shutdown sequence from the verification burn. If this increases thermal loading significantly on the injectors, the first static fire demonstrated that even if the injectors were to melt after the burn, the engine will not be violently destroyed.

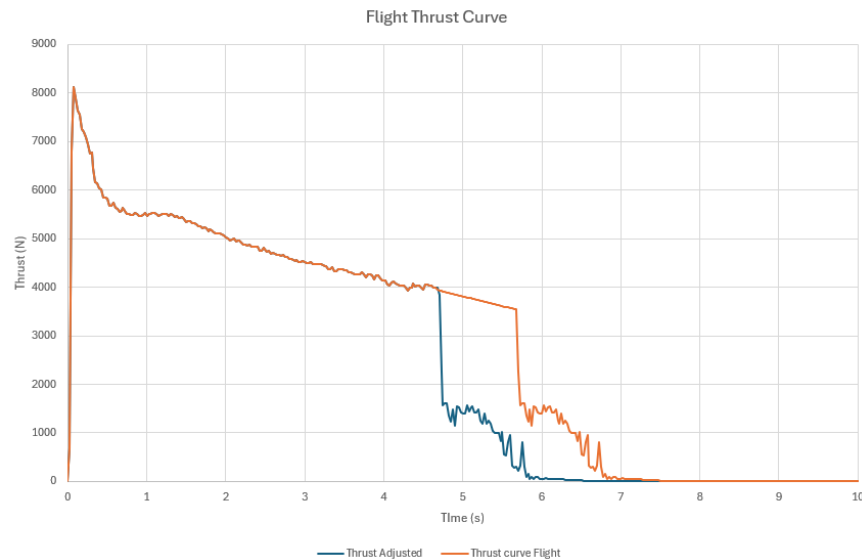


Figure 81: Flight vs Static Fire 2 Thrust Curves

## 9 AVIONICS AND TELEMETRY

The 2024 rocket's avionics system contains 3 main systems: the RocketCAN bus, two dissimilar COTS Altimeters, and an independent GPS tracking module from BigRedBee. The RocketCAN network consists of individual boards with single functionalities which communicate through a Controller Area Network (CAN) bus. This system was initially introduced in 2019 on Shark of the Sky (SotS), but has undergone significant updates since then, including new revisions of every board based on lessons learned throughout the previous years. In addition, this year, new systems have been introduced and upgraded including upgrade bit rate to 250 kbps, propulsion board for both data collection from sensors and actuation of solenoids, and a SRAD in-flight camera system.

Both avionics and Electrical Ground Support Equipment (EGESE) systems are summarized in Figure 82.

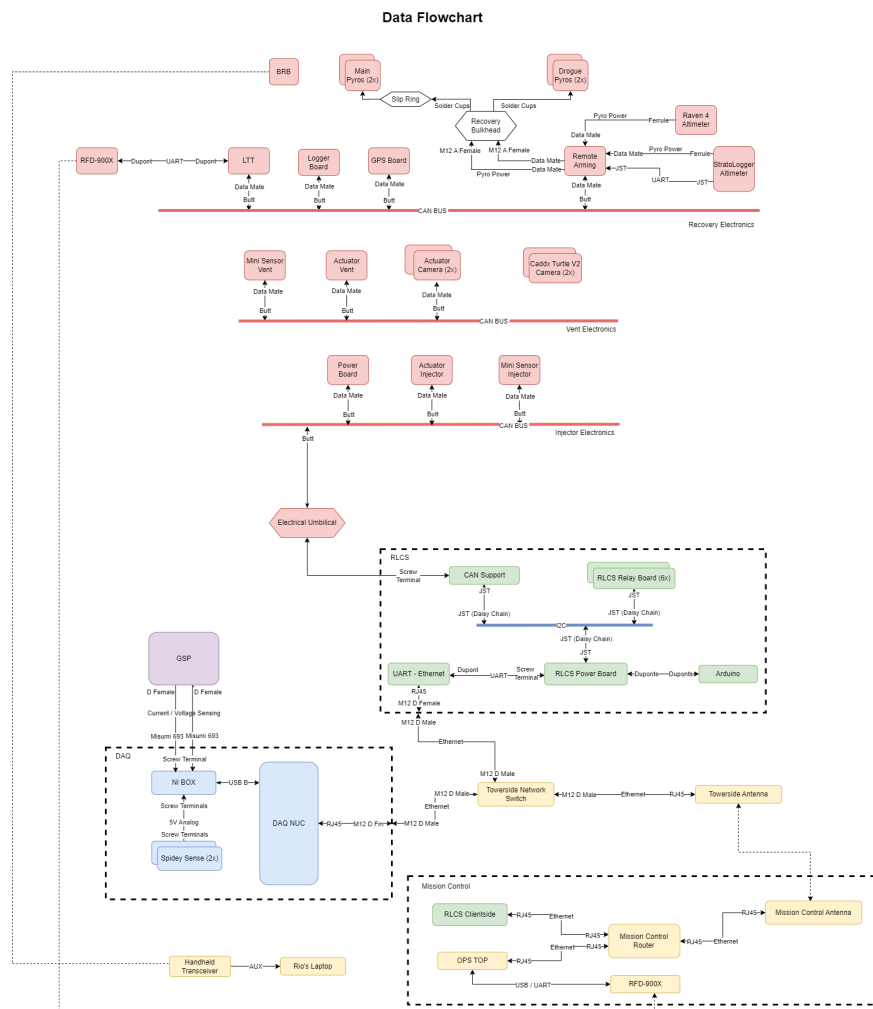


Figure 82: Block diagram of RocketCAN system and EGSE, showing the data flow between the various components

## 9.1 RocketCAN

The avionics modules on the rocket use a Controller Area Network (CAN) bus to communicate. The CAN protocol was primarily selected for its ruggedness; it has strong noise immunity and is suitable for safety-critical outdoor applications. Additionally, CAN is a democratized protocol. There is no bus 'master' or 'slave' and all boards have an equal opportunity to take control of the bus. This aids the fault tolerance of the system as any individual board can fail without affecting the rest of the bus. Each of the modules can send and receive messages independently using the bus. For example, the Live Telemetry Transmitter (LTT) board can send a message to the vent propulsion board to open the vent valve. This modular approach maximizes reliability and robustness and reduces coupling between the different avionics systems. Additionally, if any individual board fails it can quickly and easily be replaced with an identical spare copy. Table 15 gives an overview of the different avionics systems on the rocket.

Table 15: Summary of RocketCAN systems and locations

| System Name                | Location(s)                       | Description  |
|----------------------------|-----------------------------------|--|
| Propulsion Board           | Injector Section,<br>Vent Section | Used to control the pneumatic solenoids for actuating the SRAD injector, fill, and vent valves and power each flight camera. Furthermore, it is capable of measuring from a pressure transducer and thermistor, as well as an IMU and barometer. This is used to measure pressure in the combustion chamber, pneumatic lines, and oxidizer tank, as well as gather barometric and altitude data. |
| GPS Board                  | Recovery Electronics Bay          | Detects the GPS location of the rocket and relays it over the CAN bus.   |
| Live Telemetry Transmitter | Recovery Electronics Bay          | Sends and receives messages from the ground, relaying telemetry and commands to and from other systems on the CAN bus. It also controls and regulates power to the CAN bus, allowing the rest of the bus to be shut off to save power.   |
| Logger Board               | Recovery Electronics Bay          | Records all CAN messages to an SD card, including all telemetry and commands for post-flight analysis.   |
| SRAD Camera                | Vent Section (x2)                 | Records in-flight 360 degree video from the rocket. It is built around the OV5640 image sensor which provides 1080p/30fps. Records footage to an SD card.  |

|                 |   |   |
|-----------------|---|---|
| Remote Arming   | Recovery Electronics Bay                        | Allows for the redundant COTS recovery altimeters to be armed remotely via the CAN bus, as well as gathering comprehensive telemetry data about the recovery system to ensure correct operation.  |
| Charging Board  | Vent Section, Recovery Electronics Bay, Payload | Provides charging capabilities and status reporting for the rocket's LiPo battery. Prevents rocket battery drainage while on the pad and provides warnings concerning low rocket battery voltage levels. Also provides high current to the two onboard motors in the airbrakes and payload. |
| Processor Board | Recovery Electronics Bay                        | Takes in sensor data, estimates the state of the rocket, predicts the apogee of the rocket, and generate control commands for the airbrakes during flight. The board is also responsible for generating some CAN telemetry, including redundant GPS data and state estimates.               |
| Vibration Board | Payload   | Records acceleration data from a high bandwidth accelerometer on the board, and records temperature and flow data from the payload.   |

### 9.1.1 Bus Topology and Harness Design

To allow all the RocketCAN systems to communicate there is a harness that runs the length of the rocket, connecting the boards in a tree topology. The bus can be separated into multiple sections for disassembly and transport via in-line Harwin Gecko connectors, which are reconnected during final assembly.

Electrically, a CAN bus consists of a differential wire pair for communications connecting the modules together in a tree topology. Each end of the bus is terminated with a  $120\ \Omega$  resistor that ties the high and low lines together when they aren't driven. The RocketCAN implementation includes the CAN bus wire pair, a common ground line, and regulated +5VDC, unregulated +12VDC, and regulated +24VDC.

The harness is connected to each system using Harwin Datamate and Harwin Gecko connectors. These connectors, shown in Figure 84, along with the Gecko in-line connectors (Figure 89), were selected as they are shock resistant and can survive the intense mechanical vibrations experienced during flight thanks to their screw-locking mechanism. This has been confirmed through testing, including post-flight analysis of the electrical systems on LOTS and its predecessor, Shark of the Sky, which both had a high-g landing due to a failed main parachute.



Figure 83: Male (G125-FC10605F1-0150L) and female (G125-MC10605M1-0150L) gecko cable assemblies



Figure 84: Female Harwin Datamate connector assembly (M80-9410642) with a Male Harwin Datamate PCB mounted connector (M80-5400642) beside it

Since the harness is subject to high loads and wide temperature ranges, particularly the section of the harness which connects the vent and injector sections and runs along the outside of the oxidizer tank, the use of high-quality wire is critical. As such the CAN bus harness is made primarily from 6 conductor shielded cable with Tefzel jacketing, conforming to MIL-C-27500. This is connected to the COTS pre-crimped contacts provided by Harwin, which also use durable, high-temperature PTFE insulation. All connections are made using suitable butt splices and clear heat shrink complying with the LC DTEG safety-critical wiring guidelines.



Figure 85: Tefzel jacketed cable used for rocket harnessing (M27500-22TG6T14)

### 9.1.2 Common RocketCAN Hardware

Most RocketCAN boards are built around the PIC18F26K83 microcontroller (abbreviated as PIC18). The PIC18 is an 8-bit microcontroller running at 12 MHz selected for its low power draw, expansive I/O capabilities including CAN support, low price and high availability throughout worldwide chip shortages. Most of the RocketCAN boards do not perform any complicated processing that would require a larger or more powerful processor, allowing cost savings and simpler embedded code. Some boards such as Camera Board and Processor Board that need to handle a large amount of data use a 32-bit microcontroller from the STM32H7 series, selected for its higher clock speed and data bandwidth.

The PIC18 microcontrollers are wired up very similarly across all RocketCAN boards. The MCLR, ICSPDAT and ICSPCLK wires connect to the PICKit3 programmer used to load code onto the boards. OSC1 and OSC2 connect to an external 12 MHz crystal oscillator. CAN\_RX and CAN\_TX connect to a CAN transceiver such as the MCP2562. Lastly, a number of debugging LEDs are included which will often show board status or a heartbeat indicating the board is alive and well.

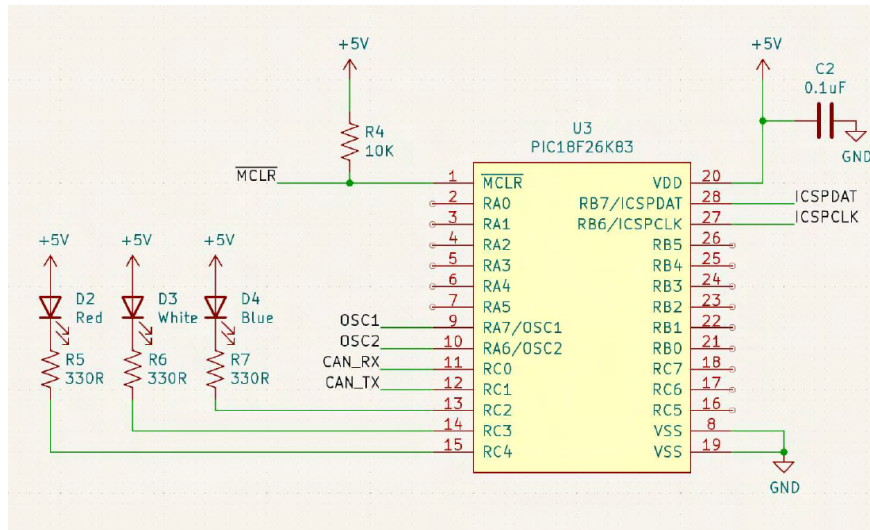


Figure 86: Schematic of Standard PIC18F26K83 Connections

Another common fixture on RocketCAN boards is the CAN transceiver. This is a chip that is responsible for converting the differential CANH and CANL signals into digital CAN\_TX and CAN\_RX signals. The MCP2562 was selected for this purpose due to its ease of use and price. Additionally, drop-in replacements are available should availability become a concern due to ongoing shortages.

The boards are programmed using a PICKit3 which can also act as an in-circuit debugger. It requires three lines to be connected to the microcontroller: MCLR, ICSPDAT and ICSPCLK. These lines along with power and ground are broken out to a Dupont connector placed on each board for ease of programming.

The last feature common across all RocketCAN boards is the CAN connector and power circuitry. Each board is equipped with a current sensing resistor on the +5 V line which allows it to measure and report how much current it is drawing. The voltage drop across the resistor is

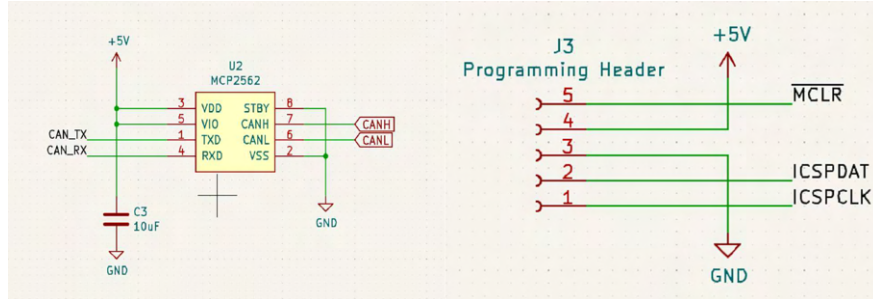


Figure 87: Schematic of the MCP2562 CAN transceiver and PICKit3 programming header schematic

amplified by an INA180 current-sense amplifier and measured by the microcontroller using its internal analog-to-digital converter. This in combination with a polyfuse allows boards to detect and appropriately react to an internal fault.

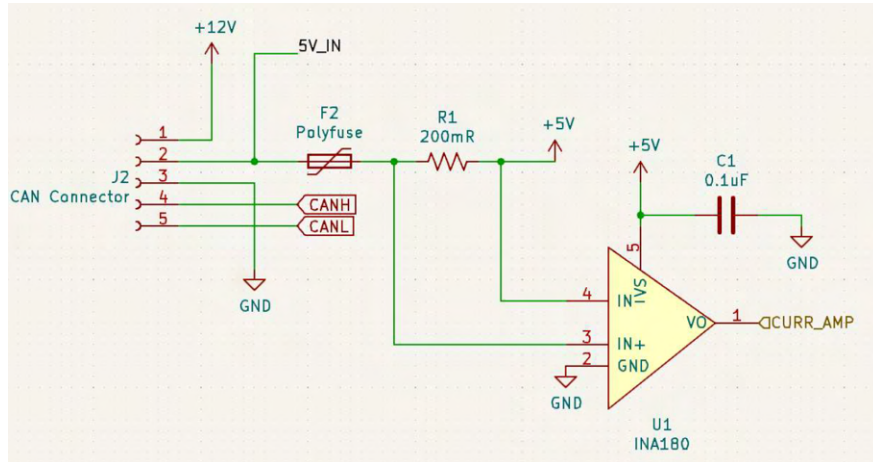


Figure 88: CAN Connector and Current Sensing Schematic

### 9.1.3 Common RocketCAN Software

To handle the intricacies of CAN and ensure a common set of message types, board IDs, and data field formats, all RocketCAN boards use a shared library known as canlib to interface with the CAN bus. Canlib provides functions to build and inspect the various CAN message types, ensuring the format of the data field is well-defined, and abstracts over the specific CAN hardware used which allows its use on the various microcontrollers in the system.

All boards on the CAN bus must fail safely, and the software is an important factor in this. Each board periodically produces a nominal status message to indicate that it is still online and functioning correctly. If any of the internal error checks on a board fails the status message will be replaced with an error message indicating the error detected, which will be relayed to the operator over the live telemetry system. Additionally, safety-critical boards will automatically go into an appropriate safe state if an error is detected. For example, if the vent propulsion board detects

a critically low battery voltage, it will send a low battery warning and open the vent valve in order to safe the rocket. The nature of the safe mode depends on the function of each board, but it is generally a state which will minimize hazards to both the rocket and the human operators. The democratized nature of the CAN bus system means that if any of the boards suddenly stops functioning, the bus will remain online and the other boards on the bus can continue functioning normally.

#### 9.1.4 Message Format and Arbitration

RocketCAN uses the standard CAN 2.0A message format, on top of which the RocketCAN message system has been designed. An example of a standard CAN message is shown in the figure below.

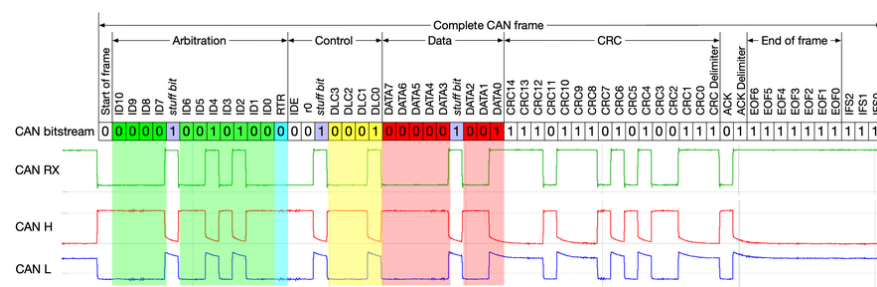


Figure 89: Example CAN Message

The key fields in the CAN message are the Arbitration, Data, and CRC bits. The CRC, or Cyclic Redundancy Check, is built into the CAN hardware, and provides robust error detection for each message, ensuring no false data or commands are read, without the need for any software. The data field of a CAN message can be up to 8 bytes long and is what carries the information in each message. The 11 arbitration bits are used to determine the priority level of a message, with all zeros being the highest priority, and all ones being the lowest. RocketCAN splits these bits into two further fields, the board ID and message type. The first six bits are the message type, these are the more significant bits with respect to priority which ensures that higher priority messages (such as valve commands) are selected to be sent over lower priority ones. The lower 5 bits are used to determine which board is sending the message, this is a convenient place to store this information and has the added benefit of breaking message ties by prioritizing more important boards such as remote arming or propulsion board.

### 9.1.5 Telemetry Architecture

The primary method of communication between the rocket and mission control is the live telemetry system. Telemetry data sent on the RocketCAN (such as position from GPS board and acceleration from Processor) are serialized by the Live Telemetry Transmitter (LTT) board as a UART stream and sent to mission control through the RFD900x radio modem and SRAD antenna. In the other directions, LTT deserializes commands from mission control into CAN messages where they can be processed by all boards on the RocketCAN bus. The RFD900x modem was selected for its long range and ease of use as a transparent UART link over radio. It operates on the 900MHz band and has transmit power up to 1 watt.

An SRAD antenna is used on the rocket side of communication. It is made by routing long traces on a PCB as two orthogonal dipoles, with dimensions designed to fit into the body tube horizontally. This approach allows the antenna to lay flat inside the rocket, reducing the vertical space required. The two traces are connected to the RFD900x modem individually; the trace with the best received signal is automatically selected for communication. This eliminates blind spots in the radiation pattern, allowing radio communication from any direction regardless of the orientation. The antenna is shown in Figure 90.

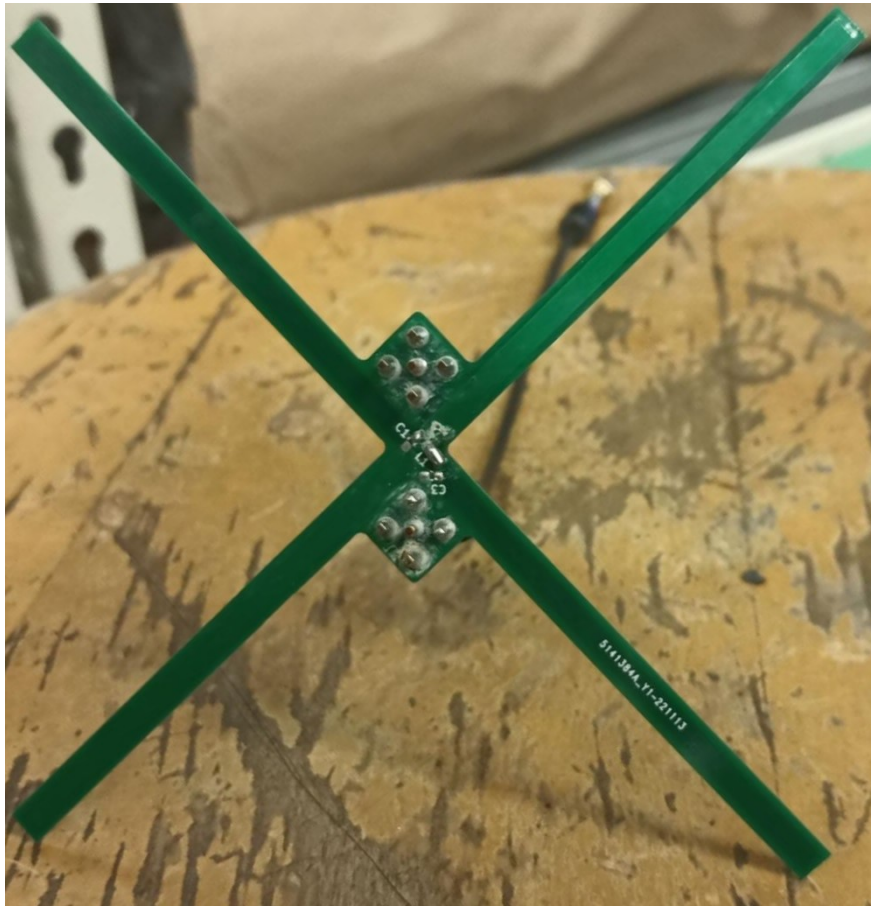


Figure 90: PCB Trace Antenna on Rocket Side

On mission control side, two antennae are used. During flight, the communication is done through a SRAD helical antenna. This helical antenna is made from light-weight fibreglass, making it easy to move around by hand and aim. Furthermore, its circular polarization helps it maintain connection even when the rocket is spinning. When the rocket is on the pad or has landed, a high-gain COTS Yagi antenna is used in parallel to improve reliability.

The ground systems communicate with mission control via a pair of Ubiquiti Litebeam 5AC Gen2 antennas which provide a high-bandwidth Ethernet link. These antennas, installed on taller towers to further improve signal quality and reliability, have been validated at the 2023 SAC. DAQ and RLCS both connect to a router located at the tower which then forwards the data over the antenna link.

Additionally, while the rocket is on the pad the ground antennas act as a backup line of communication via the electrical umbilical. The rocket's main CAN bus lines are routed through the umbilical to the DAQ system, which contains a board that can transmit and receive CAN messages over a USB connection. This data stream is then passed over the ground radio link along with the usual data from DAQ and RLCS. Because the electrical umbilical disconnects after liftoff this backup link is fully sufficient to launch the rocket in the event of a live telemetry failure.

### 9.1.6 Power Architecture

The RocketCAN bus is powered by a single 3S 2200mAh lithium polymer battery. The battery is connected through the charging board, which controls power to the rest of the CAN bus in the form of both an always-on, fused but unregulated 12V line directly from the battery for higher power systems such as actuators, and a buck converter that steps down the battery voltage to a stable 5 V which is used to operate the microcontrollers and other digital electronics on the bus. The buck converter delivers up to 2 A of current and is equipped with overcurrent protection. Furthermore, every board on the RocketCAN bus is guarded by a polyfuse, which will automatically disconnect that board from the bus if it has a short circuit. This ensures that an electrical fault on any one of the boards will not affect the operation of the RocketCAN bus as a whole.

Additionally, a backup source of power is provided through the electrical umbilical from the Ground Side Power Distribution system. This system ensures the rocket's batteries will be fully charged until personnel leave the pad, and ideally until the moment of takeoff. However, all power budgets have been designed with a worst-case scenario of the electrical umbilical disconnecting immediately after personnel leave the pad for fill operations.

Since the rocket must be able to sit for multiple hours on the pad waiting for an opportunity to launch, a long battery life is critical. To allow this charging board can shut down the rest of the CAN bus and enter a hibernation mode to conserve battery power. In addition, the cameras, which draw the most power of any system, can be individually shut down to conserve power while the rest of RocketCAN is in operation. Table 16 shows the power consumption. All of the values have been found experimentally to ensure accuracy.

Table 16: CAN Bus Power Consumption

| System         | Quantity | Active Power Draw |
|----------------|----------|-------------------|
| Charging       | 1        | 300 mW            |
| Live Telemetry | 1        | 5260 mW           |
| Actuator       | 2        | 530 mW            |
| Remote Arming  | 1        | 950 mW            |
| Camera         | 2        | 3000 mW           |
| Mini Sensor    | 2        | 170 mW            |
| Logger         | 1        | 180 mW            |
| GPS            | 1        | 300 mW            |

Based on the power draw, the expected power schedule during operations is summarized in the below table. These calculations were performed assuming the rated 24.42 Wh of the 3S lipo battery, and for the remote arming system (which is powered by a pair of 9V batteries) 4 Wh per

battery. The expected battery life for RocketCAN as well as the other electrical systems on the rocket are shown.

Table 17: CAN Bus Power Schedule

| Operational Phase          | Duration | RocketCAN          | Recovery Electronics | Big Red Bee |
|----------------------------|----------|--------------------|----------------------|-------------|
| Final integration          | 3 hours  | 0.6 Wh             | Off                  | Off         |
| Waiting for launch         | 6 hours  | -0.6 Wh (charging) | 1.38 Wh              | 6 hours     |
| Fill operations and flight | 1 hour   | 8.95 Wh            | 0.95 Wh              | 1 hour      |
| Total Usage                |          | 8.95 Wh            | 2.33 Wh              | 7 hours     |
| Remaining Margin           |          | 15.47 Wh           | 1.77 Wh              | 3+ hours    |

## 9.2 Charging Board

Charging board is the SRAD PCB responsible for power distribution on the rocket and on-board motor control. The previous iteration of this board was designed solely to distribute power and charge batteries, motivated by issues the team had in 2022 with batteries discharging while waiting to launch. However, with two servos on board this year, it was determined that all the boards should still be capable of charging batteries while also playing the role of either power distribution or motor control. Both airbrakes and the cubesat payload will have their own copy of charging board. There will also be a main power supply board, totalling to three copies of charging board on the rocket.

Power is supplied to the rocket through a external quick-disconnect connector that receives 24V from two car batteries. The 24V line runs to the power copy of the board, which converts the 24V to 12V and 5V rails, providing power to the other circuit boards. It also charges the on-board 3s LiPos while the rocket is on the pad. The board also has a redundant tethered CAN communication connection to the Remote Launch Control System (RLCS). In the case of a Live Telemetry failure, this CAN connection ensures that the rocket can still fill, pressurize, ignite, and take off successfully. The motor control copies charge their own batteries directly from the 24V line, skipping the 24V to 12V circuit conversion. Both motors are controlled via PWM, but the airbrakes draw power directly from its battery, while the payload motor runs from the 5V line.

The key design requirement for this board was that it must be "hot-swappable." While the motor control boards do not use the voltage regulator circuit and the power board does not use the motor control circuit, each copy of the board must have both circuits functioning nominally. The difference between the circuits of each type of charging board is a set of jumpers, making it easy to switch from one board to another. This requirement was intended to make debugging easier, as rather than switching boards or fabricating a new board of the required type, one could swap some jumpers and have a different copy of the board to test. The firmware can stay the same between boards (as much of the system initialization would be identical), and if statements and macros could be used for the parts of the code that are unique.

Since the motor control copies of this board were built to support airbrakes and payload, it is worth discussing the requirements of those sections in relation to this board. Payload's motor control is relatively simple: when they send a command to turn on their motor, the board is to supply power and output a PWM signal of a predetermined pulse width to their motor.

Airbrakes' requirements were significantly more complicated due to the sensitive nature of extending panels out of a rocket during flight. The airbrakes are not to be extended while the rocket is on the rail (as one panel extends directly into the rail, this would be catastrophic) and are not to be extended during the engine's boost phase to remain in compliance with DTEG R7.4.1. They are also not to be extended at apogee due to the concern of the parachute cords getting tangled in, or worse, getting cut by, the panels. While much of this is accounted for internally by processor board, charging board firmware has its own internal timer restricting power to the motor. This redundancy is for the sake of safety. When the rocket is coasting, charging board enables power to the motor and takes analog command inputs from processor board over CAN, controlling the motor accordingly. The message is in the form of an integer from 1 to 100, which is to be interpreted as a percentage extension. The board then converts this to a pulse width for the PWM signal it outputs to the motor.

The schematics for this board are available in Appendix C

### 9.3 Propulsion Board

Propulsion board is responsible for controlling the liquid engine valves and making sensor readings. It combines the functionality of the previous actuator board and mini-sensor board from last year's rocket. The two boards were merged into one for the sake of simplicity; as there is no longer a need to design, assemble and write firmware for the two boards separately.

#### 9.3.1 Actuators

Propulsion board now operates up to three valves for the liquid engine, up from two from the previous actuator board (See Figure 91). They are all designed to be fail low, meaning that in the case of under-voltage, the solenoid will fail open for vent and fill-dump valve and fail closed for injector valve. Then, the solenoid is ported to achieve the desired fail state of the valve. This prevents a premature actuation and buildup of pressure. This was achieved by utilising N-channel MOSFET in a low-side-switching configuration, since it is both simple and reliable. A flyback diode is also added to prevent voltage spikes from inductive loads. Another of the same shock-resistant Harwin Datamate connectors was used on the CAN bus to connect the three valves to the board.

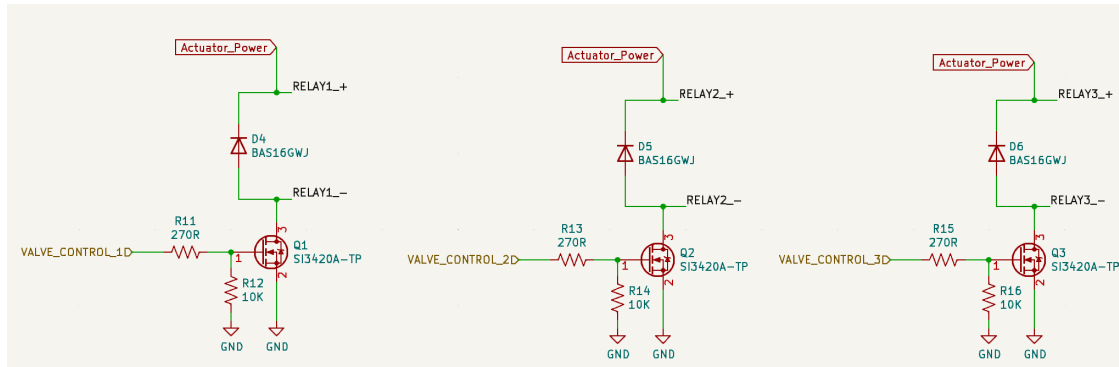


Figure 91: Propulsion Board Actuator Circuit

In addition, a safe-state mode for the actuators was implemented via firmware. The safe-state operation would turn on in the event of battery undervoltage, or if the board had not received a CAN bus command for five seconds. This would then lead to each actuator entering a predefined state.

The board was equipped with a PCA9536DR I/O expander IC. This provides the ability for the actuator output state not to be changed while the PIC18 MCU is undergoing a watchdog timer triggered reset, this allows for the actuators to be open and closed through the PIC18's I2C interface.

All these features were tested were extensively tested with hardware. A USB CAN debugger was used to send and receive actuator messages. Probing the board with an oscilloscope allowed us to confirm whether the CAN and I2C lines were working . On board LEDs signified whether the actuators were open, closed, or in their safe-state. Lastly, by shorting the CAN lines or lowering the board voltage via a power supply, the safe-state behaviour was demonstrated to be valid.

### 9.3.2 Sensors

Propulsion board contains a barometric pressure and temperature sensor (See Figure 92) and six connection points for external thermistors, hall sensors, and pressure transducers (See Figure 93). The barometric pressure and temperature sensor measures both the atmospheric pressure and temperature, they are useful for determining the altitude of the rocket as well as for characterizing the thermal conditions experienced by the rocket during flight. For the external thermistors and pressure transducers, they are responsible for generating data that characterize the performance of the engine during flight. The hall sensors measure the magnetic field produced by the valves in the pressure transducers. This allows us to accurately determine the valve position and deduce whether the pressure tranducers are behaving normally. No IMU was placed on propulsion board, as an IMU was placed on processor board instead.

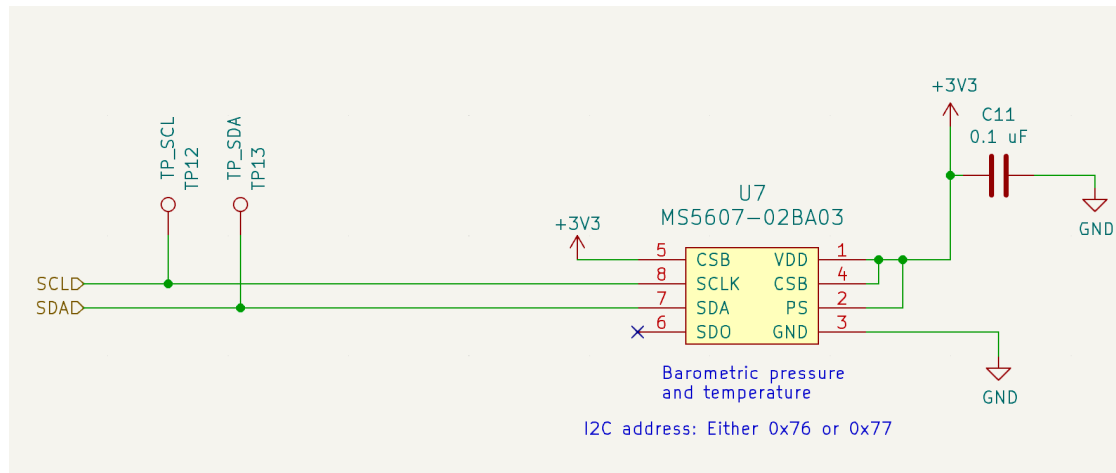


Figure 92: Propulsion Board Barometric Pressure and Temperature Sensor

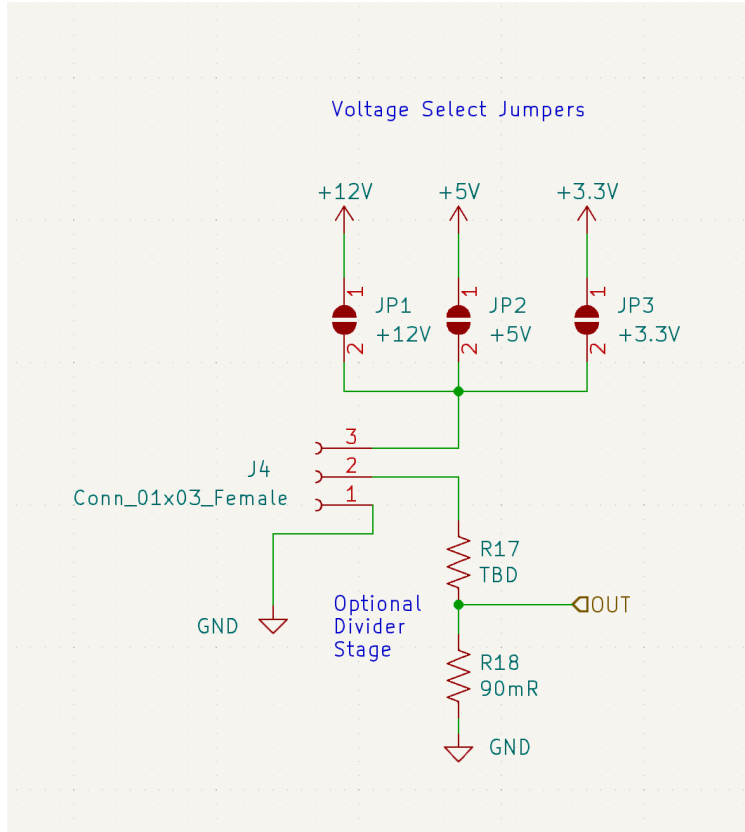


Figure 93: Propulsion Board Connection Points for External Analog Sensors

Once again, a CAN USB debugger was used to receive the values from the sensors, as well as the board's voltage and current levels. This allows easy verification of the sensor's nominal values, and whether the sensors are functional.

#### 9.4 GPS Board

With the use of an M10578-A2 GPS receiver, the GPS board locates the rocket in space and transmits this data over the CAN bus. This data is transmitted through the live telemetry system to provide a secondary method of tracking the rocket and is also stored by Logger Board to provide valuable flight data to be analyzed later. Because the GPS receives an RF signal, care was taken to match the impedance of the trace to the antenna. The maximum possible width and shortest allowable path was given, and all high-speed signals were kept away from the trace without compromising their own shortest possible path. The ground plane was also connected through vias to give as short a path as possible for the return path and to relieve any thermal concerns.

Because the GPS module can take up to 30 seconds to obtain a fix on its position when starting up from a cold state, the ability to power the GPS from an external battery was added to this board. Two diodes allow the module to be independently and redundantly powered from either the auxiliary battery or the CAN bus 5 V line. This allows the GPS module to be powered on before the rest of the RocketCAN bus to ensure a timely fix. In the event of a dead auxiliary battery both the battery voltage and GPS fix state are both reported over the CAN bus so operators can

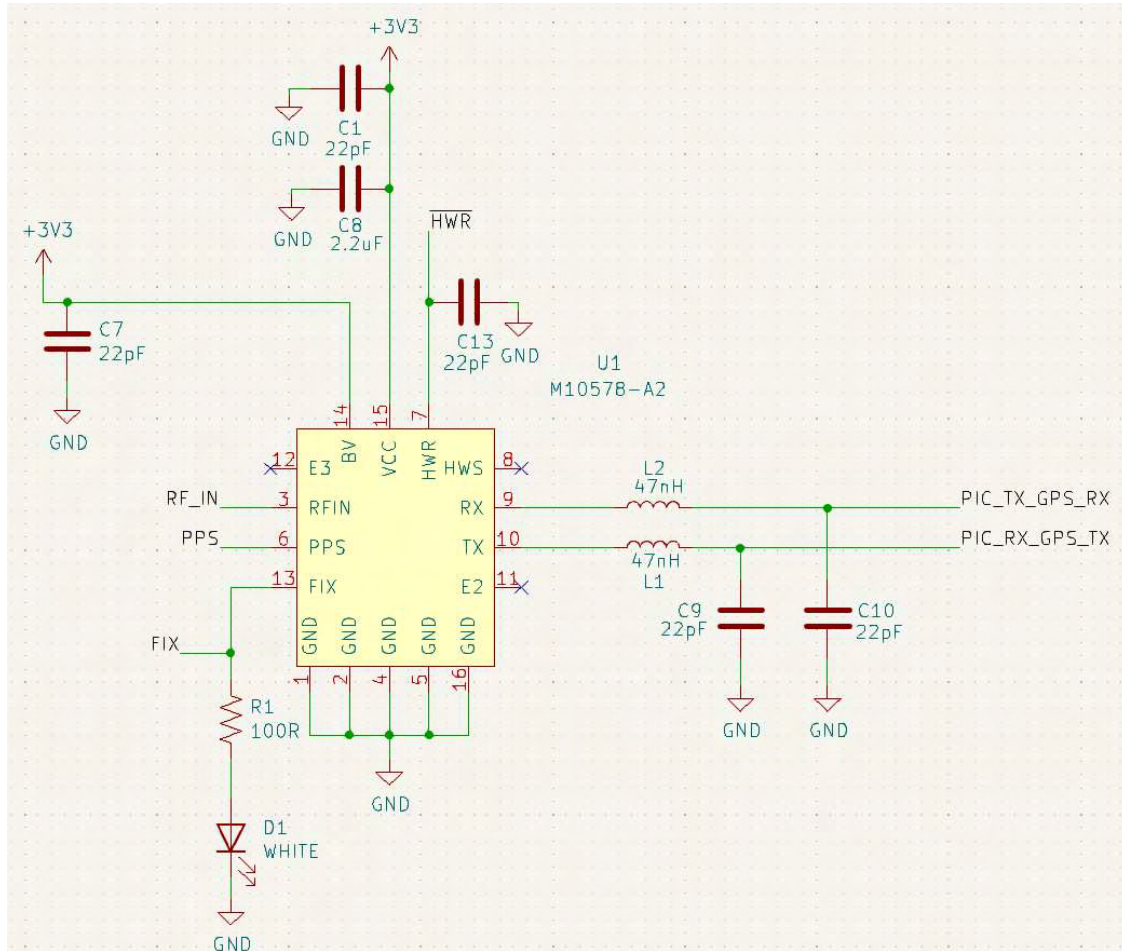


Figure 94: GPS Connections Schematic

replace the battery or delay until a fix is achieved. However, in order to save on the mass of an auxiliary battery, it was decided that the longer start-up time to achieve a fix was acceptable and an additional battery will not be flown.

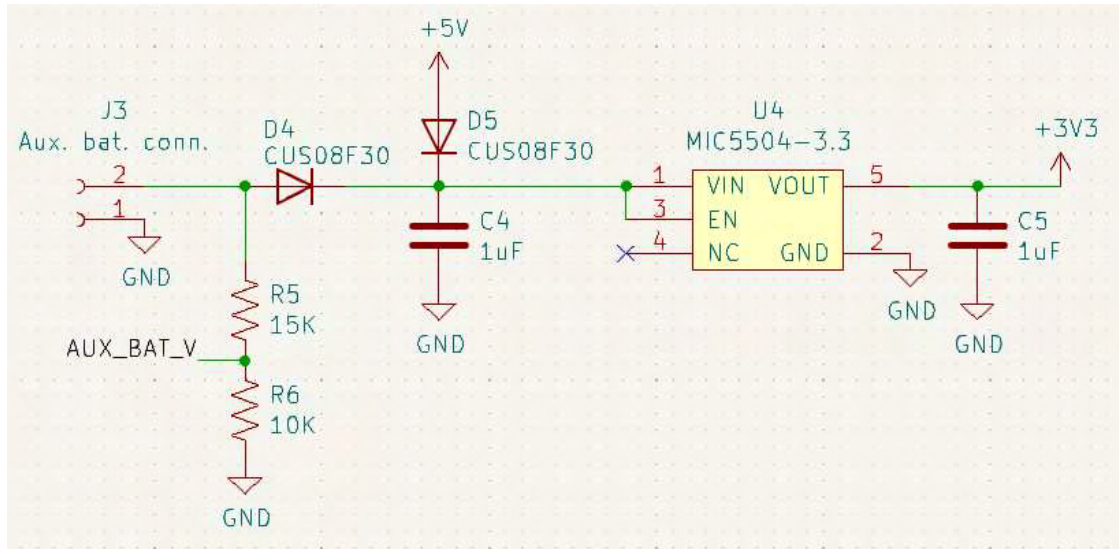


Figure 95: GPS Power Supply Schematic

## 9.5 Live Telemetry Transmitter

The purpose of the Live Telemetry Transmitter (LTT) is to act as a two-way CAN to UART converter between the RocketCAN bus and the radio modem as described section 9.5. The board uses 12V as its power source. A DC-DC switching regulator steps 12V down to 5V to supply the radio modem, and a linear regulator produces 3.3V from 5V to supply the PIC18LF26K83 microcontroller. This way, LTT can remain powered up and communicating with mission control while the 5V line on RocketCAN is turned off to conserve power. In addition, power to the radio module can be switched off or reset by the microcontroller, either manually through hard wired RLCS CAN connection or automatically through a timeout timer in the code.

The CAN messages are serialized into ASCII messages consisting of hexadecimal digits and separators. Each serialized message has a CRC8 code attached to ensure the integrity of data. This can prevent cases such as single bit error turning a "close injector" command into an "open injector" command, launching the rocket. While ASCII is not the most optimal format to transfer data in terms of bandwidth, a human readable format makes verifying the radio communication much easier using a FTDI cable and serial terminal. There is enough bandwidth over radio to accommodate for the overhead.

## 9.6 Camera/Logger Board

### 9.6.1 Scope

Camera board is responsible for recording in-flight 360 degree video from the rocket. It is built around the OV5640 image sensor which provides JPEG frames to the onboard STM32H750 mi-

crocontroller at 1080p/30fps. The board includes an SD card for storing footage, a USB port to upload footage to a computer, and a connection to the RocketCAN bus for control. The board is designed to be as compact as possible, measuring only 30x45 mm, and includes geometry to mount the image sensor and lens for easy integration. Due to limited bandwidth on the CAN bus and telemetry connection, streaming live video is not a goal of this board.

Additionally, the fast processor and SD card on camera board also allows it to be used to log all messages on the CAN bus for post-flight review. In this configuration the image sensor is not connected to the board, and RocketCAN data is instead logged to the SD card. Electrically these two modes are identical, with the only difference being what firmware is flashed to the board.

Last year, the team used COTS FPV camera modules for in-flight video, but they were not well suited for integration into a rocket. They were bulky, consisting of separate camera and recording PCBs, and drew a significant amount of power. This power draw also caused thermal concerns, which forced the inclusion of heavy copper heatsinks to prevent the cameras from overheating when being out in the sun. Lastly, there was no easy way to control or check the status of the cameras, power was simply switched via an SRAD PCB to turn them on or off. This year's design is intended to address all of these issues. By building an application-specific PCB, power draw from extraneous features is removed, and the addition of a CAN connector and custom firmware will let allow direct command and health checks of the camera module over the rocket's telemetry connection.

### 9.6.2 Electrical Design

Camera board draws from the high-power unregulated +12V line of RocketCAN so as to not put undue load on the regulated +5V line. It includes an onboard buck converter to produce a 2.8V logic level power, and a 1.5V linear dropout regulator to provide power to the image sensor. In order to conserve power when not in use, both 2.8V and 1.5V power to the image sensor can be cut off through the use of a power switch IC. Camera board is also intended to be usable as a ground camera to record static fires and launches, and as such can also be powered with 5V from its USB connector.

The STM32H750 microcontroller was chosen for its hardware peripheral support of digital cameras, SD cards, CAN and USB. These peripherals made the remainder of the electrical design simply a matter of connecting the signals from the image sensor, SD card, CAN transceiver and USB connector to their respective pins on the microcontroller. The microcontroller also supports direct memory access for both the camera and SD card peripherals which allows for high bandwidth data transfers as required by real-time video recording.

The OV5640 image sensor was selected primarily for its built-in JPEG compression engine. This greatly reduces the bandwidth required to transmit and store real-time video, thus increasing the possible resolutions and frame rates. The module supports both high-resolution 1080p/30fps and high-speed 240p/120fps, along with other configurations in between. Due to the compression engine this should only require approximately 12 MB/s of data transfer, which should be within the capabilities of the microcontroller and SD card. Lastly, the module is also widely available and fairly cheap, costing about \$20 CAD from online retailers.

## 9.7 BigRedBee GPS

Borealis, in addition to having a custom GPS on board, will also have a commercial BigRedBee GPS. This board will be stored in a mount in the nosecone and have its own independent power supply. In 2022, the team had considerable difficulty with this battery depleting for the duration it was plugged in. In 2023, the chosen mitigation involved charging the BigRedBee through the nosecone tip and shear pin coupler, which was successful but difficult to work with and required constant contact between the two outer metal surfaces. For Borealis, it was decided to arm and charge via a screw switch in the nosecone surface. Before installation, the BigRedBee will be installed into a mount and connected electrically to a screw switch and a dupont connector underneath the screw switch. The BigRedBee is then armed with a #6-32 screw to the outside, or charged by feeding a solid core wire through a #6-32 which connects to ground, and the #6-32 connects to the positive terminal of the battery. This configuration allows arming and charging of the BigRedBee through only a #6-32 hole in the nosecone, preserving surface finish and accessibility. The mount is partially bonded into the nosecone, and the two mount halves are fastened with double sided tape and two axial M3 screws. This mounting solution was validated at IREC 2023 and Launch Canada 2023. If the charging solution fails, the team is able to fly without BigRedBee charging, but will have to unpack the nosecone for every attempt at flight to keep the BigRedBee charged.

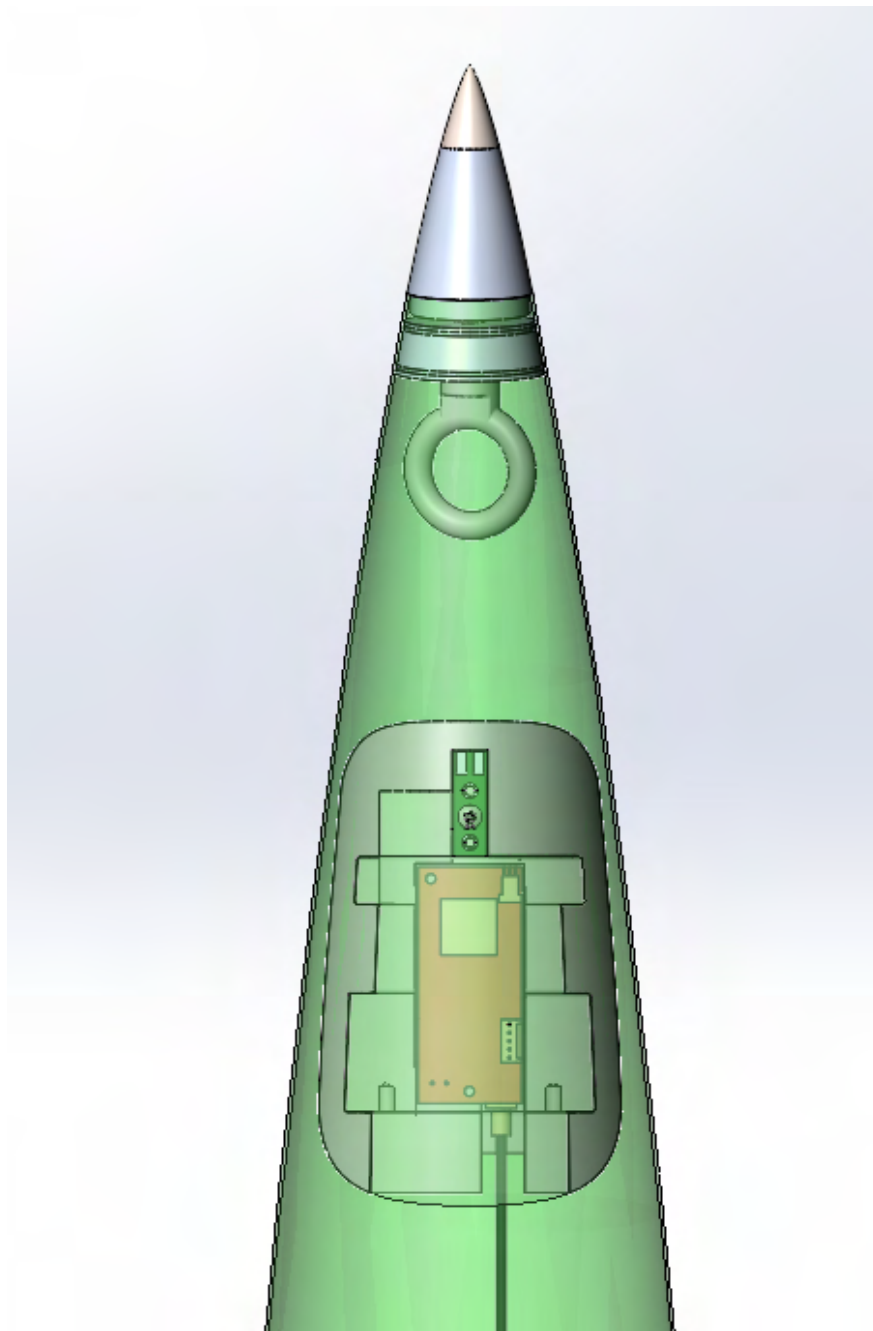


Figure 96: The BigRedBee Mount in the Nosecone

## 10 RECOVERY SYSTEM

### 10.1 Overview

The recovery system under development is a continuation of the past two attempts to successfully recover a reefed parachute system. The recovery system is a two stage reefing descent system. The single reefing parachute, released at apogee, acts as a drogue while reefed and as a main after disreefing at 457 m (1500 ft) AGL as in Figure 97. There is additionally a small, loosely-packed pilot parachute attached to the vent of the main chute that serves to pull the parachute bag and rigging out of the rocket, before then pulling the parachute out of the bag. This is a change from last years bag-first deployment, which deployed the parachute from the bag prior to stretching the lines. Additionally, after a tangling failure observed on the previous flight test, the disreefing pyrocutter are have been moved from the top of the shock chord and are now sewn into the canopy. These changes follow investigation and adaptation from past failures, elaborated on in section 10.4

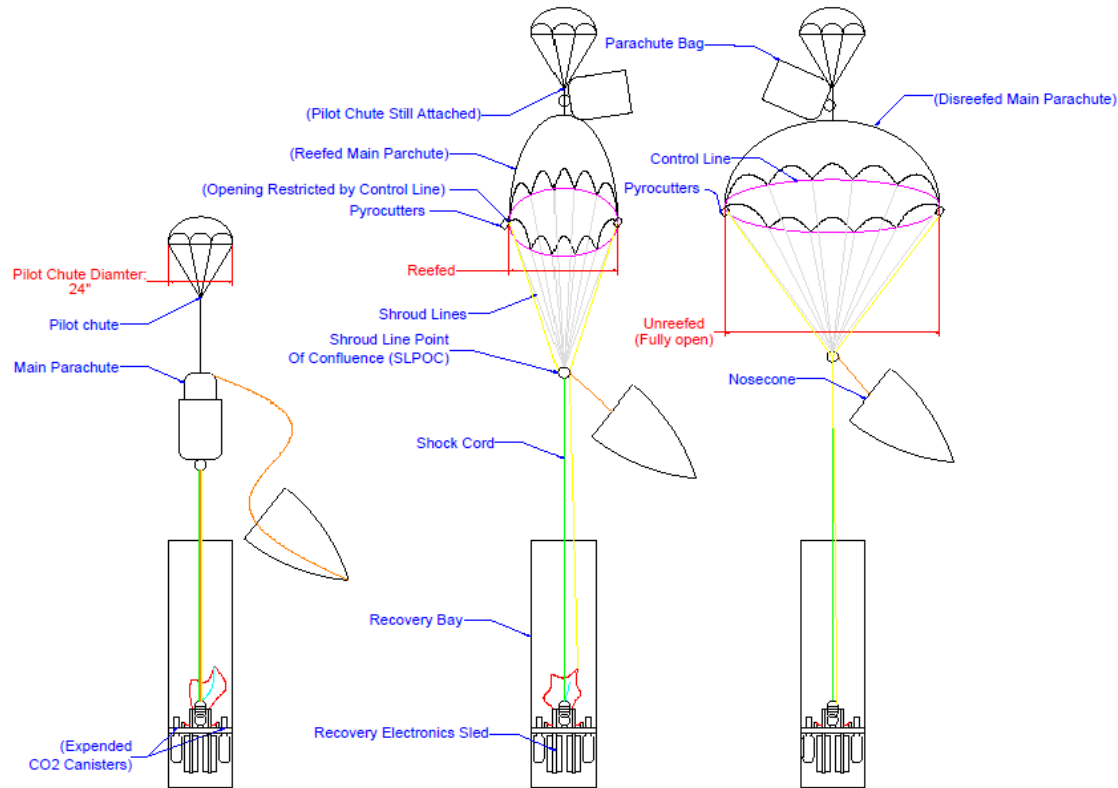


Figure 97: Deployment Architecture

## 10.2 Reefing Design

The design of the reefing system is similar to the one outlined by Sadeck and Lee in their paper in the Journal of Aircraft [13]. It uses a single prescribed-length control line that passes through rings sewn into the skirt. The length of this line is taken from a line length to drag area curve that is to be generated over the course of testing, as suggested by Knacke [14]. By shortening the control line, the parachute can be reefed in, reducing coefficient of drag. This control line is then able to be cut on-command, disreefing the parachute, inflating it back to the full size and drag.

The reefing control line (or control line) is cut via custom designed pyrocutters, which are sewn into the skirt of the parachute, and actuated via long wires that run down to the rocket.

Previous years parachutes have used large metal rings at the bottom of the parachute. This year, a new light-weight grommet ring version was created to reduce weight and increase packing ease. The control line passes through a grommet at the base of each gore on the parachute, allowing for a point to reef the parachute inwards.

This reefing design depends on the generation of the line length to drag area curve mentioned above. Over the years of developing this reefing system, a reliable and repeatable methodology for developing this curve has been developed by pulling the parachute at various reefing ratios around a test track. Code has been written to allow the team to analyze the data and size the parachute to the specified coefficient of drag. This methodology was used to size all three previous flights, and although those flights had some tangling issues preventing us from completely validating this testing method, both flights had a <30% error on main descent rate.

## 10.3 Physical Design

The recovery section consists of the parachute bay and the recovery electronics bay (see Figure 20), which are adjacent to each other. They are separated by the main recovery bulkhead, which uses a o-ring seal to hermetically separate both sections, excluding the parachute bay vent holes and upper body tube altimeter sampling ports, which vent both tubes to atmosphere. The parachute bay consists of the nosecone and the parachute bay tube. The parachute tube and nosecone are connected via a short, 1.5" slip-fit coupler held together with three nylon rivets that act as shear pins to allow the nosecone to separate from the rest of the rocket. The team understands that this is shorter than the minimum suggested coupler length requirement as per DTEG R8.7.9.3, but has used this design since 2019 with no failures in 3 flights. To ensure that there is no misalignment of the nosecone which creates offset forces, this is a metal-to-metal joint machined and finished in-house to create no more than 1 degree of nosecone tip misalignment, usually far less. Once completely finished fabrication and testing, a dial gauge will be used to calculate the as-finished total possible misalignment.

The three nylon shear pins break when at least one of the two redundantly actuated 20 g CO<sub>2</sub> cartridges eject their contents into the parachute bay, thereby pressurizing it. This CO<sub>2</sub> deployment method has been extensively tested through its use on the last four rockets flown by the team, and is tested thoroughly on the ground each year, including a preliminary test already having being completed this year (Figure 99), with more complete tests planned before launch. This verifies the new o-ring sealing technique employed this year to make the bulkhead sealing more efficient and reliable.

The parachutes and rigging are packed in both the nosecone and parachute bay tube for space



Figure 98: Truck Testing a Previous Year's Parachute

and weight savings. The main, 25-foot 0.5" tubular OneBadHawk kevlar shock cord is bundled in alternating loops with elastic bands wrapped around each loop to keep the bundles together. It is stowed around the parachute bag when packed into the rocket. Running parallel to it is the electronic reefing wire, which routes up the shock cord and provides power to the canopy pyrocutters (see Figure 101). The reefing wire is made up of a flexible, silicon stranded wire, bundled together in a sheath. To account for the stretch of the shock cord upon deployment, the wires are a prescribed length longer than the shock cord. A tensile test was performed on samples of the shock cord to determine the maximum elongation to calculate the required extra wire. The parachute bag is packed in the center of the parachute bay, with the bundled shock cord around it. Above that is the loosely stuffed pilot chute, free to catch the wind upon deployment.

Due to the necessity of a swivel on the parachute rigging, a solution to eliminate torsion from damaging the disreefing wires is required, as the wires need to connect to both sides of the swivel. A slipring was used on the two previous flights of this reefed recovery system to allow the electrical signal to swivel with the parachute as it spins. By rotating in conjunction with the 24kN breaking-strength (5400 lbf) Petzel gated swivel, the wires never build up torsion and do not rip out (see Figure 102.). A 3D printed TPU coupler is attached to the slipring rotor and the top side of the



Figure 99: Deployment test completed to verify new o-ring seal integrity with this year's flight components

gated swivel. At LC 2023, the team had a confirmed firing of both pyrocutters which indicates that the slingshot and coupler functioned perfectly during descent. The slingshot is tested at its rated maximum of 100 rpm manually to ensure it still fires reliably, and maintains continuity under an oscilloscope. It is difficult to exactly determine the required spin rating for the slingshot as the spin of the rocket on descent varies wildly in differing atmospheric conditions. The 100rpm figure is a 10x factor of safety applied to the observed descent rotation of our flight at SAC 2023. This year, an updated 3D printed shroud and a slightly more robust slingshot was sourced.

An attempt was made this year to introduce a second redundant slingshot in series with the first after it was noted by the judges of Launch Canada 2023 that the use of a single slingshot could be a single point of failure without redundancy. A second slingshot was going to be installed above the first with a mechanical link, but this was rejected by the team for two reasons. Firstly, the eyebolt length required created a packing concern for the parachute and rigging, as it creates an odd donut-shaped packing configuration. Secondly, the elongated eyebolt shank (required due to a taller stack of slingshots) means a worse bending load on the eyebolt. There was no way to use a larger eyebolt (meaning a larger slingshot), thus this idea was rejected.



Figure 100: Recovery Electronics Sled

The team contends that:

1. Four separate traces carry the signal through the slipring, meaning it is no different than the team's remote arming board, or a screw terminal block termination point. These bring both the main and backup pyro signals into a single mechanical point, despite electrical isolation.
2. A mechanical failure that causes the breakdown of the traces within the board or the bearing that allows for smooth rotation could also be a sufficiently damaging event to have damaged other parts of the parachute bay, such as the screw terminals that join the pyro lines, or by ripping wires out of ematches. Due to the high build quality of the slippings, it is expected they would survive such an event.
3. The event impacted by the operation of the slipring is disreefing. In the result of a slipring failure, the reefed parachute will still deploy and orient the rocket such that it does not tumble, as it plays no bearing in these events.
4. Adding a second slipring in series adds further mechanical points of failure such as the mechanical link or breakdown of a single bearing causing failure of both, and doesn't really accomplish a wholly redundant solution.

The team has continued with the single slipring design and has also conducted a destructive test with previous years' model to determine its integrity. After destructively damaging the slipring to the point that it could not spin, the device still maintained signal integrity and would still fire e-matches if commanded.

As mentioned above, the disreefing event fires e-matches that trigger custom SRAD pyrocutters. These custom pyrocutters are designed to increase reliability by being able to be machined,



Figure 101: Routed and Folded Reefing Wire and Shock Cord Bundles

disassembled, and cleaned in-house. The titanium body provides a high degree of safety and longevity. They allow for two e-matches to fit in each pyrocutter increasing reliability and redundancy. Ground tests for all pyrocutters are required for them to pass internal testing, and a version of these cutters flew on our most recent flight and fired, successfully cutting the line (which did not disreef due to tangling, discussed later).

The deployment events are controlled by redundant COTS altimeters: the PerfectFlite StratoLogger and the Featherweight Raven 4. Both tie into our avionics system and can trigger either set of ematches for the CO<sub>2</sub> ejectors or pyrocutters.

The recovery electronics, including the altimeters, custom remote arming board, and radio, sit on a compact recovery electronics sled attached beneath the main bulkhead. Strain relief and proper electrical routing is an important part of the design of this sled and care is taken to ensure robustness of this design.

Changes to the recovery electronics in this design cycle include the addition of a COTS inertial measurement unit (IMU), SRAD processor board to handle IMU data and control airbreaks, and an SRAD charging board to allow for charging of the on rocket-side lipo when on the pad. These boards have been integrated into the recovery electronics sled without increasing the length of the sled plates through the efficient use of interior plate space.

One change since 2023 is the addition of a 3S lipo into the recovery electronics sled. To allow for this, a new lipo mount was designed to seat the lipo, with the design constraints of allowing for easy access without the need to disassemble the plates, which would require disconnecting the connected electronics harnessing. To allow for easy insertion of the battery, side tabs were cut in the plate to allow for the battery to be gripped from the sides of the plates without the disconnection of the sled harness.



Figure 102: Integrated Recovery Bulkhead with Slipring Shroud

#### 10.4 Past Failures and New Changes

It has been possible to pinpoint the cause of failures within the recovery section in the previous two flights and these have been driving the changes outlined above. The issue with the reefed recovery system has never been one of the deployment of the reefed drogue state, as this has always performed nominally. It is the disreefing transition that has been the source of failures. The failure found in the SAC 2023 LotS rocket was two-fold. Firstly, the pyrocutter failed to sever the control line as the electrical connections were severed at reefed deployment due to opening shock. This was confirmed by the lack of electrical connection recorded by the remote arming board at apogee. On this flight the pyrocutter were located only 1m (3ft) up the shock cord, so it was thought that there just simply wasn't enough extra wiring on the pyro lines to accommodate for the stretch. The pyrocutter were found a few feet away from the rocket upon recovery which indicates the control line pulled loose from the pyrocutter. This would have normally resulted in a main at apogee event, however the nosecone and nosecone retention strap had also wrapped around the shock cord and control line, preventing the tension from being released in the line. The rocket impacted the ground under drogue, but thankfully suffered very little damage.

To fix these issues the 10K KOTS Solid rocket launched at LC 2023 moved the pyrocutter from the bottom of the shock cord up to just below the shroud line point of confluence (SLPOC) and fixed the fastening system that attaches the pyrocutter to the control line. These fixes worked, as proved by the successful firing of the pyros and severing of the control line at the 2023 LC competition. However, the failure that resulted in no disreef is attributed to the control line wrapping around the shroud lines and causing a tangle. The current theory as to why this tangle happened is due to the order in which the parachute deploys and the packing method.

Previously, with the parachute bag attached to the bulkhead, when the pilot chute is ejected it



Figure 103: Packed Parachute and Rigging



Figure 104: Lipo Mount

pulls out the rolled up parachute from the bag first. Then, the shroud lines start to be pulled out of their elastic bands on the bag. During the shroud line deployment, it's theorized that the chute could quickly inflate before the rest of the lines are deployed. If inflation of the parachute occurred before the shroud lines were fully deployed, it would have pulled on the control line which had its slack collected below SLPOC. This in turn would cause the control line to prematurely deploy ahead of the shroud lines it is bundled with, creating what was seen upon recovery, bundles of undeployed shroud line being tangled with the control line. Even though the pyrocutters cut the bottom of the line, the tangle was such that it could not be pulled through to release tension and slow the rocket down.

The team has designed two fixes for the issues found at the LC competition. The first method is to change the order of deployment. By attaching the parachute bag to the pilot chute instead of the bulkhead, the deployment order would be flipped. The shock cord would extend first, followed by the shroud lines and finally the full parachute. Since the shroud lines are deployed before the

parachute, the failure risk of the control line tangling would be mitigated. This deployment order is commonly used in a mortar based parachute deployment, but could also be used without a mortar. The second fix is to move the pyrocutters up to the inside of the parachute canopy, eliminating any control line not inside the parachute. The control line would be packed with the parachute, not with the shroud lines. This would make the two independent and therefore not able to tangle. Given it has already been demonstrated that the team can successfully route cables up the shock cord, routing the cables up to the parachute is merely an extension of already proven concepts, rather than a whole new concept. The intention is to run the wires parallel to one of the shroud lines. Canopy mounted disreefing devices are more common than other approaches due to the simplicity of lines. In industry, a wireless link, timer, or parachute-mounted altimeter is used, as opposed to a hardwired connection. Unfortunately, wireless or other systems do not conform easily to the Launch Canada DTEG, and thus have been avoided. To maximise the chance of a successful recovery, both solutions were implemented.

## 10.5 Parachute Folding and Deployment Bag

The past parachute bag has been in use for more than three years and four launches. As such it has gained a significant amount of wear and tear justifying the manufacture of a new bag. The opportunity to do so also grants the opportunity to re-evaluate the design, optimizing it for a new rocket. Moreover, previous parachute folding techniques included folding the parachute into a dart, then rolling it up to fit into the bag. Drop test analysis shows that this can introduce additional twists into the rigging that should be avoided. Analysis of skydiver parachute packing and circular military parachute folding shows the initial dart folding is acceptable. However, it is then z-folded into the bag to make for a smoother deployment. This has the benefit for the parachute exiting the bag ready to deploy, which leads to lower opening shock as the rocket has less time to accelerate. The bag will be made slightly wider near the top to accommodate the widening of the parachute and to ease deployment. Furthermore, it will be slightly longer as this pack is moderately less efficient. The bag being made about an inch longer will accommodate the looser pack, reefing grommets, and allow for easier pyrocutter access.

## 10.6 Remote Arming

Remote arming is a custom SRAD board designed to eliminate the need for operators to climb a step ladder and use a magnet attached to a pole to arm the altimeters while standing directly under the rocket. In addition, it provides valuable instrumentation that allows for constant monitoring of the recovery system health before and during flight, allowing a comprehensive check of the system performance immediately prior to launch. The system communicates via RocketCAN, which in turn receives commands from the operator via RLCS to arm or disarm the system. A block diagram of remote arming is shown in the figure below.

Remote arming is a single SRAD PCB, which all the key components of the recovery system are attached to securely, either with screws or screw locking Harwin Datamate connectors. This significantly reduces the complexity of the recovery wiring, reducing the risk of mistakes or faults in the harness such as bad crimps. The complete system is shown below.

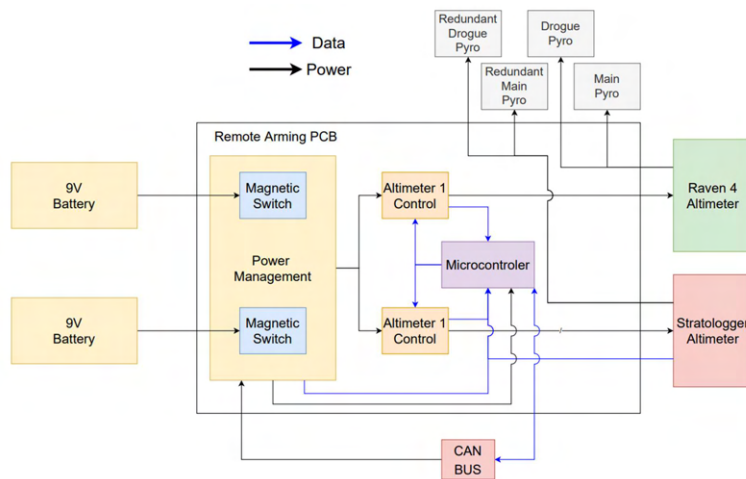


Figure 105: Remote Arming Block Diagram

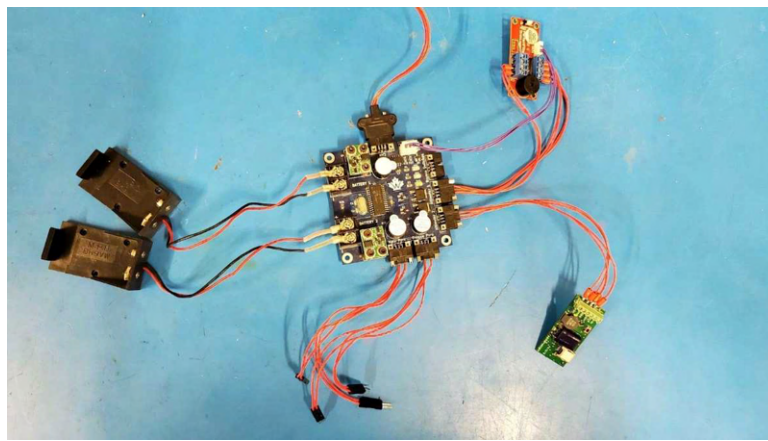


Figure 106: Complete Remote Arming System

### 10.6.1 Failing Safely

A key problem for remote arming is to create a system which always fails safe. Most systems on the rocket need to fail safe, however usually this has a well-defined, single meaning. For example, the vent valve should always fail open to ensure there is never an SRAD pressure vessel which cannot be vented. However, for remote arming, failing safely does not always mean the same thing. While the rocket is on the ground, remote arming needs to fail in the disarmed state, as if it fails armed, the pyrotechnics could accidentally be triggered, and an operator could be injured. However, once the rocket launches, the altimeters must stay armed, or the recovery system will fail. As such once in flight the system must fail armed.

It is not possible to design a system which will always fail armed and will always fail disarmed, so a compromise was made. The system has been designed such that it will always fail armed. However, a pair of magnetic switches ensure that the recovery system can always be manually disarmed with a mag-switch if needed. In addition, buzzers are continuously on whenever the altimeters are powered ensure that there is no possibility of personnel approaching the system without knowing it is armed.

Since both arming circuits are controlled by a single microcontroller, several measures have been taken to ensure that it does not cause a single point of failure:

- There is a pull up resistor which ensures that if the microcontroller fails or loses power, the circuit will keep the altimeter powered.
- The code on the microcontroller ensures that its default state on power up is armed, as such any temporary loss of power will not result in the altimeters disarming.
- A watchdog timer is used, such that if the main loop is ever hung up, the microcontroller will be reset.
- The microcontroller is powered both by the recovery batteries, and the Rocket's CAN bus, which adds redundancy and reduces the chances of a brown out.

### 10.6.2 Remote Arming ConOps

Since the logic of remote arming is designed to default to armed, some care must be taken in setting up the system for launch. The procedure is as follows:

- Since the magnetic switchs default state is on, during assembly the 9V batteries should be installed first, the magnetic switches turned off, and then the e-matches should be attached. This is true regardless of remote arming.
- Once the rocket has been full assembled, inspected, and loaded onto the launch rail, but before the rail is raised, the CAN bus should be powered up, remote arming should be commanded to disarm the altimeters, and then a magnet should be used to turn on the magnetic switches, checking the remote arming telemetry to ensure both switches are functioning correctly. The indicator buzzers will also play a distinct tone to indicate both batteries are functioning correctly.

- The CAN bus can then be powered down and remote arming will continue operating using recovery battery power.
- Once the rocket is vertical on the tower and ready for launch, remote arming will be commanded to arm. The telemetry will then be checked to ensure the system is ready for launch. This includes the following:
  - Both battery and magnetic switch voltages are good.
  - Remote arming reports both altimeters armed.
  - Current draw from the recovery batteries matches expected value for all systems armed.
  - Drogue and main pyro voltages for each altimeter read as expected for the armed state.
  - Altitude data is being received from the Stratologger altimeter.

### 10.6.3 Power Management

Remote arming is powered by two 9V batteries connected via a 4A PTC fuse, each with their own voltage sensing and magnetic switch, as shown in Figure 107. A SM74611 smart diode is used with each battery to ensure a difference in voltage between the two does not cause issues. These diodes are designed for solar power generation and have a nominal voltage drop of only a few mV thanks to an internal FET and charge pump circuit, ensuring there is minimal power loss through the diode.

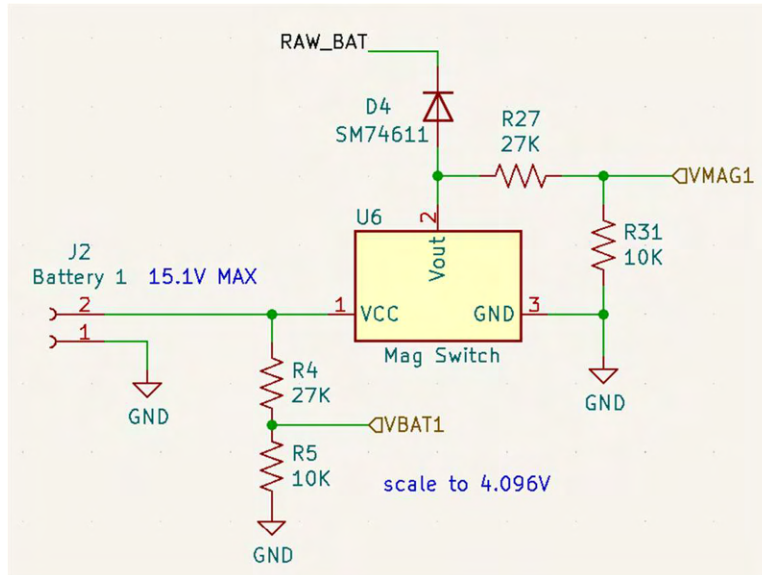


Figure 107: Remote Arming Power Circuit for One of Two Batteries

The microcontroller is powered by the CAN bus via the same PTC fuse and current sensing circuit as discussed in above, with the only difference being a CUS08F30 Schottky diode to prevent Remote Arming from powering the CANBus with its backup 5V regulator which draws power from the 9V batteries.

Current sensing from the 9V batteries is achieved using an INA180 amplifier as shown in Figure 108.

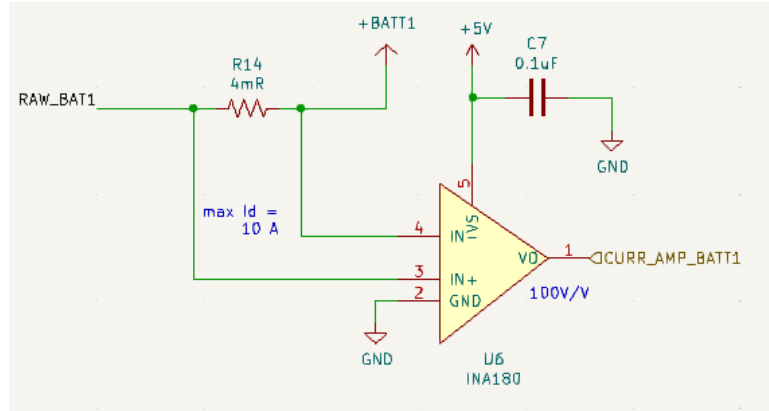


Figure 108: Recovery Batteries Current Sensing Circuit

#### 10.6.4 Altimeter Control

As seen in Figure 109, power to each altimeter is controlled by an AOD417 P-channel MOSFET, which is in turn controlled by a DMG2302UK N-channel MOSFET to allow the circuit to be controlled with the microcontrollers 5V logic. This high side switching is slightly more complex than if low side switching was implemented with a single Nchannel MOSFET but ensuring that the altimeters and remote arming have a shared ground is needed for reading altitude data from the Stratologger. This MOSFET combination has already been flown as part of the injector valve control board for the rocket Shark of the Sky at SAC 2019 without issue and continued to function even after the rocket landed under drogue and experienced significant shock loading. The pull up solder jumpers are for use with the Raven 4 altimeter which does not have a dedicated positive pin for the drogue or main e-matches, and as such requires that they are externally connected to power. As mentioned previously, each power control circuit has a buzzer that is on whenever the altimeter is powered. Two different frequencies are used to make it possible to identify which altimeters are powered.

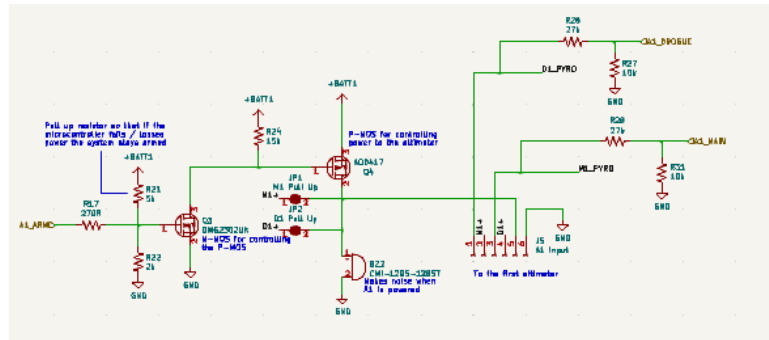


Figure 109: One of Two Altimeter Arming Circuits

### 10.6.5 Telemetry

Remote arming has a total of eleven different sources of telemetry, the telemetry channels are as follows:

- Battery 1 and battery 2 voltage
- Magnetic switch 1 and switch 2 output voltage
- Voltage reading for all four of the drogue and main e-matches. This voltage reads close to the battery voltage while the altimeters are powered, and the e-matches connected, and close to zero if not. As such it is easy to verify that the recovery system is entirely functional immediately prior to launch.
- Current draw from the 9V recovery batteries, this has a maximum value of 4A so that the current draw of the e-matches firing can be measured. As such the signal is very noisy and imprecise when reading the passive current draw of the microcontroller. This is mitigated via the use of software low pass filters which allow reasonably accurate measurements down to approximately 20mA.
- Current draw from the CAN bus using the same architecture used on all other RocketCAN boards.
- Remote arming parses the UART altitude stream from the Stratologger altimeter and transmits it over the CAN bus so that the altitude can be monitored live during flight. The level shifting circuit can be seen in the figure below.

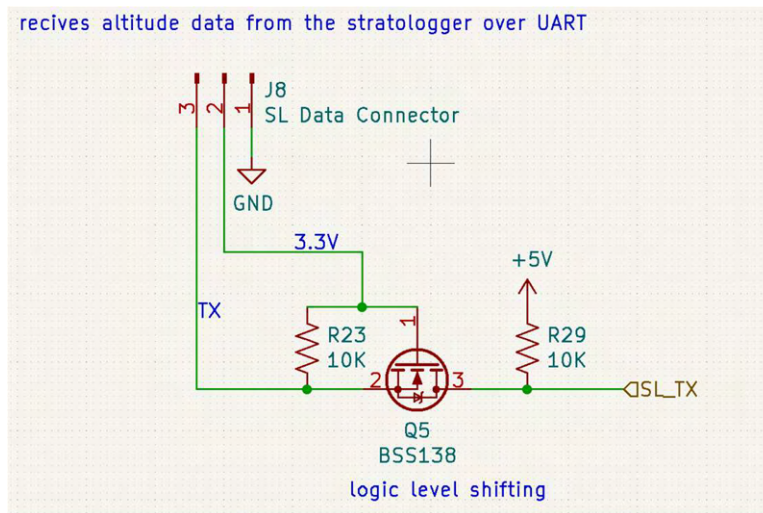


Figure 110: Stratologger Telemetry Level Shifting Circuit

### 10.6.6 Remote Arming Testing

As of present the remote arming system has undergone full system testing under benchtop conditions. It has also undergone a series of simulated flights where the complete recovery electronics system was put in a vacuum chamber. A partial vacuum was pulled to simulate an increasing altitude, then air was slowly introduced back in to simulate apogee and descent. Referencing an aircraft altimeter, it was confirmed that the drogue channel fired at apogee, and the main channel fired at a reading of 1500 ft. Throughout the process, remote arming reported all the correct telemetry. Unfortunately, this test only works with the Stratologger altimeter since its altitude measurement is solely barometer based, while the Raven 4 uses an accelerometer along with the barometer. Both the Raven and Stratologger altimeters were tested with remote arming by connecting them to a computer and using their respective simulated flight tests. The system has successfully flown twice in 2023 on rockets LoTS and 10K KoTS Solid.

The remote arming system uses a common power bus supplied by two redundant batteries. This single bus provides power to both redundant altimeters. This provides an advantage over the past system which had two isolated redundant systems as it allows for a single battery failure as well as a single altimeter failure without a failure of the recovery system. This was deemed valuable as in 2019 both a battery failure and altimeter failure were experienced, and due to the isolated nature of the systems, this caused both recovery systems to fail. This situation is prevented with the use of a joined power bus. While a joined power bus was deemed valuable for added reliability, a new potential failure mode was identified. It is possible that a short-circuited e-match could cut power to both altimeters leading to a failure. To test this the main parachute pyro line was intentionally short circuited on one altimeter and that channel was fired while monitoring the status of the other altimeter. This test was then conducted with the two altimeters in opposite roles. This test confirmed that the brownout protection capacitors on each altimeter allow them to keep their state in the event of a drop of bus voltage due to a short-circuited e-match on the other altimeter. Therefore, this failure mode does not affect the operation of the other altimeter. As an extra safety measure, the single point of connection between the two circuits is a 4A PTC fuse. The fuse value was chosen heuristically from testing current draw of the e-matches while firing. This will prevent a short in one battery from taking out both systems, maintaining dual redundancy.

### 10.6.7 Revisions

Remote arming has flown several successful flights as mentioned above, however key areas of improvement and points of failure have been identified. This has resulted in some small revisions being for the 2024 rocket.

Firstly, both battery channels have been separated except at a single PTC fuse. This update removes the possibility of having a short in one battery from breaking both recovery systems while still providing the advantages of cross linking both batteries.

Secondly, the pinout on the connectors to the pyrotechnics has been modified. Previously, each connector would connect to both mains and the other would connect to both drogues. This presents the possibility that a faulty connection could prevent a parachute deployment. The new pinout has both a main and drogue connected to each connector.

Lastly, some smaller changes have been made such as jumper connections between the two systems being removed. This further isolates the two systems. The shunt resistors for current

sensing involved two parallel resistors, that way a failed resistor will not take down a system. This was deemed unnecessary and removed.

## 10.7 Bulkhead and Cameras

The bulkhead underwent a series of improvements this design cycle to ensure faster and more reliable sealing, electrical pass through and improved strength.

Due to the CO<sub>2</sub> gas ejection system, it is imperative to seal the bulkhead with the body tube coupler to maximize the chances of nosecone ejection. On previous rockets this has been done through the use of aluminum tape and lithium grease to seal any gaps due to machining in the bulkhead coupler seal. This sealing was extremely difficult during flight assembly due to the small space available for application and tight gap between pre-installed recovery hardware and the physical gap. Furthermore, it is an extremely long procedure, having taken upwards of three hours in previous years. To address this concern, the addition of an o-ring face seal was implemented. This o-ring seals between the coupler and the bulkhead can be seen in Figure 111. This seal was then successfully tested in a worst case deployment test as mentioned above. The addition of sealing M8 connectors to the bulkhead improves the quality of the electrical harness, ensuring reliable and easy connection and disconnection of the recovery electronics sled. These use an o-ring seal and are countersunk in to the bulkhead to ensure a tight seal. The bulkhead is made of Aluminum 6061-T6. The bulkhead was validated through the use of FEA sims as seen in Figure



Figure 111: CNC Recovery Bulkhead

112. With a FOS of 4 at maximum recovery loading, the bulkhead is strong enough to withstand recovery loading. The main eyebolt was also sized by calculating the shock loads the rocket would experience at both deployment and dis-reef. Due to the increased height of the slip ring, compared to last year the eyebolt was increased to a half inch diameter eyebolt. This ensured the FOS was above 2 throughout the entire deployment sequence and greatly reduced the deflection the eyebolt would experience, ensuring it would not contact the sliring at any point. Furthermore, the integration of a camera was being developed to gain more useful data from a recovery event. Unfortunately, due to time constraints, this was cut from scope this year.

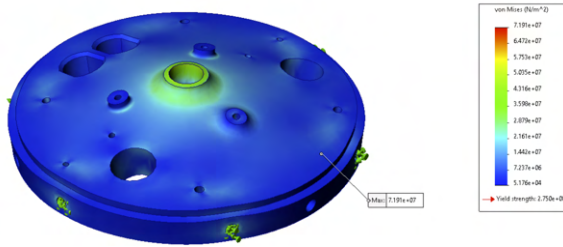


Figure 112: FEA of the Recovery Bulkhead

## 10.8 Potential Sources of Failure

When considering the new recovery system, it is critical to try and predict any new potential sources of failure and what effect they would have on the system in flight. Four main sources of failure were identified for the new design. Given the partial success of previous flight, most of these failure modes are a result of the enacted changes. Having never repeated the same failure mode twice, and by only changing hardware that directly caused the failure, the goal is for a reliable reefed recovery system to be established.

### 1. Tangles in the Rigging:

The most unpredictable source of failure is a tangle in the rigging. From past experience, we have determined that this can come from one of three places. Interactions with the nosecone strap, interactions with the reefing line, and incorrect deployment. The severity of a tangle involving the parachute or reefing line is dangerous, having the potential to prevent either main or drogue chute inflation. However, the team has never had a reefed chute deployment failure. By following previously established guidelines internal to the team and performing drop tests to simulate parachute deployment, we can minimize the risk of a deployment related tangle as much as possible. This comes through consistent parachute packing and well written procedures. By moving the pyrocutter up to the canopy of the parachute, it is now almost impossible for the control line to be affected by either the nosecone strap due to it not exiting the skirt of the parachute. Furthermore, restraining the control line to the skirt of the chute means it cannot tangle with the shock cord or shroud lines below it. An improved deployment order means that each part of the rigging is deployed in sequence, ensuring that there are no tangles.

### 2. Pyrocutters Sever the Reefing Line Prematurely

A potential source of failure is the movement or grinding of the reefing line on the pyrocutter body abrading it to the point it breaks mid flight leading to a main deployment before the selected altitude. The most likely source are the pyrocutters. The material selected for the reefing line (cypress line) is very durable and the reefing line is made out of new material prior to competition, so the risk is already quite small. To minimize this risk further, the pyrocutters are being tested extensively to ensure any sharp edges are removed, to ensure all edges are bevelled or filleted and ultimately by attempting to use the pyrocutters to cut the cypress line manually. This is unlikely if the slack in the reefing line is managed correctly to prevent any unnecessary movement in the reefing line during flight and after deployment.

### 3. Pyrocutters Compromise the Integrity of Chute on Activation

A low risk failure mode are the pyrocutters damaging the structural integrity of the parachute. This is mitigated through two methods, firstly, by using fire-retardant rip-stop nylon, the parachute melts rather than burns, meaning any damage would be localized. Furthermore, the gas ejection port on the pyrocutters is pointed down and away from the parachute, aimed towards the much more sturdy straps that run the edge of the parachute. Pyrocutters were set off on the skirt of the chute in the flight configuration. The design of the pyrocutter holder effectively caught and deflected the hot gasses away from the critical parachute features.

### 4. Pyrocutters Disconnect Electrically Before Activation

This is a moderate risk failure mode that has been partially tested through the flight of the 2023 rocket "10K KOTS Solid". The team has already successfully routed cabling up a shock cord. By tensile testing the shock cord and determining the maximum elongation at deployment, the team was able to adequately determine the amount of slack required in the system. The cypress lines and utilised knots were also tensile tested to characterise the line at high force values.

## 10.9 Risk Assessment

Table 18: Recovery Programmatic and Technical Risks, Hazards and Mitigation Strategies

| Risk   | Likelihood | Severity | Description   |
|--|------------|----------|---|
| Pyrocutters cut / degrade reefing line consistently                      | Low        | High     | Deburr any sharp edges, consider the addition of a paper sheath around cypress line to promote sliding or the addition of lubrication   |
| Parachute undergoes a significant rip or tear during handling or testing | Low        | Low      | If required the damaged gore can be removed and sewn back in if a patch is ineffective, avoid the use of the flight parachute for high risk testing (drop test) and instead use previous rocket's parachute |
| Falling behind timelines   | High       | Low      | Build a significant amount of buffer into the manufacturing and testing timelines, ask for manpower from non recovery team members to complete work   |

## 10.10 Testing

Multiple tests have and will be conducted to ensure that the recovery system works nominally. The system must be approximated though ground tests and small crane drop tests.

Table 19: Recovery Tests

| Test                               | Comments  |
|------------------------------------|---|
| CO2 ejection ground testing        | Couplers, nosecone and parachute bay have passed initial testing and are waiting on final assembly for final complete testing.  |
| Bulkhead seal verification testing | Passed this test by successfully sealing the bulkhead and deploying the nosecone without any internal components.   |
| Drop test parachute deployment     | A mock air frame was 3d printed to contain all parachute components. The assembly was then elevated via the use of a crane and it was then be dropped to investigate parachute bag deployment and parachute inflation.        |
| Pyrocutter qualification tests     | A new pyrocutter pellets were machined and qualified. This involves the pyrocutter being actuated and ensuring it can reliably cut the cypress line more than once.   |
| Parachute burn test                | To ensure the pyrocutters cannot harm the parachute, a pyrocutter qualification test was conducted while tightly wrapped in parachute material. This aided in understanding how the pyro ejection gasses affect the material. |

## 11 GROUND SUPPORT EQUIPMENT

The Waterloo Rocketry team has a variety of SRAD and COTS ground support equipment which will be used during the launch of Borealis. The proposed layout of the launch pad is shown in Figure 113

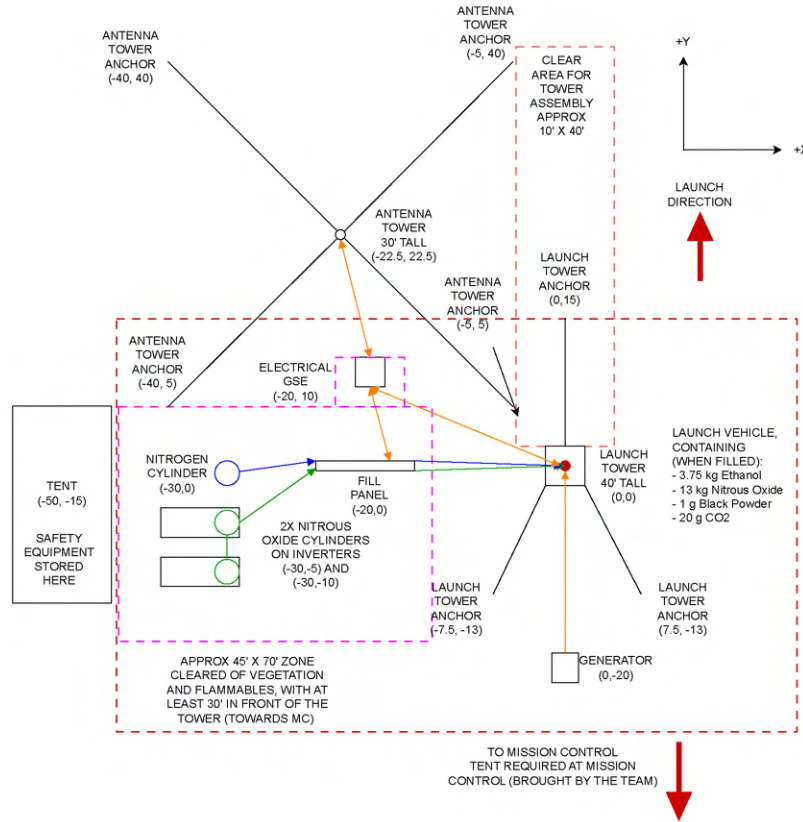


Figure 113: Site Layout

### 11.1 Remote Launch Control System

The Remote Launch Control System (RLCS) is the primary means of interfacing with the rocket and supporting fill plumbing during launch operations. The main objective of the system is to allow remote operation of the rocket from up to 3,000 ft from the tower during all phases of operations. Once the RLCS operator takes control of the launch process, no human intervention

shall be required at the launch site at any time when the fluid systems are pressurized. In the event of total failure, the system must put all engine and fill systems into a known safe state so that personnel can approach the rocket without placing themselves in danger.

RLCS is made up of two halves, Clientside and Towerside, which communicate over a radio link formed by a pair of Litebeam 5ac gen2. Towerside is located beside the launch tower and handles actuating motorized valves and ignition. Clientside is located at mission control and houses switches that map to the various actuators and an LCD to display data to the operator. Both halves are built into weatherproof and robust Pelican cases to protect them from the elements.

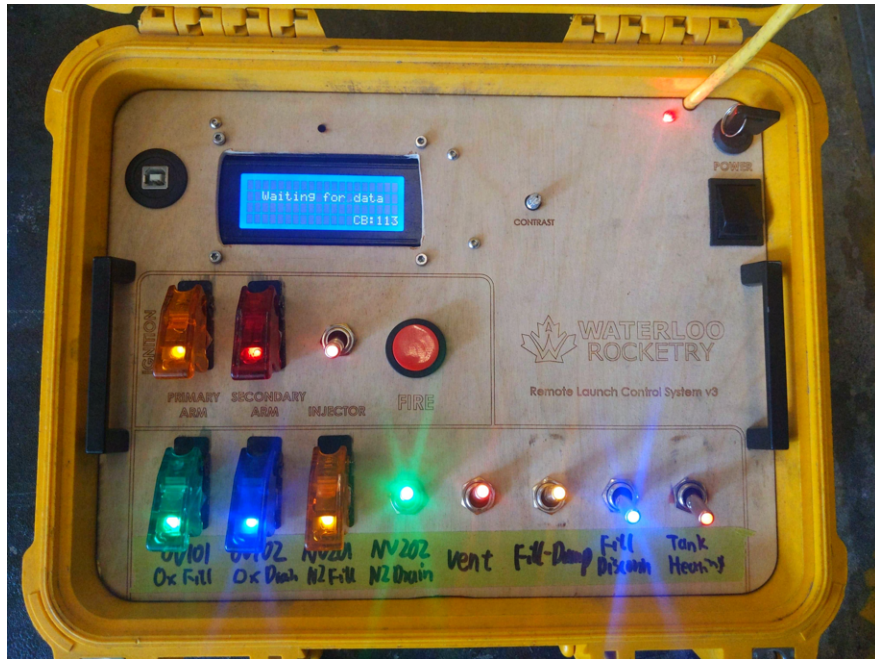


Figure 114: RLCS Clientside

### 11.1.1 Clientside

Clientside is used by the RLCS Control operator to control motorized valves and ignition. Clientside is a relatively simple system composed of an Arduino Mega, a LCD module, several missile switches, and a custom arduino shield for power regulation and expanded GPI/O to screw terminals. Additionally, it exposes a USB port which allows it to send data to a computer for plotting and logging. Clientside contains a set of missile switches, each matched to a motorized valve or rocket on-board solenoid valve. There is also the ignition button paired with an arming missile switch for controlling the current that passes through the nichrome ignition coil. The LCD module displays the state of all motorized valves (open, closed, and not connected), the voltage of the LiPo batteries, and the ignition coil current. Clientside dumps all RLCS sensor data periodically through USB UART link to the DAQ operator laptop. This connection provides a path for monitoring the state of tank heating.

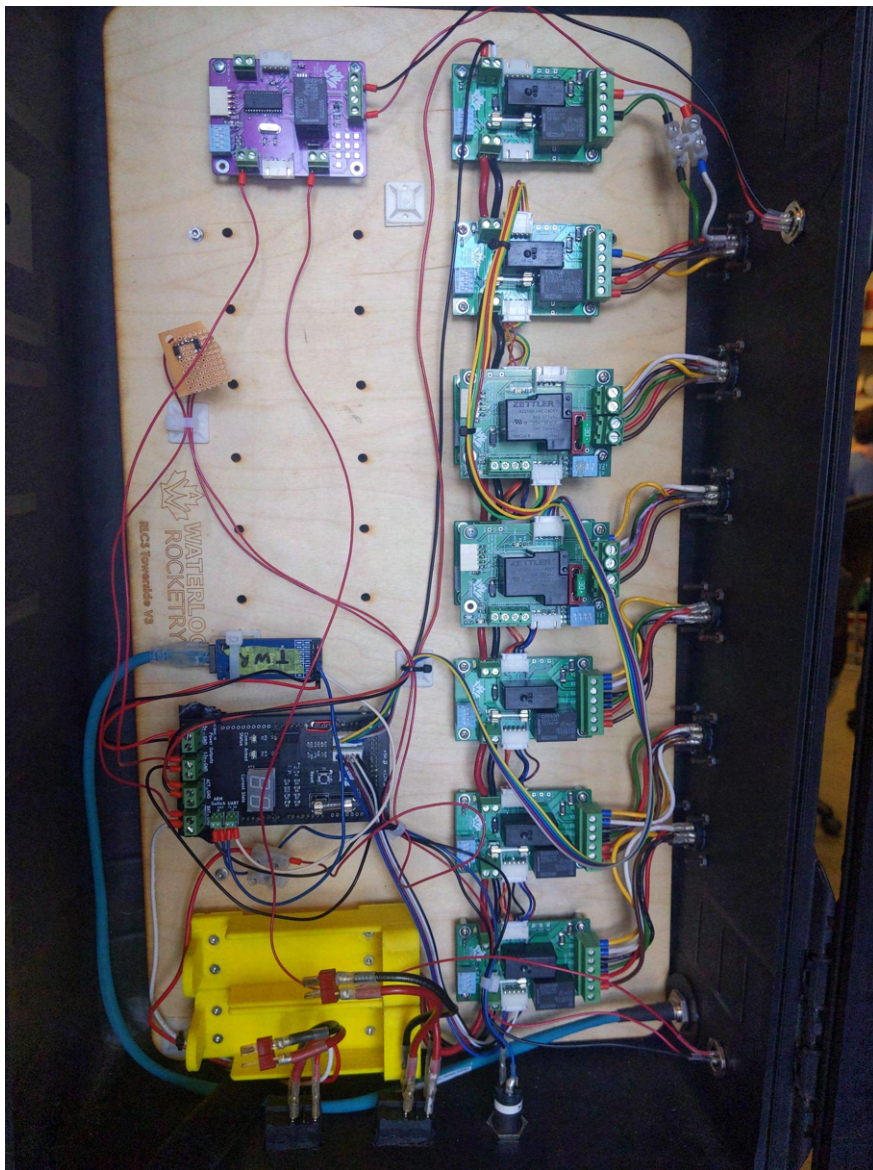


Figure 115: RLCS towerside

### 11.1.2 Towerside

Towerside receives and enacts the commands of the clientside operator. Its architecture is similar, but made more complicated as it needs to handle the high current draw of motorized valves and tank heaters. It is made up of a set of identical relay boards and two tank heating relay boards connected over a I2C bus to a master Arduino Mega.

The various I2C boards in Towerside are connected over a I2C bus in a daisy-chain configuration. In addition to the two I2C wires SDA and SCL, there is a regulated 5V line, an unregulated 12V line, and a ground line. The 5V line drives the various microcontrollers on the boards and the 12V line is used to drive the relays on I2C Relay boards. The I2C Relay boards additionally have a secondary daisy-chained power connection which uses low-gauge wire and is used exclusively to drive the actuators. This ensures that the high current draw of the actuators does not cause

brownouts on the MCU power lines. The tank heating relay board have a point to point connection to car batteries, and does not draw power from low-gauge actuator wires.

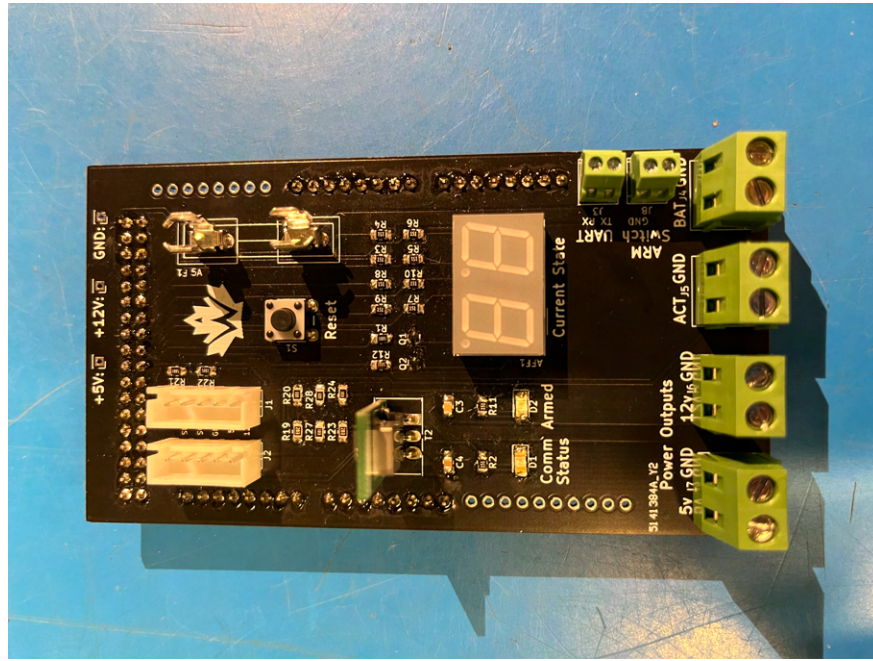


Figure 116: RLCS Towerside Power Board

The main purpose of the Towerside Power Board is to supply 5V power to the Arduino, provide power output, provide UART screw terminal for communication to Clientside, and provide a keylock switch connector and JST I2C connector. The seven segment display on the board displays the current status of each motorized valve and ignition, with binary each bit representing a valve or ignition coil.

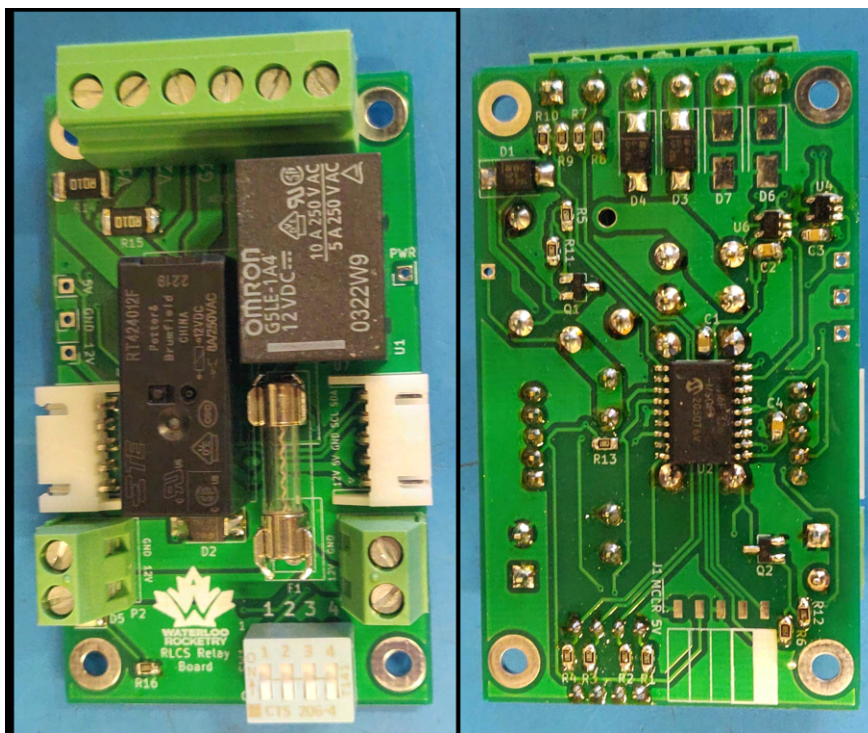


Figure 117: RLCS Relay Board

The main purpose of the RLCS Relay board is to operate the motorized valves that control the flow of oxidizer into the rocket during fill operations. Each Relay board is connected to one motorized valve. Relay board also detects the states of limit switches built into the valves, which are activated whenever the motor shaft arrives at a fully closed or fully open state. These limit switches indicate the current position of the motor shaft; this information is provided to human operators at mission control so that the operators are continually aware of the current position of every motorized valve in the system. Accurate tracking of the states of each of the launch control devices is critical for safety. In addition to operating motorized valves, the relay board can also apply an electric current to an ignition coil to ignite the engine. The typical ignition current is approximately 5 A. The Relay board is equipped with a current-sense amplifier which continually measures the current sunk through whatever actuator or coil is connected. These measurements are reported to the human operators at mission control so that the operators are aware of the current flowing to the motors and ignition coils. Thus, if any of these electrical devices are malfunctioning, the human operators can easily identify the faulty component and take appropriate action.

Relay board uses a pair of relays to control actuation direction and power to the actuator independently. This requires two actions to be taken in order to actuate a valve or fire an ignition coil (where the coil is wired to the normally open contacts of the direction relay).

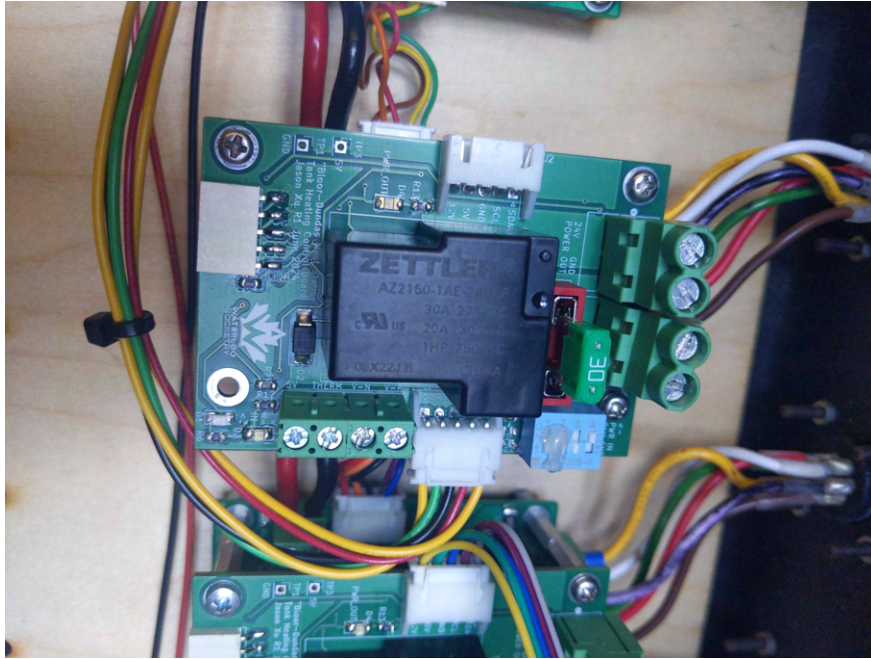


Figure 118: RLCS Tank Heating Relay Board

The RLCS tank heating relay board shares a similar design to RLCS relay board, except it only have one high current relay for controlling power to the tank heater. The tank heating relay board takes power input from two car batteries connected in series. This then goes through the power input terminal. The 24V path goes through a 30A automotive blade fuse, which then goes through the relay and to the output terminal. The ground path has a 0.001 ohm shunt resistor for current sensing. The board also has a 4 terminal screw terminal, two of the ports are for connecting to heater's thermistor, sensed by forming a voltage divider with it, and the other two ports are for measuring voltages across the heater, for accurate measurement of the heater resistance for calculating temperature.

### 11.1.3 System Safety

RLCS is designed to prevent unintended actuation of valves and fail safely. Both Clientside and Towerside have keyed-alike arming and disarming switches respectively, both of which retain the key when turned. This means that whenever the tower is approached the key is removed from Client Side, disarming it, and then inserted into Towerside, also disarming it. In this configuration it is physically impossible to arm Clientside while personnel are at the tower since the key is also physically with them, and even if a fault caused either Clientside or Towerside to unintentionally arm the other half would still be disarmed.

Within Towerside, two relays are required to actuate in order to trigger any action. The relays are wired in series such that one provides power to the actuator and the second determines which direction the actuator should move. The plumbing system is also set up such that if any individual actuator fails the system can still be safely vented.

Clientside and Towerside continually send command and sensor data messages to each other. This means that if either one unexpectedly fails, or the radio link between them drops, both can

detect this by noticing silence on the line. If Towerside does not hear from Clientside for 10 seconds, it will automatically set all actuators to a predefined 'safe state' that is defined in firmware. This means opening all vent valves and closing or de-energizing all others in order to make the system safely approachable by personnel. Clientside will also report any silence of at least 3 seconds to the operator, which could indicate a flaky radio connection or an issue with Towerside.

RLCS controls the following actuators necessary for fill and engine start:

- The Remote Oxidizer Fill Valve
- The Remote Oxidizer Drain Valve
- The Remote Nitrogen Fill Valve
- The Remote Nitrogen Drain Valve
- The linear actuator that triggers the remote disconnect mechanism
- Two nichrome coils inside the engine ignition puck
- Two sets of tank heaters
- The Injector Valves, via RocketCAN
- The Tank Vent Valve, via RocketCAN
- The Fill Dump Valve, via RocketCAN

Moreover, RLCS uses sensors to collect the following data, and report that data back to the operator:

- The current state of all motorized valves (open/closed)
- All error codes
- The amount of current flowing through each nichrome coil inside the ignition puck
- Voltage, Current and Temperature sensed from tank heating
- Voltage of all LiPo batteries

## 11.2 Data Acquisition System

The goal of the Data Acquisition (DAQ) system is to provide a more convenient and accurate method of obtaining ground sensor data during fill and launch operations. It also allows data to be plotted and logged in real time on a computer in a more user-friendly visualization than the LCD on RLCS Client Side.

The DAQ system uses a pair of Ubiquiti Litebeam AC to communicate between mission control and itself. These antennas have been fully qualified at multiple cold flows, static fires, and parachute tests providing reliable communication between the tower side DAQ and mission control.

The heart of the DAQ system is a National Instruments USB-6218 Multifunction I/O Device (the NI module). It supports up to 32 analog input channels with a sensitivity down to  $4.8 \mu\text{V}$ . This makes it suitable for both 0-5 V / 4- 20 mA sensors and mV/V strain gauges such as load cells with no external amplification. New to this year's DAQ comes in the form of sensor wiring and processing. Previously sensors were wired into the NI module through a set of DIN rail terminal blocks with sensors which read a 4-20 mA signal supported by placing an 100-ohm resistor between the negative sensor wire and ground, and measuring the voltage drop across the resistor linearly with the current. Thermistors were also supported with the same internal resistor configuration forming a voltage divider with the external thermistor.

This year, this hardwired processing has been replaced by a SRAD DAQ Patch Panel PCB, which enables easy switching between sensor types through the use of jumpers on the board. DAQ Patch Panel allows for interchangeability of sensors through the use of external pin headers. These allow for the input voltage for each sensor type to be selected individually. To prevent shorting between the header pins when selecting voltages, a star design for the header pins with selection in the middle was adopted to only allow connection to one voltage rail at a time.

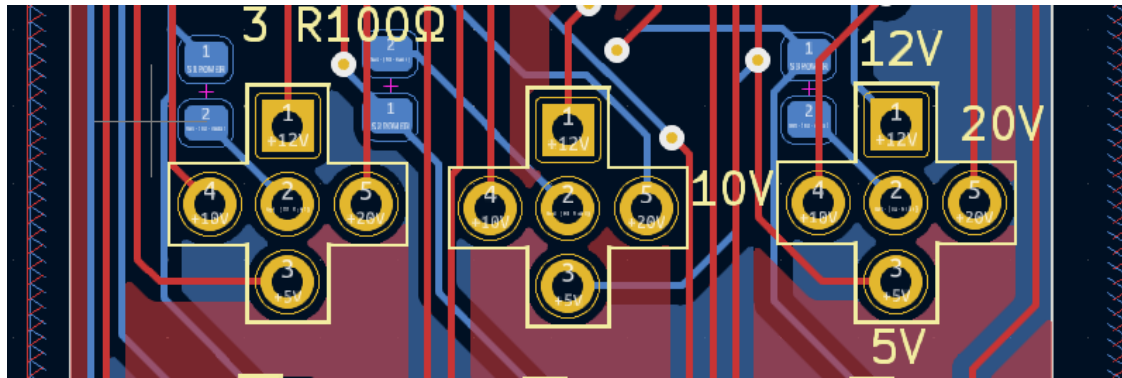


Figure 119: Star Shaped Voltage Headers

Additionally to allow for the use of 4-20mA and thermistor sensors without external output resistor, an additional jumper set for output resistor selection was included. Furthermore, when using 4-20mA sensors, the ground port can be set to a secondary voltage input to allow for two 4-20mA sensors to run from one sensor terminal, doubling the maximum number of 4-20mA sensors without increasing the number of terminals. These jumpers allow configuration of a total of three sensor ports per board. To allow for all four copies of the board to be installed and draw from the same voltage rail, two terminals per board were utilized to allow for daisy chaining of DAQ Patch Panel voltages. This board has been tested through a coldflow, static fire, and WDR's to ensure reliability.

Once the sensor voltages are collected by the NI module, they are passed over USB to the integrated Framework mainboard, a compact single-board computer running the necessary software to send the data over to mission control. At startup, the mainboard automatically runs the DAQ server in preparation to connect and send data to computers at mission control over the same Ubiquiti Litebeam 5AC antennas and radio link as RLCS uses.

At mission control, a custom robust laptop built around the framework mainboard is used to display and log all DAQ and telemetry data. It is enclosed in a watertight aluminum case with three

built-in monitors, along with standard laptop functionality such as a keyboard, trackpad, camera, microphone, speakers, and Wi-Fi.



Figure 120: DAQ Connectors

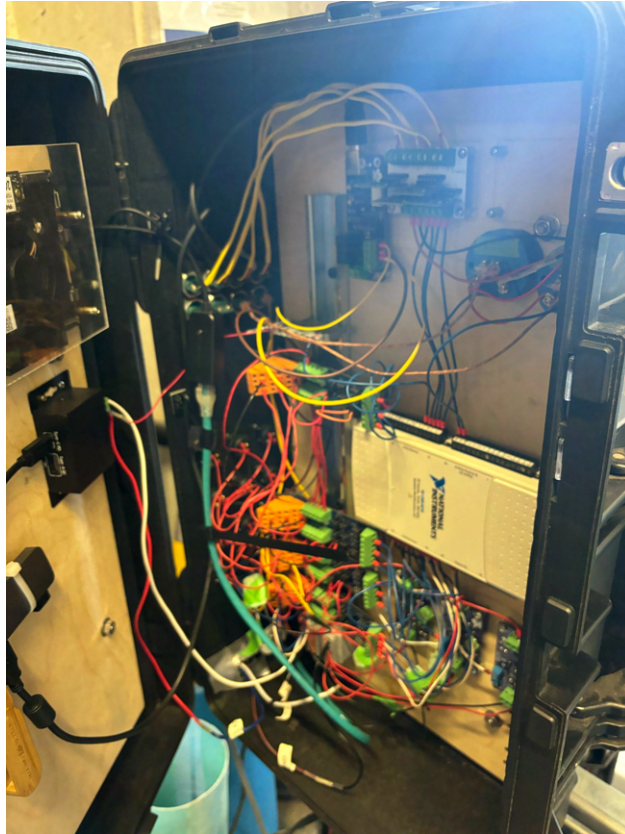


Figure 121: DAQ Interior

Once the sensor voltages are collected by the NI module, they are passed over USB to the local Framework mainboard. This computer then relays them in real time over an ethernet link to a computer at mission control, which plots and logs the data. Since ethernet cables have a maximum length of only 100 m, the Ubiquiti Litebeam AC antennas were selected to act as a transparent link that can span the distance between the launch tower and mission control.

Power to the sensors is delivered by a DAQ Power Board, a custom PCB designed for ultra-low output noise. This is achieved by a dual step-down design where a high-efficiency buck converter regulates the input voltage down to 2 V above the desired output voltage and the final regulation is achieved by a pair of less efficient but ultra-low-noise linear dropout regulators (LDOs). Three copies of this board power the +5 V, +10 V, and +12 V power rails within the DAQ system. The output noise of the board was too low to be measured accurately but is at most  $10 \mu\text{V}$  peak to peak. DAQ Power board was designed for 1 A output at a configurable voltage between 5 and 15 V. To achieve this a 1 A buck converter is followed by two 500 mA LDOs which share the output load. Additionally, pairing up the LDOs reduces the output noise by a factor of 1.4.

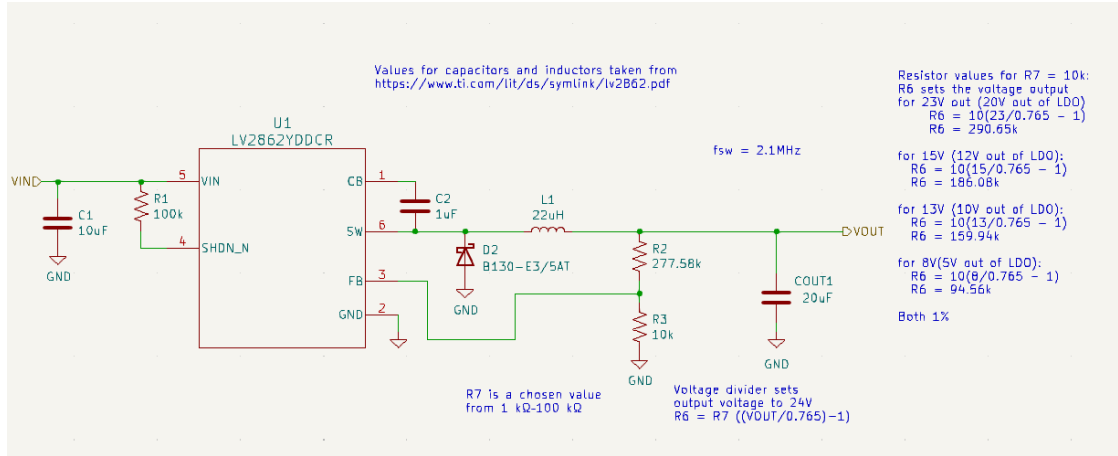


Figure 122: DAQ Power Buck Schematic

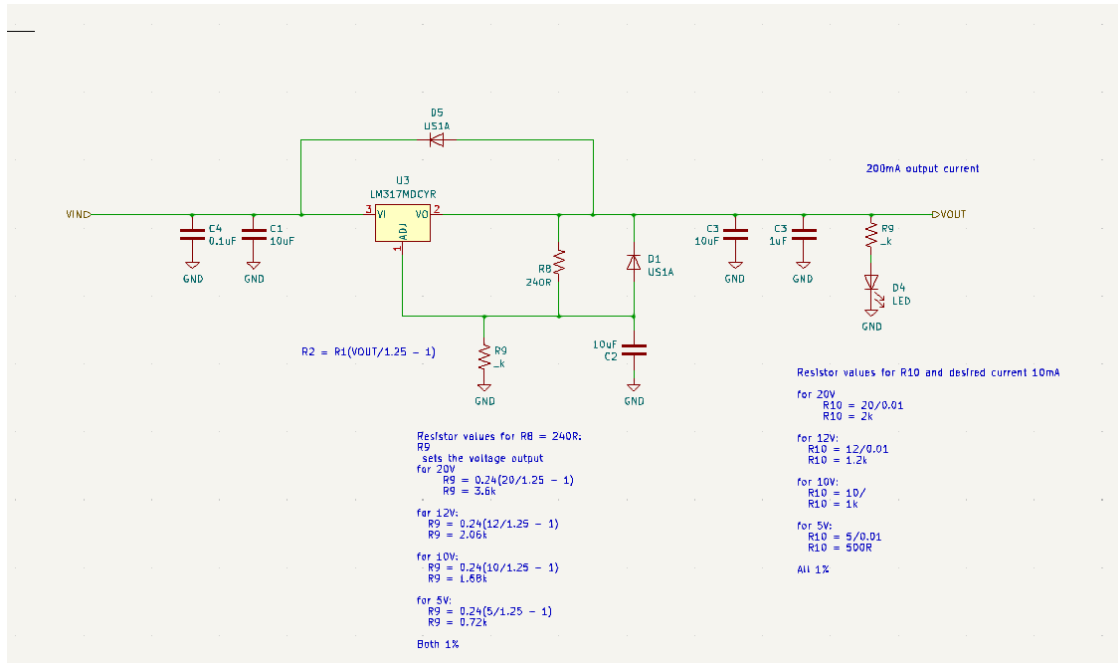


Figure 123: DAQ Power LDO Schematic

Power to the integrated computer is delivered by a COTS USB-C PD DC-DC charger. This module is able to accept voltage from the +12 V power rail and convert it to the appropriate PD voltage required to operate the Framework mainboard. This charger was not only chosen due to its viability in providing power to the computer but also its considerably large input voltage tolerance between 9-36V - helpful in case of voltage noise - and in addition, has low voltage protection to protect both itself and the computer from damage due to high current drawn from dangerously low voltage levels.

## 11.3 Omnibus

Omnibus is a unified data bus which manages the connection of various data sources (such as DAQ and RLCS) and sinks (such as plotting software and logging). This allows real-time data from Borealis to be sent wirelessly to mission control and displayed in useful formats.

The DAQ and RLCS systems are connected to an Omnibus source, which packages their data, serializes it, and broadcasts it on a private Wi-Fi network. At mission control, a custom robust laptop built around the framework mainboard runs an Omnibus sink (such as the Dashboard). It is enclosed in a watertight aluminum case with three built-in monitors, along with standard laptop functionality such as a keyboard, trackpad, camera, microphone, speakers, and Wi-Fi. The Omnibus sink can listen for a particular Omnibus source and continuously receive data from it. This data is then unpacked, interpreted, and displayed in the desired format.

For example, a pressure transducer feeding into DAQ will have its data transmitted through the Omnibus source for the NI module, then received by the Omnibus Dashboard sink and passed to plotting software. This allows mission control to see the pressure visually on a graph that updates in real time. Most data passed through Omnibus is read-only (i.e. source → sink), however, there is some write functionality that enables Omnibus to send commands to electrical boards over RocketCAN.

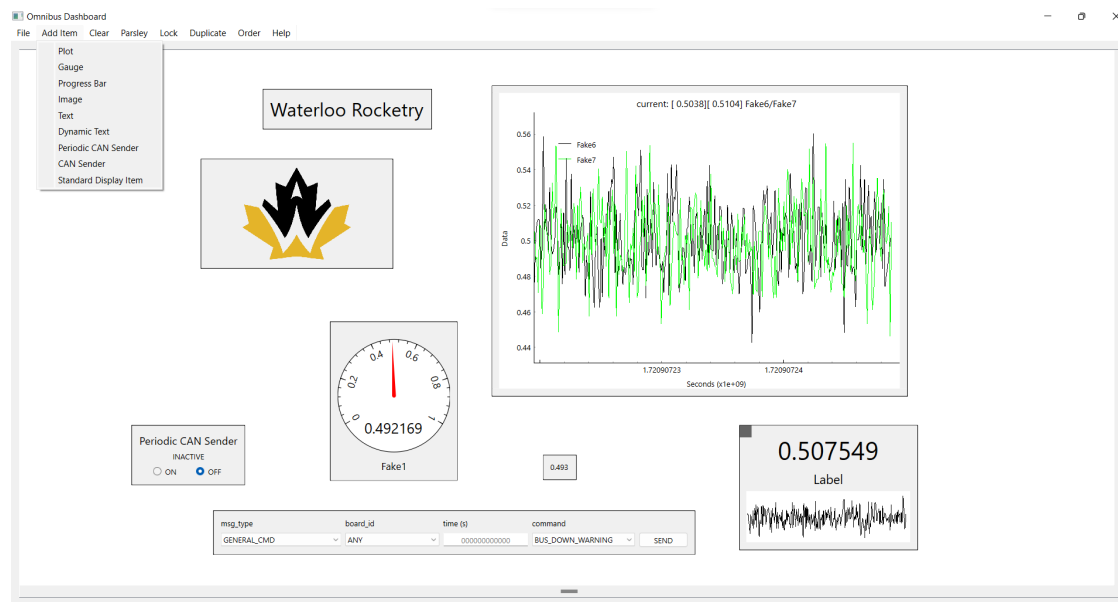


Figure 124: Omnibus Dashboard Screenshot

The Omnibus Dashboard is designed to allow for easy modifications to allow DAQ operators to make quick changes as necessary. Dashboard items can be locked and resized, with keyboard shortcuts to simplify common actions. Dashboard configurations can be saved and loaded. Data visualization features including an analog gauge, progress bar, and sparkline display provide clear updates.

## 11.4 Ground Side Power Distribution

Ground Side Power Distribution (GSPD) is a new SRAD system that supplies power to our ground side equipment (GSE). The intention of GSPD is to have a central hub in which all our GSE; DAQ, DAQ Laptop, RLCS, Ethernet box, and Antenna can be powered simultaneously using up to four car batteries or by generator. The system takes in 12V from the car batteries or the ATX 430W power supply (which is used to convert the generator voltage to 12VDC) and filters it. The 12VDC is then fed through a 5V and 24V converter and filtered. The 5V, 12V, 24V and GND lines along with voltage, current, and temperature sensing data are distributed to the GSE via an array of M12 connectors and cables. The components of GSPD are housed in a water and dust proof pelican case, modified for ease of usage and cooling.

### 11.4.1 GSPD Boards

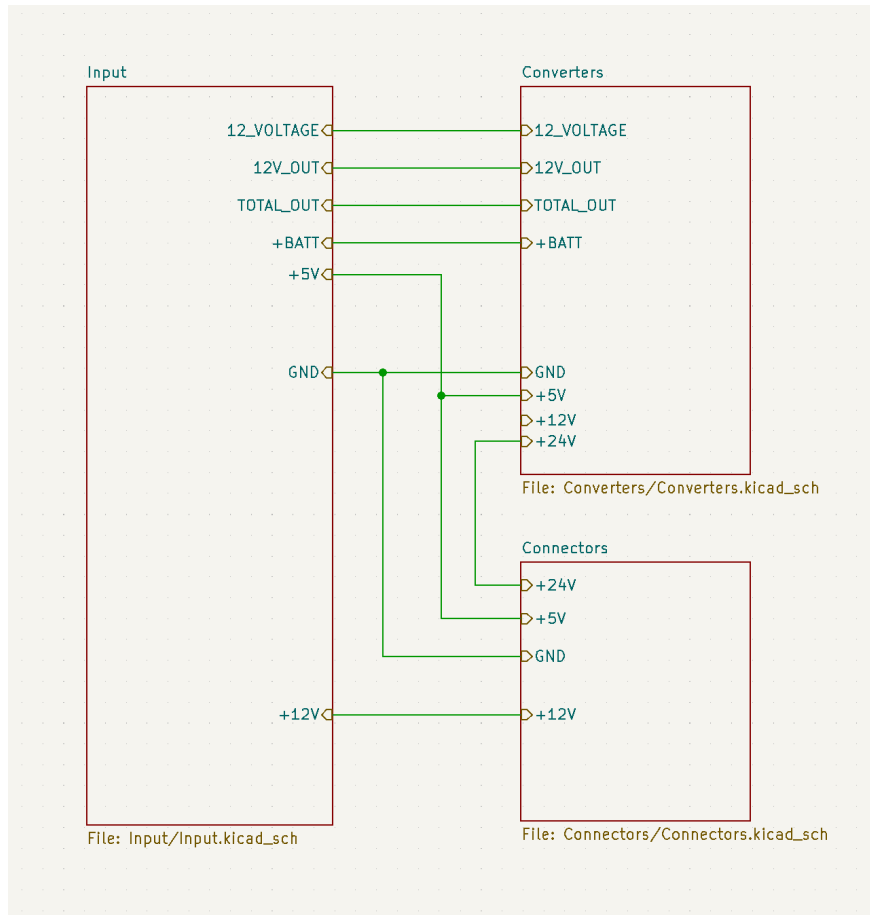


Figure 125: Connections Between Boards for GSPD

The input board's primary purpose is to receive power from either the car batteries or ATX power supply. Looking at the input section of the schematic below, a three position switch is used to flip between battery power, generator power, and off. The input incorporates several safety features including a fuse, inrush current limiter and reverse polarity protection. Originally, the input voltage

was to be filtered using several 22mF caps. However, testing demonstrated the voltage line was clean enough without the 22mF caps and that the 100uF capacitor alone is able to handle sudden variations in voltage. This board also displays battery voltage on a digital voltmeter, uses a resistor divider so the voltage can be monitored by DAQ and incorporates two current sensors, one for 12V and the other for the entire system. We then pass both the raw 12V and filtered 12V line to the converter board.

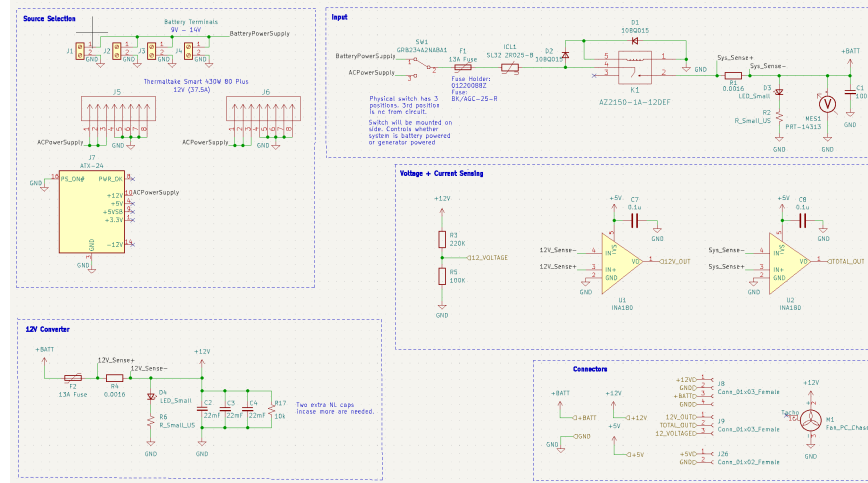


Figure 126: Schematic for Input Board

Converter board takes the raw 12 volts from either the battery or power supply and converts the voltages to 5V and 24V using buck converters. The 5V converter used is the K7805-3AR3 with a max current of 3A and efficiency of 93%. This converter incorporates a 10uF capacitor at the input and 22uF capacitor at the output to help reduce ripples. The 24V converter used is the URB2424LD-20WR3 with a max current of 834mA and efficiency of 90%. This converter incorporates a 100uF capacitor at the input and output. High efficiency converters were selected to reduce heating and power losses. The 5V and 24V lines each have fuses rated under the maximum current the converters can handle along with a 10uF buck capacitors. This board is also home to the voltage and current sensing for the 5V and 24V lines along with a thermistor to measure the temperature of the surrounding air. The sensing data is directly fed to DAQ via an M12 connector/cable assembly.

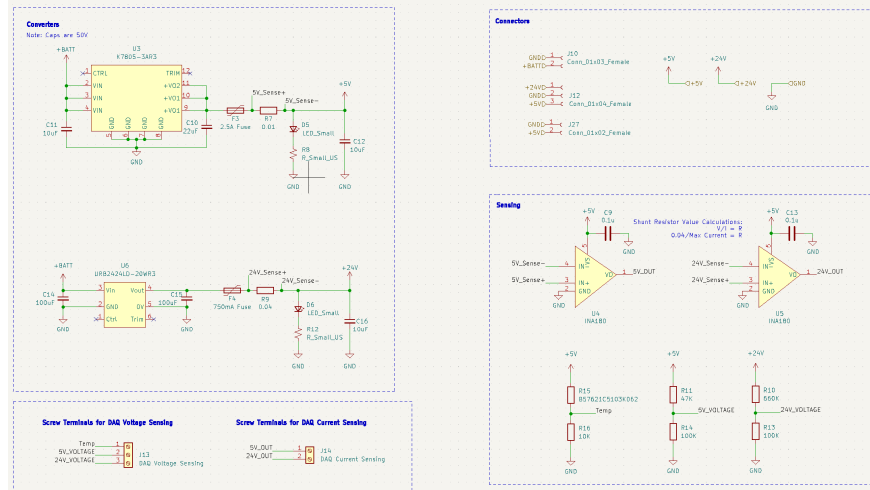


Figure 127: Schematic for Converter Board

Connector board receives all the voltage lines and ground from the input and converter board and connects these lines to 9 4-pin screw terminals. Each screw terminal is partnered with an M12 connector, capable of providing power to any of the GSE. The team recently decided to standardize our connectors, with A type M12's being used for lower power demands, D type M12's used for data transmission to DAQ (voltage, current and temperature sensing) and T type M12's used to transmit power to equipment with high current draw (such as the DAQ laptop). These connectors are mounted on the back of the GSPD case.

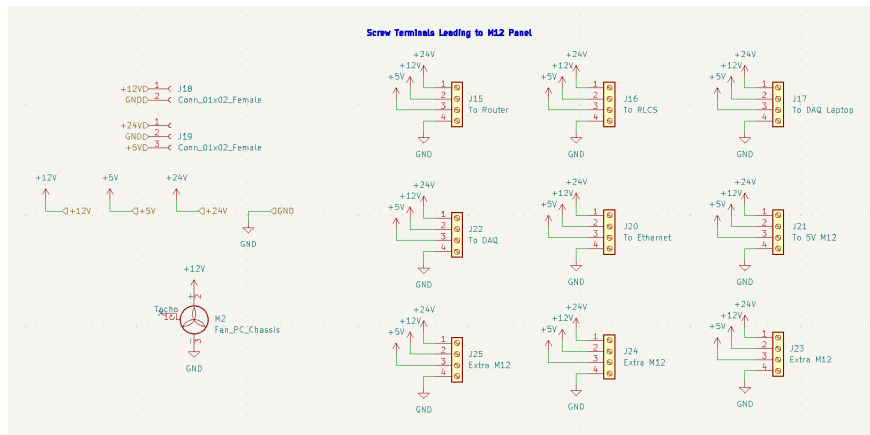


Figure 128: Schematic for Connector Board

### 11.4.2 GSPD Case

In order to safely house all electrical components, a weatherproof pelican 1506 air was selected. All components are mounted to a laser cut wooden boardm which is securely fitted to the bottom of the case (Figure 129). Connections to components outside the box are done through waterproof M12 connectors, which pass through watertight holes drilled into the the sides of the box.



Figure 129: Inside the Fully Assembled GSPD Case

At the top of the box there are connections to data lines leading to the DAQ box, which can handle up to 6A of current. The PSU is mounted to the wooden base using a bent aluminum sheet plate, a hole was drilled and caulked near the bottom for the AC power cable. There are also four wire feeds for the four car batteries the system can support. In the bottom right, a hole was carved for a switch and digital voltmeter. It was also caulked for waterproofing. For cooling, two 12V PC fans were installed, one for intake, other for outtake. A water/dust proof mesh was added to prevent debris from entering through the fans. A 3D modelled cover was also added to protect the fans from the rain.

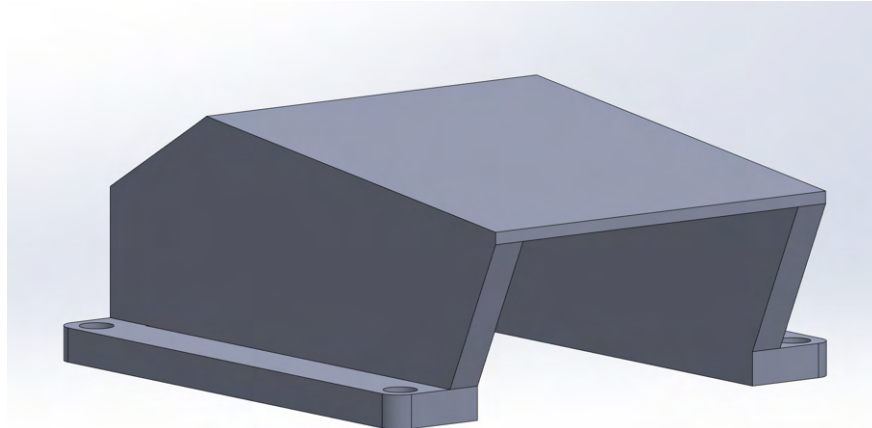


Figure 130: CAD for the Fan Cover

## 11.5 Tank Heating

This year, due to the climate at Northern Ontario, a need for active tank heating was established. The SRAD heater is made of single layer flexible PCB with adhesive, which is glued to the Ox Tank. The heater has a resistance under ambient temperature of approximately 1 , and a power draw of 625W. The heater's resistance varies by temperature, the higher the temperature the higher the resistance, when the heater reaches 75 degree Celsius, the resistance is approximately 1.2 ohms. The variation of the resistance will be used for calculating the temperature of the heater.



Figure 131: Tank Heater Flex PCB  
Page 160

The power to the heater is connected via a XT-30 connector, with the female side soldered to the flex PCB and connected to the PCB traces. The male connector is connected via a pair of 12 awg wires to power and a pair of 22 awg wires to tank heating relay board for voltage sensing. The voltage sensing line, which senses the voltage across the heater, along with the current sensing provided by the relay board, makes it possible to do a 4-terminal sense of the heater's resistance in real time. The extra voltage sensing line is required for avoid inaccurate data caused by voltage drop at the power wires. There is also a thermistor on the heater which is being used for redundancy of the 4-terminal sensing. The thermistor connector is a standard female 2-pin dupont connector. All of the connectors are friction fit and pointing towards ground. This makes the connectors disconnect during launch.

## 11.6 Electrical Umbilical

The rocket's main CAN bus lines are routed through the umbilical to the DAQ system, which contains a board that can transmit and receive CAN messages over a USB connection. This data stream is then passed over the ground radio link along with the usual data from DAQ and RLCS. Because the electrical umbilical disconnects after liftoff this backup link is fully sufficient to launch the rocket in the event of a live telemetry failure.

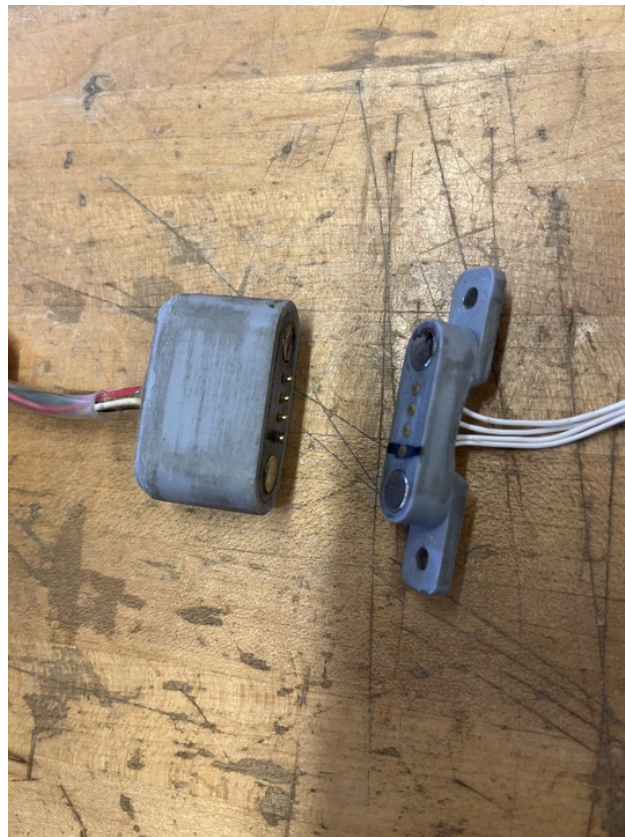


Figure 132: Electrical Disconnect

The electrical disconnect connectors have 4 conductor pins and two magnets which mate the two halves together. The connectors are for GND, CANL, CANH and 24V. The contact pins are

spring loaded for maintaining contact. The two magnets are in opposite polarity to ensure the connector can only be connected in one way. The case is 3d printed from PETG.

## 11.7 Launch Tower

The launch tower used by the team is comprised of four 10' segments of triangular aluminum lattice, connected to an 18" x 18" plate. This truss was sourced new for this year, as the previous truss used by the team was at least 12 years old and was beginning to warp meaning the rail would not run straight. The new aluminum truss is much lighter, and simpler to assemble. The assembly of the truss and the 18" x 18" plate is connected to a larger base frame via a hinge, allowing the base to be secured to the ground before the tower is raised. When raised, the tower is angled 6° from vertical as per LC DTEG R10.1.1, and secured by a series of three guy wires as shown previously in Figure 113. The guy wires are sized to ensure a FOS of at least 1.5 on tipping at the maximum wind speed recorded in Timmins during the launch period, 60km/h. A 32' launch rail made up of 1.5" square aluminum T-slotted extrusion segments is mounted onto the tower using clamps that wrap around the vertical tubes of the aluminum truss. During initial testing, it was discovered that the clamps could rotate if not tightened sufficiently, which would be a significant issue if it occurred while the rocket was on the rail. To fix this, neoprene rubber was bonded to the surface of the clamps to increase the friction and allow the clamps to be tightened further without damaging the tower, and the wingnuts supplied with the clamps were replaced by standard hex nuts for easier tightening. The rail interfaces with the two launch lugs on the rocket which slide into the slot of the rail. A load cell is mounted at the base of the tower such that the rocket rests on it, allowing the mass of the rocket to be remotely monitored during propellant filling. The launch tower is shown in Figures 133 and 134.



Figure 133: Assembled Launch Tower



Figure 134: Raised Launch Tower

In 2022, there was an incident where the gin pole used to raise the tower snapped due to improper sizing. The gin pole mount was resized in 2023 to account for the bending loads when raising the heavier steel lattice tower, so this sizing is still valid for the lighter aluminum tower. This new gin pole was validated in tower raising tests in 2023 and 2024, and at competition in 2023. In previous years, the load cell data has been unreliable. In 2023, an attempt to solve this issue was made by placing the load cell mount on a set of linear bearings to reduce binding. This solution showed improved results during a static loading test using water, however when the rocket was placed on the rail the data became unreliable and was therefore not used to monitor filling in 2023 (filling was monitored instead both visually and via temperature data confirming when liquid reached the diptube and began exiting the vent valve). The root cause of the load cell data issue has since been theorized to be the force being applied to the rocket by the spring-loaded quick disconnect mechanism causing the launch lugs to bind on the launch rail. Given that the quick disconnect mechanism is disconnected using pressure and gravity this year, it should not exert a binding force on the rocket and so it is hoped that the load cell data will improve.

The major upgrades for 2024 are the new truss, the use of clamps for mounting the launch rail and guy wire mounts, and a 2500lb electric winch to replace the drill driven winch which was used in previous years. The use of clamps to mount guy wires and the launch rail instead of drilling bolt holes through the tower as was done with the steel truss, as well as the use of a standard aluminum triangular truss, means that the launch tower can be reconfigured much more easily to accommodate changes in height. The current tower is sized to ensure sufficient off-rail velocity for Borealis, but it could be shortened or extended for future rockets as needed.

## 11.8 Antenna Towers

At competitions in 2022 and before, the antenna at the launch site was mounted on the launch tower, and the antenna at mission control was affixed to a shovel or vertical piece of wood. This created issues when connecting the antennas, as the towerside antenna needed to be rotated independent of the launch tower in two axes - horizontally to point towards base camp and vertically as the antennas were at different elevations. The low elevation of the basecamp antenna also presented connectivity issues as signals were blocked by surrounding vegetation or the terrain.

In 2023, two identical towers with metal extendable bases and telescoping carbon fiber masts were sourced so that the antennas can be mounted independently and at a high enough elevation to be clear of any obstructions. The towers can be raised to a maximum height of 33ft, and the height can be adjusted as desired by extending some or all the telescoping mast segments to properly align the antennas vertically. The telescoping masts can also be rotated once they are raised, allowing fine tuning of antenna pointing to improve connection. The towers are secured by three guy wires similar to the launch tower, and were used successfully at IREC 2023.

## 11.9 Fill Plumbing

For competition in 2023, a panelized approach to groundside plumbing was implemented to reduce pad setup time and increase plumbing standardization and reliability. The current fill plumbing stand has two panels, one for loading nitrous oxide into the rocket, and one for loading nitrogen gas into the rocket's pneumatics. The P&ID of the plumbing panels that will be used for flight is included in the system P&ID provided as an appendix.

The panel includes many features to make operations easier and safer. Remote valves and pressure transducers at key locations allow for the system to be monitored and operated at a distance, and mean that operators only need to open supply cylinders and set the nitrogen regulator before retreating. This means no operators are ever near the rocket when it is filled with propellant. Additionally, manual bypass valves with ropes attached are located so that there is no point where there can be pressure trapped without a way to vent it from a distance. The panel also includes a pressure gauge, as well as a pressure relief valve set to 1000 psi for safety. To allow the panel to be used without full sanitation after each use, a swappable filter element is included at the inlet of the panel to catch debris. Additionally, an inlet for a nitrogen purge is included to remove remaining nitrous oxide vapor after use. Quick disconnects interface from hoses to the panel, for quick assembly in the field. Tubing was used for as much of the panel as possible to allow for easy assembly without the major clocking issues caused by NPT. Additionally, it will be easy to modify the tubing in the future if changes are required. Both JIC flared connections and Swagelok are used on the panel to connect tubing and interface with NPT components. The fully assembled panel is shown in Figure 135.



Figure 135: Assembled Nitrous Oxide Panel

Both the nitrous oxide and nitrogen panels have passed hydrostatic test at 1.5x the maximum expected operating pressure (1500 psi), and have successfully supported three static fires (one for the 2023 hybrid engine, and 2 for the Eridium engine) as well as the successful launch of the 2023 rocket. Using the same plumbing setup in all tests has also allowed all operators to become much more familiar and comfortable with the system, and has allowed the team to validate the reliability of both panels.

## 12 AIRBRAKES

### 12.1 Mechanical

#### 12.1.1 Constraints and Criteria

The goal of the airbrakes subsystem is to hit a target apogee through the use of active aerodynamic control surfaces that are able to adjust the rocket's flight trajectory mid-flight more closely than can be achieved through purely passive controls such as propellant mass fill. Historically, precision was achieved exclusively through rigorous simulations and precision manufacturing, which in 2023 brought LOTS to within 1500ft of the 30,000ft target apogee. To further improve this result, Borealis will fly active in-flight controls in the form of airbrakes. The addition of this new rocket subsystem demanded a set of constraints and criteria that would influence its independent mechanical design, as well as the integration with the other sections of the rocket. This presented unique challenges when considering integration with the new liquid bipropellant propulsion system, which requires significant integration considerations compared to solid propellant rockets where airbrakes are most often flown.

1. To ensure symmetry between the control surfaces, lest they produce an uneven drag force causing the rocket to tip, the following must be maintained:
  - (a) System must only use one motor to drive the mechanism, so that there is no potential for individual motor failure (electrical, software, or mechanical)
  - (b) Mechanically, the halting of one panel must result in the halting of the others; they must be mechanically coupled, even in the case of mechanical failure in multiple subsystem areas.
2. To assist in simplifying the control system, the distance rotated by the servo should be directly proportional to the distance the control surfaces stick out of the rocket.
3. Be as compact and lightweight as possible.

#### 12.1.2 Conceptual Design

Two initial concepts were considered for the airbrakes mechanism. The first involved flaps that started flush along the body of the rocket and then pivoted away from the body of the rocket into the airstream. The second concept involved horizontal panels extended and retracted from the body tube by a mechanical linkage. The second concept was chosen to eliminate the requirement of a drive motor strong enough to actuate against the drag force produced. In addition, potential implementations of the first concept suggested the linkage would take up considerable space and/or require multiple independent motors. Both of these ideas and various mechanical linkages were referenced from past reports of teams who flew airbrakes.

### 12.1.3 Implementation

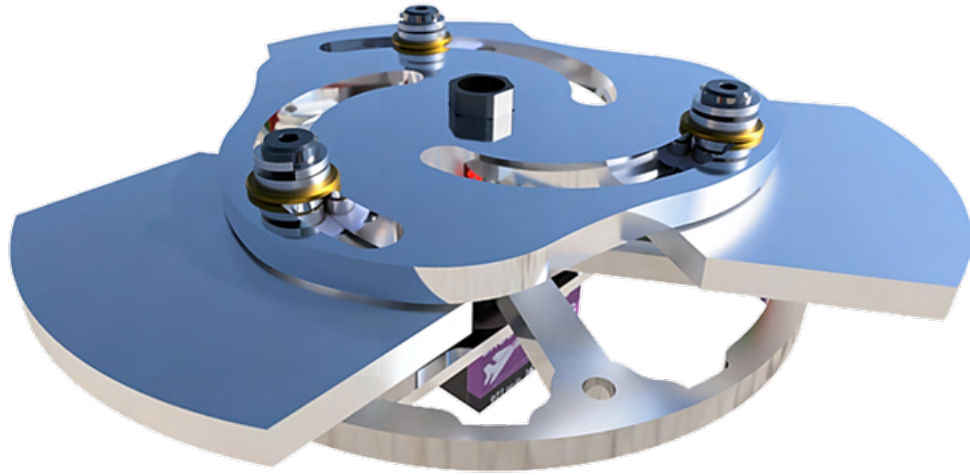


Figure 136: Airbrakes mechanism Top View

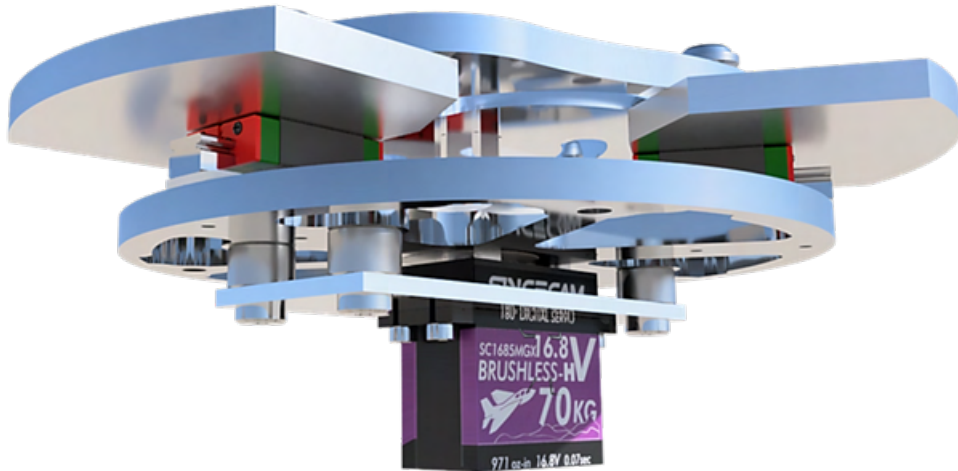


Figure 137: Airbrakes mechanism Bottom View

The final implementation of the first design concept is shown in Figure 138. The design can be broken down into a few key areas that all work together to ensure the servo has minimal mechanical load, even under intense flight loading:

1. Slot Geometry
2. Linear Rails
3. Bearing Stack

#### 4. Servo Selection

#### 5. Servo Placement

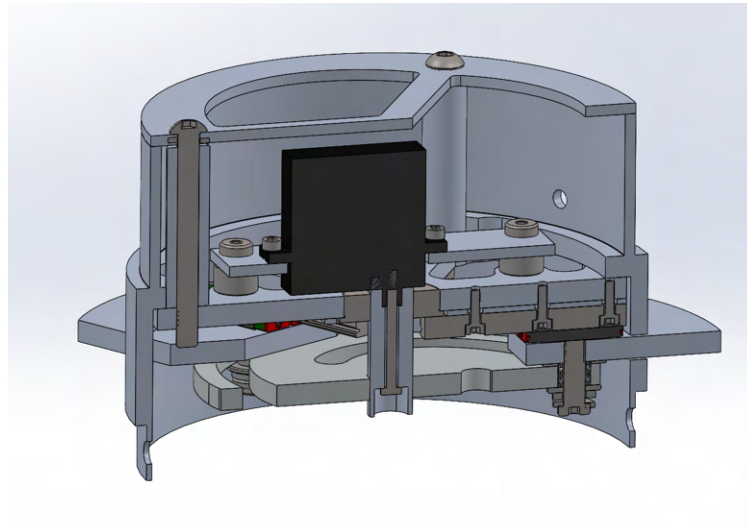


Figure 138: Airbrakes assembly section view showing integration and final body tube

There are several mechanisms that can couple one rotational input to 3 synchronous linear outputs, however finding one that had a linear relationship between degrees and linear distance extended was challenging. One of the mechanisms thought to provide maximum flexibility while being much more robust and reliable than other options involving gears or linkage arms was a cam and slot mechanism. However the typical cam and slot profile does not result in this linear relationship. Instead, using parametric curves, a custom slot geometry was modeled that ensured the rotational motion linearly coupled to the straight extension of the panels. This can be seen in Figure 139:

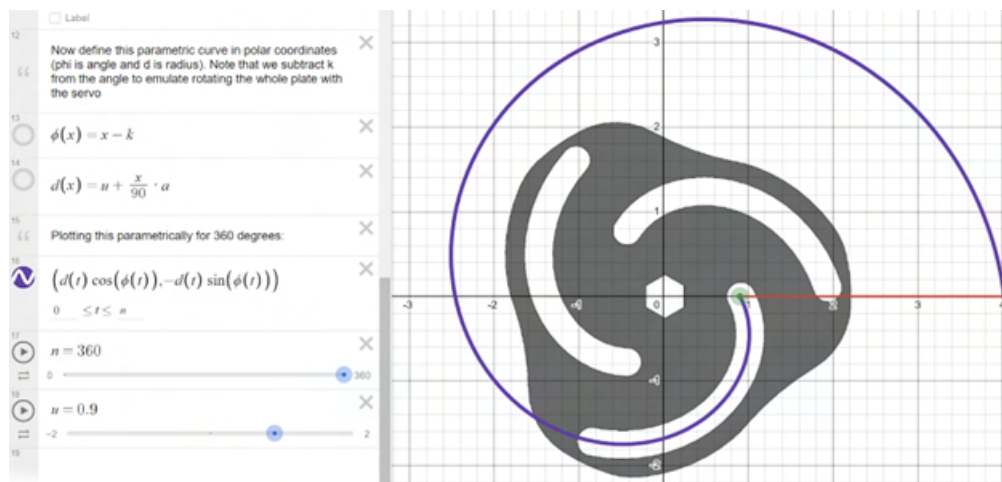


Figure 139: Airbrakes parametric curve graphed in desmos

Two sections of the system, the bearing stack and the linear rails, are utilized to have the servo essentially move zero load, under no mechanical stress, even during peak flight loading. These two sections guarantee that the motor will not stall under the stresses of flight. The linear rails provide the majority of the support to the panels, allowing them to sustain the bending moments caused by the drag generated moving at high velocities. The largest load is the drag force acting on the panels, both pulling down on the linear rails creating a moment along their length shown below.

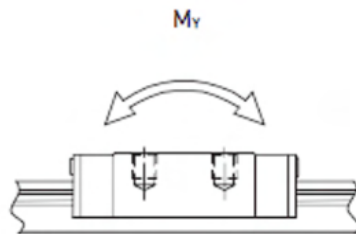


Figure 140: Moment about linear rails

The drag results from CFD were used to calculate the maximum loading the panels would experience, and the smallest linear rail that could sustain that load (with a safety factor) was selected. The size of the rail height and length were both important considerations. The height being smaller helps satisfy the criteria of the entire subsystem being compact, and in addition lower rails mean the servos shaft is not cantilevered as far above the support bearing thus improving rigidity. The length being short is far more critical, since the systems diameter is constrained to 6 inches, a longer block takes up valuable space, reducing how much the panels can extend from the rocket. However, as the blocks become smaller their load ratings decrease significantly. As the smaller blocks also allow more of the panel to stick out, this simultaneously increases the surface area, increasing the drag force, and also the moment arm distance, so overall as block size decreases the load rating decreases significantly. The shortest possible block that could handle 7 Nm of torque was selected, the Hiwin MGN9CZ0C. 7Nm was the torque calculated using that length of block, which consequently led to having 0.86" of panel sticking out of the rocket at maximum extension.

The other design consideration for minimizing loads on the servo is the bearing stack for the pins. The bearing stack minimizes friction between the panels and attached 1/4"-28 bolts and the spinning plate. Many iterations of the bearing stack were assembled in CAD, and two of those were selected for further physical testing. The first included thrust bearings on the top and bottom of the spinning plate, low profile bearings that ran through the slots, and a split washer to keep the whole assembly held together at a constant force. This worked but had considerable friction and a tendency to become stuck or bind. The balls of the thrust bearings could catch when they dropped into the slots and the split washers were not consistent enough to provide only a very light force and so often increased friction significantly. The flight iteration solves those problems by replacing the thrust bearing with oil impregnated bushings and the split washer with three flat washers that only allow the spinning plate to shift a small amount but do not force it onto the panels.

The whole assembly must also maintain each of the panels in an extremely similar extension state. This is so no uneven drag forces are created which would affect stability. Therefore the connection from the spinning plate to the bearings to the 1/4"-28 bolts must have as little slop as possible. Originally the spinning plate was going to be water-jet along with the rest of flat



Figure 141: Bearing stack components and assembled

aluminum pieces in the section and a test with different clearance slots was cut to determine what was the smallest slot that could still allow the bearing stack to move. However, the rough surface finish of the water-jet meant that some areas of the slot would be loose while others would catch. Because a wire EDM was available it was decided to cut the plate that way and not attempt sanding of the slots to a perfect fit. The final plate has slots only 1 thousandth of an inch larger than the outer diameter of the bearings and the bearing stack both moves with almost no friction and restricts the panels to all being at the same extension. This has been further validated during testing, where when a significant gap and resultant slop was observed between the spinning plate and the shaft, the extension of the panels relative to one another was unaffected.

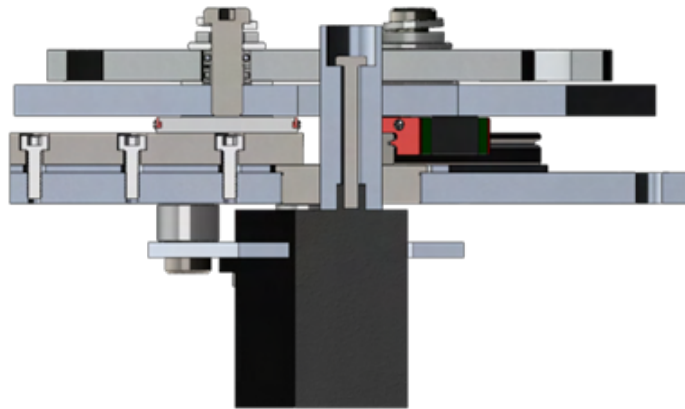


Figure 142: Airbrakes Mechanism Cross Section

The final aspect of the design which helps completely eliminate loading of the servo is the arrangement of the mechanism and its connection to the servo. The mechanism and servo are mounted to either side of the base plate and connected by a hex shaft. This arrangement was chosen to minimize the section height, minimize the number of structural plates needed and because it integrated well with the rest of the rocket. This arrangement places the servo very close to the bearing held in the base plate, allowing the bearing to take almost all lateral loads.

One of the earlier components that was selected in the design process was the motor. This is because most of the design would have to conform around the size and mounting of the motor. This was also critical to inform the design of the control electronics for the motor. Ultimately a servo motor was selected rather than a DC motor with an external encoder, for two primary reasons. First, servos are much more compact, and brushless servos include considerable power in a small form factor, compared to an SRAD solution with a DC motor. Also, since servo motors have built-in position control, the system would not rely on the SRAD avionics for this functionality, reducing complexity and the need to pass additional data back and forth over the already rate-limited data connections in the rocket. Based on the requirements established by the mechanism design, a brushless servo that had the best combination of actuation time (a function of the speed of the servo) and acceleration (a function of the torque of the servo) was selected. This was a Sincecam 16V 70kg steering servo.

#### 12.1.4 Integration

Integration of the airbrakes subsystem with the rest of the rocket was highly iterated on. Very early on, the team considered putting the airbrakes towards the back of our rocket to ensure that the center of pressure (CP) is always behind the center of gravity (CG) (for rocket stability). However this was deemed infeasible because the only location this would be permissible would be in the injector section (between combustion chamber and tanks), a section too crowded to also contain airbrakes. Thus simulations in Openrocket were performed and it was determined that placing the airbrakes above the vent section would still retain the rocket's aerodynamic stability as discussed in Section 6.10. These simulations were later verified to be very similar to higher fidelity CFD modelling. Once this location was decided it was further decided to keep the airbrakes as their own separate section that would couple to the vent section below it and the payload above, rather than integrate it within the same tube as the vent section. This was done because the high loads on the airbrakes section and cuts in the aerostructure required an aluminum frame. Additionally, because the airbrakes are quite thin, they did not significantly interfere with the rest of the rocket architecture. After several iterations of coupler designs the one shown below was selected. The airbrakes assembly added 2 bolt circles to the vehicle, which was deemed acceptable. The airbrakes top plate also serve as the baseplate of the payload, reducing the requirement for a structural payload bond.

The final manufacturing consideration was not creating a pocket in the center of the coupler that would be difficult to machine out. Instead the decision was made to leave the ID the same from the vent section coupler to the airbrakes. This did mean a slight reduction in the ID where the airbrakes are housed (so a reduction to airbrakes system OD) and increased weight but both trade-offs were deemed acceptable.

#### 12.1.5 Testing

To test the airbrakes system 15 pounds were hung from each panel then the system was actuated 100 times. 15 pounds is the maximum force each panel was designed to withstand. The system performed as expected maintaining a quick and smooth response. The testing setup can be seen in Figure 144.

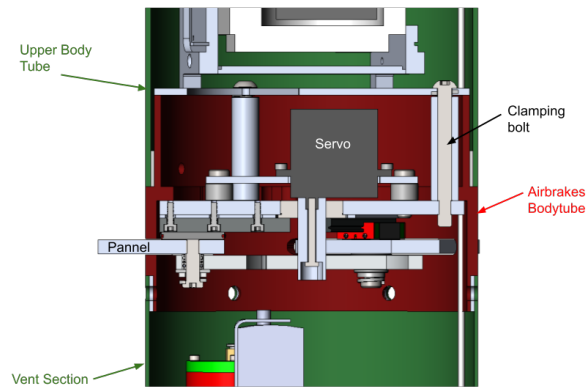


Figure 143: Airbrakes system integration and body tube drawing



Figure 144: Airbrakes Testing setup

Some final images of the airbrakes mounted inside their body tube can be seen below:



Figure 145: Top and Bottom View of Assembled Airbrakes in Bodytube

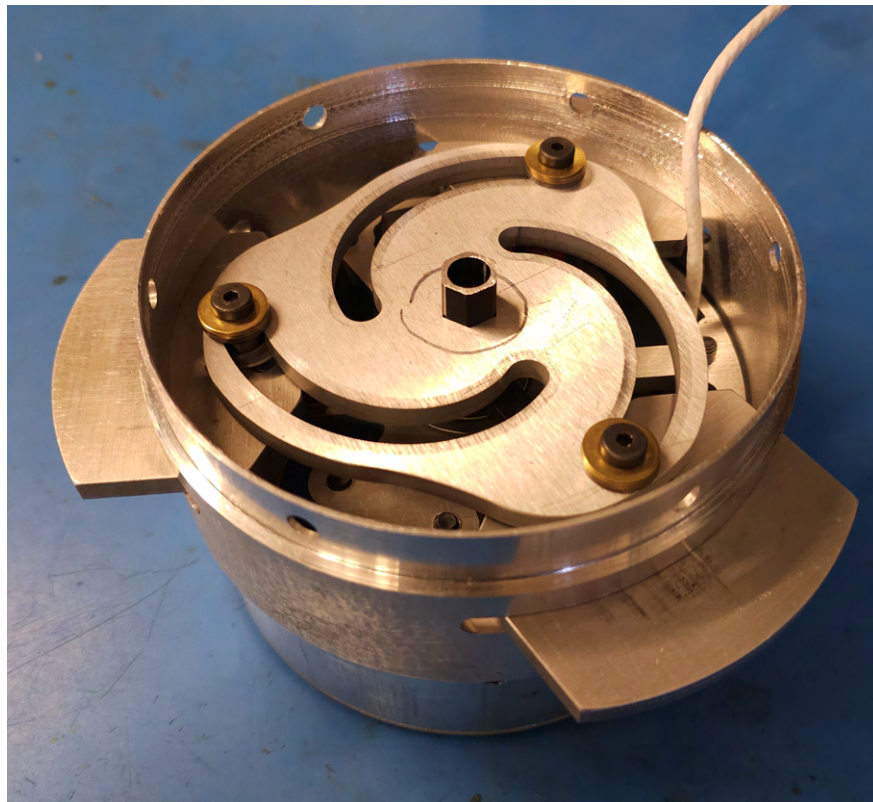


Figure 146: Isometric View of Final Assembled Airbrakes in Bodytube

### 12.1.6 Conclusion

The final mechanical design of the airbrakes meets all of the established requirements. The mechanism is smooth and easy to assemble, and does not bind even when binding is induced. Additionally upon powering up the servo the actuation of the panels remains fast even under load. Integration within the rest of the rocket is simple due to ease of manufacturing and assembly being heavily considered in the joint design.

## 12.2 Controller

The extension of the airbrakes is determined by an onboard implementation of a proportional-integral-derivative controller. The error function is defined as the difference between the predicted apogee given the current rocket state and with the current extension of the airbrakes assumed to be held constant, and the target apogee. The parameters of the controller are determined and verified through as discussed in section 6.12.

## 12.3 Processor Board

### 12.3.1 Scope

The purpose of the processor board is to take in sensor data, estimate the state of the rocket, predict the apogee of the rocket, and generate control commands for the airbrakes during flight. The board is also responsible for generating some CAN telemetry, including redundant GPS data and state estimates. The majority of sensor data and state information is supplied from a Vectornav VN-300 Rugged Dual INS. The VN-300 is used to supply raw accelerometer, gyroscope, and magnetometer data to an SRAD state estimation pipeline. To provide optimal flight data for future simulation efforts and design refinement, the output of the VN-300s Inertial Navigation System (INS), which provides a full state estimate significantly more accurate than what the team's srad system can be expected to achieve, is output and logged separately. The only external source of data to the processor board is the Remote Arming board, which forwards the altitude values read by the Stratologger COTS altimeter over the RocketCAN bus. The SRAD state estimation and apogee estimation is based on reducing a full 6-DOF rigid body model of the rocket to a 2-DOF, 4 state model. Linear acceleration (accelerometer), angular velocity (gyroscope), and heading (magnetometer) data are first fused using a Madgwick filter to produce three Euler angles which fully describe the orientation of the rocket in space with respect to the fixed Earth reference frame. These angles are transformed to yield an elevation angle with respect to the fixed frame. The rockets vertical velocity in the fixed frame can be estimated by differentiating the altitude readings with respect to time. Using the assumption that the rocket travels at approximately zero angle of attack due to the stabilizing effect of the fins, the elevation angle and vertical velocity can be used to calculate the net velocity of the rocket. Given the estimated altitude and net velocity at a point in time, as well as an empirical model of the drag force acting on the rocket, the rockets apogee can be estimated numerically. Once an estimated apogee is generated, this is provided to a feedback controller which compares it to a fixed target apogee and modulates the airbrake extension target. Although the primary reason for feeding the SRAD state estimation results to the apogee predictor is for the purpose of flight testing our own software, the INS and GPS on the VN-300 itself is disabled once the unit begins traveling over 500 m/s (this is standard on all commercially available

GPS/GNSS systems), and the unit only continues to provide raw IMU data. Although airbrake operation begins well below 500 m/s, since the exact operation of the VN-300 in this mode is unknown, the only flight objective for the INS is to passively collect as much data as possible. This will also give some indication of if and when the INS will be reenabled during flight, for future use.

### 12.3.2 Electrical Design

As part of the RocketCAN distributed avionics system, the processor board communicates with other rocket systems and mission control via the RocketCAN bus. It draws power from the 5V onboard regulated supply and uses the same standard connector, current sense amplifier, and CAN transceiver circuits as other RocketCAN boards. The processor board is directly connected to the VN-300 and supplies power and data through a 10 pin Harwin Datamate connector. Unlike most of the teams flight hardware, the VN-300 is worth many thousands of dollars and essentially irreplaceable. Therefore, the 5V supply to the VN-300 is equipped with reverse voltage protection and transient voltage suppression (TVS) diodes.

The processor board mounts an STM32H733 microcontroller. This handles CAN and UART communication, as well as performing all the computation for state estimation, apogee prediction, and control. The processor board has a local, dedicated SD card, which is connected to the MCU over a high speed Secure Digital and MultiMediaCard (SDMMC) interface. This is necessary for effective data logging since the bandwidth of the RocketCAN bus is extremely small compared to the volume of data available for logging and the speed at which the STM32 can log. The board is capable of and designed to log all incoming CAN traffic, acting essentially as a spare for the Logger board. For testing purposes, the board also integrates an I2C interface which can be used to communicate with external sensors.

### 12.3.3 Firmware

Unlike other RocketCAN boards which generally use low power microcontrollers, perform relatively simple individual functions, and have real-time requirements on the order of thousands or hundreds of milliseconds, the processor board has extensive functionality and a target operating frequency for the core estimation and control loop of 100 Hz. Thus, to structure firmware development and make the most out of the available processing power on the STM32, and to give undergraduate students interesting technical challenges, the choice was made to run the processor board firmware on top of a real-time operating system (RTOS). The initial RTOS of choice was ZephyrOS, however this was abandoned due to a lack of support and large development overhead. Instead, the project eventually settled on FreeRTOS, which is directly supported by STM.

The diagram in Figure 147 gives an overview of the code architecture. The code is split up into threads (blue) whose execution on the CPU is managed by the FreeRTOS scheduler. Each hardware peripheral (yellow) is only assigned to a single task, preventing the need for hardware resource management. Threads communicate with each other primarily through FreeRTOS's thread-safe queue system (green). Where large amounts of data need to be transferred, such as with logging, a set of dedicated RAM buffers (also green) with mutual exclusion (which FreeRTOS also provides support for) is used instead. Sensor data is received and parsed through the FDCAN1 and USART1 peripherals, before being sent to the state estimation and apogee prediction subsystems.

The apogee prediction is rate-limited by the COTS altimeter, which outputs at significantly lower than 100 Hz. Due to the modular nature of the code, the state estimation task can continue to update the estimated orientation of the rocket, with apogee prediction taking over as soon as new altitude data arrives.

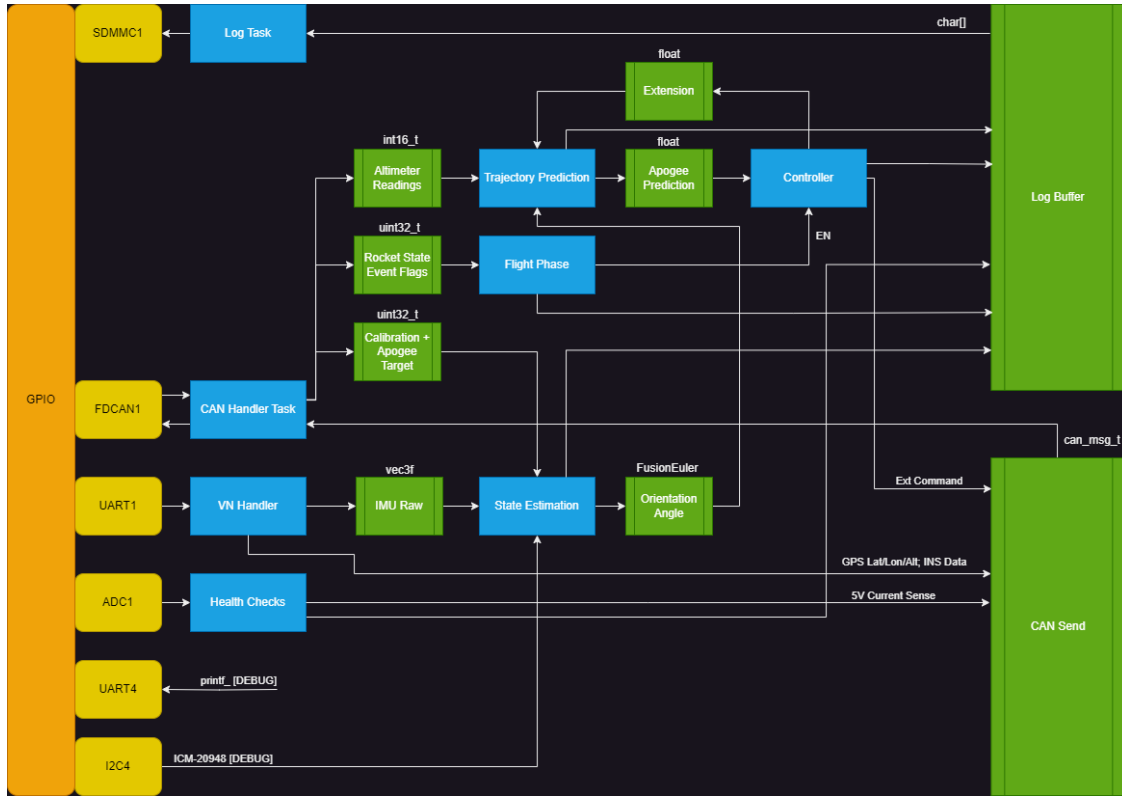


Figure 147: Processor Board Firmware Architecture

## 12.4 Simulations

Given the practical integration concerns with placing the airbrakes system in the injector section, the aftmost placement available was the area immediately above the vent section. Preliminary simulations using OpenRocket (see Section 6.10) suggested this placement was likely acceptable and so design proceeded under that assumption. These simulations were not, however, sufficient for verification of the design or for development of drag profiles necessary for effective rocket control using the airbrakes. It was decided that a commercial CFD package, Ansys Fluent, should be used to conduct simulations of the aerodynamic behaviour of the rocket over the relevant flight regime.

As the team had never conducted direct CFD analysis of the rocket, it took a great deal of time to become familiar with the software and understand aspects of the process such as geometry meshing that were abstracted by prior analyses in OpenRocket. Further complicating this was the lack of available rocket geometry, given that the Borealis project was still in its infancy and little to no mechanical CAD existed. For a number of reasons, it had been well established at the infancy of the project that the airbrakes would only operate in the coast phase of flight. This allowed for a considerable simplification of simulations, as it enables the airbrakes to be simulated

in an isolated and standalone environment, without consideration of the engine burn, which can drastically change the flow regime surrounding the rocket body.

The first true rocket analysis was performed using a simplified model of LOTS - the team's 2023 flight vehicle, which has an extensive set of OpenRocket data, with the only protrusions being the rocket fins. This was compared against the results of Cycle 6 flight dynamics simulations for verification and allowed the team to refine CFD parameters such as mesh bodies of influence and the solver to fit this specific use case. A mesh refinement study was also conducted on this model, which informed later simulation efforts. Once these preliminary simulations were performed, the model of LOTS was modified with three instead of four fins to match the Borealis architecture (section 6.5) and airbrakes at various fractions of their total extension. Fluent does support parametric workflows for geometry, but this was descoped due to time constraints, and instead the team settled on using a minimal set of fixed extensions with individual surface CAD for each. For the final simulations, an accurate model of the rocket is created, with airbrakes, bolt circles and the combustion chamber modelled.

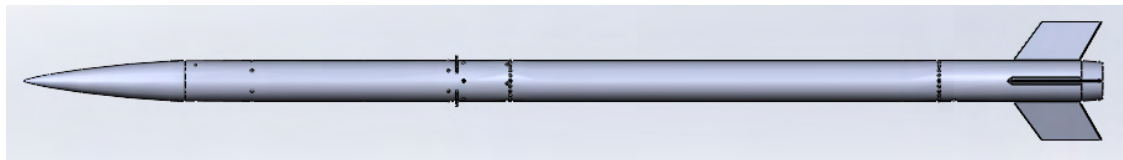


Figure 148: Rocket Model Used for CFD Simulation

Setup starts by importing the geometry of the rocket, with the interior completely solid and watertight, into Spaceclaim. Various geometry fixes are performed to ensure there is no broken or skewed geometry. Bodies of influence (BOIs) are created at the region of interest, including nosecone, airbrakes, bolt circles and fins. A cylindrical enclosure of 1000in length and 300in radius is created with the rocket geometry subtracted away.

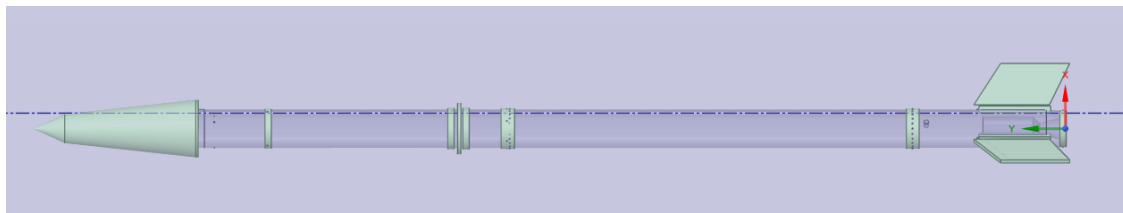


Figure 149: Enclosure Created from Rocketry Geometry, with Bodies of Influence

This geometry is then brought over to Fluent mesher. With all the BOIs set, the surface mesh is created with an initial target maximum skewness under 0.7. Then, the regions are set, 5 layers of boundary layers are added to ensure an acceptable  $y+$  value for the turbulence model. If no error arises, the skewness, orthogonality and aspect ratios are checked. The maximum skewness target is 0.85, and the minimum orthogonality target is 0.2, with an average of 0.01-0.1 and 0.95-1, respectively. The cells that are close to the maximum skewness are individually checked to ensure they are not in the critical region of the rocket.

The simulation starts by setting the air density and dynamic viscosity at the altitude of simulation according to the 1976 U.S. Standard Atmosphere[15]. Boundary equations are set with

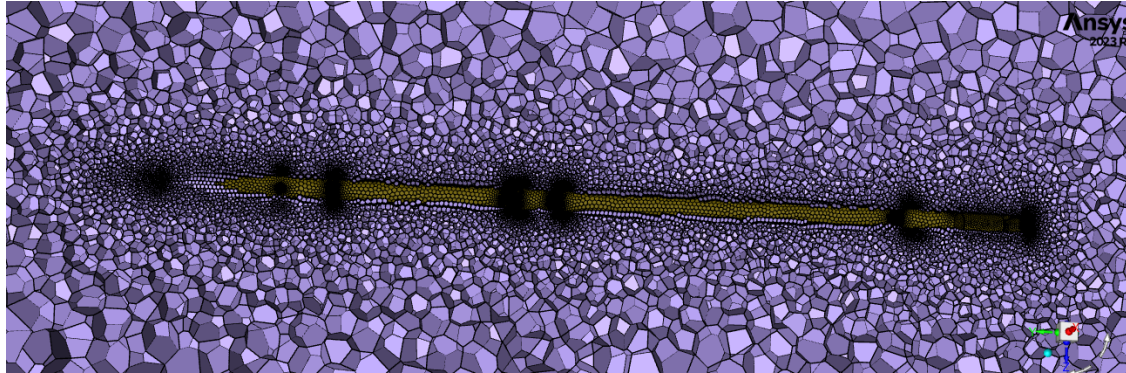


Figure 150: Closeup View of the Mesh

the inlet as the velocity of the rocket, with the direction of the inlet parallel to the rocket and in the opposite direction (pointing towards the tail). The angle of attack is added by resolving the velocity with angle into components with trigonometry. The outlet is set to be a pressure outlet with a gauge pressure of 0.

To resolve the velocity components with angle of attack, given an angle of attack  $\alpha$ , the formula is:

$$V_{parallel} = V_{total} \cdot \cos(\alpha)$$

$$V_{perpendicular} = V_{total} \cdot \sin(\alpha)$$

The enclosure wall is set to be free slip, allowing airflow to be undisturbed. The rocket wall is set to a specific roughness according to the final surface finish of the rocket, 0.5 roughness constant for the rocket is used as this is the way it is predicted in OpenRocket.

The system model used is shear stress transfer (SST)  $k-\omega$ . It combines the advantages of the  $k-\epsilon$  and  $k-\omega$  models to improve accuracy in predicting the onset and amount of flow separation. The SST  $k\omega$  turbulence model is particularly suitable for modelling the aerodynamics of the rocket due to its accurate prediction of flow separation under adverse pressure gradients, enhanced near-wall treatment, and robustness across a wide range of flow conditions. The model solves two transport equations: one for the turbulent kinetic energy ( $k$ ) and one for the specific dissipation rate ( $\omega$ ). These equations describe how turbulence is generated, dissipated, and transported throughout the flow field.

Reference values are computed from inlet, with the reference zone being the air surrounding the exterior of the rocket. Length is set to the length of the rocket, and area set to the frontal cross-section area of the rocket. These dimensions are computed from OpenRocket and SolidWorks.

The solution method is coupled for pressure-velocity coupling, with least squares cell-based gradient and second-order upwind for every other discretization.

Two distinct products of CFD simulation were established. The first was stability verification. Since OpenRocket is not capable of simulating the airbrakes geometry, and the airbrakes were expected to have a meaningful impact on the location of the rocket center of pressure once extended, it was necessary to recalculate the center of pressure and static stability margin. These values are computed with the following equation, which calculates the center of pressure by taking the moment of pressure distribution along the rocket's major axis (y-axis in this model) and dividing it by the total pressure force [16]:

$$CP_y = \frac{\int_A (Y * Pressure) @ rocket}{\int_A (Pressure) @ rocket}$$

The second was the drag force at any particular combination of airbrake extension (reference area of the rocket body), velocity, and altitude, which is computed with a vector set parallel and in the opposite direction of the rocket's heading.

The location of concern is the axis parallel to the rocket, the CP values along the other axes should evaluate very closely to 0. Hybrid initialization and residuals are set accordingly depending on the precision requirement, and the calculation is run until convergence, defined by all residuals reaching 1E-3.

The solution is opened up in Ansys Post, planes are drawn on different axis and cut through the rocket at different angles. Velocity streamlines are drawn both forward and back, flows over airbrakes and fins are evaluated to determine if there are any concerning patterns.

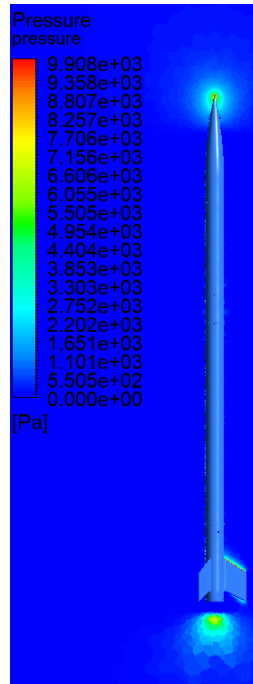


Figure 151: Pressure Contour of the Rocket at Mach 0.8 and 0% Airbrake Extension

Drag force curves were produced for 0, 50, and 100% extension of the airbrakes across a range of velocities and at fixed altitude. A second-order polynomial was fit to these data points to generate a continuous mapping from velocity to drag force. The drag coefficient was approximated as independent from altitude, allowing the air density  $\rho$  to be extracted as a linear scaling parameter of the force. The model which was eventually settled on linearly interpolates between these "extension curves" to determine the drag force, which is then scaled by the altitude ratio. The drag force at a given altitude  $a$  and velocity  $v$ , is:

$$F_{d,ext}(a) = \left[ (F_{d,50}(v) - F_{d,0}(v)) \cdot \frac{ext}{50} + F_{d,0}(v) \right] \cdot \frac{\rho(a)}{\rho(a_0)} \quad (1)$$

For the final drag tabulation, this was refined to steps of 10% extension, which were simulated across velocity of Mach 0.1 to 1.6 in 0.1 increments and altitude of 0m to 10 000m in 1000m increments. For simplicity by avoiding another domain of simulation, the rocket is always assumed to travel upright orthogonal to the ground reference frame, or angle of attack of 0. This resulted in a modification to the model to directly evaluate drag force as a function of both velocity and altitude. Between 40 and 50% extension:

$$F_{d,ext}(a, v) = \left[ (F_{d,50}(a, v) - F_{d,40}(a, v)) \cdot \frac{ext - 40}{50 - 40} + F_{d,40}(a, v) \right] \quad (2)$$

The results are plotted with drag against velocity and altitude, as shown in Figures 152 and 153.

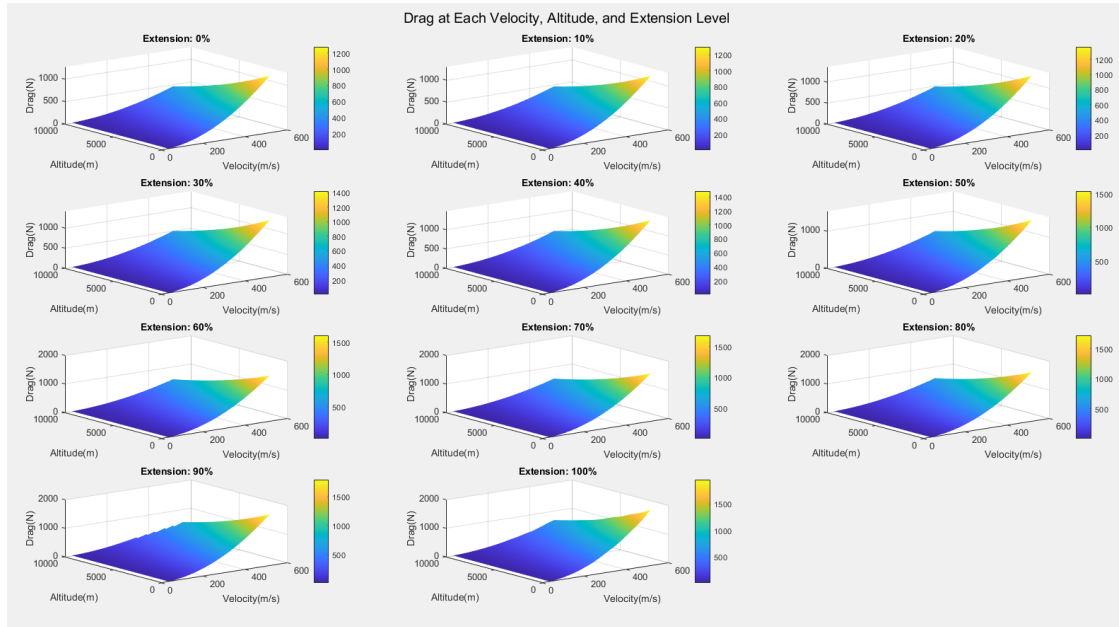


Figure 152: Drag Plot at 0-100% Extension

The plots can be overlaid on each other to visually see the effect of each parameter on the total drag value.

In parallel with simulations, the team developed an OpenRocket plugin [17] which is capable of overriding the drag force calculation normally performed by OpenRocket. This was used to determine the expected flight profile with minimum and maximum extension. The trajectory prediction and controller algorithm was also built into the plugin, allowing the controller parameters to be refined in simulation and loaded directly into the flight firmware.

## 12.5 PyAnsys Automation

In order to reduce the total number of person-hours configuring and running each individual simulation, it was decided to use the Ansys Python API, PyAnsys, to automate all the simulations. This allowed for minimal human intervention and error as well as allowing the team to run multiple simulations in batches overnight using a university provided supercomputer.

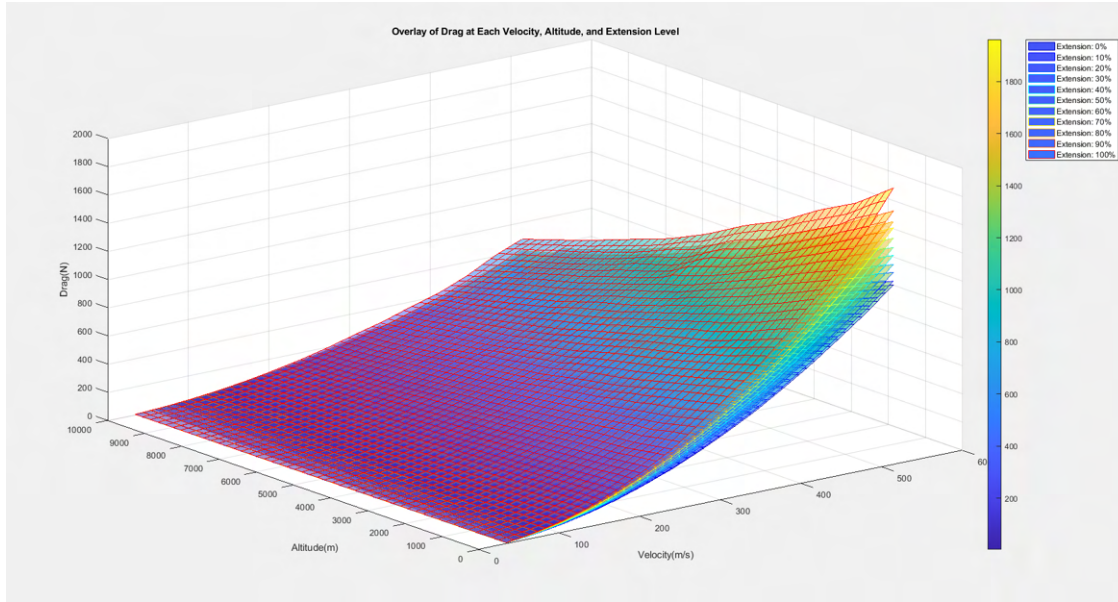


Figure 153: Drag Plot of 0-100% Extension Overlaid

Using PyAnsys in no way modified or altered the simulation data, this simply automated and sped up the process, allowing for the team to collect a larger amount of data points and construct more accurate plots.

The program allows a user to input all meshes into a folder, where each mesh represents a different extension of air brakes, and update a configuration file for all necessary parameters. The current configurations used for the simulation are altitude, velocity, and angle of attack. Using this information, the program also calculates air density and viscosity using the 1976 U.S. Standard Atmosphere [15]. All other values (rocket length, convergence values, etc.) are constant but can be modified by altering .csv files in the configurations folder of the program.

Once all input cases have been added, the user can hit run and leave the computer running overnight or for several days. Every input case will be run on every mesh and all data will be outputted into a .csv file for easy use. Furthermore, the velocity and pressure contour of each simulation case is saved into a directory as well. This is helpful to visualize any discrepancies. The full program can be found on the team's GitHub page. [18]

CFD development was a large project and this report is not intended to cover the full scope of development work. Further discussion of airbrakes mechanical design, integration and simulations is included in Section 12.1. However, several topics including the automation of simulation cases, further mesh refinement study details, geometry modelling of protrusions, and a few other details are left out of this report for the sake of brevity. These are discussed in an in-depth airbrakes CFD report written by Waterloo Rocketry in fall 2023 [19].

## 13 PAYLOADS

Waterloo Rocketry will be flying a payload consisting of two separate experiments this year. The first is an experiment designed to evaluate the affects of vibrations experienced in flight by fasteners of various sizes, torques, and thread engagements. The second experiment is a modular closed loop peristaltic pump designed to test the feasibility of maintaining laminar flow during the conditions of a rocket launch.

### 13.1 Vibration

At IREC 2023, the payload subsystem nearly had a catastrophic failure as multiple fasteners holding the payload in place were drastically loosened in flight by the vibrations they experienced. This prompted the need for an experiment designed to quantify the effect on the fasteners used on the rocket both in the payload bay and elsewhere.

The vibration experiment is split into two parts: an electrical circuit board designed to read three axis accelerometer data during launch to quantify the vibrations experienced in flight, and 12 plates with tapped through holes to qualitatively determine the vibrational effects on fasteners under several different conditions.

#### 13.1.1 Vibration Board

The vibration board began solely as a way to write three axis accelerometer data to a micro SD card to quantify vibration during flight. Since this is a 3 axis accelerometer, it has the ability to measure vibration modes in all axes, eliminating the need to consider the board's orientation. This remained the main purpose of this board, however as the pump matured, the scope of the board increased to also write flow sensor and thermistor data. This fairly small scope meant this board was not very challenging to design, but there were many difficulties in writing the firmware. The main difficulty came from the inability for the small PIC18 micro-controller to utilize the team's logger board code due to its lack of memory. To remedy this, two options were proposed, the first was to write raw data sector by sector, then process the data post flight. The second was to find and utilize an MCC library to write to the SD card in the way it was originally planned to. The MCC library option was chosen and implemented, but both options were explored to ensure payload data is logged.

#### 13.1.2 Vibration Plates

The mechanical section of the vibration experiment consists of several plates with tapped and/or clearance holes through them. These plates are designed to test all of the common fasteners, torques and thread engagements found on the rocket. The orientation of the fasteners is also being tested, as fasteners have their heads facing up, down, and horizontally. To do this testing, all fasteners will be torqued to one of four specified torques, then torque stripe will be added to all the fastener heads and photos will be taken of all initial positions. Then, the plates will be fastened into the payload and fly the experiment. Upon recovery, all plates will be photographed to compare any differences in torque. The test parameters will include four different torques based on common torque specifications used in other sections, 1/4" thread engagement, 1/8" thread engagement,

threading into aluminum, threading into cold-rolled steel, M3, #6-32, #8-32 and 1/4"-28 fasteners, nuts and bolts of the same sizes, and Loctite 242 on fasteners.

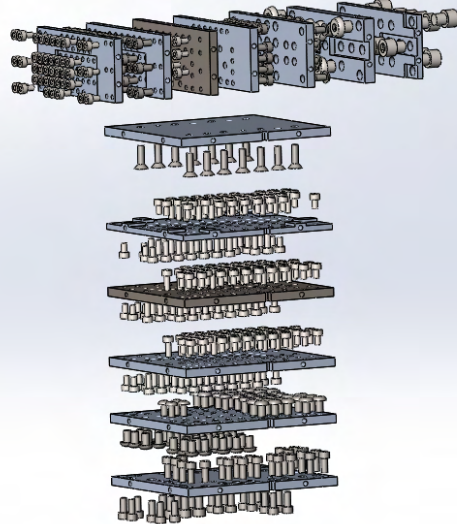


Figure 154: Exploded view of the vibration plate experiment

## 13.2 Peristaltic Pump

The ethics of medical research in aerospace also present their own list of challenges. When it comes to mitigating risk to human health and maintaining a high quality of life, modern spaceflight does not tick the boxes of acceptable test conditions.

The team has become interested in a number of questions surrounding human physiology and medical devices in zero gravity. The team is invested in questions around blood clots, stents, and blood transfusions in zero Gs.

In response to this need, a focus of this year's payload subsystem has been to develop a closed loop system capable of replicating the conditions of the human cardiovascular system in a CubeSat environment. This was done in the hopes of gathering information on what is necessary to create an analogous testing environment to combat this issue. Specifically, testing how the laminar flow created of the fluid will withstand the high levels of acceleration experienced during launch, and the freefall experience during descent.

The experiment will be considered a success if the Reynolds number of the fluid is able to successfully be determined at all points during launch, flight, and descent. The variables affecting the fluid's Reynolds number are flow area, flow velocity, flow viscosity, and fluid density. Flow area will effectively be treated as a constant, and determined by the ID of the chosen tubing. Change in flow velocity will be measured with the use of a SLF3S-400B Liquid Flow Sensor. Change in temperature will be measured using an Amphenol MA100BF103BN thermistor, which will then be used to calculate possible changes in fluid density and viscosity.

Reynolds number will be calculated using the following formula:

$$Re = \frac{\rho VL}{\mu} [20]$$

If the Reynolds number remains below 2000 for the entirety of the flight, the fluid flow will be considered to have remained laminar. Otherwise, it will be considered to have become turbulent and not a suitable analogy for a human cardiovascular system without further iteration.

### 13.2.1 Arms

A peristaltic pump functions by using a rotating mechanism, referred to as the arms of the pump, to push fluid along a flexible tube. As the liquid moves forward, an area of low pressure is created in the space vacated by the fluid, and more fluid is then pulled into the space. This creates continuous flow.

These arms consist of structural supports attached to a revolving motor, with a certain number of contacts points with the tubing. The most common numbers of contacts range from 2-4. 3 points of contact were chosen to save space while still keeping a relatively steady flow rate.

Rollers were chosen as the mechanism for the points of contact, to reduce friction and prolong tubing lifespan. This is as opposed to other mechanisms that slide directly along the tubing as opposed to rolling. A 3D CAD model of the chosen arms design is shown below:

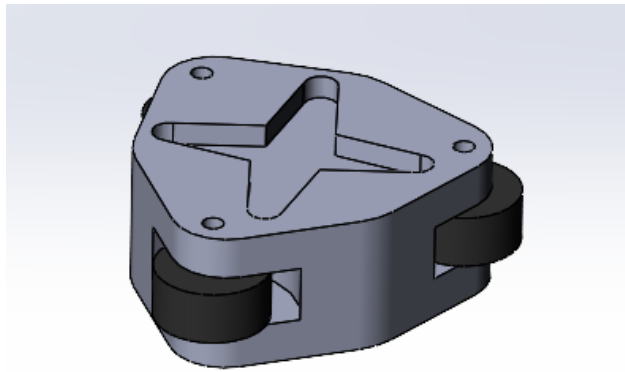


Figure 155: Peristaltic Arms

The mechanism press-fits directly onto the rotor of the HITEC-HRS motor, via the tightly toleranced cross-shaped groove in its centre.

Clearance was a very important factor to consider, as a significant concern was that the tubing would shift as the pump pushes the fluid. This concern was validated during testing, as the rollers pulled the tubing backwards along the track due to the clearance being too tight. In response, a set of different diameter rollers were tested to determine which size would be best. The final radius of revolution of the arms was 31.1 mm, providing a clearance of 0.4 mm from the edge of the track, which had a diameter of 31.5 mm. This provided the necessary overlap with the 4.0 mm OD tubing to allow the pump to rotate smoothly while still creating enough pressure to push the fluid along its path.

### 13.2.2 Tubing and Bagging

Two prospective designs were considered for the path of the liquid in the pump. The first involved using the pump to transfer fluid from one bag to another bag, connected by a tubing pathway. However, this design limits the available testing time as it can only be run once, therefore there is no guaranteed data from any specific stage of flight.

The second, and chosen, design includes a looped system of tubing with both ends attached to a bag reservoir of fluid. This allows the experiment to run for the entirety of the launch and descent of the rocket, providing more data capture throughout different stages of flight. The single bag design also saved space, which was a very important factor to consider given that the sealed area of the CubeSat is only 103.5mm tall. A picture of this setup is displayed the figure below.



Figure 156: Bagging and tubing setup

The chosen tubing has an OD of 4.0 mm and an ID of 3.0 mm. This was lightly influenced by spacing factors and majorly influenced by the average coronary blood vessel diameter, which is within 3.5-4.5 mm[21].

### 13.2.3 Fluid

There were two requirements for the fluid in the pump system. The first was that it must be similar to blood in viscosity, as the main goal of this specific experiment is to model using an IV pump to transfuse blood. The second was that, as part of a triple-redundancy system to prevent shorting out

the rocket avionics, the fluid must register as low-conductivity when tested. As a result, the chosen blood-analogous fluid is a homogeneous solution of 26% glycerol and 74% distilled water, which has the same density as blood at 25°C. This density is 1.062 g/cm<sup>3</sup>. [22]. Calculations for these percentages are shown below:

$$\rho_{blood} = 1.062 \text{ g/cm}^3 \text{ at 25 degrees Celsius.}$$

$$\rho_{water} = 0.997 \text{ g/cm}^3 \text{ at 25 degrees Celsius [23].}$$

$$\rho_{glycerol} = 1.25 \text{ g/cm}^3 \text{ at 25 degrees Celsius [24]}$$

$x$  will represent the unknown decimal percentage of glycerol in the solution.

$$1.062 = 0.997(1 - x) + 1.25x = 0.997 - 0.997x + 1.25x$$

$$1.062 - 0.997 = -0.997x + 1.25x$$

$$0.065 = 0.253x$$

$$0.257 = x$$

### 13.3 Tubing Track

The last important element of the pump assembly is the track, which provides a pathway around the arms for the tubing to follow, as well as a surface on which the rollers compress the tubing. A CAD model of this component is shown below:

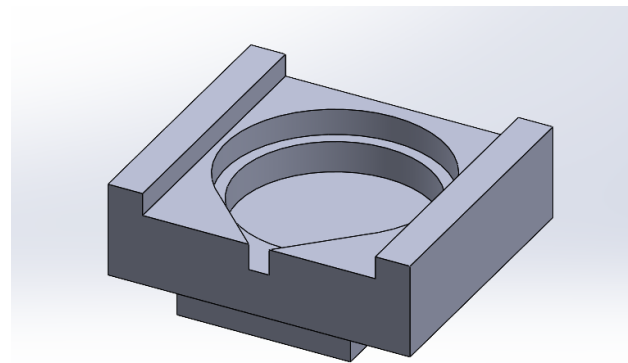


Figure 157: Tubing track CAD model

It was considered to add an anchor of revolution for the arms to rotate around, however testing revealed that this was unnecessary as the arms did not deviate from their proper position. However, testing did show that the tubing tended to move upwards and out of the track when the motor was turning. In response, a flat cover was added to the track to resist this migration.

#### 13.3.1 Pump Assembly

An exploded view of the pump assembly 3D model is shown below, excluding the tubing and bagging:

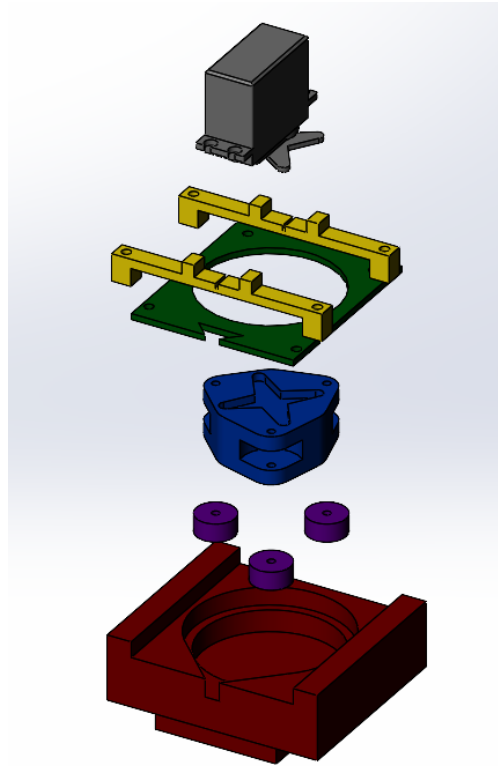


Figure 158: Exploded view of the pump assembly

The tubing track (red) fits directly into the CubeSat frame, which is described in the next section. Tubing is fed into the dedicated tubing path. The pump arms (blue) are then attached to the motor (grey), which is then fastened directly to the tubing track. The tubing cover (green) is then placed on top of the tubing path, and supports (yellow) are added to increase stability of the motor mount. An image of the fully assembled pump is shown in Figure 159:

### 13.4 CubeSat

The payload this year, as with all previous payloads of Waterloo Rocketry, is based off of a 3U CubeSat standard. Because of this standard, the payload was required to be at least 300 millimeters tall, 100 millimeters wide, and 100 millimeters long. This payload was designed to be 307.5mm by 100mm by 100mm to conform to the standard while also adding extra height to assure the CubeSat does not interfere with the screw heads below the payload. This year's payload was also entirely machined in house by students. The figures below show both an exploded view of the entire assembly and the machined assembly's profile.

As is mentioned in section 13.6, this payload was also made to have gasket seals to avoid a failure of the pump where the test fluid leaks out of the pump loop (Figure 162). These seals split the payload into two distinct sections of sealed and unsealed as to avoid shorting the harness or the battery in the unsealed section. To allow cables to pass into this sealed section, a cable pass-through similar to ones used in the recovery section was used and connectors were soldered on.

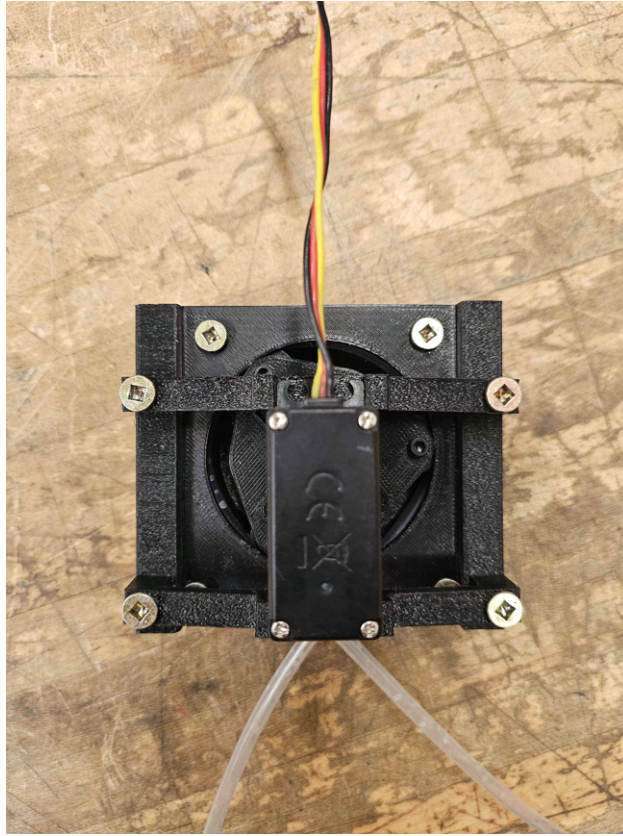


Figure 159: As machined pump assembly

### 13.5 Fabrication

The payload was fabricated using two main materials, PETG and 6061-T6 aluminum. All aluminum parts were either milled by students or water jet in the student machine shop. While this resulted in multiple parts having to be re-machined or altered to fit together, it provided a great learning opportunity and allowed an iterative approach to designing parts. The milled parts include the entire structure of the CubeSat and all of the panels.

The PETG parts were 3D printed in house as well using student designs. PETG is favoured over the more common PLA due to its increased strength and heat resistance which was experimentally tested on a past Waterloo Rocketry payload. The 3D printed parts include the pump assembly and the zip-tie mounts used for electrical routing and fastening the flow sensor.

### 13.6 Testing & Risks

With fluids in the payload this year, testing and risk analysis was a very high priority when designing the CubeSat.

In order to consider the payload as flight ready, the payload has been put through numerous tests to mitigate these aforementioned risks. The most critical test was the sealing test, where the payload was filled with water to evaluate the performance of the gasket seals to hold in water in the case of a catastrophic pump failure. The other flight critical test was WDR. This was critical

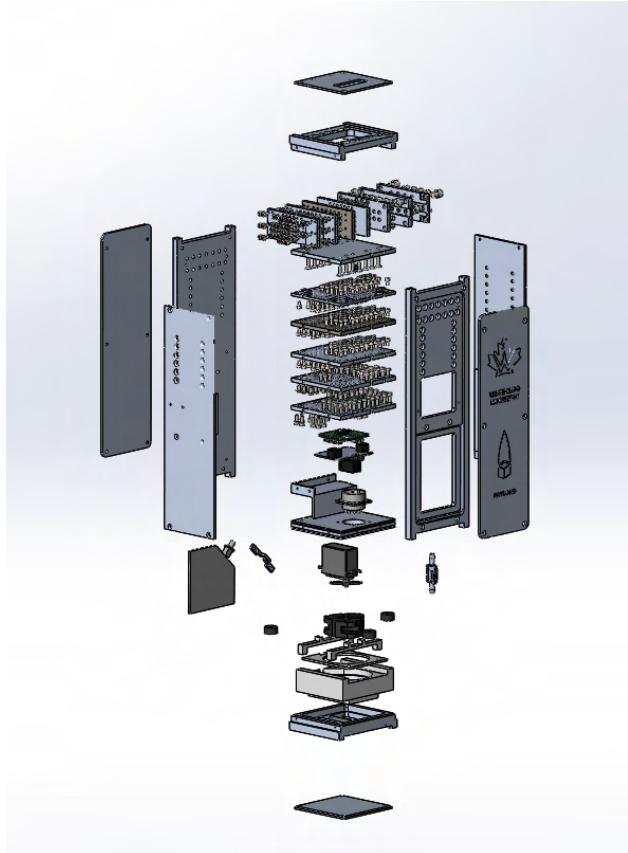


Figure 160: Exploded View

for interfacing tests and evaluating the performance of the two electrical boards being controlled over the RocketCAN harness. Other tests done include independent board tests, where each board is independently tested to verify their function, harnessing tests, done to confirm the cable pass-through was correctly soldered, and battery drain tests, to determine the specific battery life of the experiment before it is unable to gather data.



Figure 161: Machined CubeSat

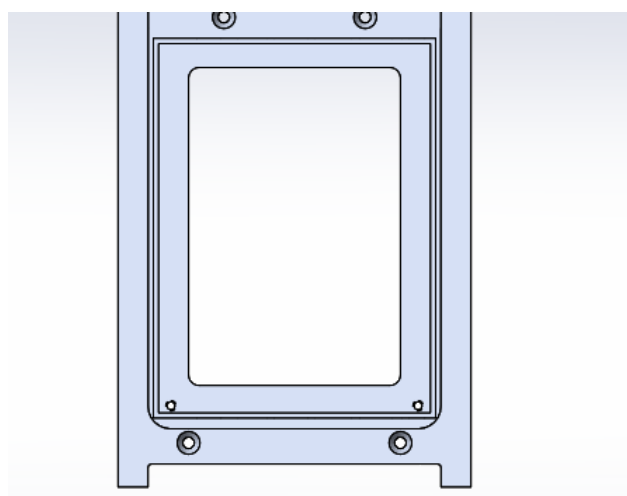


Figure 162: Gasket seal found on the front and back braces of the structure

Table 20: Payload technical risks, hazards, and mitigation strategies

| Risk  | Likelihood | Severity | Section  |
|---|------------|----------|--|
| Fluid leaks out of CubeSat and shorts avionics.                                       | Low        | High     | Add gasket seals to a designated area of the CubeSat, use low-conductivity fluids, do extensive leak testing of the tubing and bagging system as well as the sealed environment. |
| Screw or bolt falls out of vibration plate and damages electrical connections/boards. | High       | Low      | Attach screws and bolts with their heads on the far side of the plate from the avionics, such that if they dislodge, they will become trapped between other vibration plates.    |
| Run out of power from LiPo batteries.   | Low        | High     | Have multiple batteries for redundancy, fully charge both batteries before assembly, establish a maximum battery life of the experiment.   |

## 14 COMPLETED AND PLANNED SYSTEM TESTING

### 14.1 Static Fire

The Waterloo Rocketry Team has conducted two static fire tests of the Eridium Liquid engine. The first test, in December 2023, was primarily to verify the performance of the injectors. This test was successful, and demonstrated the Eridium engine could successfully start up, achieve steady state, and burn until propellant depletion without damage. The engine achieved a peak thrust of about 6kN, and during disassembly of the engine it was discovered that the injector sleeves had partially melted. From analysis of the data, it was concluded that the melting occurred during shutdown as there was no evidence of the mixture ratio of the engine changing during the burn. Additionally, during shutdown the chamber experienced blowback and was observed to have briefly relit due to nitrous oxide and ethanol vapours being introduced by the tanks which were operating independently in blowdown, meaning both nitrous and ethanol vapour were injected into the chamber after the chamber was extinguished for the first time.

The second static fire test, which was completed on June 8th, was a test of the engine in its final flight configuration. The concentric tanks which use the nitrous vapour pressure to pressurize the ethanol using a piston performed better than expected, with less than 15psi pressure drop across the piston. This test went very smoothly, with no issues encountered during ops. The engine achieved a peak thrust of 8.1 kN, and the injectors did not melt.

Videos of the two static fire tests can be found at <https://www.youtube.com/watch?v=ZWvHEy1VRlg>..

### 14.2 Rocket Assembly

The rocket assembly test was completed on June 29th. This test involved assembling the entire airframe of the rocket to ensure all components fit, and to begin final harnessing of the rocket. The fully assembled rocket is shown in Figure 163.

### 14.3 Wet Dress Rehearsal

The first wet dress rehearsal (WDR) test was completed on July 7th. The purpose of the first WDR was to verify all flight critical rocket avionics work as desired, all sensors are operational and provide sensible data, and practice nominal launch operations. All engine and critical avionics components were assembled with the exception of the combustion chamber internals (liners, ignition puck, and nozzle). The test was conducted using nitrogen to fill the oxidizer tank and water to fill the fuel tank in order to minimize risk to personnel and allow this test to be safely conducted outside the building where the team's design bay is located, allowing for easy access to tools and supplies to fix any issues that may occur.

The operations procedures were run through twice. On the first attempt, an issue was found with the fill/dump pneumatic valve, where we aborted. On the second attempt, we were able to send nitrogen and water through the injectors as desired. Some notable conclusions from these two operations are

- Fill/dump was unable to close past 550psi of tank pressure. This is related to a manufacturing error with the valve. As of July 9th, rework has been completed to the existing valve that



Figure 163: Assembled Rocket

allows it to seal at 700 psi, which should be sufficient as a last resort at competition, but in order to reduce risks as much as possible a new version of the valve has been sent for machining and should be ready for the next WDR attempt.

- Both new rocket avionics systems were able to stay healthy and function nominally throughout the procedure.
- Several gaps in the flight procedure were found, noted, and corrected
- The ground side connection is not reliable on Wi-Fi, and must be connected directly via ethernet. This has been added to our "prior to start" checklist

The second WDR test is scheduled for the weekend of July 13th. In this test, the rocket oxidizer will be filled with carbon dioxide (used to simulate nitrous oxide). The fuel tank will likely be left empty to avoid freezing. The primary purpose of this test will be to validate the fluid systems which were not able to be validated in the static fire setup, which are the pneumatically actuated fill/dump valve, the flight tank heating system, the fill-disconnect mechanism, and the ability to accurately determine propellant mass filled using the launch tower load cell. This test will follow the nominal launch operations procedure, meaning the simulated propellant will be loaded remotely, and conditioned by the tank heating system to determine the fill-to-fire time for the launch vehicle. Once



Figure 164: Nitrogen and Water Being Sent Through the Injector Valves During WDR 1

the carbon dioxide reaches firing pressure, the test will move into a simulated abort to determine the time required to abort and safe the system.

Depending on the outcomes of the first two WDR tests, additional tests are being considered. These tests include attempting to run a nominal procedure with the electrical disconnect detached (requiring communication to and from the rocket via the onboard antennas), and simulated aborts where the operations team must react to failures both from previous year's vehicles and input from system experts about how their systems could fail. These tests would be conducted using CO<sub>2</sub> and water with the primary goal of making sure the launch operations crew is fully familiar and comfortable with the launch vehicle and ground systems.

#### 14.4 Competition Simulator

The 'competition simulator' test will be the final dress rehearsal test of the rocket once any and all issues discovered during WDRs have been fixed. This test will start with the rocket in the state it will be in after the conference days. The team that will be responsible for setting up the launch pad at competition will be sent in the morning to assemble all launchpad infrastructure, while a second team works to assemble the rocket (minus ignition and recovery pyrotechnics). Once the pad infrastructure and rocket are prepared, the rocket will be brought out to the 'pad', railed, and raised. The team will then conduct a wet dress rehearsal following the nominal operations procedure (minus ignition) which will conclude by flowing CO<sub>2</sub> through the injectors. The goal of this test is to give team members practice for what they will be doing during the competition, and to identify and solve any issues that come up or delays that occur during the test so that competition will go as smoothly as possible. This test is tentatively scheduled for July 20th pending the results of WDRs, but will be no later than July 27th to ensure team members have time to study for final exams.

## 15 PROGRAMMATIC/TECHNICAL RISKS AND MITIGATION STRATEGIES

Technical risks have been explored in each systems relevant section. As such, this section will explore programmatic and organizational risks to a successful launch and successful flight. The tables below summarises the most severe or likely programmatic risks associated with development and testing of the vehicle. This section also explores some risks the team may encounter at competition and in preparation for flight

Table 21: Likelihood and Severity Categories for overall programmatic risks

| Severity | Explanation  |
|----------|--|
| Low      | Event is unfavourable, but relatively easy to recover from.  |
| Medium   | Event is severe, but primary mission goal is still possible. |
| High     | Event is detrimental; team will be unable to compete.        |

Table 22: Team-wide programmatic risks

| Risk  | Likelihood | Severity | Mitigation Strategy  |
|---|------------|----------|--|
| Team funds deplete                                  | Low        | High     | Careful financial planning and seeking of outside funding sources  |
| Critical Illness/Injury incapacitating team members | Medium     | Medium   | Commonly known as the "bus factor", the team is careful to not be too reliant on any singular person, and to crosstrain as much as possible. The team is also careful to finish things early so that illness doesn't affect timelines                                      |
| Spring Term Exams using team time                   | High       | Low      | Waterloo has exams that most in-person students will be participating in for the 2-3 weeks before Launch Canada. No team schedule currently has work taking place during the exam period except for rocket painting, which is being done by students who do not have exams |

|   |        |        |  |
|---|--------|--------|--|
| Damage critical hardware                | Low    | Medium | Depending on the hardware, circumstances, and timelines, irreparably damaging flight hardware could be extremely detrimental. We treat all flight hardware carefully, and make spares of as many components as possible (longerons, boards, etc) to avoid damage ruining flight opportunities  |
| At competition                          |        |        |  |
| Poor weather conditions                 | Medium | High   | In the case of rain or fire ban, there is very little the team can do to mitigate these events. However, the team can ensure it is maximally prepared to launch as soon as the window opens. This way, if it is too windy only in the afternoons, or it is raining only at the end of competition, the team is still able to fly early |
| Insufficient Transportation             | Low    | Low    | In addition to planning out every phase of competition, including vehicle allocations, the team also has options to bring spare vehicles in case one becomes unavailable   |
| Mistake in Assembly                     | Medium | Low    | The team will continuously rehearse assembly procedures, as well as build in dedicated checks to test that an assembly procedure was followed correctly  |
| Insufficient time to prep on launch day | Low    | Medium | Much of the work can be done before leaving for competition, and the team is careful to minimize the work that must happen day of to give the best attempt at flight   |

|   |        |        |   |
|---|--------|--------|---|
| Illness/Injury incapacitating critical team members | Low    | Medium | Crosstraining and sufficient diffusion of responsibilities has allowed Waterloo to be effective when encountering this issue in the past. At Launch Canada last year, a team lead became ill and was unable to attend conference day, but conference day planning and organization was able to be resolved by the rest of the team. Thorough testing also allows other team members to learn critical systems and serve as backups for assembly |
| Vehicle breaks down to or at competition            | Medium | Medium | All past competitions have had a vehicle break down, and the team has been able to reallocate resources and materials such that the rest of the team can continue as that vehicle gets repaired   |
| Rocket cannot be located prior to Rocket Retrieval  | Low    | High   | Two independent GPS modules with independent power and charging, as well as live onboard telemetry and a dedicated retrieval drone reduce the likelihood that the rocket will not be found  |
| Launch attempt failure                              | Medium | Medium | Every critical rocket system will have spares, and the team has purchased sufficient propellants for three launch attempts. Igniter failure, failure to open valves, FOD, power failure, etc are all failure modes that shall be tested and characterized for the best opportunity to fly the vehicle.  |

## References

- [1] J. Godard. (2024, Jan.) Increasing Rocket Apogee by 23% Through Iterative Design. Waterloo Rocketry. (Accessed: 07.08.2024). [Online]. Available: <https://drive.google.com/file/d/1CygsVuvnB14k3kH8S6ockkXLSafdzxK7/view>
- [2] J. Godard and T. Fairhead, "Increasing Apogee by 23% Through Iterative Design Approach," Waterloo Rocketry, 2024, (Accessed: 07.09.2024). [Online]. Available: <https://www.youtube.com/watch?v=fDDOLux1RgE>
- [3] A. Leszkowiat. (2024) A Practical Method For Reducing Skin Friction Drag In, Sounding Rockets. Waterloo Rocketry. (Accessed: 07.09.2024). [Online]. Available: [https://drive.google.com/file/d/1HQf1ckOifeKUsRN-epp1EaRBEbp\\_2skI/view?usp=drive\\_link](https://drive.google.com/file/d/1HQf1ckOifeKUsRN-epp1EaRBEbp_2skI/view?usp=drive_link)
- [4] (2018) ASTM D3518. ASTM International. [Online]. Available: [https://www.astm.org/d3518\\_d3518m-18.html](https://www.astm.org/d3518_d3518m-18.html)
- [5] (2024) Aluminum 6061-T6; 6061-T651. Aerospace Specification Metals inc. [Online]. Available: <https://asm.matweb.com/search/SpecificMaterial.asp?bassnum=ma6061t6>
- [6] B. Waxman, "An investigation of injectors for use with high vapor pressure propellants with applications to hybrid rockets," Ph.D. dissertation, Stanford, 2014. [Online]. Available: <https://purl.stanford.edu/ng346xh6244>
- [7] Injector Bulkhead Flange FEA Report. Waterloo Rocketry. [Online]. Available: [https://docs.google.com/document/d/17p5fIE\\_rBdS5GiKhEkEHQ2vbW409gDEhI81v6huSrZI/edit?usp=sharing](https://docs.google.com/document/d/17p5fIE_rBdS5GiKhEkEHQ2vbW409gDEhI81v6huSrZI/edit?usp=sharing)
- [8] Parker o-ring handbook. Parker. (Accessed: 07.13.2024). [Online]. Available: <https://www.parker.com/content/dam/Parker-com/Literature/O-Ring-Division-Literature/ORD-5700.pdf>
- [9] Sticky Drawer Effect. Kalsi Engineering. (Accessed: 07.13.2024). [Online]. Available: [https://www.kalsi.com/handbook/D21\\_Sticky\\_drawer\\_effect.pdf](https://www.kalsi.com/handbook/D21_Sticky_drawer_effect.pdf)
- [10] M. Zhou. (2023) Design and Testing of a Coaxial Propellant Valve . Waterloo Rocketry. (Accessed: 07.10.2024). [Online]. Available: <https://drive.google.com/file/d/1D03cqj1evIAFhh7zxqJHqAipTtUOeJ30/view?usp=sharing>
- [11] M. Gordon. (2024, May) Design of a Remotely Operated Fill/Dump Valve . Waterloo Rocketry. (Accessed: 07.10.2024). [Online]. Available: [https://drive.google.com/file/d/1bzky83p\\_3DFZrTO0oN1y\\_qT1im5U-eZw/view?usp=sharing](https://drive.google.com/file/d/1bzky83p_3DFZrTO0oN1y_qT1im5U-eZw/view?usp=sharing)
- [12] Leviathan of the sky hybrid rocket project technical report. Waterloo Rocketry. (Accessed: 07.13.2024). [Online]. Available: <https://drive.google.com/file/d/1y9teKByS1LoSF9aj4fo1byQsZomRpGke/view>
- [13] J. E. Sadeck and C. K. Lee, "Continuous disreefing method for parachute opening," *Journal of Aircraft*, vol. 46, no. 2, pp. 501–504, 2009. [Online]. Available: <https://doi.org/10.2514/1.37444>

- [14] T. Knacke, *Parachute Recovery Systems: Design Manual*. Para Pub., 1992. [Online]. Available: <https://books.google.ca/books?id=5pzgAAAAMAAJ>
- [15] (1976) Us standard atmosphere, 1976. National Oceanic and Atmospheric Administration. [Online]. Available: [https://www.ngdc.noaa.gov/stp/space-weather/online-publications/miscellaneous/us-standard-atmosphere-1976/us-standard-atmosphere\\_st76-1562\\_noaa.pdf](https://www.ngdc.noaa.gov/stp/space-weather/online-publications/miscellaneous/us-standard-atmosphere-1976/us-standard-atmosphere_st76-1562_noaa.pdf)
- [16] (2022) Center of pressure. NASA. [Online]. Available: <https://www1.grc.nasa.gov/beginners-guide-to-aeronautics/center-of-pressure/>
- [17] (2024) OR Airbrake Plugin. Waterloo Rocketry. [Online]. Available: <https://github.com/waterloo-rocketry/or-airbrake-plugin>
- [18] (2024) PyAnsys. Waterloo Rocketry. [Online]. Available: <https://github.com/waterloo-rocketry/PyAnsys>
- [19] R. Ding and J. Dolina. (2023, Oct.) Airbrakes CFD Report. Waterloo Rocketry. (Accessed: 07.08.2024). [Online]. Available: <https://docs.google.com/document/d/1Z-oG1jZdk96txgp5OGYvELsAUv6tGQymU-YJx3D068/edit?usp=sharing>
- [20] (2023) What is reynolds number? Ansys. [Online]. Available: <https://www.ansys.com/blog/what-is-reynolds-number>
- [21] J. T. Dodge, B. Brown, E. L. Bolson, and H. T. Dodge, “Lumen diameter of normal human coronary arteries. influence of age, sex, anatomic variation, and left ventricular hypertrophy or dilation.” *AHA/ASA Journals*, vol. 86, no. 1, p. 239, 1992. [Online]. Available: <https://doi.org/10.1161/01.CIR.86.1.232>
- [22] F. Knuppel, I. Thomas, F.-H. Wurm, and B. Torner, “Suitability of different blood-analogous fluids in determining the pump characteristics of a ventricular assist device,” *Fluids*, vol. 8, no. 5: 151, 2023. [Online]. Available: <https://doi.org/10.3390/fluids8050151>
- [23] Density of water (g/cm<sup>3</sup>) at temperatures from 0°C (liquid state) to 30.9°C by 0.1°C increments. California State University. [Online]. Available: <https://www.csus.edu/indiv/m/mackj/chem1a/docs/h2oden.pdf>
- [24] Glycerin safety data sheet. Fisher Science Education. [Online]. Available: [https://beta-static.fishersci.com/content/dam/fishersci/en\\_US/documents/programs/education/regulatory-documents/sds/chemicals/chemicals-g/S25342.pdf](https://beta-static.fishersci.com/content/dam/fishersci/en_US/documents/programs/education/regulatory-documents/sds/chemicals/chemicals-g/S25342.pdf)
- [25] Canadian Climate Normals 1991-2020 Data. Government of Canada. (Accessed: 02.20.2024). [Online]. Available: [https://climate.weather.gc.ca/climate\\_normals/results\\_1991\\_2020\\_e.html?searchType=stnProv&lstProvince=ON&txtCentralLatMin=0&txtCentralLatSec=0&txtCentralLongMin=0&txtCentralLongSec=0&stnID=205000000&dispBack=0](https://climate.weather.gc.ca/climate_normals/results_1991_2020_e.html?searchType=stnProv&lstProvince=ON&txtCentralLatMin=0&txtCentralLatSec=0&txtCentralLongMin=0&txtCentralLongSec=0&stnID=205000000&dispBack=0)
- [26] Atmospheric Pressure vs. Elevation above Sea Level. Engineering Toolbox. (Accessed: 02.20.2024). [Online]. Available: [https://www.engineeringtoolbox.com/air-altitude-pressure-d\\_462.html](https://www.engineeringtoolbox.com/air-altitude-pressure-d_462.html)

- [27] AISI Internal Screw Threads Size and Tolerances Table Chart. Engineers Edge. (Accessed: 07.08.2024). [Online]. Available: [https://www.engineersedge.com/thread\\_strength/internal\\_screw\\_threads\\_chart.htm](https://www.engineersedge.com/thread_strength/internal_screw_threads_chart.htm)
- [28] Black-Oxide Alloy Steel Socket Head Screw 6-32 Thread Size, 3/4" Long. McMaster-Carr. (Accessed: 07.08.2024). [Online]. Available: <https://www.mcmaster.com/91251A151/>

# Appendices

## A Aerostructure Component Calculations

### A.1 Bodytube Safety Factor Calculation Example

This section contains a sample calculations for safety factor at body station 143.1 (143.1 inches aft of the nosecone tip), which corresponds to a point on the fin can, at MaxQ. Many calculations were performed to analyze the bodytubes at multiple stations along its length at both takeoff and MaxQ. However, all the calculations follow the same procedure with limited variation so only one calculation is shown to demonstrate the methodology. One global conservative assumption is that there are no vent holes in any bodytube. For the calculations, this implies that all the bodytubes are now pressure vessels where the gauge pressure inside the bodytubes is equal to the difference between the ground level and 30,000 ft. Another thing to note is that the loads used are preliminary and conservative. These are the worst case scenario. Updated loads since the time of these calculations have dropped significantly so the safety of the bodytubes still holds true.

Table 23: Bodytube Parameters

| Parameter                   | Value            | Unit      | Source                         |
|-----------------------------|------------------|-----------|--------------------------------|
| Outer Radius ( $r_o$ )      | 3                | in        |                                |
| Inner Radius ( $r_i$ )      | 2.96             | in        |                                |
| Area (A)                    | 0.749            | $in^2$    | $\pi(r_o^2 - r_i^2)$           |
| Second Moment of Area (I)   | 3.326            | $in^4$    | $\frac{\pi}{4}(r_o^4 - r_i^4)$ |
| Polar Moment of Inertia (J) | 6.651            | $in^4$    | $\frac{\pi}{2}(r_o^4 - r_i^4)$ |
| Compressive Strength        | 70 (10152.64)    | MPa (psi) | Airstone 780E/786H Datasheet   |
| Estimated Launch Elevation  | 294.699 (966.86) | m (ft)    | [25]                           |

Table 24: Bodytube Loads

| Parameter                                       | Value           | Unit      | Source  |
|---|-----------------|-----------|---|
| MaxQ Axial Force ( $F$ )                        | -0.3            | lbs       | Loads Analysis  |
| MaxQ Shear Force ( $V$ )                        | -38.5           | lbs       | Loads Analysis  |
| MaxQ Moment Force ( $M$ )                       | 1249.2          | lb-in     | Loads Analysis  |
| MaxQ Fin Shear Force ( $V_{fin}$ )              | 0.076           | lb        | Loads Analysis  |
| MaxQ Fin Moment ( $M_{fin}$ )                   | 2386.99         | lb-in     | Loads Analysis  |
| Axial Stress ( $\sigma_{axial}$ )               | -0.134          | psi       | $\frac{F}{A}$   |
| Bending Stress ( $\sigma_{bend}$ )              | 1126.873        | psi       | $\frac{Mr_o}{I}$  |
| Total Normal Load ( $\sigma_{normal}^{total}$ ) | -1127.007       | psi       | $\sigma_{axial} + \sigma_{bend}$  |
| Transverse Shear ( $\tau_s$ )                   | 75.774          | psi       | $\frac{2*( V +V_{fin})}{A}$   |
| Torsion ( $\tau_t$ )                            | 1076.623        | psi       | $\frac{M_{fin}r_o}{J}$  |
| Total Shear Loads ( $\tau$ )                    | 1179.635        | psi       | $\tau_s + \tau_t$   |
| Pressure at Ground Level                        | 14.190 (97.834) | psi (kPa) | $101325((1 - (2.25577(10^{-5})) * AltitudeASL)^{5.25588})$ [26]   |
| Pressure at 30,000 ft AGL                       | 4.175 (28.788)  | psi (kPa) | $101325((1 - (2.25577(10^{-5})) * AltitudeASL)^{5.25588})$ [26]   |
| Gauge Pressure at 30,000 ft                     | 10.014 (69.046) | psi (kPa) | Pressure at 30,000 ft - Pressure at ground  |
| Hoop Stress ( $\sigma_{hoop}$ )                 | 751.071         | psi       | $\frac{GaugePressure*r_o}{r_o - r_i}$   |
| Longitudinal Stress ( $\sigma_{long}$ )         | 375.535         | psi       | $\frac{GaugePressure*r_o}{2(r_o - r_i)}$  |
| $\sigma_1$                                      | -751.471        | psi       | $\sigma_{normal}^{total} + \sigma_{long}$   |
| $\sigma_2$                                      | -751.071        | psi       | $\sigma_{hoop}$   |
| $\tau$  | 1179.635        | psi       |   |
| Von Mises Stress ( $\sigma_{VM}$ )              | 2242.362        | psi       | $\sqrt{\frac{(\sigma_1 - \sigma_2)^2 + (\sigma_2 - \sigma_3)^2 + (\sigma_1 - \sigma_3)^2 + 6(\tau_{12}^2 + \tau_{23}^2 + \tau_{13}^2)}{2}}$ |
| Safety Factor                                   | 4.19            |           | $\frac{CompressiveStrength}{\sigma_{VM}}$   |

## A.2 Longeron Calculations

The geometrical parameters of the longerons are provided below.

Table 25: Longeron Calculation Parameters for Column Buckling

| Property                                | Value                           |
|---|---------------------------------|
| Young's Modulus                         | 10,010,000 psi                  |
| End Condition for a Fixed Support       | 1                               |
| Yield Strength                          | 40,000 psi                      |
| Limiting Slenderness Ratio              | 70.28326261                     |
| Moment of Inertia (X-Axis)              | 0.008287"                       |
| Cross-Sectional Area                    | 0.174826 <i>in</i> <sup>2</sup> |
| Least Radius of Gyration                | 0.2177186631 in                 |
| Length of Longeron                      | 9 in                            |
| Slenderness Ratio of Longeron           | 41.33775153 in                  |
| Johnson Parabolic Stress                | 38,948 psi                      |
| Critical Johnson Buckling               | 6809.192001 lbf                 |
| Idealized Compressive Load per Longeron | 676 lbf                         |
| FoS                                     | 10.07276923                     |

Table 26: Longeron Calculation Parameters for Tensile Failure

| Property                             | Value           |
|--------------------------------------|-----------------|
| Tensile Load at Deployment           | 330 lbf         |
| Idealized Tensile Load per Longeron  | 110 lbf         |
| Expected Tensile Stress per Longeron | 629.1970302 psi |
| Ultimate Tensile Strength            | 45,000 psi      |
| FoS                                  | 71.51972727     |

Table 27: Longeron Calculation Parameters for Compressive Failure

| Property                                 | Value            |
|--|------------------|
| Expected Compressive Stress per Longeron | 3,866.701729 psi |
| FoS                                      | 10.34474474      |

### A.3 Payload Bay Calculations

To calculate bolt failure, internal thread shear, and bolt-tear out, the loads shown below in Table 28 were used in the calculations in the next few sections. It is assumed that there is no shear load on the rocket as it was determined to be minimal during load analysis.

| Parameter                  | Value | Unit | Source         |
|----------------------------|-------|------|----------------|
| CubeSat Mass               | 4     | kg   | Payload Team   |
| Acceleration               | 25    | g's  | Loads Analysis |
| Tensile Force from CubeSat | 220   | lbf  | F=ma           |

Table 28: Payload Bay Bolt Loads

#### A.3.1 Bolt Failure

The clamping plate uses (4x) #6-32 bolts to prevent the payload from moving upwards during descent. Table 29 shows the #6-32 bolt properties used in the payload bay. The shear stress is calculated from the tensile stress by dividing by 3 as per Von Mises criterion.

| Parameter              | Value   | Unit | Source            |
|------------------------|---------|------|-------------------|
| Major Diameter         | 0.138   | in   | [27]              |
| Minor Diameter         | 0.104   | in   | [27]              |
| Threads Per Inch (TPI) | 32      |      | N/A               |
| Length                 | 0.75    | in   | N/A               |
| Tensile Strength       | 170 000 | psi  | [28]              |
| Shear Strength         | 98150   | psi  | Tensile Strength/ |

Table 29: Payload Bay Bolt Parameters

Von Mises stress was used for the bolt failure safety factor calculations. The bolt was approximated as a rod with a diameter equal to its minor diameter. The full load was tested on a singular screw as a conservative calculation. If a singular screw does not fail, then 4 screws should not fail. Table 30 below summarizes the bolt failure calculations. As mentioned earlier, it is assumed that there is no shear load on the rocket as it was determined to be minimal during load analysis. Thus, the calculations assume pure axial loading on the bolts.

| Parameter                 | Value    | Unit   | Equation                                     |
|---------------------------|----------|--------|--|
| Area                      | 0.008495 | $in^2$ |  |
| Tensile Stress            | 25898    | psi    |  |
| Von Mises Stress          | 25898    | psi    |  |
| Safety Factor (Tension)   | 6.564    |        | Bolt Tensile Strength/Plate Tensile Strength |
| Safety Factor (Von Mises) | 6.564    |        |  |

Table 30: Payload Bay Bolt Failure Calculations

### A.3.2 Bolt Thread Engagement

The minimum thickness of the plate to ensure proper bolt thread engagement length was calculated. The #6-32 bolt parameters used in Table 29 was used in the calculation, and with aluminum 6061-T6 as the plate material. Table 31 below shows the minimum thread engagement, in which the top centering plate exceeds with a plate thickness of 0.5 inches.

| Parameter                        | Value   | Unit      | Equation  |
|----------------------------------|---------|-----------|-----------|
| Tensile Stress Area              | 0.009   | $in^2$    |           |
| Thread Pitch (TPI)               | 0.03125 | in/thread | $1/TPI$   |
| Minimum Thread Engagement Length | 0.098   | in        |           |
| Thread Engagement Ratio          | 4.5     |           |           |
| Thread Engagement Length         | 0.418   | in        | $J * L_e$ |

Table 31: Minimum Thread Engagement

## B Remote Arming Schematics

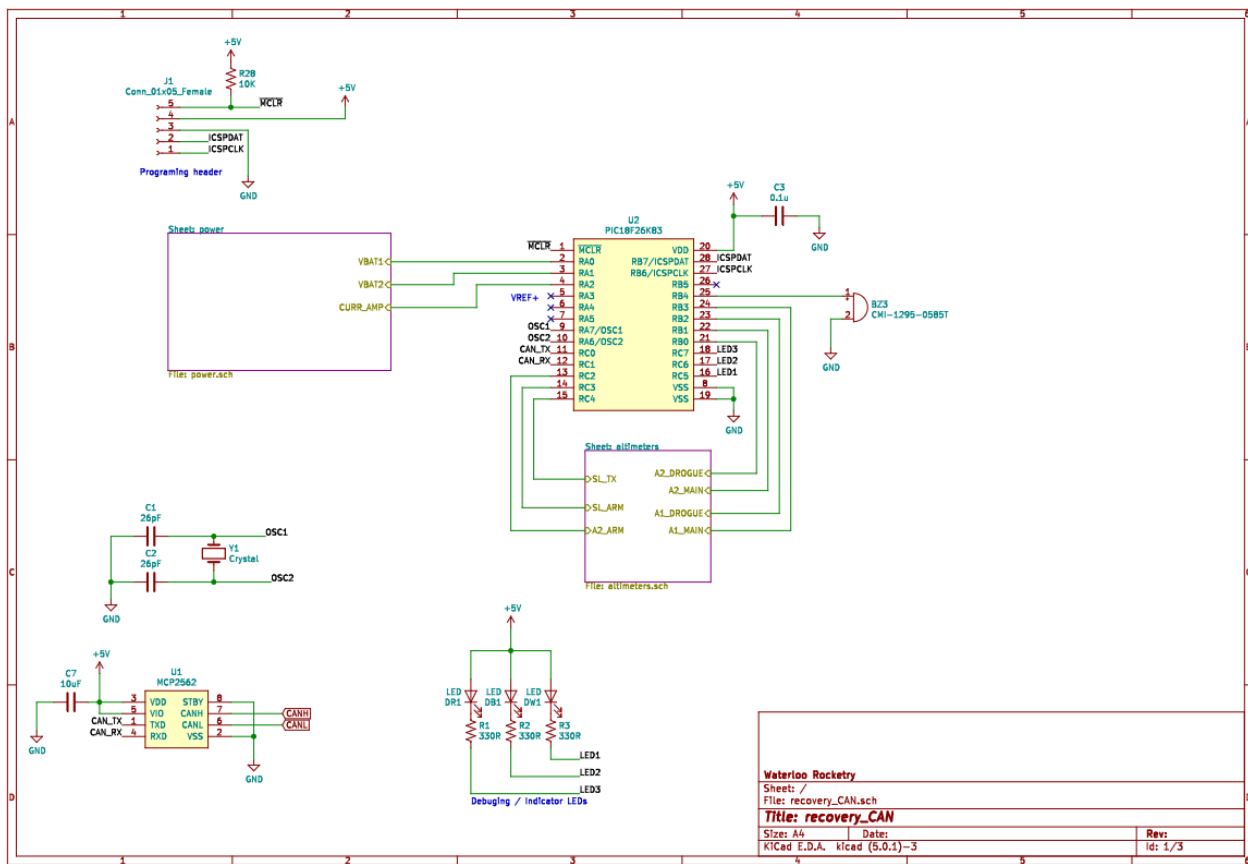


Figure 165: Remote Arming Schematic - Microcontroller

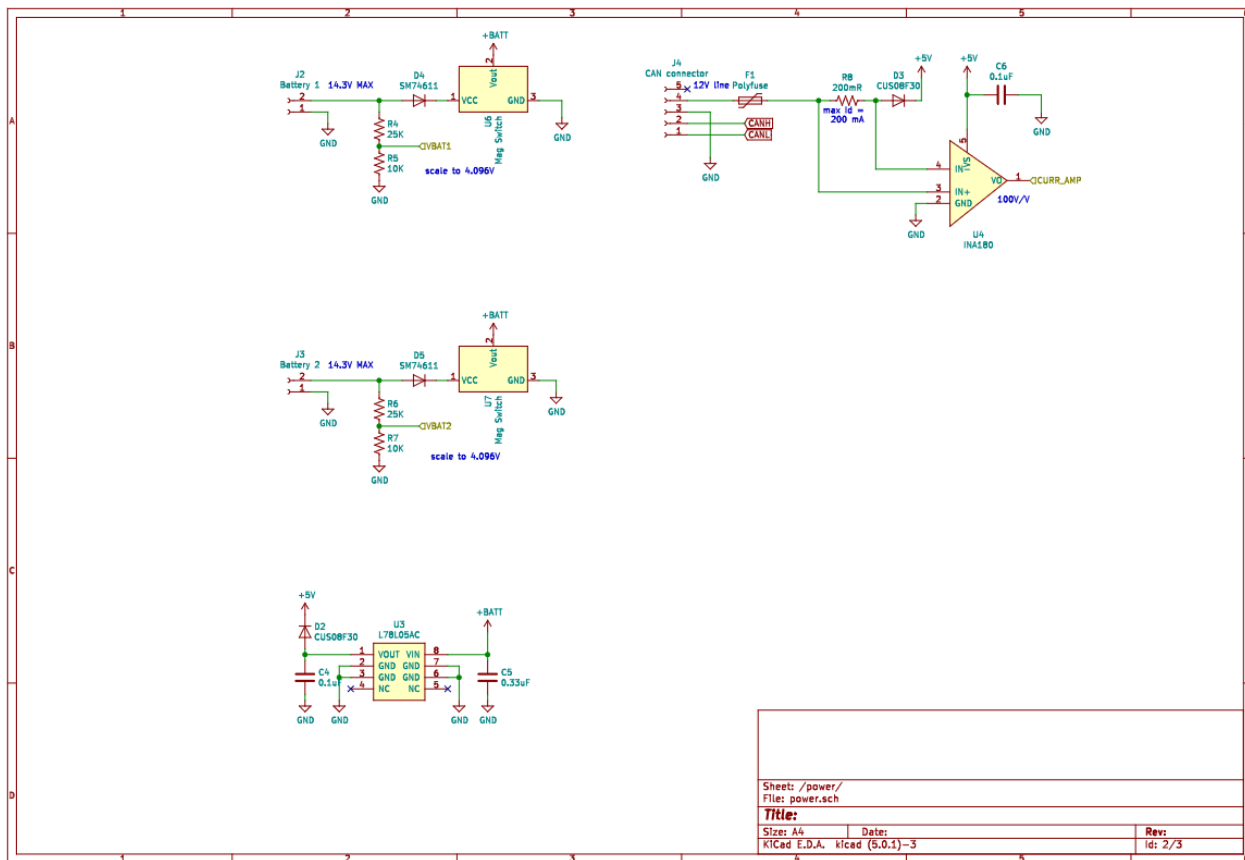


Figure 166: Remote Arming Schematic - Power

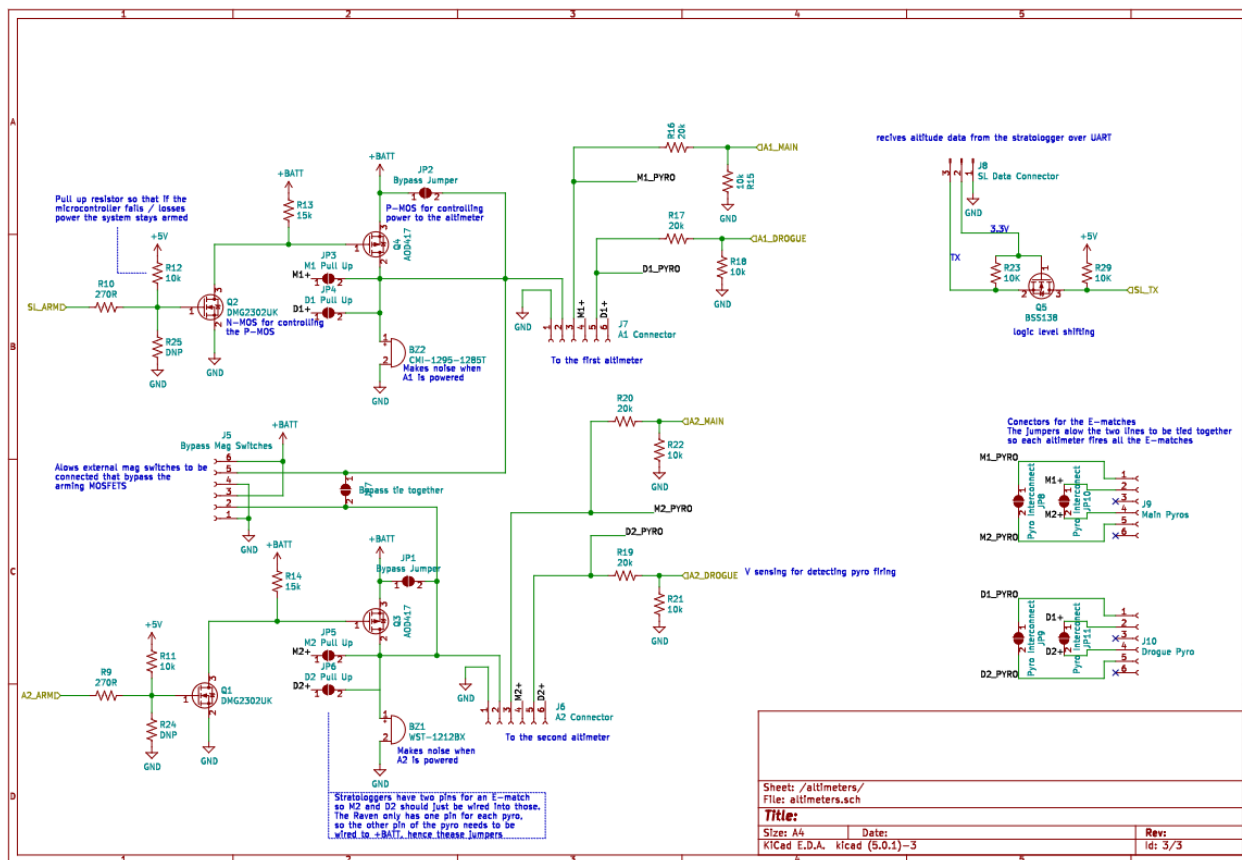


Figure 167: Remote Arming Schematic - Altimeters

## C Charging Board Schematics

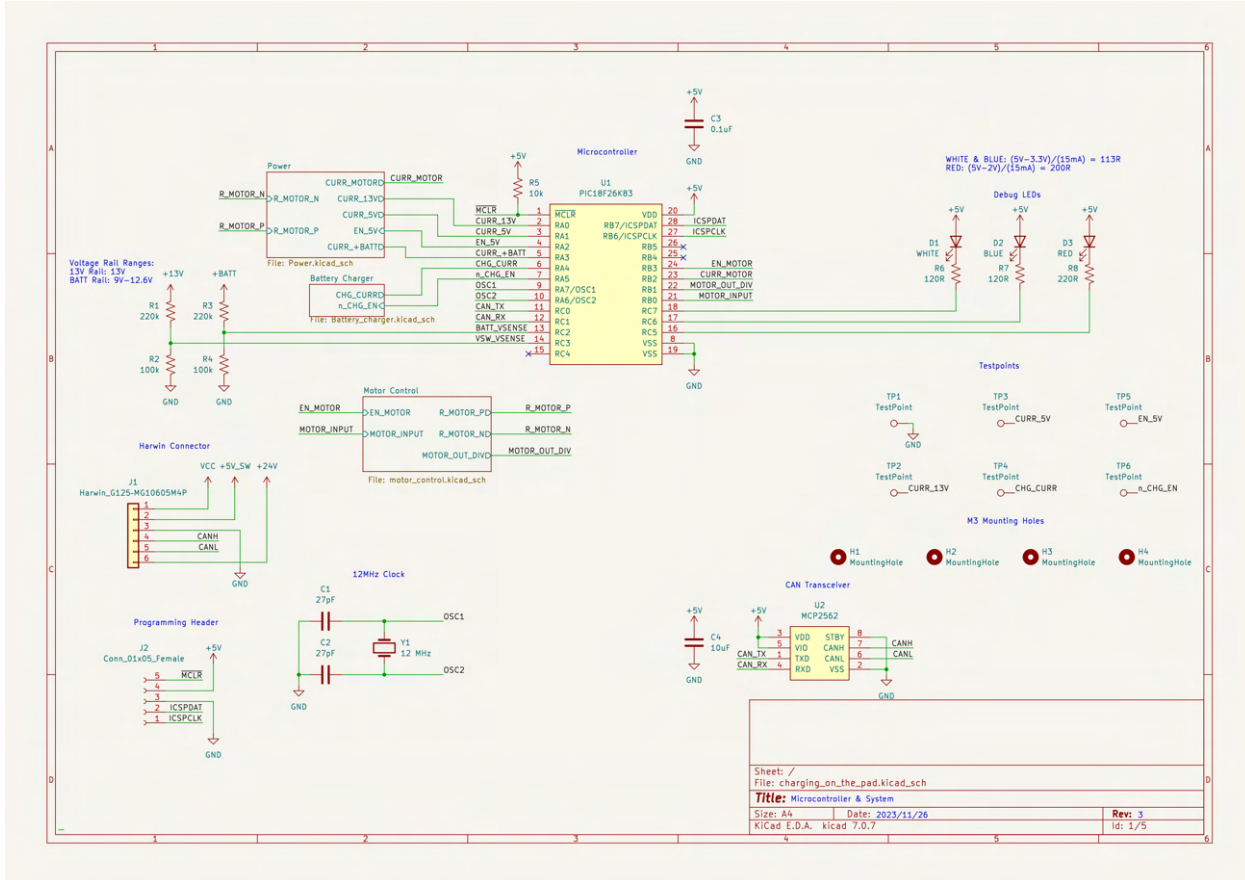


Figure 168: Charging board - Microcontroller and System

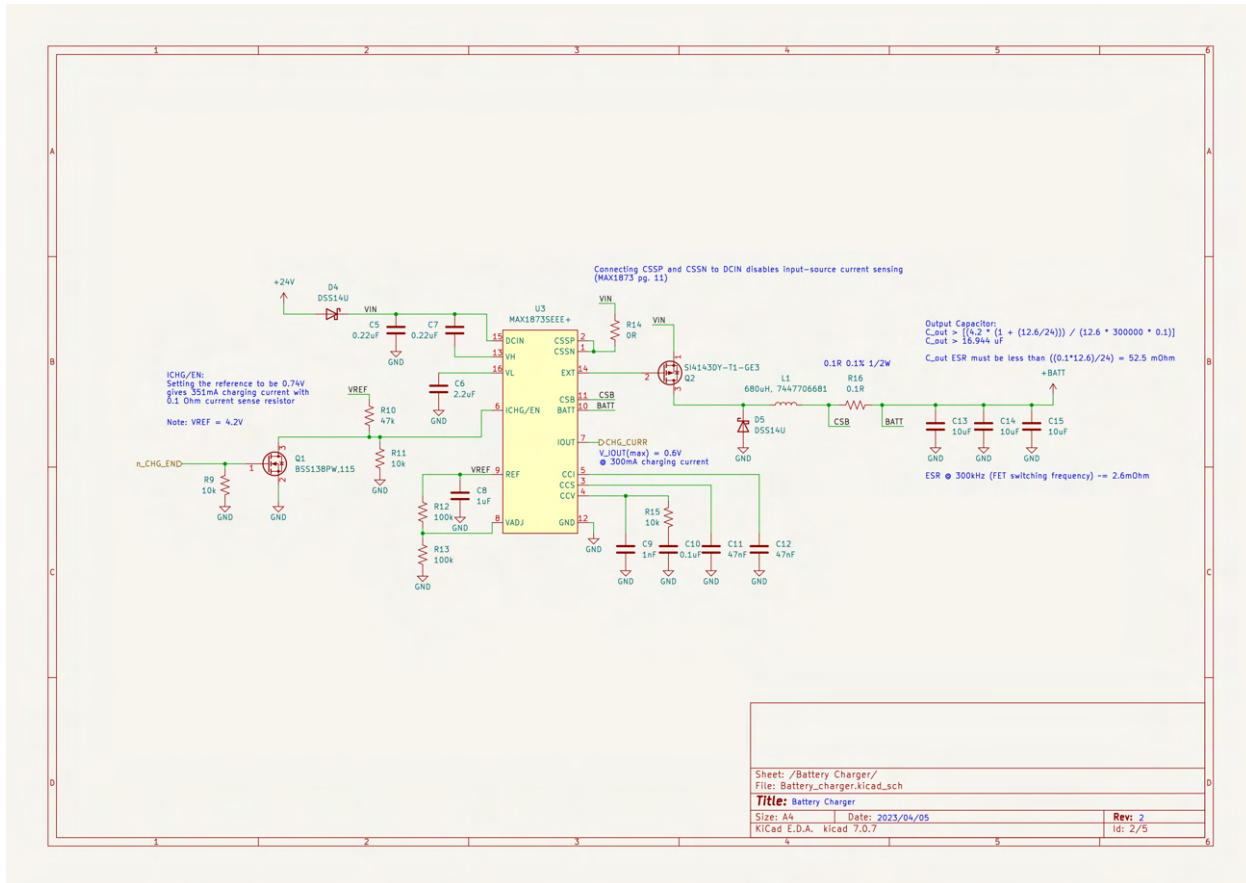
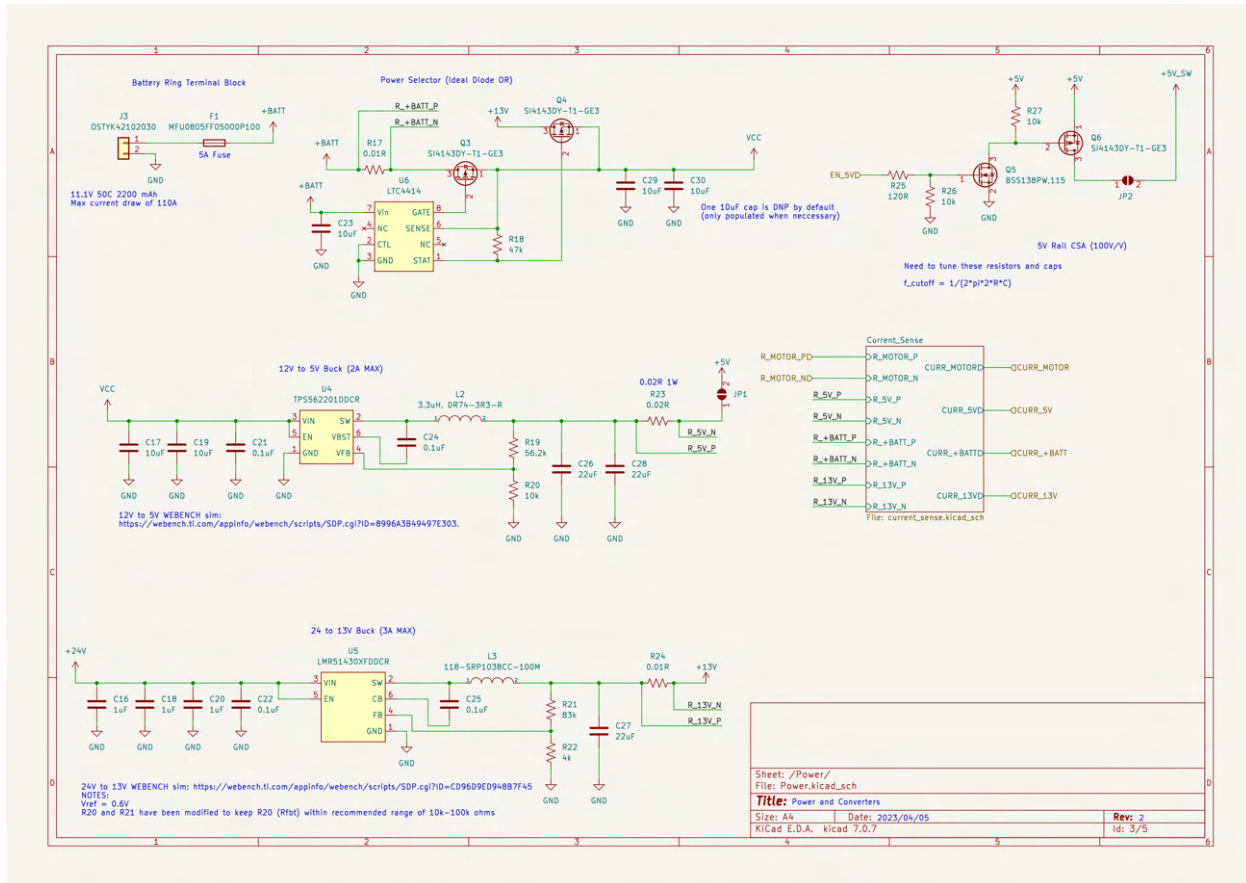


Figure 169: Charging Board - Battery Charger



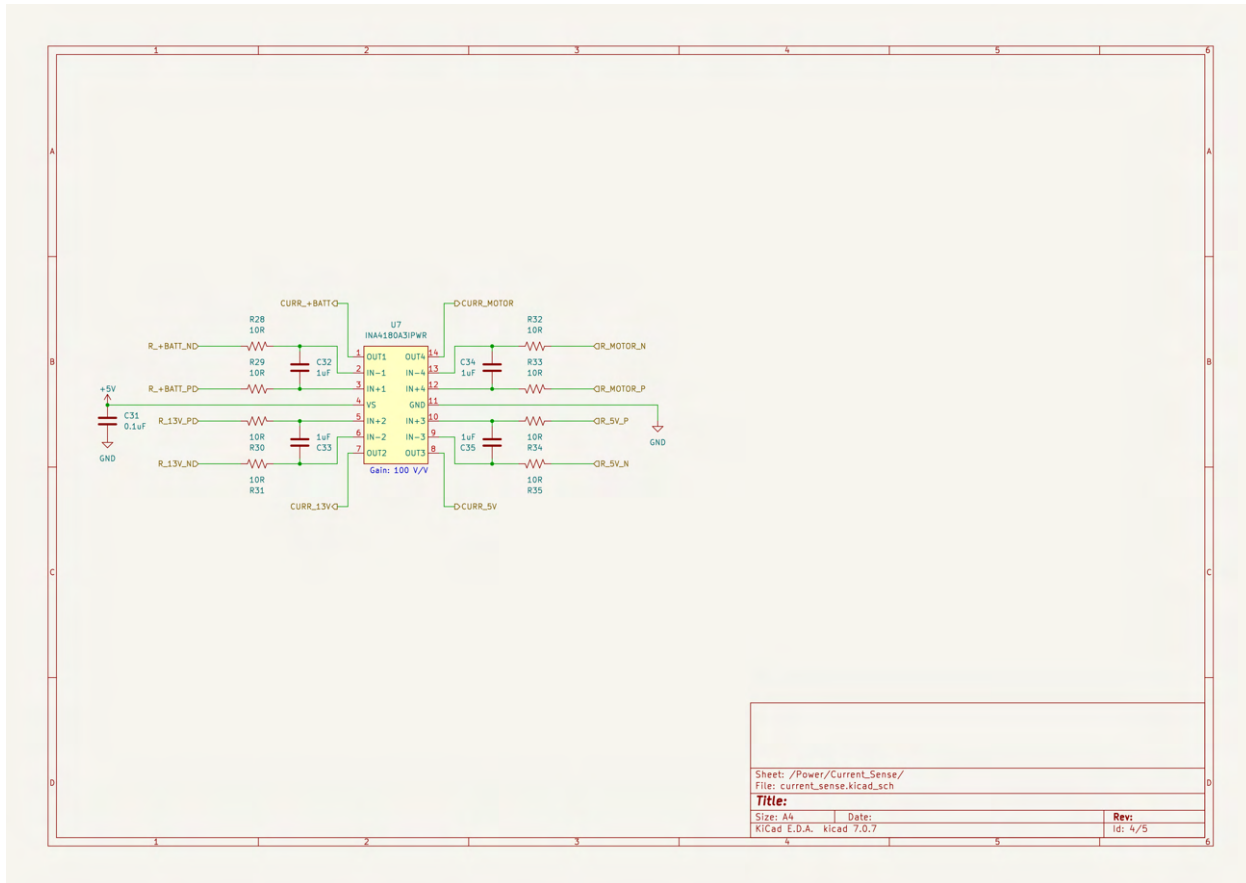


Figure 171: Charging Board - Current Sense

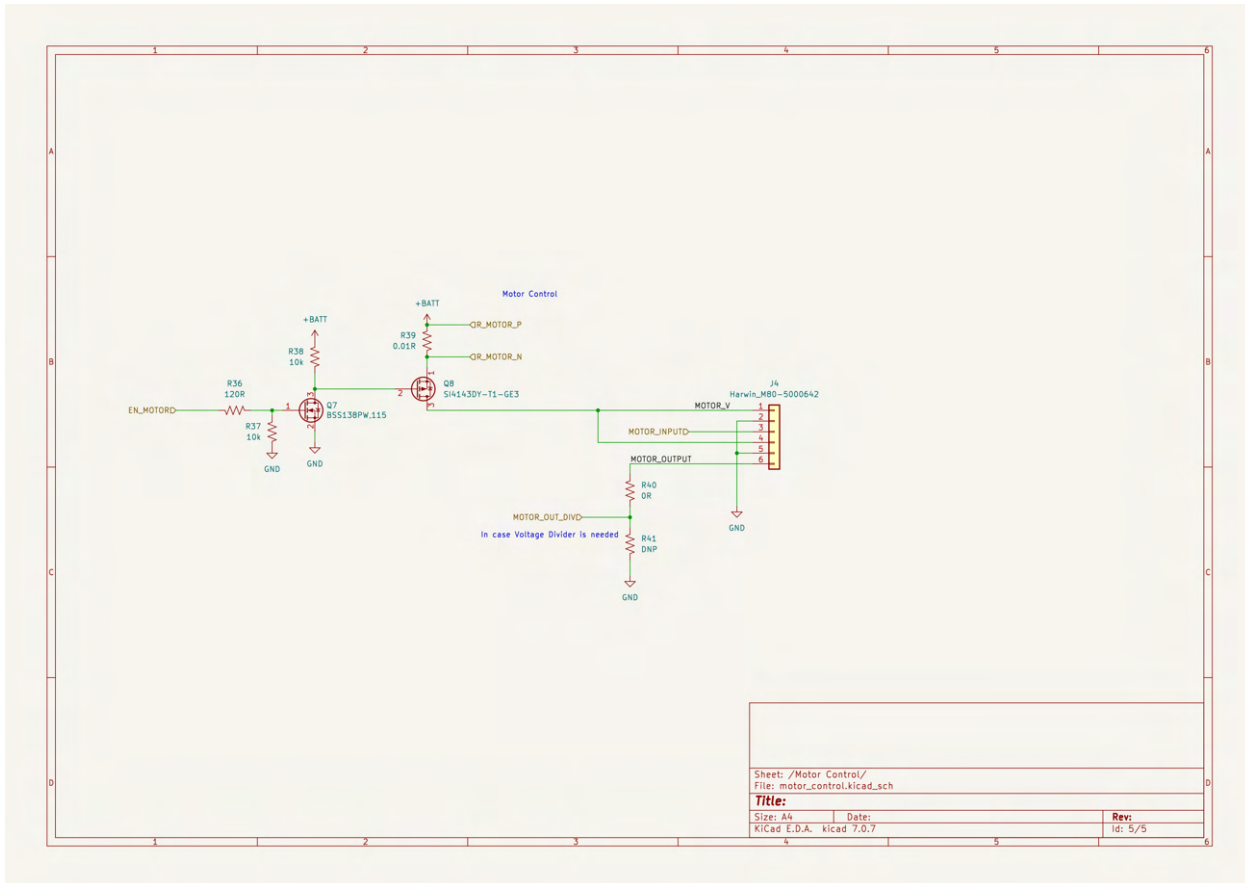


Figure 172: Charging Board - Motor Control

D Borealis P&ID

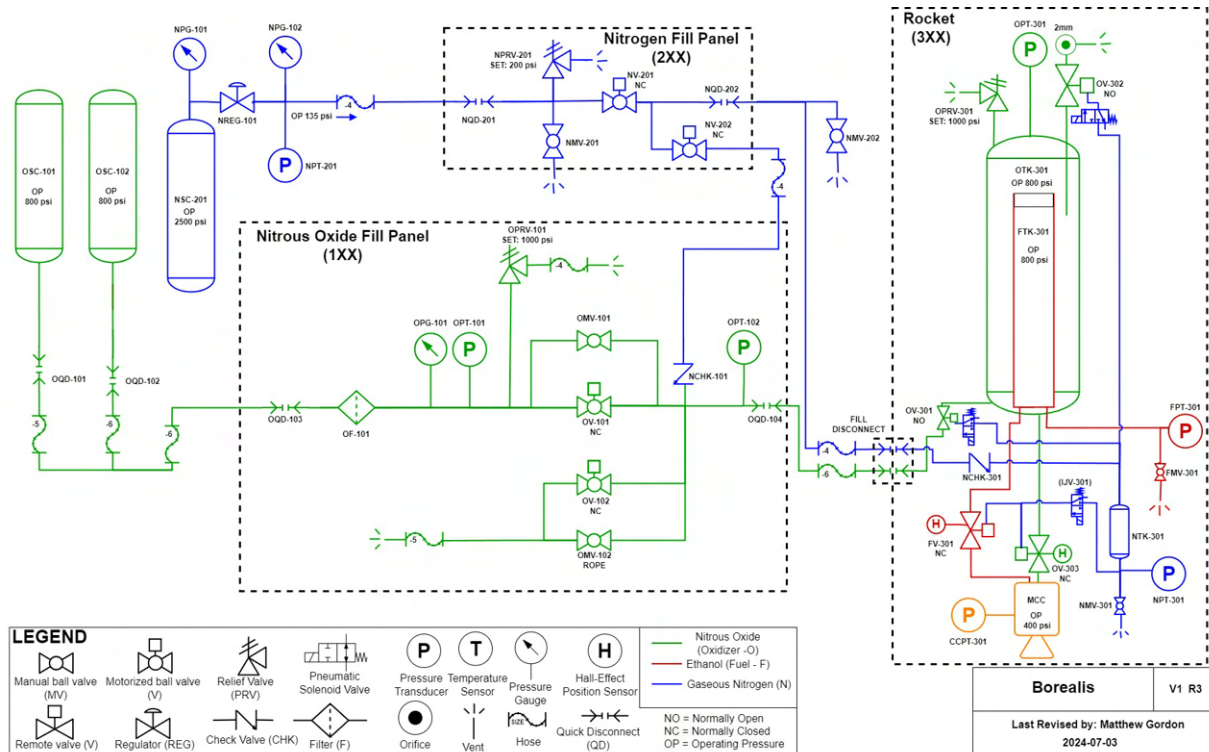


Figure 173: Borealis P&ID

## **E Launch Operations Procedure**

THIS PAGE INTENTIONALLY LEFT BLANK



---

Borealis  
Launch

Launch Operations Procedure

Compiled on 2024-07-11

# Launch Operations Procedure

---

## Contents

---

This document contains the following five procedures:

- The *Launch Operations Procedure* comprises steps for operating the fill system, conducting preflight check-outs, launching the Borealis Vehicle, and safing the system after launch.
- The *Alpha Abort* comprises steps for aborting and safing the system in the event of an anomaly during the launch operations procedure when contact is maintained between **FLIGHT** and **SECONDARY** and Remote Launch Control System (RLCS) is functional.
- The *Beta Abort* comprises steps for aborting and safing the system when contact is maintained between **FLIGHT** and **SECONDARY** and the RLCS is experiencing an anomaly.
- The *Gamma Abort - Pad* comprises steps for **PRIMARY** and **SECONDARY** for aborting and safing the system in the event contact between **SECONDARY** and **FLIGHT** is lost.
- The *Gamma Abort - Mission Control* comprises steps for the Mission Control team for aborting and safing the system in the event contact between **SECONDARY** and **FLIGHT** is lost.

## Personnel Required

---

The test operations team consists of nine personnel:

- The **Flight Director [FLIGHT]** directs operations and communicates with all other test personnel
- The **Primary Operator [PRIMARY]** is the main system operator. **PRIMARY** operates all manual valves on the fill and nitrogen pressurization system.
- The **Secondary Operator [SECONDARY]** is the backup for **PRIMARY**, and communicates with **FLIGHT**. If **PRIMARY** becomes incapacitated, **SECONDARY** is responsible for removing them from danger.
- The **Control System Operator [CONTROL]** operates the test control system, including actuating remote valves and engine ignition.
- The **Data Acquisition System Operator [DAQ]** monitors and operates the ground side data acquisition system.
- The **Telemetry System Operator [TELEMETRY]** monitors and operates the rocket telemetry system.
- The **Chief Propulsion Engineer [PROP]** is responsible for providing input to **FLIGHT** on all propulsion systems.
- The **Weather Officer [WEATHER]** is responsible for monitoring weather conditions, specifically wind speeds, and ensuring they are acceptable for launch.
- The **Range Safety Officer [RSO]** is a Launch Canada personnel responsible for supervising the launch pad and range, and provides permission to fill propellants and launch.

## Sign-Off

---

*To be completed by all test personnel after reading and familiarization with procedures*

- **FLIGHT** \_\_\_\_\_
- **PRIMARY** \_\_\_\_\_
- **SECONDARY** \_\_\_\_\_
- **CONTROL** \_\_\_\_\_
- **DAQ** \_\_\_\_\_
- **TELEMETRY** \_\_\_\_\_
- **PROP** \_\_\_\_\_
- **WEATHER** \_\_\_\_\_

## General Notes

---

- If any event fails to occur as specified in this procedure **FLIGHT** should proceed to the Alpha abort procedure, unless alternate steps are provided in the procedure.
- Flags are used to indicate risk level of the system. The colours indicate the following:
  - **GREEN**: Normal risk level, pad open.
  - **YELLOW**: Moderate level of risk - single item of concern, pad must be at yellow flag.
  - **ORANGE**: Moderate risk - multiple points of concern, pad must be at yellow flag.
  - **RED**: High level of risk, pad must be cleared before entering this state.
  - **DARK RED**: Highest level of risk, single action/failure causes launch.

## Prior to Launch Operations Start

---

- 1     Ensure the following items are complete before beginning the launch procedure
  - 2     Rocket fully assembled per all relevant assembly procedures.
  - 3     Rocket raised on launch tower.
  - 4     Ground side plumbing set up per Borealis P&ID.
  - 5     Fuel tank filled with 4.25kg of ethanol
    - 6     Fuel tank should be filled using the piston pump until pumping causes pressure to increase in the fuel tank, indicating the piston has topped out.
  - 7     DAQ system checkouts, including validating all sensors are displaying reasonable values.
  - 8     Valve safe state checks for all remote valves.
  - 9     RLCS power on, including:
    - 10     Both lipos installed.
    - 11     Actuator and Main switches set to "ON".
    - 12     GSPD on connected to 2 car batteries in parallel.
  - 13     Correct plumbing is connected to cylinders and safety caps are installed.
  - 14     Both tank heating PCB power wires connected to RLCS towerside box.
  - 15     Both tank heating PCB sensing wire assemblies connected to DAQ.
  - 16     Security cameras in the correct positions and communicating over DAQ.
  - 17     Media Remote cameras (GoPros) in position and recording.
  - 18     Anemometer installed on the launch tower and sending data to DAQ.
  - 19     Set all regulators to the minimum position.
  - 20     Ensure ropes are installed on Manual Oxidizer Drain Valve (OMV-102) and Manual Oxidizer Fill Bypass Valve (OMV-101) and tested.
  - 21     Ensure all personnel as defined above are available and have completed sign-off.
  - 22     Ensure a blank copy of the procedure is available or a unique symbol will be used to cross off steps.
  - 23     DAQ logs cleared from DAQ computer.
  - 24     Lockout key is installed in towerside box.
  - 25     Ignition cables are disconnected from the towerside box.
  - 26     The following tools are present at the launch pad:
    - 27     Multimeter
    - 28     Wrench set
    - 29     DAQ screwdriver
    - 30     OTAS screwdriver
    - 31     Allen Key set
  - 32     The yellow generator is filled with fuel and running at the ops table.
  - 33     Verify the voltages of the following systems are within the acceptable range:
    - 34     RLCS Lipos: 11V or greater
    - 35     GSPD Car Batteries: 11.5V or greater
    - 36     Tank heating car batteries: 11.5V or greater
  - 37     A laptop is on the ops table with a live feed from the remote cameras.
  - 38     Ops Audio is being recorded.
  - 39     The following personnel have walkie-talkies and that communication is functional:

- 40            **FLIGHT**  
41            **SECONDARY**  
42            Ensure **PRIMARY** and **SECONDARY** are wearing face shields and have no exposed skin.  
43            Ensure **PRIMARY** is wearing thermal gloves.  
44            Ensure **SECONDARY** has a back-up walkie talkie.  
45            Verify permission to begin pre-launch ops is received from **RSO**.

## Launch Operations Procedure

---

- 1            **DAQ**: Begin DAQ data logging.
- 2            **SECONDARY**: Confirm that the ignition wire is not connected to the towerside control box.
- 3            **DAQ**: Confirm the zero points of all sensors have been recorded and offset.
- 4            **PRIMARY**: Confirm the following valves are initially closed:
- 5            Remote Oxidizer Fill Valve (OV-101).  
6            Manual Oxidizer Fill Bypass Valve (OMV-101).  
7            Remote Oxidizer Drain Valve (OV-102).  
8            Manual Oxidizer Drain Valve (OMV-102).  
9            Nitrogen Fill Valve (NV-201).  
10            Nitrogen Drain Valve (NV-202).  
11            Upstream Manual Nitrogen Drain Valve (NMV-201).  
12            Downstream Manual Nitrogen Drain Valve (NMV-202).  
13            Manual Fuel Dump Valve (FMV-301).  
14            Manual Pneumatics Drain Valve (NMV-301).
- 15            **CONTROL**: Confirm the commanded state for the following valves is 'closed':
- 16            Injector Valve (IJV-101).
- 17            **DAQ**: Verify the displayed states for the following valves is 'closed':
- 18            Fuel Injector Valve (FV-301).  
19            Oxidizer Injector Valve (OV-303).
- 20            **CONTROL**: Confirm the commanded state for the following valves is 'open':
- 21            Oxidizer Tank Fill/Dump Valve (OV-301).  
22            Oxidizer Vent Valve (OV-302).
- 23            **PRIMARY**: Confirm the resistance across the primary and secondary ignition cables is 2.0 +/- 0.5 ohms.
- 24            **SECONDARY**: Confirm there are no personnel at the launch pad except for **PRIMARY**, **SECONDARY**, and any range safety personnel or operators from other teams.
- 25            **DAQ**: Confirm all sensors are reading their determined zero points.
- 26            **FLIGHT**: Verify drone is not at the pad.
- 27            **PRIMARY**: Slowly open Nitrogen Supply Cylinder NSC-201.
- 28            **PRIMARY**: Communicate cylinder supply pressure as read by NPG-201.

- 29     **PRIMARY**: Slowly adjust pneumatics regulator NREG-101 until a pressure of 135psi is read on NPG-202.
- 30     **DAQ**: Confirm the pressure reading on NPT-201 is 135psi.
- 31     **PRIMARY**: Slowly open the first Nitrous Oxide supply cylinder, OSC-101.
  - If leaks are observed proceed to the Alpha Abort Procedure.
- 32     **PRIMARY**: Slowly open the second Nitrous Oxide supply cylinder, OSC-102.
- 33     **PRIMARY**: Communicate the oxidizer supply pressure as read by gauge OPG-101.
- 34     **DAQ**: Communicate the oxidizer supply pressure as read by OPT-101.
- 35     **FLIGHT**: Confirm the two values are in agreement.
- 36     **TELEMETRY**: Command remote arming to arm altimeters.
- 37     **PRIMARY**: Verify altimeters have been armed by listening for the beeping pattern.
- 38     **SECONDARY**: Connect the ignition wire to the towerside box.
- 39     **SECONDARY**: Remove lockout key from towerside box.
- 40     **PRIMARY** and **SECONDARY**: Retreat to mission control. Bring the multimeter.
- 41     **FLIGHT**: Proceed when **PRIMARY** and **SECONDARY** have reached mission control and the pad is clear.
- 42     **FLIGHT**: Request permission to fill from **RSO**.
- 43     **CONTROL**: Insert system control key into clientside box and engage control.
- 44     **CONTROL**: Open Nitrogen Fill Valve (NV-201).
- 45     **TELEMETRY**: Continuously communicate pressure as read by Pnuematics Pressure Transducer NPT-301.
- 46     **FLIGHT**: Proceed when pressure reaches 135 +/- 5 psi.
- 47     **CONTROL**: Open Remote Oxidizer Fill Valve (OV-101).
- 48     **DAQ**: Continuously communicate oxidizer tank mass as read by oxidizer tank load cell.
- 49     **FLIGHT**: Proceed when tank mass has increased by 13 kg (+ 0.5kg, - 0 kg), or a plume is observed from Oxidizer Vent Valve (OV-302).
  - If supply and oxidizer tank pressure equilibrate or mass stops increasing before target conditions are met proceed to the Alpha Abort Procedure.
- 50     **CONTROL**: Close Remote Oxidizer Fill Valve (OV-101).
- 51     **CONTROL**: Close Oxidizer Vent Valve (OV-302).
- 52     **CONTROL**: Close Oxidizer Tank Fill/Dump Valve (OV-301).
- 53     **CONTROL**: Open Remote Oxidizer Drain Valve (OV-102).
- 54     **DAQ**: Constantly communicate upstream supply pressure as read by Upstream Oxidizer Fill Transducer OPT-102.
- 55     **FLIGHT**: Proceed when OPT-102 reads atmospheric.
- 56     **CONTROL**: Close Remote Oxidizer Drain Valve (OV-102).
- 57     **DAQ**: Verify pressure reading on Upstream Oxidizer Fill Transducer OPT-102 is atmospheric.

- If pressure on OPT-102 increases, cycle Oxidizer Tank Fill/Dump Valve (OV-301), then repeat lines 53 to 57.
  - If cycling Oxidizer Tank Fill/Dump Valve (OV-301) causes oxidizer tank mass to drop below 12.5 kg, verify supply (OPT-101) is higher than the oxidizer tank pressure (OPT-301), then open Oxidizer Vent Valve (OV-302) and then return to line 47.
  - If cycling Oxidizer Tank Fill/Dump Valve (OV-301) does not fix the issue, proceed to the Alpha abort procedure.
- 58     **FLIGHT**: Verify tank pressure is below firing pressure of 750psi.
  - If tank pressure is above firing pressure, re-open Oxidizer Vent Valve (OV-302) until tank pressure is 750psi, then close Oxidizer Vent Valve (OV-302) and proceed to line 77.
- 59     **CONTROL**: Engage tank heating.
- 60     **TELEMETRY**: Communicate oxidizer tank pressure as read by OPT-301 in increments of 50psi.
- 61     **DAQ**: Monitor all sensors and report any deviations or anomalies to **FLIGHT** immediately.
- 62     **FLIGHT**: If oxidizer tank mass drops below 12.5 kg proceed to the Alpha abort procedure.
- 63     **FLIGHT**: If the difference between the fuel tank pressure and oxidizer tank pressure is more than 100psi, proceed to the Alpha Abort Procedure.
- 64     **FLIGHT**: Proceed when the oxidizer tank pressure has reached 700psi.
- 65     **FLIGHT**: Ensure all spectators are wearing safety glasses
- 66     **CONTROL**: Close Nitrogen Fill Valve (NV-201).
- 67     **CONTROL**: Open Remote Oxidizer Drain Valve (OV-102).
- 68     **CONTROL**: Open Nitrogen Drain Valve (NV-202).
- 69     **CONTROL**: Actuate Fill Disconnect.
- 70     **CONTROL**: Close Remote Oxidizer Drain Valve (OV-102).
- 71     **CONTROL**: Open Nitrogen Fill Valve (NV-201).
- 72     **FLIGHT**: Verify with remote cameras that fill disconnect has detached from the rocket.
- 73     **CONTROL**: Close Nitrogen Fill Valve (NV-201).
- 74     **TELEMETRY**: Verify rocket pneumatic pressure as read by NPT-301 is stable.
- 75     **FLIGHT**: Proceed when the oxidizer tank pressure has reached firing pressure of 750psi.
- 76     **CONTROL**: Disengage tank heating.
- 77     **TELEMETRY**: Set the rocket to internal power by turning off the 24V groundside supply.
- 78     **PAUSE POINT**
- 79     **FLIGHT**: Verify the following test commit criteria are met:
  - Oxidizer tank mass stable at 13 +/- 0.5 kg.
  - Fuel tank mass stable at 4.25 +/- 0.25 kg.
  - Oxidizer tank pressure stable at 750 +/- 25 psi.
  - Fuel tank pressure stable at 750 +/- 25 psi.
  - Pad clear.

- 85        Fill disconnect mechanism disconnected.  
86        Altimeters armed.  
87        GPS is connected.  
88        Verify airbrakes are not extended via remote camera.  
89        **TELEMETRY**: Verify all rocket avionics are configured for launch.  
90        **DAQ**: Confirm all sensors are reading steady values.  
91        **DAQ**: Confirm wind gust speeds are less than 37 km/h or 23 mph.
- 92        **FLIGHT**: Request permission to launch from **RSO**.
- 93        **FLIGHT**: Conduct a final Go/No-Go poll of the following operators:
- 94        **DAQ**  
95        **CONTROL**  
96        **TELEMETRY**  
97        **PROP**  
98        **WEATHER**  
99        **FLIGHT**
- 100       **TELEMETRY**: Command the payload servo to turn on.  
101       **TELEMETRY**: Begin onboard cameras recording.  
102       **CONTROL**: Conduct the engine startup procedure.  
103       Arm primary ignition.  
104       Hold down the fire button and continuously communicate ignition current.  
105       Proceed when either primary or secondary ignition current reads 0 amps, or when smoke is observed on the remote cameras.  
106
  - In the event of a failed ignition (criteria are not met within 1 minute) immediately release the ignition button and proceed to the Alpha Abort Procedure

107       Conduct the launch by opening Injector Valve (IJV-101).  
107       **ALL**: Observe the launch.

108       **TELEMETRY**: Provide continuous callouts of rocket altitude, and events including apogee and recovery system deployment.

109       **FLIGHT**: Confirm with remote camera operators that there is no visible fire on or around the test stand.  
109      
  - In the event fire is observed inform **RSO** immediately.

110       **TELEMETRY**: Record the final location of the rocket GPS for the recovery team.  
111       **DAQ**: Verify DAQ systems are functional and ground side plumbing is in a stable configuration.  
112       **CONTROL**: Disengage control and remove system control key.  
113       **FLIGHT**: Wait for permission from **RSO** to return to the pad.  
114       **PRIMARY** and **SECONDARY**: Return to the pad.  
115       **SECONDARY**: Insert lockout key into the towerside box.  
116       **PRIMARY**: Close Nitrous Oxide supply cylinder OSC-101.  
117       **PRIMARY**: Close Nitrous Oxide supply cylinder OSC-102.

- 118     **PRIMARY**: Close Nitrogen supply cylinder NSC-201.
- 119     **SECONDARY**: Remove lockout key from towerside box.
- 120     **PRIMARY** and **SECONDARY**: Retreat to a safe distance.
- 121     **CONTROL**: Insert system control key into clientside box and engage control.
- 122     **CONTROL**: Open Remote Oxidizer Fill Valve (OV-101).
- 123     **CONTROL**: Open Nitrogen Fill Valve (NV-201).
- 124     **DAQ**: Confirm all Ground-Side sensors are reading their determined zero points.
- 125     **CONTROL**: Disengage control and remove system control key from the clientside box.
- 126     **DAQ**: Stop DAQ logging and save data files.
- 127     **FLIGHT**: Inform **RSO** that the system is safed.
- 128     **FLIGHT**: Proceed with teardown when the **RSO** gives permission for all personnel to return to the pad.

## Alpha Abort Procedure

---

- 1     **CONTROL:** Release the ignition button if pressed.
- 2     **DAQ:** Verify DAQ is operational and receiving data.
  - If DAQ or RLCS is not operational, proceed to the Beta Abort Procedure.
- 3     **FLIGHT:** Confirm communication with **SECONDARY** is functional.
  - If communication is non-functional, proceed to the Gamma Abort Procedure.
- 4     **CONTROL:** Disengage tank heating.
- 5     **TELEMETRY:** Return the rocket to ground-side power by turning on the 24V ground supply.
- 6     **TELEMETRY:** Command remote arming to disarm altimeters.
- 7     **CONTROL:** Open Oxidizer Vent Valve (OV-302) if not already open.
- 8     **CONTROL:** Close Remote Oxidizer Fill Valve (OV-101) if not already closed.
- 9     **CONTROL:** Open Remote Oxidizer Drain Valve (OV-102) if not already open.
- 10    **CONTROL:** Open Oxidizer Tank Fill/Dump Valve (OV-301) if not already open.
- 11    **FLIGHT:** Proceed when the oxidizer tank is fully vented.
- 12    **CONTROL:** Close Nitrogen Fill Valve (NV-201) if not already closed
- 13    **CONTROL:** Open Nitrogen Drain Valve (NV-202) if not already open.
- 14    **CONTROL:** Disengage control and remove the system control key.
- 15    **FLIGHT:** Inform **RSO** of abort.
- 16    **FLIGHT:** Proceed when **RSO** gives clearance for personnel to return to the launch pad.
- 17    **PRIMARY** and **SECONDARY:** Return to the launch pad.
- 18    **PRIMARY:** Confirm altimeters are disarmed and no beeping is heard.
- 19    **SECONDARY:** Insert lockout key into towerside box.
- 20    **SECONDARY:** Disconnect the ignition wires from the towerside box.
- 21    **PRIMARY:** Close Nitrous Oxide supply cylinder OSC-101.
- 22    **PRIMARY:** Close Nitrous Oxide supply cylinder OSC-102.
- 23    **PRIMARY:** Close Nitrogen supply cylinder NSC-201.
- 24    **SECONDARY:** Remove lockout key from towerside box.
- 25    **PRIMARY** and **SECONDARY:** Retreat to a safe distance.
- 26    **CONTROL:** Insert the system control key and engage control.
- 27    **CONTROL:** Open Remote Oxidizer Fill Valve (OV-101).
- 28    **CONTROL:** Open Nitrogen Fill Valve (NV-201).
- 29    **DAQ:** Verify all sensors are reading their determined zero point.
- 30    **CONTROL:** Disengage control and remove system control key.

- 31     **PRIMARY** and **SECONDARY**: Approach the launch pad.
- 32     **PRIMARY**: Remove the front left OTAS panel.
- 33     **PRIMARY**: Open Manual Pneumatics Drain Valve (NMV-301).
- 34     **FLIGHT**: Abort and revisit plumbing and controls setup.

## Beta Abort Procedure

---

- 1     **CONTROL** and **DAQ**: Attempt to troubleshoot the issue.
  - If RLCS and DAQ become at any time operational, have **PRIMARY** and **SECONDARY** retreat to a safe distance and return to the Alpha Abort Procedure.
- 2     **CONTROL**: If able, set the rocket and GSE to safe state.
- 3     **FLIGHT**: Have the drone operator confirm the rocket has gone to safe state.
- 4     **FLIGHT**: Inform **RSO** of the abort.
- 5     **FLIGHT**: Proceed when **RSO** gives permission for personnel to return to the pad.
- 6     **PRIMARY** and **SECONDARY**: Return to the pad and approach the manual valve ropes.
  - If venting is heard, report approximate source to **FLIGHT**, and do not proceed until cleared by **FLIGHT**.
  - If a connection issue is suspected send a DAQ technician with a laptop and walkie talkie to the pad with **PRIMARY** and **SECONDARY** and attempt to connect to the local wifi to provide sensor data.
- 7     **PRIMARY**: Open Manual Oxidizer Drain Valve (OMV-102) using the attached rope.
- 8     **FLIGHT**: Proceed when **PRIMARY** and **SECONDARY** report no venting is heard.
- 9     **SECONDARY**: Insert lockout key into towerside box.
- 10     **SECONDARY**: Disconnect the ignition wires from the towerside box.
- 11     **PRIMARY**: Disarm altimeters with the magnet on a pole.
- 12     **PRIMARY**: Close Nitrous Oxide supply cylinder OSC-101.
- 13     **PRIMARY**: Close Nitrous Oxide supply cylinder OSC-102.
- 14     **PRIMARY**: Close Nitrogen supply cylinder NSC-201.
- 15     **PRIMARY** and **SECONDARY**: Retreat to the manual valve ropes.
- 16     **PRIMARY**: Open Manual Oxidizer Fill Bypass Valve (OMV-101).
- 17     **FLIGHT**: Proceed when **PRIMARY** and **SECONDARY** report no venting is heard.
- 18     **PRIMARY**: Open Downstream Manual Nitrogen Drain Valve (NMV-202).
- 19     **PRIMARY**: Open Upstream Manual Nitrogen Drain Valve (NMV-201).
- 20     **PRIMARY**: Remove the front left OTAS panel.
- 21     **PRIMARY**: Open Manual Pneumatics Drain Valve (NMV-301).
- 22     **PRIMARY**: Verify the following gauges read zero pressure:
  - Oxidizer fill panel gauge OPG-101.
  - Nitrogen cylinder gauge NPG-201.
  - Nitrogen fill panel guage NPG-202.
- 23     **DAQ**: If able, confirm all sensors are reading their determined zero points.
- 24     **FLIGHT**: Abort and revisit plumbing and controls setup.

## Gamma Abort Procedure - Pad

---

- 1     **SECONDARY**: Attempt to contact **FLIGHT** using the backup radio or by phone at +249-385-6237.
- 2     **SECONDARY**: If contact is not restored in 1 minute, proceed with the abort.
- 3     **SECONDARY**: Insert lockout key into towerside box if not already inserted.
- 4     **SECONDARY**: Disconnect ignition wires from the towerside box, if connected.
- 5     **PRIMARY**: Disarm altimeters with the magnet on a pole, if armed.
- 6     **PRIMARY**: Close Nitrous Oxide supply cylinder OSC-101.
- 7     **PRIMARY**: Close Nitrous Oxide supply cylinder OSC-102.
- 8     **PRIMARY**: Close Nitrogen supply cylinder NSC-201.
- 9     **PRIMARY** and **SECONDARY**: Retreat to the manual valve ropes.
- 10    **PRIMARY**: Open Manual Oxidizer Fill Bypass Valve (OMV-101).
- 11    **PRIMARY**: Open Manual Oxidizer Drain Valve (OMV-102).
- 12    **PRIMARY** and **SECONDARY**: Proceed when no venting is heard.
- 13    **PRIMARY**: Open Downstream Manual Nitrogen Drain Valve (NMV-202).
- 14    **PRIMARY**: Open Upstream Manual Nitrogen Drain Valve (NMV-201).
- 15    **PRIMARY**: Remove the front left OTAS panel.
- 16    **PRIMARY**: Open Manual Pneumatics Drain Valve (NMV-301).
- 17    **PRIMARY**: Verify the following gauges read zero pressure:
  - Oxidizer fill panel gauge OPG-101.
  - Nitrogen cylinder gauge NPG-201.
  - Nitrogen fill panel gauge NPG-202.
- 18    **PRIMARY** and **SECONDARY**: Return to Mission Control.

## Gamma Abort Procedure - Mission Control

---

- 1     **FLIGHT**: Attempt to re-establish contact with **SECONDARY** for no more than 1 minute.
- 2     **CONTROL**: Remove system control key from clientside box if inserted.
- 3     **FLIGHT**: Inform **RSO** of the abort.
- 4     **DAQ** and **TELEMETRY**: Monitor all sensors and provide updates on any changes.
- 5     **FLIGHT**: Wait for **PRIMARY** and **SECONDARY** to return.
- 6     **FLIGHT**: Abort and revisit plumbing and controls setup.

## Variable Recording